

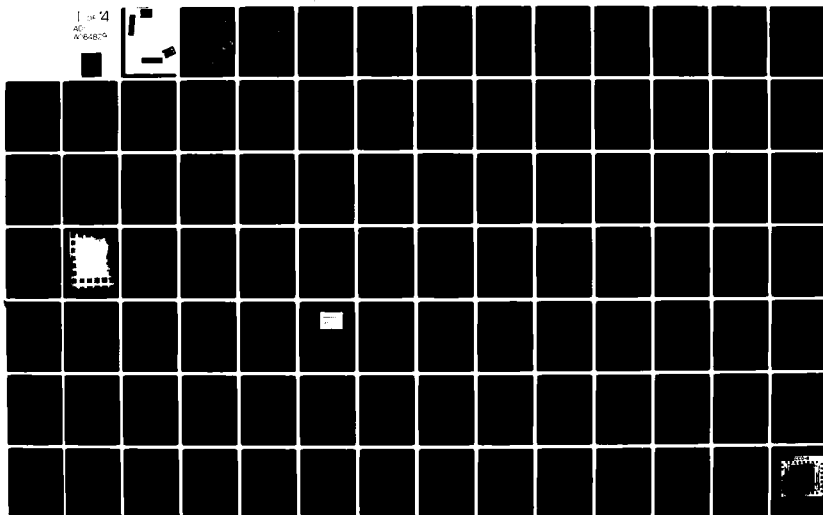
AD-A084 829

TRW DEFENSE AND SPACE SYSTEMS GROUP REDONDO BEACH CA F/6 9/1  
CHARGE COUPLED DEVICES IN SIGNAL PROCESSING SYSTEMS. VOLUME V. --ETC(U)  
DEC 79 R A ALLEN, J M ANDERSON, F G HAMILTON N00014-74-C-0068

UNCLASSIFIED

NL

1 of 4  
AD  
A-64829



ADA084829

LEVEL III

DTIC  
ELECTE  
MAY 29 1990

C

This document has been approved  
for public release and is  
distributed in unlimited quantities.

# **CHARGE COUPLED DEVICES IN SIGNAL PROCESSING SYSTEMS**

---

## **VOLUME V. FINAL REPORT**

DECEMBER 1979

SPONSORED BY:

THE NAVAL ELECTRONICS SYSTEMS COMMAND

DIRECTED BY:

THE NAVAL RESEARCH LABORATORY

NAVY

CONTRACT NO. N00014-74-C-0068

DTIC  
ELECTED  
MAY 29 1980  
C

**TRW**

DEFENSE AND SPACE SYSTEMS GROUP

ONE SPACE PARK • REDONDO BEACH, CALIFORNIA 90278

This document has been approved  
for public release and sale; its  
distribution is unlimited.

Unclassified

SECURITY CLASSIFICATION OF THIS PAGE (When Data Entered)

REPORT DOCUMENTATION PAGE		READ INSTRUCTIONS BEFORE COMPLETING FORM															
1. REPORT NUMBER	2. GOVT ACCESSION NO.	3. RECIPIENT'S CATALOG NUMBER															
	AD-A084 829																
4. TITLE (and Subtitle) Charge Coupled Devices in Signal Processing Systems, Volume V, Final Report, December, 1979.		5. TYPE OF REPORT & PERIOD COVERED Final Report: October, 1973 to December, 1979															
		6. PERFORMING ORG. REPORT NUMBER															
7. AUTHOR(s) R. A. Allen, J. M. Anderson, F. G. Hamilton, W. H. Huber, M. Penberg, T. A. Zimmerman, R. Nicas, N. Schneider		8. CONTRACT OR GRANT NUMBER(s) N00014-74-C-0068															
9. PERFORMING ORGANIZATION NAME AND ADDRESS TRW Systems Group OneSpace Park Redondo Beach, CA 90278		10. PROGRAM ELEMENT, PROJECT, TASK AREA & WORK UNIT NUMBERS 15-5151															
11. CONTROLLING OFFICE NAME AND ADDRESS		12. REPORT DATE Dec 1979															
		13. NUMBER OF PAGES															
14. MONITORING AGENCY NAME & ADDRESS (if different from Controlling Office)		15. SECURITY CLASS. (of this report) Unclassified															
		15a. DECLASSIFICATION/DOWNGRADING SCHEDULE															
16. DISTRIBUTION STATEMENT (of this Report) Approved for public release; distribution unlimited (9) F. T. for Oct 73-Dec 79																	
17. DISTRIBUTION STATEMENT (of abstract entered in Block 20, if different from Report)																	
18. SUPPLEMENTARY NOTES																	
19. KEY WORDS (Continue on reverse side if necessary and identify by block number) <table border="0"> <tr> <td>Charge Coupled Device</td> <td>Half Adder</td> <td>LSI</td> </tr> <tr> <td>CCD</td> <td>Digital Multiplier</td> <td>CAD</td> </tr> <tr> <td>Digital Functions</td> <td>Digital Adder</td> <td>Radiation</td> </tr> <tr> <td>Full Adder</td> <td>DCCD</td> <td>Floating Gate</td> </tr> <tr> <td></td> <td>Pipeline Arithmetic</td> <td>Floating Diffusion</td> </tr> </table>			Charge Coupled Device	Half Adder	LSI	CCD	Digital Multiplier	CAD	Digital Functions	Digital Adder	Radiation	Full Adder	DCCD	Floating Gate		Pipeline Arithmetic	Floating Diffusion
Charge Coupled Device	Half Adder	LSI															
CCD	Digital Multiplier	CAD															
Digital Functions	Digital Adder	Radiation															
Full Adder	DCCD	Floating Gate															
	Pipeline Arithmetic	Floating Diffusion															
20. ABSTRACT (Continue on reverse side if necessary and identify by block number) <p>This report provides a comprehensive treatment of the entire digital charge coupled device (DCCD) program. The design history, starting from SSI logic circuits and continuing through MSI and LSI multipliers and adders, is discussed. The process development is traced from the early metal gate P-channel process to the final double poly n-channel process. Results of radiation testing on DCCD circuits is presented. Several computer aided design techniques are described which were developed during the course of the program. Finally, other programs related to and resulting from this effort are described.</p>																	

DD FORM 1 JAN 73 1473

Unclassified 409637  
SECURITY CLASSIFICATION OF THIS PAGE (When Data Entered)

# FORWARD

This report has been prepared by TRW Defense and Space Systems Group. The work summarized in this report was performed under contract N00014-74-C-006P. The scientific officer for this contract was Dr. D. F. Barbe of the Naval Research Laboratory. The sponsor was L. W. Sumney of the Naval Electronics Systems Command. The period of performance was from mid 1973 to December 1979.

Accession For	
NTIS GRA&I	
DDC TAB	
Unannounced	
Justification	
By	
Distribution/	
Availability Codes	
Dist	Avail and/or special
A	

## CONTENTS

	<u>Page</u>
1.0 INTRODUCTION	1-1
1.1 DCCD Implementation	1-2
1.2 Program History	1-3
1.3 Phase I Report Summary	1-6
1.4 Phase II Report Summary	1-6
1.5 Phase III Report Summary	1-6
2.0 SUMMARY AND CONCLUSIONS	2-1
2.1 Summary	2-1
2.1.1 Design	2-1
2.1.2 Layout	2-1
2.1.3 Wafer Processing	2-3
2.2 Conclusions	2-4
3.0 SMALL SCALE INTEGRATION (SSI) DEVELOPMENT	3-1
3.1 Introduction	3-1
3.2 Floating Gate/Floating Diffusion Designs and Results	3-5
3.3 Full-Adder Designs and Results	3-6
3.3.1 Full Adders Implemented from Dual Half Adders	3-10
3.3.2 Conversion to N-Channel Designs	3-12
3.3.3 Computer Model of a Full-Adder	3-15
3.3.4 Advantages of Full-Adders Over Dual Half-Adders	3-22
3.3.4.1 Power Dissipation	3-22
3.3.4.2 Transfer Efficiency	3-22
3.3.4.3 Pipeline Delays	3-22
3.4 Half-Adder Designs and Results	3-22
3.4.1 Half-Adder Gain and Operating Margins	3-28
3.4.2 Other Uses of Half-Adders	3-31
3.4.2.1 Refresh and Invert	3-31
3.4.2.2 Fan-Out	3-31
3.4.2.3 Frequency Divider	3-32
3.4.3 Advantages of Half-Adders over Full-Adders	3-32
3.4.3.1 Clock Frequency	3-32
3.4.3.2 Signal-to-Noise Ratio	3-34

	<u>Page</u>
3.5 I/O Circuitry	3-34
3.5.1 Input Circuits	3-34
3.5.1.1 DCCD Input Charge Generation	3-34
3.5.1.2 Input Buffers	3-36
3.5.2 Output Circuits	3-37
3.5.2.1 Source Follower Output Circuit	3-37
3.5.2.2 Two Stage Source Follower Output Circuit	3-39
3.5.2.3 DCCD to TTL Tri-State Output Circuit	3-39
3.6 Memory Cells	3-42
3.6.1 The Offset Gate Device Configuration	3-43
3.6.1.1 LSM-3 Device Test Results	3-72
4.0 LARGE SCALE INTEGRATION (LSI) DEVELOPMENT	4-1
4.1 Introduction	4-1
4.2 Evolution of DCCD Adder/Subtractor Designs	4-4
4.2.1 DP1 Adder Array	4-4
4.2.2 The DP2 4 + 4 Bit Adder Array	4-9
4.2.3 The DP2 8 + 8 Bit Adder Array	4-14
4.2.3.1 The Cascaded Dual Half Adder Design	4-14
4.2.3.2 Full Adder Design	4-14
4.2.4 The DP3 Adder Array	4-21
4.2.5 The DP5, Adder/Subtractor Array	4-24
4.2.6 Azimuth Correlator Device (ACD) 10 + 10 Bit Adder	4-28
4.3 Evolution of Multipliers	4-30
4.3.1 The DP1 Multiplier Arrays	4-30
4.3.2 The DP2 Multiplier Arrays	4-38
4.3.3 The DP3 Multiplier Array	4-45
4.3.4 The DP4 Multiplier Array	4-49
4.3.5 The Azimuth Correlator Device (ACD $\emptyset$ ) Multiplier Array	4-51
4.3.6 The ACD2 Multiplier Array	4-52
4.4 Fast Hadamard Transform (FHT) Cell	4-56
4.4.1 FHT-0 Test Chip	4-61
4.4.2 A-Hadamard Functional Block	4-61
4.4.3 Charge Fan-Out	4-65
4.4.4 Transfer Efficiency	4-70
4.4.5 AND Function	4-70
4.5 Memories	4-74

	<u>Page</u>
5.0 RADIATION TEST RESULTS	5-1
5.1 Introduction	5-1
5.2 Prompt-Ionizing Radiation Upset Tests	5-4
5.2.1 Test Setup and Discussion of Results	5-4
5.2.2 Prompt-Ionizing Radiation Upset Test Data	5-7
5.3 Total Ionizing Dose Tests	5-7
5.3.1 Test Setup and Discussion of Results	5-7
5.3.2 Total Ionizing Dose Test Data	5-21
6.0 SIGNAL AND DATA PROCESSING APPLICATIONS	6-1
6.1 Introduction	6-1
6.2 Applying the DCCL Concepts	6-1
6.3 Specific NRL/DCCL Applications	6-4
6.3.1 Itakura Transform Application	6-6
6.3.2 Sort and Merge Applications	6-9
6.3.2.1 DCCL Sort and Merge Technique No. 1	6-9
6.3.2.2 DCCL Sort and Merge Technique No. 2	6-16
6.3.2.3 DCCL Sort and Merge Technique No. 3	6-21
6.3.2.4 The Sort and Merge (SAM) FIFO, LIFO Design	6-27
6.3.2.4.1 Interlaced FIFO SPS Design	6-27
6.3.2.4.2 Interlaced FIFO/LIFO SPS Memory Design	6-32
7.0 DCCD WAFER PROCESSING	7-1
7.1 Introduction	7-1
7.2 Processing Evolution	7-1
7.3 Processing History	7-4
7.3.1 Introduction of the "DP" Mask Series	7-5
7.3.1.1 The Double Polysilicon Process	7-8
7.3.1.2 The Switch to N-Channel DCCD Technology	7-9
7.3.1.3 The DP3 Series	7-10
7.3.1.4 The Nitride Sandwich Experiment	7-13
7.3.2 NE-1 and NE-2 Test Patterns	7-14
7.3.2.1 SILMAT-Processed Wafers	7-16
7.3.2.2 Buried Channel Operation	7-17
7.4 The Impact of the DCCD Program on TRW's Processing Technology	7-22
7.4.1 Mask-to-Wafer Alignment	7-22
7.4.2 Photoresist Coating, Developing and Removal	7-22
7.4.3 Microprocessor-Controlled Diffusion Furnaces	7-23
7.4.4 Dry Etching of Polysilicon, Nitride, Oxide and Metal Patterns	7-24

	<u>Page</u>
7.5 DCCD Technology Summary	7-24
7.5.1 Mask Generations	7-26
7.5.2 Gate Technology	7-27
7.5.2.1 Gate and Field Oxide Undercut Problems	7-28
7.5.2.2 Gate Control by Means of Gate Oxide Thickness Adjustment	7-30
7.5.2.3 Thermally Grown Field and Gate Oxides	7-31
7.5.2.4 Clean Gate Oxide Technology	7-33
7.5.2.5 Polysilicon Gate Technology	7-34
7.5.2.5.1 The Single Level Polysilicon Process	7-35
7.5.2.5.2 The Double Polysilicon Process	7-36
7.5.3 Progress Towards an Isoplanar Technology	7-39
7.5.4 Metallization Problems and Solutions	7-40
8.0 COMPUTER AIDED DESIGN	8-1
8.1 Introduction	8-1
8.2 Developing a CCD Design/Layout CAD System	8-1
8.3 Evolution of DCCD as an LSI Technology	8-2
8.4 Present MOS/CCD Design and Layout System	8-3
9.0 RELATED DCCD PROJECTS	9-1
9.1 Fast Hadamard Transform Project (FHT)	9-1
9.2 Azimuth Correlator Device (ACD)	9-2
9.3 Sort and Merge (SAM)	9-6
9.4 The Twente Report	9-9
10.0 RECOMMENDATIONS FOR FUTURE WORK	10-1
10.1 Design	10-1
10.2 Processing	10-2
11.0 PATENTS AND PUBLICATIONS	11-1
11.1 Patents	11-1
11.2 Publications	11-2
12.0 REFERENCES	12-1

## ILLUSTRATIONS

	<u>Page</u>
1-1 Chronology of Program	1-5
2-1 Power dissipation versus clock frequency for full adders constructed from various semiconductor technologies	2-6
3-1 DCCL OR Gate	3-1
3-2 DCCL OR gate with correction for 1 + 1 logic	3-2
3-3 DCCL AND gate	3-2
3-4 DCCL exclusive-OR gate	3-3
3-5 DCCL half-adder	3-4
3-6 DCCL full-adder	3-5
3-7 Implementation of a LSM-1 full adder	3-8
3-8 A full-adder logic cell implemented with dual cascaded half-adders	3-10
3-9 Schematic diagram of NE2 and DP5 full adder	3-13
3-10 DP5 full-adder and half-adder	3-14
3-11 Implementation of the ACD-0 full-adder. This is a 4-phase, double-polysilicon, N-channel device formed from 2 half adders, 2 1-bit delays and an OR-gate	3-15
3-12 Capacitor model of the charge transfer electrode	3-17
3-13 Surface potential diagram of the T-cell to charge transfer electrode interface	3-20
3-14 Schematic of the 1975 DPO half-adder	3-23
3-15 Schematic of the NE-1 half-adder	3-26
3-16 Oscilloscope display of sum and carry outputs of a half-adder during margin testing	3-30
3-17 Sum and carry outputs of a DP5 full-adder showing a 25% fat zero margin and a 70% thin binary one margin	3-32
3-18 Schematic diagram showing the basic charge input generation technique	3-35
3-19 Schematic of the TTL to DCCD input circuit	3-37
3-20 Schematic of a simple source follower CCD output circuit	3-38
3-21 Schematic of the two stage source follower	3-40
3-22 Schematic of a tri-state DCCD to TTL output circuit transmitter	3-41

	<u>Page</u>
3-23 Offset gate device	3-44
3-24 Organization of a serial-parallel-serial shift register	3-49
3-25 Location of parallel channels for maximum density	3-51
3-26 A typical SPS structure	3-52
3-27 Serial to parallel interlaced SPS structure	3-53
3-28 Clocking system required to change from LIFO read-out to read-in	3-54
3-29 Comparison of device structures	3-55
3-30 Normalized required length per bit as a function of the ratio of mask misalignment tolerance, $r$ , to minimum geometry length, $\lambda$	3-57
3-31 Normalized required area per bit as a function of the ratio of mask misalignment tolerance, $r$ , to minimum geometry length, $\lambda$	3-58
3-32 CCD-2 SPS memory device	3-68
3-33 Photomicrograph of a typical LSM-2 chip	3-69
3-34 16 K-bit SPS unit designed for 7.5 micron photolithography	3-70
3-35 16 K-bit SPS unit designed for 5.0 micron photolithography	3-71
3-36 LSM-2 plan view and cross sectional diagrams	3-73
3-37 LSM-2 process for CCD device fabrication	3-77
4-1 Block diagram of 2-word, 16-bit adder	4-2
4-2 A 2-word, 16-bit adder array of digital charge-coupled devices	4-3
4-3 A block diagram of a 4-bit x 4-bit parallel multiplier array	4-3
4-4 An 8-bit x 8-bit multiplier array of digital charge-coupled devices	4-4
4-5 Schematic diagram of the DP1 4-bit + 4-bit adder array using half-adders	4-5
4-6 Schematic diagram of the DP1 4-bit + 4-bit adder array using full-adders	4-6
4-7 Output signals from the 2-word, 4-bit adder array when a-word = 1110 and the b-word = 0000	4-8
4-8 4 + 4 bit adder array utilizing dual half-adders	4-10
4-9 DP2 4 + 4 adder array utilizing three cascaded half-adders and a single half-adder	4-11
4-10 Input to 2-word 4-bit adder	4-12
4-11 Input to 2-word 4-bit adder	4-12
4-12 Input to 2-word 4-bit adder	4-13
4-13 Input to 2-word 4-bit adder	4-13
4-14 8 + 8 bit adder array utilizing cascaded dual half-adders	4-15

	<u>Page</u>
4-15 DP2 8 + 8 adder array utilizing seven cascaded half-adders and a single half-adder	4-16
4-16 Input to 2-word, 8 bit adder	4-17
4-17 Input to 2-word, 8 bit adder	4-17
4-18 Input to 2-word, 8 bit adder	4-18
4-19 Input to 2-word, 8 bit adder	4-18
4-20 8 + 8 bit adder array utilizing full-adders	4-19
4-21 DP2 8 + 8 adder array utilizing a half-adder and seven full-adders	4-20
4-22 Logic diagram of a DP2 16 + 16 adder array	4-22
4-23 The DP3 16 + 16 adder array	4-23
4-24 Logic diagram of the two least significant bit logic cells of the 32-bit DP5 array	4-26
4-25 Block diagram of a DCCD electrically alterable adder/subtractor array	4-27
4-26 DP5 32-bit adder/subtractor/exclusive-OR chip	4-29
4-27 ACD2 10-bit + 10-bit adder array	4-31
4-28 Photos of carry input and 11 output bits of the 10 bit adder	4-32
4-29 10-bit + 10-bit adder	4-33
4-30 3 x 3 bit multiplier using half adders and "or" circuits	4-35
4-31 3 x 3 bit multiplier using full adders and half adders	4-36
4-32 Half adders	4-37
4-33 Full and half adders	4-37
4-34 3 x 3 bit multiplier utilizing half adder	4-39
4-35 3 x 3 bit multiplier utilizing full adders	4-40
4-36 DP2	4-41
4-37 Input to the 2-word, 3-bit multiplier	4-42
4-38 Input to the 2-word, 3-bit multiplier	4-42
4-39 Input to the 2-word, 3-bit multiplier	4-43
4-40 Input to the 2-word, 3-bit multiplier	4-43
4-41 Input to the 2-word, 3-bit multiplier	4-44
4-42 Input to the 2-word, 3-bit multiplier	4-44
4-43 Schematic diagram of the 8-bit x 8-bit multiplier	4-47
4-44 DP2 8 x 8 multiplier array	4-48

	<u>Page</u>
4-45 ACD0 2's complement 4 x 6 bit multiplier	4-53
4-46 ACD2 2's complement 4-bit x 6-bit multiplier	4-54
4-47 ACD2 6 x 4 multiplier	4-55
4-48 Block diagram of the 64 point fast hadamard transform chip	4-57
4-49 Block diagram of A1 through A12 functional block	4-58
4-50 A1 Hadamard transform block timing diagram	4-59
4-51 Schematic and operational diagram of the charge transfer node (CTN)	4-60
4-52 Functional block diagram of the A-FHT cell test arrangement	4-62
4-53 A-FHT functional block state variable timing diagram	4-63
4-54 A-FHT outputs with MUX.IN equal to all zeros	4-64
4-55 A-FHT outputs the proper one-zero pattern on MUX.IN	4-64
4-56 Schematic of the test arrangement consisting of the charge fan-out, labeled M1000, and the half adder, labeled R1A	4-66
4-57 Output characteristic curve of the FHT charge fan-out circuit showing how the binary one and zero levels change as a function of frequency	4-68
4-58 A normalized plot of the fat zero level of a FHT-OB charge fan-out circuit vs. clock frequency	4-69
4-59 Comparative logic level truth table (a) and corresponding plot (b) for the half adder AND (output = x) and the simple AND (output = y) functions	4-71
5-1 Half-adder bonding diagram	5-2
5-2 Shift register bonding diagram	5-3
5-3 Shift register upset test set-up	5-5
5-4 CCD shift register, prompt ionizing radiation upset	5-8
5-5 CCD shift register, prompt ionizing radiation upset	5-9
5-6 CCD shift register, prompt ionizing radiation upset	5-10
5-7 CCD shift register, prompt ionizing radiation upset	5-11
5-8 CCD shift register, prompt ionizing radiation upset	5-12
5-9 CCD shift register, prompt ionizing radiation upset	5-13
5-10 CCD shift register, prompt ionizing radiation upset	5-14
5-11 CCD shift register, prompt ionizing radiation upset	5-15
5-12 CCD shift register, prompt ionizing radiation upset	5-16

	<u>Page</u>
5-13 Shift register output vs. total dose (sample #1)	5-22
5-14 Shift register output vs. total dose (sample #3)	5-23
5-15 Half-adder output vs. total dose (sample #58)	5-24
5-16 Half-adder output vs. total dose (sample #58)	5-25
6-1 DCCL arithmetic unit chip	6-2
6-2 DCCL controller chip	6-5
6-3 Itakura analyzer	6-7
6-4 A sort and merge chip comparator schematic diagram	6-12
6-5 Block diagram showing how four registers are interleaved	6-14
6-6 Block diagram of a sort and merge algorithm with the features of allowing the bit length of the numbers being compared to be expandable in the row direction and the quantities of sorted numbers to be expandable in the column directions	6-17
6-7 Logic diagram of the DCCL sort and merge cell for technique no. 2	6-20
6-8 First step of the radix exchange sort and merge algorithm	6-22
6-9 Second step of radix exchange sort and merge algorithm	6-24
6-10 Step 3, repeat step 2 for register no. 2. Step 4, reverse procedure no. 1.	6-25
6-11 Block diagram of test cell FIFO/LIFO CCD memory	6-26
6-12 Block diagram of a standard SPS structure	6-28
6-13 Serial to parallel interface of an interlaced SPS structure	6-29
6-14 Timing diagram for the serial register and a serial-to-parallel transfer	6-30
6-15 Potential diagram showing transfer of charges from the serial to parallel register in the interleaved SPS memory	6-31
6-16 Potential diagram showing transfer of charges from parallel to serial register in the interleaved SPS memory	6-33
6-17 Parallel to serial interface for the interleaved SPS structure	6-34
6-18 Timing diagram for the serial register and the parallel-to-serial transfer	6-35
6-19 Forward and reverse four-phase clocks	6-36
6-20 Clocking system required to change from LIFO read-out to read-in	6-38
6-21 Input and output data flow block diagram for the LIFO memory	6-39

	<u>Page</u>
7-1 An SEM photograph showing the vertical tilt at the end of the poly I gate	7-12
7-2 Polysilicon protect configuration	7-29
7-3 Fixed charge as a function of quartz tube age	7-34
7-4 LSM-2 process for CCD device fabrication	7-37
7-5 Undercut polysilicon step covered by a TEOS film	7-39
7-6 Breaks in the Al metallization - DP-0 circuit	7-40
7-7 Source/drain contact to poly contact structure	7-42
8-1 Index of schematic symbols and descriptions	8-4
8-2 Flow diagram of the complete die design and layout procedure taken from the DCCD design/layout manual	8-6
9-1 Block diagram of the 64 point fast hadamard transform chip	9-3
9-2 Four typical FHT cells	9-4
9-3 Developmental model SAR processor block diagram	9-5
9-4 Functional block diagram of the ACD	9-7
9-5 EW pulse processing algorithm	9-8

## TABLES

		<u>Page</u>
2-1	Estimates for the active area in square millimeters of various arithmetic technologies constructed from different semi-conductor technologies	2-6
3-1	Full-adder truth table	3-6
3-2	Process shrink/growth factors	3-18
3-3	Half-adder truth table	3-23
3-4	Half adder truth table with one input always a binary one	3-31
3-5	Implementation comparison for equal channel widths	3-46
3-6	CCD-1 shift register devices	3-47
3-7	Required area per bit for the devices of Figure 3-29	3-59
3-8	Basic SPS relationships	3-60
3-9	Optimized SPS parameter values	3-61
3-10	Comparison of the minimum number of transfers and minimum power optimizations for SPS units	3-62
3-11	Comparison of offset gate and standard structure SPS units for both optimizations	3-64
3-12	CCD-2 mask levels	3-66
3-13	Comparative SPS layout values of CCD-2	3-67
3-13	Comparative SPS layout values of CCD-2	3-74
3-14	Summary of LSM-2 and LSM-3 lots processed	3-75
4-1	Selectable functions of the DP5 array	4-24
4-2	Algorithm for a 8 x 8 bit multiplier	4-46
4-3	Algorithm for a 16-bit x 16-bit multiplier	4-50
4-4	Multiplication of 6 x 4, 2's complement numbers producing a positive product	4-51
4-5	FHT-OB high level briefing	4-72
4-6	FHT-OB design/layout changes, incorporated in FHT-1 and FHT-OC	4-73
5-1	NE1 Radiation Test Result Summary	5-2
6-1	Truth table for the generation of a carry from a full-adder	6-11
6-2	Signal and control lines for a single sort and merge logic block	6-19
7-1	The DCCD double polysilicon process flow chart	7-19
7-2	DP and NE design generations	7-25

## 1.0 INTRODUCTION

This report is exclusively concerned with the theory, development and fabrication of digital charge coupled devices (DCCD's). In general any digital domain function can be performed with charge coupled devices. This means, in particular, digital charge coupled device logic and arithmetic functions. The development of DCCD was undertaken with the goal of achieving both the traditional advantages associated with all digital circuits as well as some unique to the CCD technology. Before addressing DCCD's unique characteristics, a review of the basic advantages of digital logic in general is provided below for reference:

- (1) Freedom from parameter variations
- (2) Freedom from environmental variations
- (3) Application flexibility
- (4) Easily programmed
- (5) Flexibility in selection of bit accuracy
- (6) Well known characteristics that are easily modeled and simulated
- (7) Widespread use reduces costs

These traditional reasons have facilitated the acceptance and widespread use of digital devices. DCCD's also provide some unique advantages. These include:

- (8) Relatively low power requirements
- (9) Very high device/circuit density when compared to various bipolar (digital) signal processing technologies

A review of the unique aspects of digital CCD technology indicates a variety of device characteristics that are otherwise unobtainable with other technologies; low power is clearly desirable for applications that are space or man-pack related. The high functional density of CCD's can be used in those instances where a large number of arithmetic calculations are required to perform an overall system function. DCCD permits the circuit designer to place a large number of arithmetic functions on a single chip thereby eliminating interface and overhead circuitry and significantly reducing such factors as chip count, power supply weight, and subsystem volume.

## 1.1 DCCD IMPLEMENTATION

DCCD technology is most adaptable to binary logic applications; each CCD storage position represents either a one or a zero, depending up whether or not it contains a stored charge. CCD's can therefore be used to implement Boolean arithmetic in a straight-forward manner.

The catalog of CCD devices includes half-adders and full-adders, along with logic functions such as AND's and OR's; these can be used to implement any arbitrary logic or arithmetic function. Because the charge stored under each gate is shifted at each clock pulse, all functions must be performed in pipeline sequence, rather than by "ripple-through" logic. Pipeline calculations in arithmetic units are required due to the generation of the "carry" bit at each stage. For example, in the addition of two N-bit words, the two least significant bits can be added immediately and produce both sum and carry outputs. The carry bit is then combined with the next significant bit and produces a new sum and carry output. The carry is delayed during each operation, requiring the delay of the next significant bit by an equal amount; this necessitates the use of delays on DCCD device input lines. An analogous set of delays is also inserted in series with the output lines, so that the entire output word is available during one subsequent clock pulse. These delays can easily be provided by CCD shift registers with the attendant penalty that delays require a larger active area for DCCD logic functions. This added area can be removed in large-scale functions, where skewed arithmetic is permitted (skewed output of one function driving the skewed input of another function).

Employing skewed arithmetic involves synchronous data inputs to the chip that pass through a set of delays which properly skew all of the bits. Then an arithmetic operation (such as addition or multiplication) is performed and the resultant data is then shifted to another operation. When all arithmetic operations have been completed, the data is once more passed through a set of delays that again synchronizes all bits, to make them simultaneously available to the output pins during a single clock period.

In general, the majority of the delays associated with arithmetic operations can be deleted for functions performed internal to the chip. Only initial skewing delays and final de-skewing delays are required. During arithmetic operations on such a chip, all data can be manipulated in skewed fashion. There are other implications resulting from the use of pipeline arithmetic; since data inputs at one clock pulse and exits during a subsequent clock pulse, random calculations cannot be handled in an efficient manner. DCCD technology is therefore best suited to random calculations that occur only occasionally. A larger number of algorithms are already available in pipeline organization, or can be restructured for pipeline use, so that the application of DCCD's is not significantly restricted.

It is worth noting that pipeline arithmetic calculations can provide a very high throughput rate; data enters the device at the maximum clock rate and subsequently exits at the same clock rate. The designer need only consider the series delay that is necessarily a part of pipeline operation.

## 1.2 PROGRAM HISTORY

In 1973, the Naval Research Laboratory issued a Request for Quotation, for a study program aimed at defining and analyzing the impact of CCD technology on signal processing systems. Implicit in such a statement, was the requirement to determine those areas of signal processing systems where CCD's offered an economic advantage. The extent of that advantage or eventual impact could then be projected. This projection could not be made in terms of dollars and cents alone; it was to be made on the basis of a direct comparison with identical functions provided by competing technologies. Parameters such as speed, power requirements and parts count could be tabulated for subsequent comparisons.

As a result of the proposal submitted to the Naval Research Laboratory, TRW initiated a study of the impact of digital CCD's on signal processing systems. The results have been issued under the title, "Charge Coupled Devices in Signal Processing Systems; Volume I: Digital Signal Processing."\*

---

\*Available from the National Technical Information Services, a companion report titled, "Charge Coupled Devices in Signal Processing Systems; Volume II: Analog Signal Processing" is also available.

This study indicated that digital CCD's combine the inherent advantages of any digital technology (such as high noise immunity, freedom from device parameter variations, stable operating conditions and ease of simulation with the advantages peculiar to CCD's (such as high density and low power requirements). In addition, digital CCD's are best suited to signal processing applications where the signal flow can be handled by pipeline operations that require little or no feedback; this permits relatively high data throughput, with relatively low CCD clock frequencies. The impact of DCCD's is most dramatic in those applications where a large number of functions and/or high computational accuracy is demanded. A large number of these potential applications for existing and projected systems were identified and analyzed in detail.

At the conclusion of this study, TRW recommended experimental verification that would go beyond basic device operation and verification. An opportunity was sought to demonstrate the real advantages of the digital CCD approach. The design of a digital CCD Fast Forier Transform (FFT) on a chip was selected as a useful vehicle. This function would be quite flexible and suited to a number of diverse applications. Accordingly, a technology development program was initiated.

The objective of the first phase of this DCCD Program was the investigation and characterization of fundamental DCCD building blocks that would be employed in a typical signal processing system application. The results of this Phase I program included further development of a full adder circuit function, the design and test of a  $4 + 4$  adder, and a  $3 \times 3$  multiplier array. A study was initiated to provide a method of interconnecting a number of FFT Charge Coupled Devices in Signal Processing Systems; Volume III: Digital Function Feasibility Demonstration.\*

The objective of the second phase of this program was to develop large logic building blocks suitable for implementing a FFT or similar function. Near the end of Phase II, a potential application in voice processing arose that would require 16-bit arithmetic blocks, i.e., a  $16 \times 16$  multiplier and a  $32 + 32$  adder/subtractor. At the end of the thirteen-month Phase II effort,

---

\*Available from the National Technical Information Services Center.

work was completed on an 8-bit arithmetic block design. Work on larger blocks was continued into Phase III, including the design of a 32 + 32 adder/subtractor.

The objective of the third phase, described in this report, was to complete the work on the 32 + 32 adder/subtractor; then to work on the 16 x 16 multiplier and smaller, associated circuitry. As the work on the 32 + 32 bit adder/subtractor layout neared completion, two factors influenced a change in program objectives:

1. The need for the Phase III DCCD circuits was eliminated as a result of a change in the voice processor program.
2. The visibility provided by the 32 + 32 adder/subtractor design and layout effort indicated that the cost and schedule associated with a 16 x 16 multiplier was beyond the remaining resources of the Phase III program.

At that time, mutual customer/contractor interest arose in a unique application area, involving manipulation of lists of digital words that were arranged in order of their magnitude. This sort-and-merge-type application appeared well suited to the characteristics of DCCD functions. Various algorithms for performing these functions were examined and DCCD layouts were investigated. A specialized LIFO (Last In - First Out) memory, needed to implement the sort and merge function, was designed and layout completed. Due to program cost and schedule limitations, no further LIFO activities were pursued.

The chronology of events is summarized in Figure 1-1.

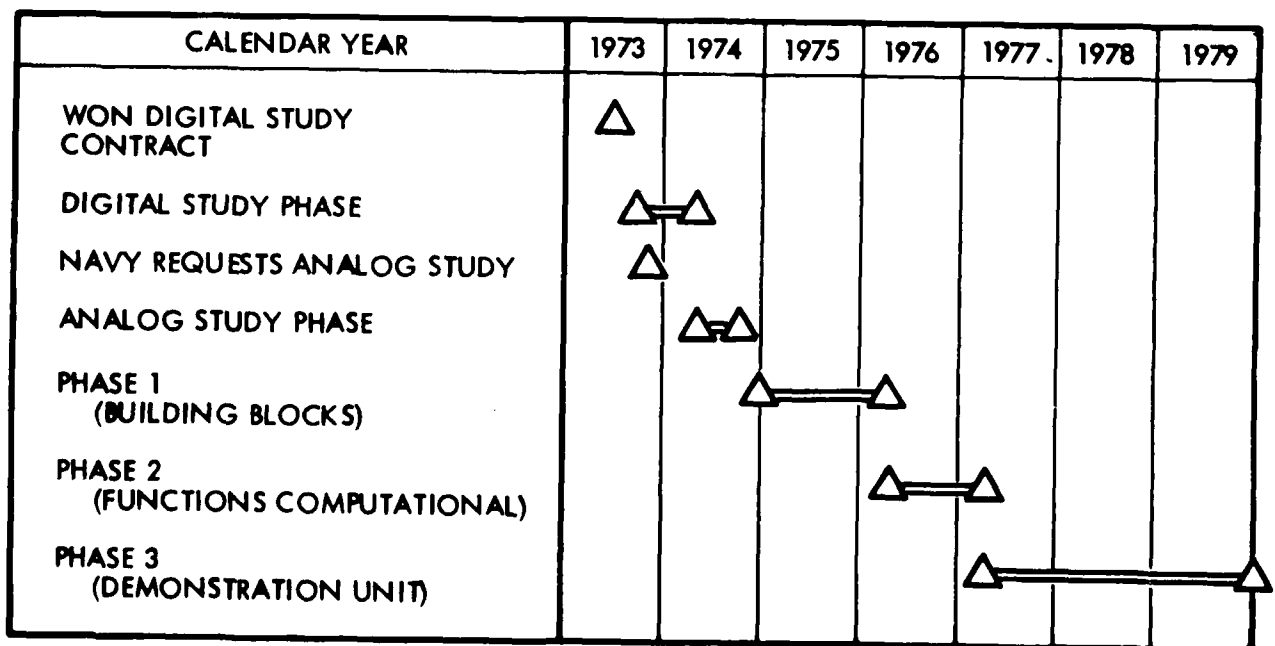


Figure 1-1. Chronology of Program.

### 1.3 PHASE I REPORT SUMMARY

This report contained an overview of the entire program and a brief statement of goals and approaches. This was followed by a discussion covering development of the full-adder circuit function. The original concept was explained and subsequent alternations to the original layout was described. Both two and three input adders were discussed and hardware implications in the several computational algorithms available were examined. The primary test mask that was designed during Phase I was presented, along with a summary of the test results. The process sequences employed to produce these devices were explained, and cross-sectional views of the devices were provided. This was followed by the results of a study to determine methods of inter-connecting a number of the projected FFT chips into a single system. The report concludes with recommendation for future work.

### 1.4 PHASE II REPORT SUMMARY

This report contained a commentary on the advantages of digital charge coupled logic (DCCL) and made a comparison with other current high density/ lower power LSI technologies. A description of the basic equations necessary for designing DCCL logic gates was included and the design of various logic cells and arithmetic functions were discussed. The principles used in the design of the pipelined multiplier and adder/subtractor arrays were discussed and the clocking schemes and test results obtained for both arithmetic arrays and single arithmetic functions were described. The metal/polysilicon and double polysilicon fabrication processes used to fabricate these devices was described. The report concluded with recommendations for future work.

### 1.5 PHASE III REPORT SUMMARY

This report contains a history of the complete DCCL program. It traces the development of the small scale building blocks (the half adder, full adder and AND and OR gates) up through the larger scale arithmetic functions of multiplication, addition, and subtraction. This report also deals, in generic terms, with the signal and data processing applications that are suited to DCCL technology. The programs that have used this technology to date are described. This is followed by a description of the computer aides and fabrication techniques developed specifically for this technology. This report concludes with recommendations for future work and a list of patents and publications resulting from this effort.

## 2.0 SUMMARY AND CONCLUSIONS

### 2.1 SUMMARY

The development of digital charge coupled device (DCCD) circuits at TRW has evolved through a number of identifiable stages since its inception in 1973. The primary areas of design, layout, and processing have all experienced this evolutionary growth in significant ways.

#### 2.1.1 Design

The design realization of DCCD logic and arithmetic circuits presented a number of very difficult concept and modeling problems during the course of the program. The basic adder cells emerged as both the most difficult and the most essential circuits for performing DCCD logic and arithmetic functions. Both a full adder and a half adder cell were developed during the course of this program and are described in detail elsewhere in this report. Basically, the full adder cell possesses the advantages of higher density and fewer throughput delays than the dual half adder while the half adder cell is faster and less sensitive to operating biases and threshold shifts. The half adder has the additional features of being easily configurable into other essential DCCD functions such as charge refresh and logical "AND" circuits. The overall flexibility and performance characteristics of the half adder cell resulted in its selection for the majority of analysis and test efforts over the full adder cell. This report delineates the logical development of these adder cells from a totally isolated (floating) gate design, through two floating gate reset techniques, leading to the present floating diffusion design. Computer models, which were developed and verified during this program, have been used to refine the present adder design into a stable, predictable configuration exhibiting high noise immunity and speeds of 5-10 MHz.

#### 2.1.2 Layout

The layout of DCCD circuits presented a number of unique problems not previously encountered by other digital technologies. Two major layout obstacles were the lack of a standardized symbology for DCCD circuits and the inability to directly interconnect two physically separated signal points by means of a metal conductor. The immense difficulty posed by the lack of

schematic circuit representation can be easily appreciated by everyone in the electronics industry. The difficulty posed by the inability to directly connect two signal points together with metal is perhaps less obvious. A DCCD circuit functions by transporting discrete charge packets along the surface of the Si/SiO<sub>2</sub> interface through a set of sequentially clocked, overlapping, MOS gate structures. Consequently, moving a signal from one physical location to another involves interconnecting these locations through a series of gates. This method of interconnect has several major disadvantages from a layout standpoint:

- (1) Additional refresh cells may be required due to the transfer loss of the interconnecting gates.
- (2) The delay associated with the interconnecting gate structure increases the overall throughput delay and may require additional delays elsewhere in the circuit to provide synchronism between interacting charge packets.
- (3) Signal path crossovers are complex and impose additional timing constraints on the design.

During the performance of this program, major progress was achieved in overcoming both of these obstacles. At this writing, a complete system of DCCD schematic symbols exist along with a technique for assembling these symbols into final circuit schematics using the Applicon Computer Aided Design (CAD) system. This DCCD schematic capability greatly reduces the opportunity for layout errors by permitting drafting personnel participation in the visual check cycle. Prior to this, only the design engineer could effectively check the layouts.

A technique for interconnecting physically separated points directly (i.e. without gate structure) was also devised. This technique has been termed the "charge transfer node," and is described in more detail in Section 4.4 of this report. Basically, the charge transfer node consists of two diffusions connected by a metal line. Charge is transferred onto the diffusion at the sending end of the node causing a current to flow (through the interconnecting line) to the receiving end (diffusion) of the node. This current flows for a time which corresponds to the sending node charge level. A storage well at the receiving node collects this charge thereby

accomplishing a charge packet transfer through a direct metal connection. The completeness (efficiency) of this transfer is a function of time allowed and the capacitance (including interconnect) of the node. Results to date indicate that, for frequencies of 5-10 MHz, total node capacitance can be on the order of 100 ff. This technique has been demonstrated and is in use on another major DCCD project.

One final layout obstacle encountered by DCCD (as well as other technologies) was the lack of computer aided design rule checking. As a result of the complexity presented by the LSI designs being undertaken by this program, the need for a computer aided design rule check was soon recognized. Since the inception of the device development phase of this program in 1975, significant progress has been made towards this end and work continues. For the past two years, a computer aided design rule check routine written for bipolar circuits has been utilized to perform a partial check of the DCCD layouts. A new routine which will provide a complete design rule check on DCCD layouts has been in development since early 1979. New algorithms have been created which permit both intra-and inter-level checking. Completion of this effort is anticipated in early 1980.

### 2.1.3 Wafer Processing

In 1975, when the DCCD device processing activity was first begun, the existing fabrication technology was P-type, surface channel employing 7.5 micron, metal/polysilicon gate structures. Since that time, a continuum of processing improvements have been implemented. These improvements have been directed at the goals of increased density, higher device operating frequencies, minimum wafer process complexity, and the achievement of reliable and repeatable process sequences capable of delivering high DCCD functional yields.

In-as-much as the history of DCCD wafer processing is complex and intricate, a comprehensive summary of these activities is difficult. A listing of some of the salient changes occurring in DCCD processing since 1975 include:

- (1) Conversion from metal/poly to poly/poly gate structures
- (2) Conversion from p-channel to n-channel
- (3) A general reduction in lithography from 7.5 micron to 5 micron
- (4) Incorporation of dry etching techniques in place of entirely wet chemistry processes
- (5) Replacement of field oxide channel definition with a ion implantation (channel stop) technique

A complete chronological history of the DCCD wafer processing evolution is provided in Section 7.0 of this report.

In addition to the continued improvement in techniques and procedures, corresponding improvements in both lot size and lot fabrication time were achieved. These improvements were a result of streamlined procedures and efficient utilization of existing resources. Increased lot sizes and reduction in fabrication time had a significant impact on the achievements of this project. Since circuit development is iterative, the value of quick turn around and the opportunity for several experimental options per lot cannot be overstated.

Efforts to further improve present wafer process capabilities are still in progress. At the time of this writing, equipment has been purchased and facilities changes initiated for further upgrading and automation of the DCCD wafer fabrication laboratory. These improvements will provide the capability for parallel plate plasma etching; automatic photoresist coating, developing, and scrubbing; dual flash evaporation metalization; microprocessor control of critical furnaces; and 1 micron resolution proximity alignment with the attendant yield improvements associated with non-contact printing. These items are scheduled for installation by the end of 1979.

## 2.2 CONCLUSIONS

The past four years of DCCD development, from the initial building block phase through the final demonstration phase, have witnessed a continuous sequence of improvements in the three central areas of device design, layout, and processing. In retrospect, the absence of a schematic representation for DCCD circuits and the lack of a comprehensive computer design rule check capability imposed the greatest obstacles to the timely development of DCCD circuits.

At this point in time, the basic elements required for the successful integration of some of the larger DCCD functions, conceived during the initial study phases of this program, are available. The fundamental logic and arithmetic DCCD cell, the half adder, has been modeled and successfully demonstrated good performance margins at frequencies in excess of 5 MHz. A system of layout procedures has been developed around the specific problems presented by DCCD designs. The major aspects of this system are a comprehensive set of design and layout rules, complete schematic documentation, the ability to nest large functional cells, an automatic design rule check procedure, and a DCCD/MOS design and layout manual. With this system it is currently possible to produce LSI chips with a turn around time of two to four months depending on the complexity of design. Finally, wafer processing has been developed for DCCD circuits which, with present design rules, provides repeatable, functioning circuits.

The present design status of DCCD logic cells, exhibiting good noise margins at frequencies of 5-10 MHz, provides an opportunity to review and update power and density estimates for this technology. A comparison of DCCD with other technologies was performed in 1977<sup>(1)</sup> using the full adder as the basis for comparison. These DCCD power estimates have been updated (based upon latest design configurations) and presented in Figure 2-1. Although an update of the power estimates for the other technologies was not possible within the schedule constraints of this program, it should be recalled that the original comparisons were for 5 micron designs. Figure 2-1 shows that, although DCCD power requirements have increased, it still compares favorably with 5 micron  $I^2L$  and CMOS. Current industry efforts to reduce NMOS and CMOS designs from 5 microns to 1-2 microns, if successful, should reduce the power requirements of these circuits by factors of 10 to 20. A corresponding scaling of DCCD's would be expected to provide similar power reductions. The ease of and degree to which DCCD circuits can be scaled is a task suggested (in Section 10.0 of this report), for future program efforts.

Revised area figures for DCCD arithmetic functions (also presented originally in 1977) are provided in Table 2-1. These areas have, with the exception of the 16 x 16 multiplier, been obtained from actual circuit layouts, excluding pads and borders. The 16 x 16 multiplier area has been extrapolated from the 8 x 8 multiplier area. Again, updated area estimates for the other technologies could not be obtained for this report so Table 2-1 reflects the original 5 micron designs.

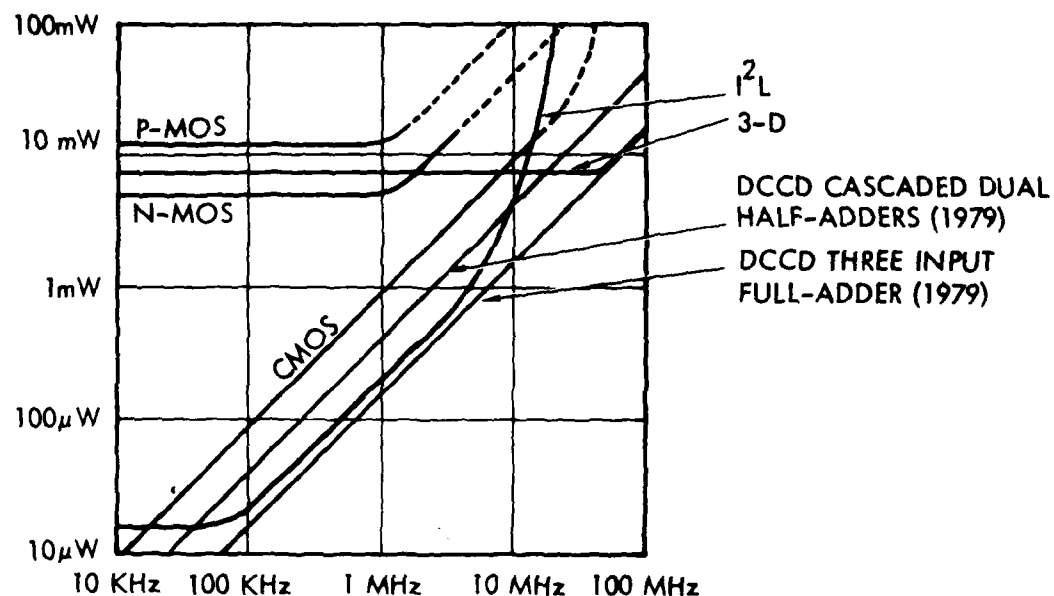


Figure 2-1. Power dissipation versus clock frequency for full adders constructed from various semiconductor technologies.

Table 2-1. Estimates for the active area in square millimeters of various arithmetic technologies constructed from different semiconductor technologies.

Technology	16+16	32+32	8x8	16x16
DCCD	6.0	20.5	7.0	38.5
P-MOS	11.3	49.2	12.2	67.7
N-MOS	7.8	34.7	7.7	44.2
CMOS	16.5	70.2	19.5	104
I <sup>2</sup> L	14.9	64.9	26.2	137

Table 2-1 indicates that in spite of a factor of two growth, from a density standpoint, DCCD still compares favorably with other 5 micron technologies. The areas presented in Table 2-1 assume the use of the DCCD full adder cell. If these full adders were implemented with dual half adders, the DCCD area values will increase by approximately a factor of two. Density comparisons, such as presented by Table 2-1, will require frequent review as the present industry drive for micron and submicron designs progress.

### 3.0 SMALL SCALE INTEGRATION (SSI) DEVELOPMENT

#### 3.1 INTRODUCTION

Digital logic functions in CCD's can be implemented with the same fabrication techniques as used in standard analog CCD's. A logical one is simply defined as a charge quantity which is equal to the capacity of a minimum geometry storage electrode, and a logical zero is defined as an empty storage electrode.

The logical OR function is the easiest function to implement. The logical OR function is shown in Figure 3-1.

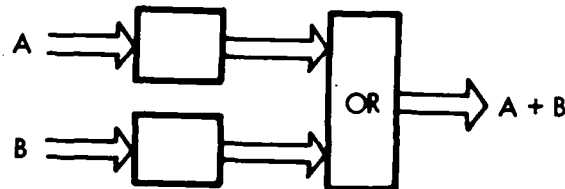


Figure 3-1. DCCL OR Gate.

When a logical one is transferred from either the A or B input under a common storage electrode the OR function occurs. In this simple OR gate, the common storage electrode will contain a charge quantity which is twice that of a logical one when both A and B are ones. This condition can be corrected by providing a potential barrier and charge sink for the excess charge as shown in Figure 3-2.

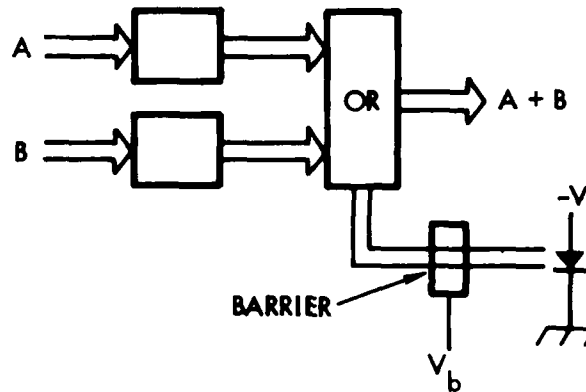


Figure 3-2. DCCL OR Gate with Correction for 1 + 1 Logic.

Realizing that the charge which is discarded is the AND function of A and B, it is a natural extension of the basic OR gate to form an AND gate. As shown in Figure 3-3, a AND function is implemented by saving the charge which spills over the barrier electrode and sinking the OR function on an alternate clock phase.

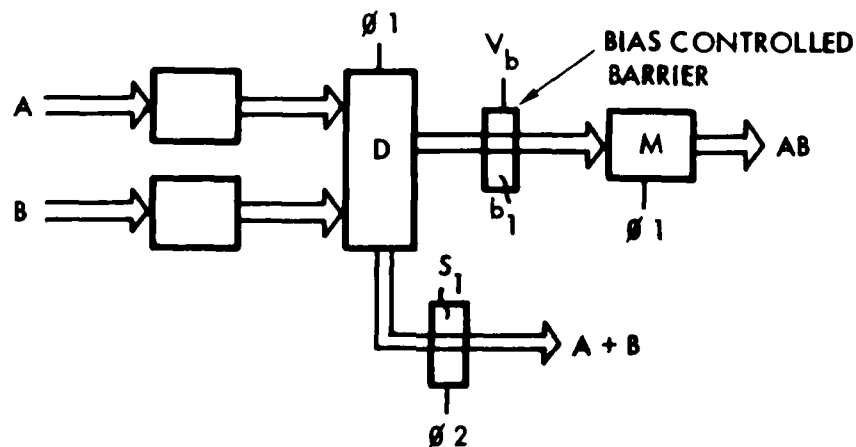


Figure 3-3. DCCL AND Gate.

The AND gate may be altered to perform the exclusive-OR function as shown in Figure 3-4.

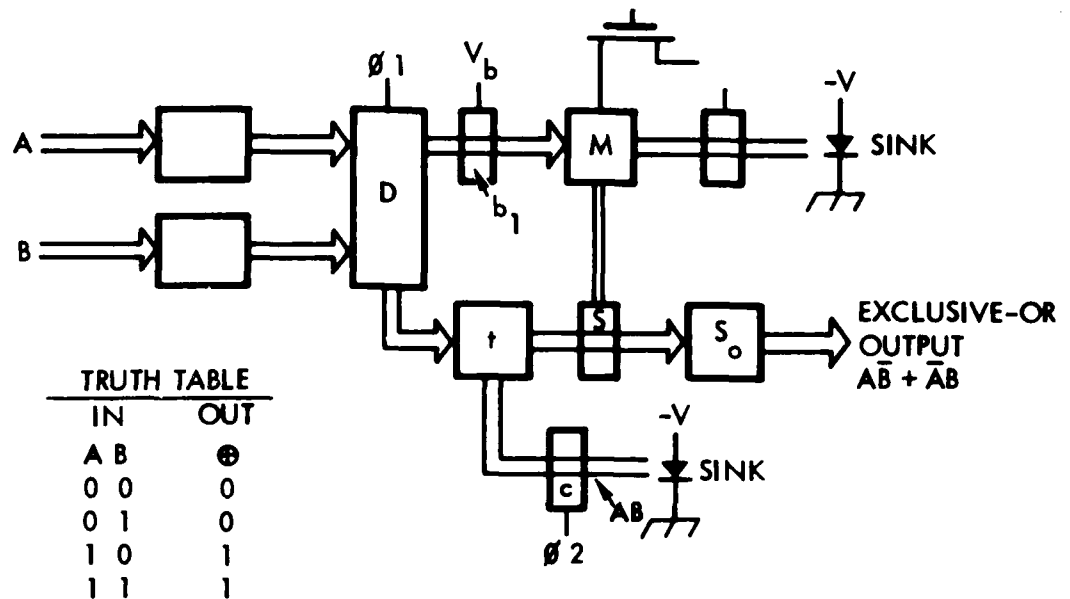


Figure 3-4. DCCL Exclusive-OR Gate.

The schematic of a DCCL exclusive-OR gate is shown in Figure 3-4. As described above, if either of the two input channels transfers a binary "1" into the D storage area, it will transfer across t and s to produce the function  $AB + \bar{A}\bar{B}$ . However, when both input channels transfer binary "1" packets into the D storage area so that it overflows across  $b_1$  to fill M, the resulting change in surface potential under M induces a potential change on the floating-gate or floating-diffusion. The potential change is transferred to the s end of the floating-gate causing it to switch from a transfer level to a charge barrier level. Now when t is switched to a positive voltage, the charge packet transferring from D will be retained under t by the s acting as a barrier. During the next clock phase when c is switched to a positive voltage, the packet of charges held in t will transfer out under c to produce the function  $C = AB$  and no charges will transfer out of  $s_0$ .

The DCCL exclusive-OR and the half-adder are identical, the  $S_0$  output is the SUM and the C output is the CARRY to the next level as shown in Figure 3-5. A full-adder can be implemented by increasing the input channels to three, and by adding the  $b_2$  and I areas as shown in Figure 3-6. The S1 and S2 are connected together in a DCCL OR gate to form the SUM output.

DCCL is a dynamic system, the D, M, and I storage areas must be completely emptied of charge between input charges. If any of the three specific functions are not required for further signal processing the charge packet at that exit port must terminate at a sink diode.

It is a simple matter to modify a half-adder DCCL cell so that it will perform the digital refresh function. All that is required is that a diode fill and spill gate be arranged to insert a binary "1" into the D storage cell on each clock phase, synchronous with the signal charge packet in the other channel.

The B input channel is designated the continuous "1" channel and channel A the input signal channel, then the SUM and CARRY outputs becomes  $S = \bar{A}$  and  $C = A$ . Since the  $C = A$  charge packet is a binary "1" only when D overflows, it must be a completely full charge packet no matter what the quantity of charges in the original A input; thus A is refreshed.

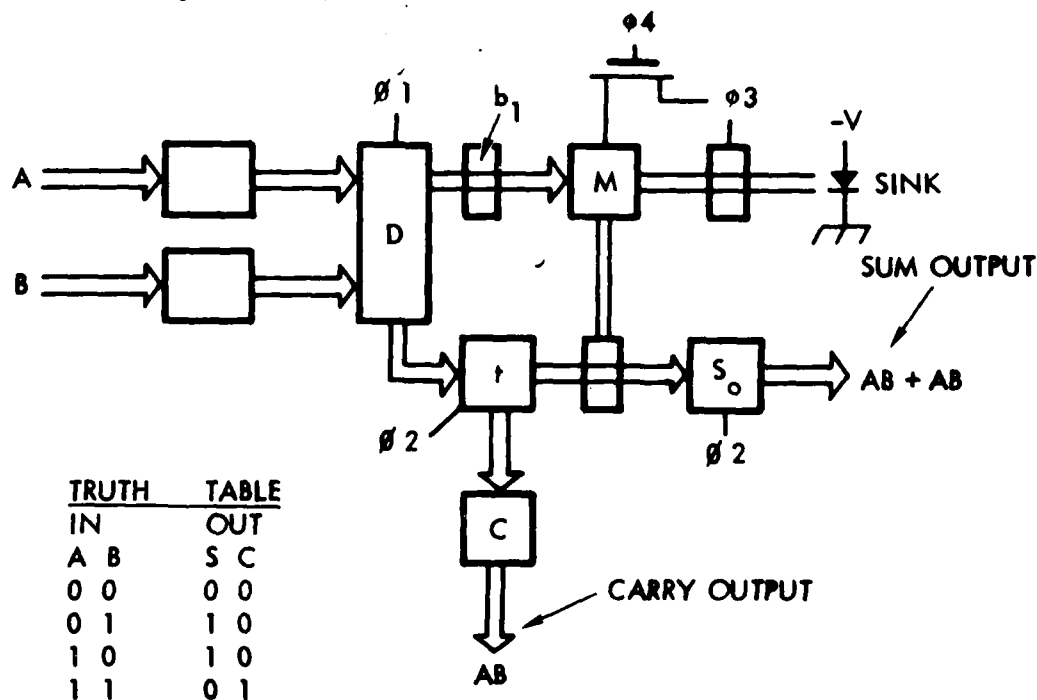


Figure 3-5. DCCL Half-Adder.

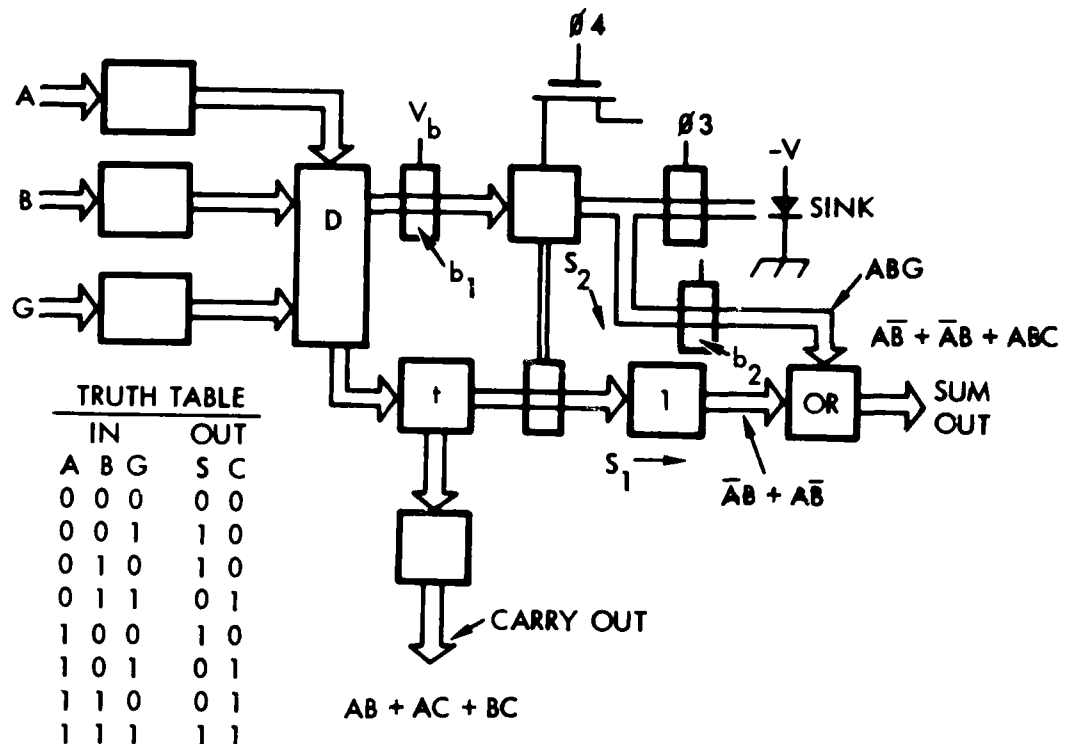


Figure 3-6. DCCL Full-Adder.

The following paragraphs provide a detailed description of the evolution and development of the basic DCCD building blocks which form the nucleus of subsequent LSI circuit designs.

### 3.2 FLOATING GATE/FLOATING DIFFUSION DESIGNS AND RESULTS

In 1972 M. F. Tompsett published<sup>(2)</sup> a description of a CCD charge regenerator that used a floating-diffusion as the sensing-node of a charge transfer electrode. From the first full-adder design on the LSM-1 layout, made in early 1975, TRW used a floating-gate as the charge sensing element. This design requires a FET switch for resetting the floating gate to a preset transfer level at the beginning of each cycle and a gated sink diode to remove charge from under the floating-gate at the end of each cycle. The floating-gate was used as a sensing-node until 1976. In July 1974,

T. A. Zimmerman mentioned the floating diffusion as an alternative in a paper containing the description<sup>(3)</sup> of a digital CCD exclusive-OR gate. The floating diffusion approach provided a significant improvement in the sensitivity of the charge sensing element. Elimination of the capacitance associated with the floating-gate and gated sink diode reduced the total parasitic capacitance loading on the charge transfer switch which was the primary factor in increasing its sensitivity.

In September 1976, at the start of the DP3 design, it was realized that by using the source diffusion of the FET switch as the sensing-node the FET would remove the unwanted charge on the node at the end of the cycle while simultaneously resetting it to the preset transfer level. Subsequent designs utilized the floating diffusion approach for all DCCD logic circuit charge sensing elements.

### 3.3 FULL-ADDER DESIGNS AND RESULTS

A full-adder is the basic arithmetic function used in many parallel adders, subtractors and multipliers. It has three inputs and two outputs. All three inputs have the same binary significance, usually two inputs are addendums while the third input is the carry-bit from a less significant full-adder. The outputs are the sum-bit and the carry-bit as shown in Table 3-1.

Table 3-1. Full-Adder Truth Table.

Inputs			Outputs	
A1	B1	C1	S1	C2
0	0	0	0	0
0	0	1	1	0
0	1	0	1	0
0	1	1	0	1
1	0	0	1	0
1	0	1	0	1
1	1	0	0	1
1	1	1	1	1

A description of how a full-adder performs the arithmetic function is given in Section 3.1.

The first full-adder design was implemented in March 1975 on the LSM-1 mask set using design concepts published<sup>(3)</sup> eight months earlier. A schematic diagram of this early full-adder is shown in Figure 3-7.

In common with all of the circuits included on the LSM-1 wafer, a metal/polysilicon gate configuration was employed, with gate oxides of 1000/2000 Å under the polygate and metal gate structures respectively. The field oxide was 15,000 Å thick.

The polysilicon charge transfer electrode was precharged to create a transfer mode surface potential; this occurred by applying a voltage pulse to a capacitor formed by the metal-oxide-polysilicon charge transfer electrode. Two problems prevented this full-adder from functioning properly.

The first problem was a race condition that occurs when two or more of the inputs have a binary value of "1" (full charge packets); in this mode, both the "D" and "M" storage areas are filled. The charge packet under the master-side, "M", of the charge transfer electrode causes the surface potential of the slave-side, "N", to switch from its initial transfer state to a barrier (blocking) state. One deficiency of this design was that a part of the charge packet that should have filled M also transferred into N. Consequently, as the surface potential of the charge transfer electrode changed from a transfer state to a barrier state, the charges under N were forced to either the sum state or to the sink diode.

A second problem existed because of a fixed charge that is produced at the polysilicon-SiO<sub>2</sub> interface as the oxide is grown. The variability of this semiconductor process-induced charge made it extremely difficult to accurately preset the charge transfer electrode to the required transfer surface potential.

Both problems were eliminated in the full-adder design completed in August 1975 for the DP-0 evaluation wafer. The race condition was eliminated

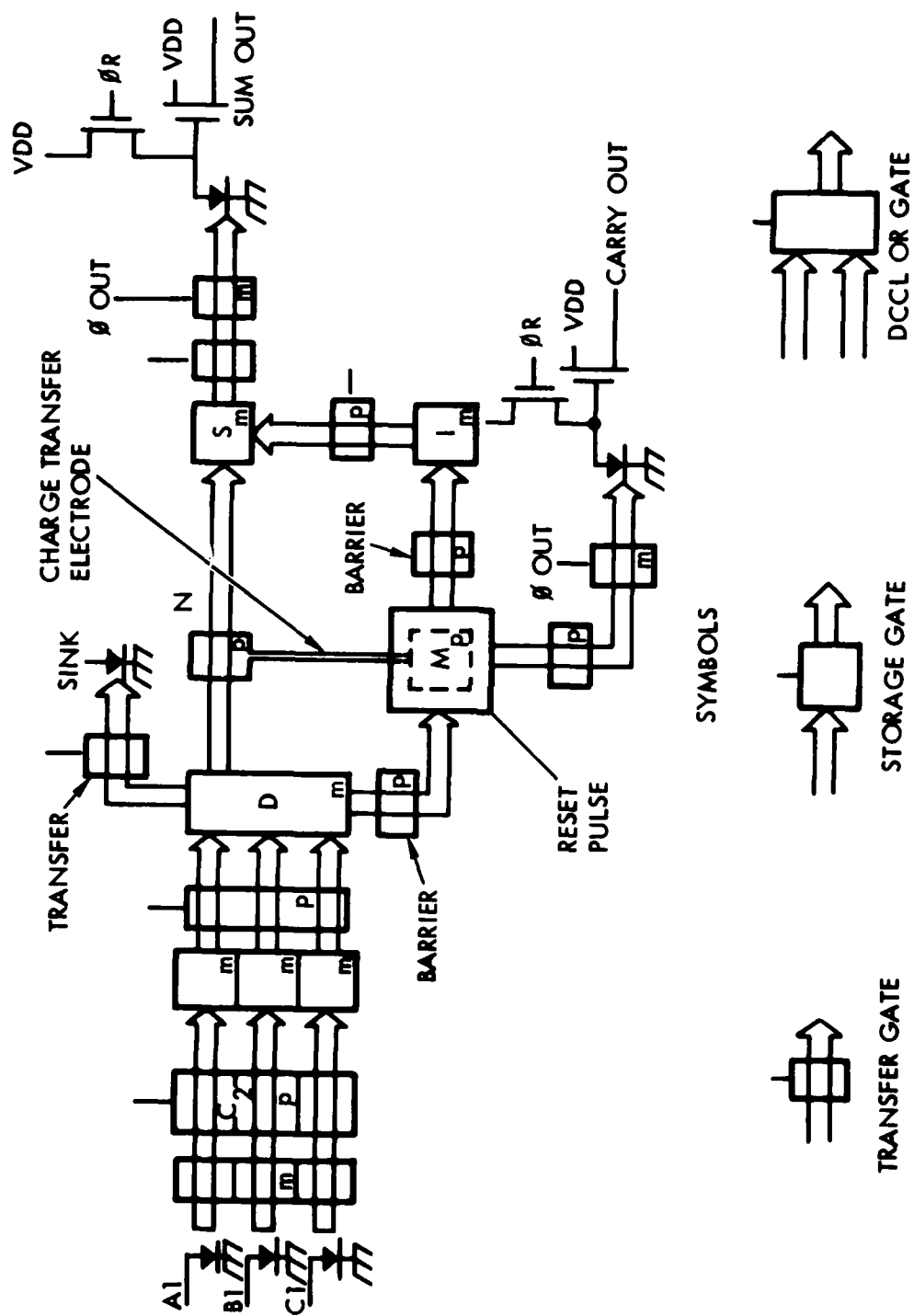


Figure 3-7. Implementation of a LSM-1 Full Adder.

by adding a transfer gate between the "D" input storage gate and the slave-node, "N", of the charge transfer electrode. The initial process-induced charge on the charge transfer electrode was removed by connecting the source of a small FET to the charge transfer electrode; also, connecting the drain of the FET to the substrate and switching the FET "on" to remove the charge just prior to inducing the required potential on the charge transfer electrode via the precharge capacitance. These two modifications produced a full-adder that performed all the correct arithmetic functions, however, the yield of good devices was low due to metal line breakage over oxide-covered polysilicon steps. With the first successful demonstration of a CCD full-adder in November 1975, the decision was made to use it as a building block in the  $3 \times 3$  multiplier and  $4 + 4$  adder; this chip was designated DP1. The layout of the full-adder was eventually modified to provide identical cells that would fit together topologically on the Applicon System; additional gates were added so that the full-adder cells would interconnect with the appropriate clock phases.

In order to digitize the multiplier and adder arrays, the sum output channel was aligned so that it could be connected with one of the three inputs to the next cell. The carry output channel had to be aligned to enable it to line up with one of the three inputs of the full-adder cell in the next more significant column of the array.

Two conceptual layout changes were made to the DP1 full-adder to correct anomalies that occurred in testing. An additional storage area was placed between the "I" and "S" storage areas (see Figure 3-7) in order to correct the phasing of the two sum packages at the sum output "OR-gate." The SINK diode output port was moved from the slave-node, "N", of the charge transfer electrode to the "D" input storage area, thus enabling the slave-node to be correctly used only as a barrier or transfer gate.

The DP1 full-adder, multiplier and adder arrays used  $1000 \text{ \AA}$  polysilicon gate oxides and  $2000 \text{ \AA}$  metal gate oxides to direct charge flow in a typical 2-phase CCD shift register. The DP1 full-adder,  $4 + 4$  adder and  $3 \times 3$  multiplier were all successfully demonstrated at clock speeds up to 175 kHz in February 1976.

### 3.3.1 Full Adders Implemented from Dual Half Adders

Early in 1976, we reviewed the capabilities of half-adders and full-adders and concluded that the half-adder had the potential for higher speeds and higher charge transfer electrode sensitivity.

A full-adder can be easily implemented from two cascaded half-adders, two one-bit shift-registers and an OR-gate as shown in Figure 3-8. The validity of the Figure 3-8 configuration can be shown through the following explanation. A half-adder accepts two inputs  $a$  and  $b$ , and produces a sum  $S = 1$ , if either input is 1, but not when both inputs are a 1. The carry  $C = 1$  if both inputs are 1. Hence  $S = a + b$  and  $c = ab$ . A full-adder accepts three inputs and produces a sum  $S = 1$  when one or all three inputs are 1, thus, in logical terms  $S = g + (a + b)$ . A carry  $C = 1$  is produced, when two or three inputs are 1's;  $C = g(a + b) + ab$ . Hence, a full-adder can be realized using two half-adders plus an OR gate as shown in 3-8.

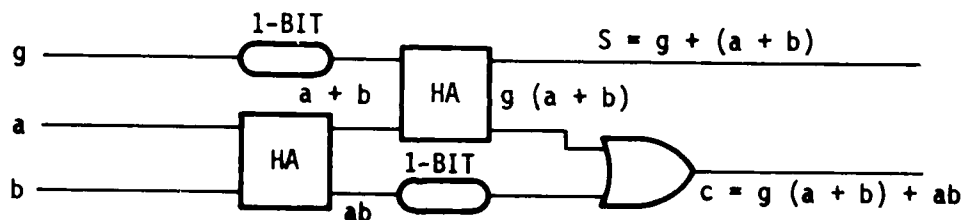


Figure 3-8. A Full-Adder Logic Cell Implemented with Dual Cascaded Half-Adders.

Two separate 8 + 8 adder arrays were included on the next mask set (designated DP2). One adder used the original full-adder, while the other used cascaded half-adders.

The single DP2 full-adder was similar to the DP1, with the exception that the additional storage cell between the "I" storage and the "S", OR-gate was removed. The "S" storage area was used for storage of the sum charge packet that occurs via the slave-node, when a single input is a binary "1" and also when the charge packet provided by the master-node is such that all three inputs are a binary "1".

Both the half-adders and the full-adders used on DP2 designs were further simplified from earlier DP1 designs by eliminating the precharge capacitance. The DP2 design used a FET to preset the charge sense electrode to the transfer state as well as removing any initial charge from a preceeding bit.

A significant DCCD technology advance was made on the DP2 series by changing from a metal-polysilicon gate combination to a double polysilicon gate structure. However, processing difficulties were experienced with the slip mask fabrication technique then in use and few DP2 working devices were available for testing.

Changing the location of the output port of the carry-out charge packet from under the master-side of the charge sensing electrode to the "D" input storage gate generated a full charge packet each time there were two or more binary "1" inputs to the D input area. An automatic charge refresh capability was thereby provided with each half-adder and full-adder of the DP3 design.

Another major improvement included on the DP3 full-adder was the elimination of the floating-gate capacitance as the charge sensing element in favor of the floating-diffusion design. This was accomplished by replacing the oxide capacitance with the depletion capacitance of the precharge FET source.

Both the  $16 + 16$  adder and the  $8 \times 8$  multiplier were designed from full-adders implemented using two cascaded half-adders as shown in Figure 3-8. Two separate full-adder test cells were included on the DP3 design; both were of the cascaded half-adder type; one had a floating-gate as the charge sensing node and the other had a floating-diffusion.

Tests were performed on both full-adders. It was determined that the full-adder designed with the floating-gate charge sensing node had less transfer efficiency than the full-adder employing floating-diffusion. The low transfer efficiency of the floating-gate version was traced to connection of the sink diode gate and carry-out gate to the same clock line. This approach was used in an effort to reduce the number of clock lines required to operate the adder. The floating-diffusion design has no sink diode since the precharge FET removes any residual charge. This feature also eliminates the possibility of the condition described previously in Section 3.3. A decision was made at that time to standardize on the use of the floating-diffusion design.

A cascaded full-adder comprised of two floating-diffusion charge sensing elements performed arithmetic operations correctly at clock speeds up to 2 MHz.

Additional details of the DP0 and DP1 designs and test results are published<sup>(4)</sup> in Vol. III and details of the DP2 and DP2 full-adders are published<sup>(5)</sup> in Vol. IV, of this series.

### 3.3.2 Conversion to N-Channel Designs

In December 1977, an effort was made to achieve higher clock speeds by replacing the existing two-phase, P-channel circuits with the inherently faster three-phase n-channel designs

An N-channel evaluation mask, designated NE-1, was designed. It contained a single binary level full-adder as well as many other DCCD evaluation devices. This full-adder was shown to perform correct arithmetic functions in February 1978. However, the gain of the charge sense electrode was too low to permit cascading of full-adders to achieve a working multiplier or adder array.

Consequently, the full-adder was redesigned for higher sense electrode gain and incorporated into the DP5 mask design. A schematic diagram of the DP5 full-adder is shown in Figure 3-9 and a photograph of the processed device is shown in Figure 3-10.

The cascaded dual half-adder approach to a full adder function has several system application advantages over a single full-adder (see Section 3.4.3). It was therefore decided to only use cascaded half-adders in future LSI applications. Only minimal tests were performed on the DP5 full-adder. Sufficient tests were carried out to show that it performed all of the correct arithmetic functions at clock speeds up to 800 kHz and that its switching margin agreed with that predicted by the model (i.e. acceptance of a 25% full charge packet as a binary "zero" and 75% of a full charge packet as a binary "one."

The last full-adder was included in the design of the Azimuth Correlator Program, described in Section 9.3. The ACD full-adder is of the cascaded dual half-adder type and was used in a 10 + 10 adder. A schematic of the ACD full-adder is shown in Figure 3-11; it was shown to operate correctly at clock speeds up to 1.25 MHz (see Section 9.3 for results).

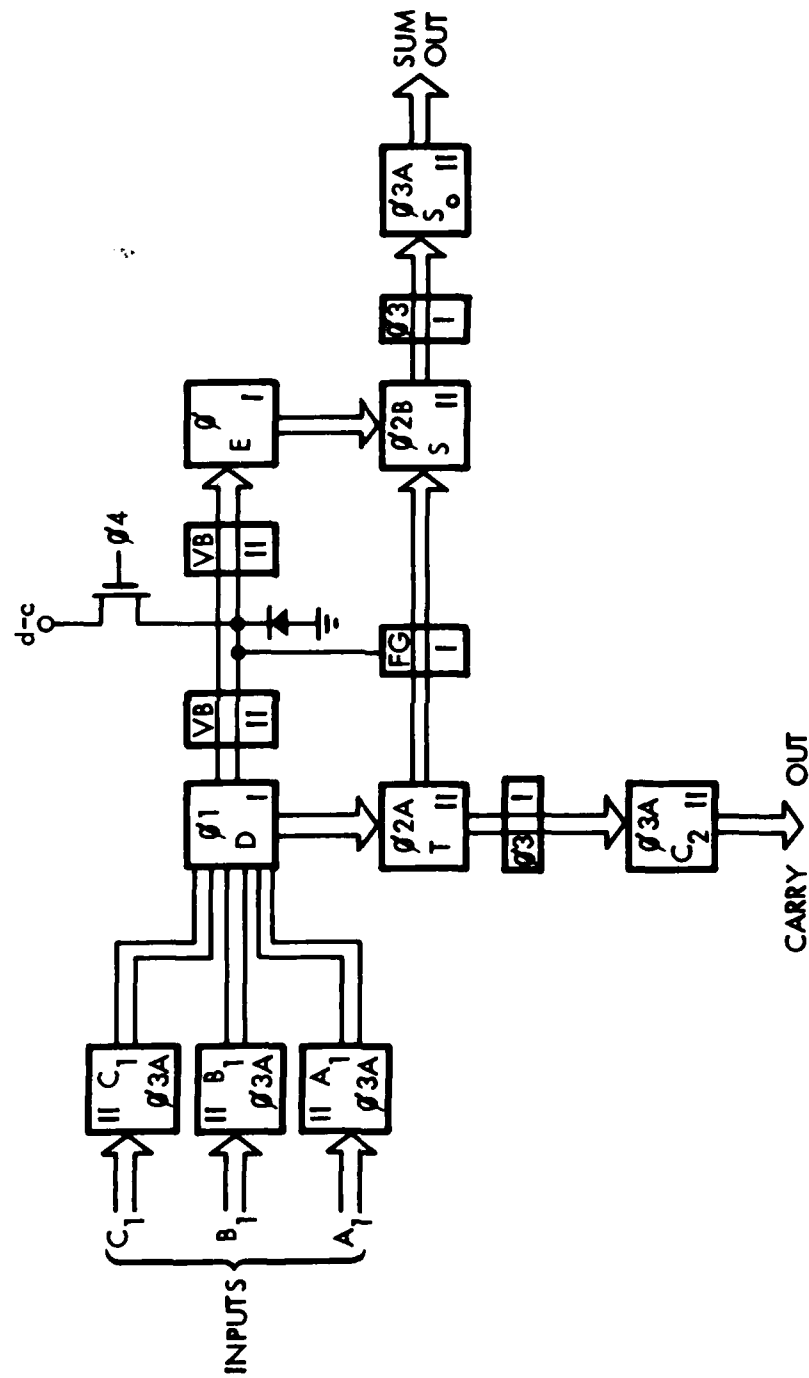


Figure 3-9. Schematic Diagram of NE2 and DP5 Full Adder.

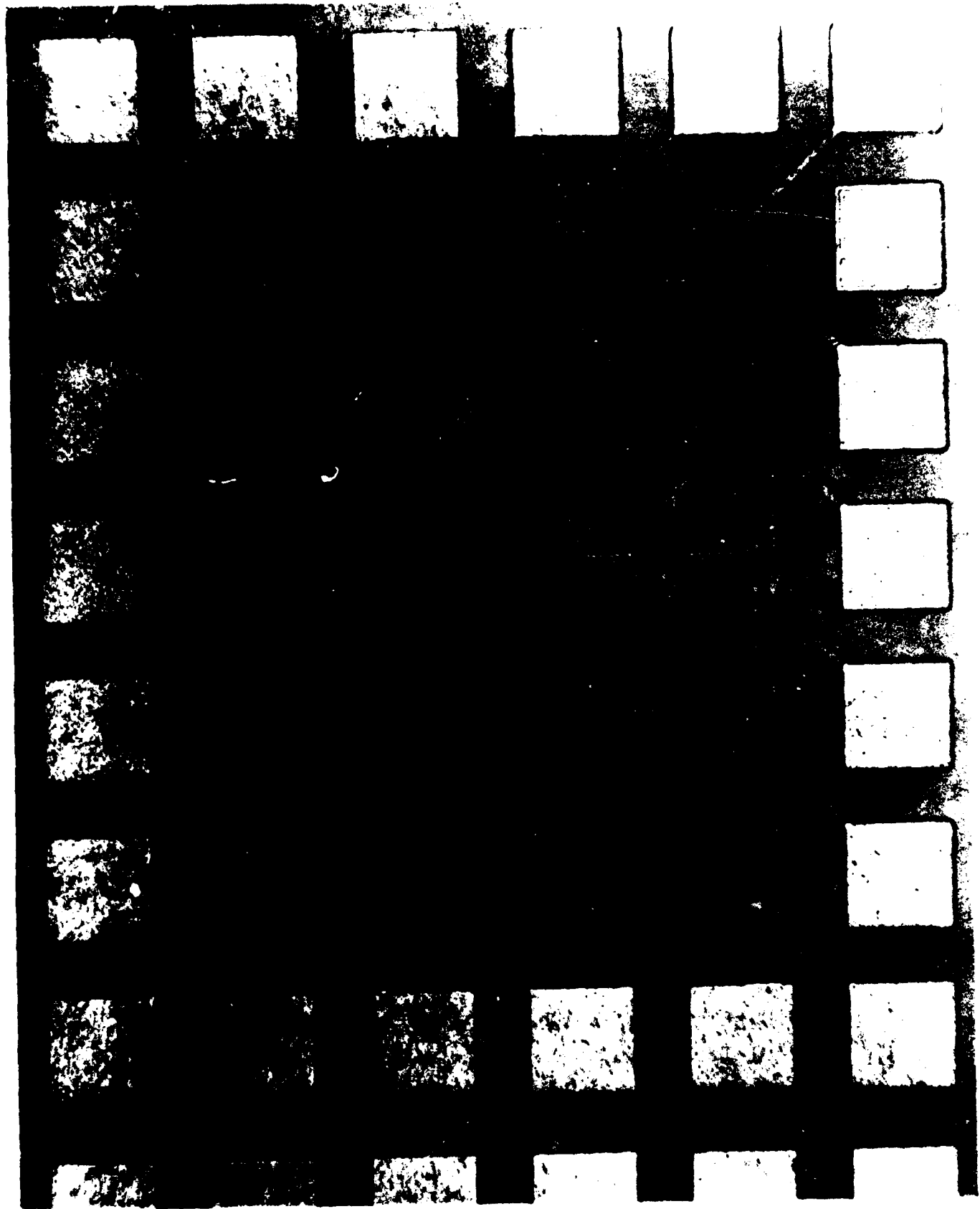


Figure 3-10 DPE Full Adder and Half-Adder

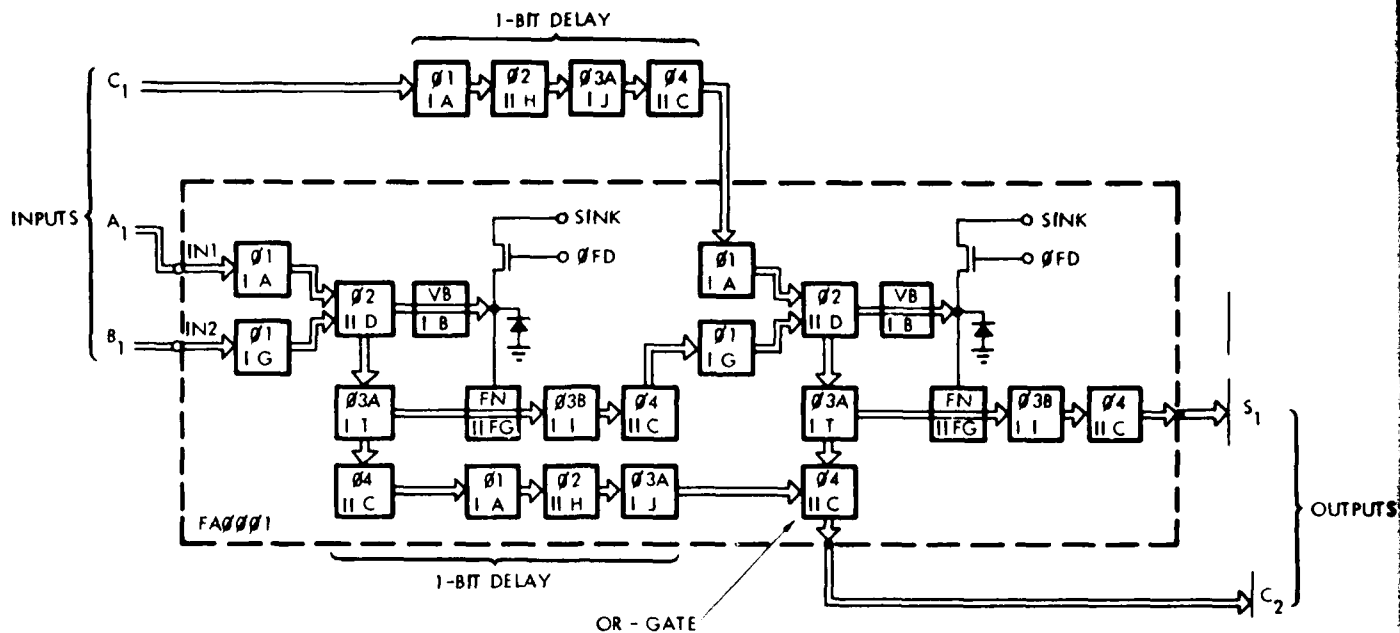


Figure 3-11. Implementation of the ACD-0 Full-Adder. This is a 4-Phase, Double-Polysilicon, N-Channel Device Formed from 2 Half-Adders, 2 1-Bit Delays and an OR-Gate.

### 3.3.3 Computer Model of a Full-Adder

Digital components such as full-adders, exclusive-OR gates, logic inverters have as a single common element, the electrode that senses and logically controls the direction of charge transfer. It is essential that this charge sense electrode operate correctly with large variations in size of input charge packets. During the design phase of the DP5 full-adder, we formulated mathematical and computer models of the charge sense electrode which accurately predicted the operational margin of these digital CCD components. Clock voltages, maximum tolerable temperature and operating frequency were also derived from the computer model.

Although the model was designed specifically for a single full-adder, it can be adapted for other digital CCD logic circuits. The computer model predicted the switching margins of the DP5 full-adder as well as the ACD half-adder.

A capacitor model of the charge transfer electrode is shown in Figure 3-12. The Computer model was used to calculate the depletion capacitance,  $C_d$ , the gate oxide capacitance,  $C_{ox}$ , and the total parasitic capacitance,  $C_p$ . The basis for these calculations included the digitized area parameters and semiconductor processing parameters such as oxide thickness, bulk impurity concentration, and fixed oxide charge density ( $Q_{ss}$ ).

The total parasitic capacitance is the sum of many small parasitic capacitances, such as the adjacent gate overlap capacitance, the metal strap to substrate capacitance and the slave node gate to channel stop overlap capacitance.

The computer program also takes into account the expansion or shrinkage of areas due to over-exposure or etching during processing in accordance with the factors listed in Table 3-2. Calculations can be based on maximum, nominal, or minimum shrinkage values. An RSS program is available that calculates the RSS variation of every surface potential based on the fluctuations of Table 3-2.

For a given amount of charge ( $\Delta Q$ ) spilling across the barrier to the charge transfer electrode, the change in voltage at the charge transfer electrode is defined as:

$$\Delta V_g = \frac{\Delta Q}{C_F}$$

where  $C_F$  is the total capacitance on the charge transfer electrode:

$$C_F = C_p + \frac{C_{ox} + C_d}{C_{ox} C_d}$$

$C_p$  = parasitic capacitances including the FET source depletion capacitance

$C_{ox}$  = oxide capacitance under the slave node of the charge transfer node

$C_d$  = depletion capacitance under the slave node of the charge transfer node

$C_F$  = OVERLAP CAPACITANCE FLOATING DIFFUSION TO FET GATE  
 $C_T$  = OVERLAP CAPACITANCE FLOATING GATE TO Ø 2A POLY  
 $C_S$  = OVERLAP CAPACITANCE FLOATING GATE TO Ø 2B POLY

$C_{CS}$  = CHANNEL STOP CAPACITANCE

$C_M$  = METAL LINK CAPACITANCE

$C_{df}$  = FET SOURCE (FLOATING-DIFFUSION) CAPACITANCE

$C_{ox}$  = FLOATING GATE OXIDE CAPACITANCE

$C_d$  = FLOATING GATE DEPLETION CAPACITANCE

$C_p$  = PARASITIC CAPACITANCE

$C_p = C_F + C_T + C_S + C_{CS} + C_M + C_{df}$

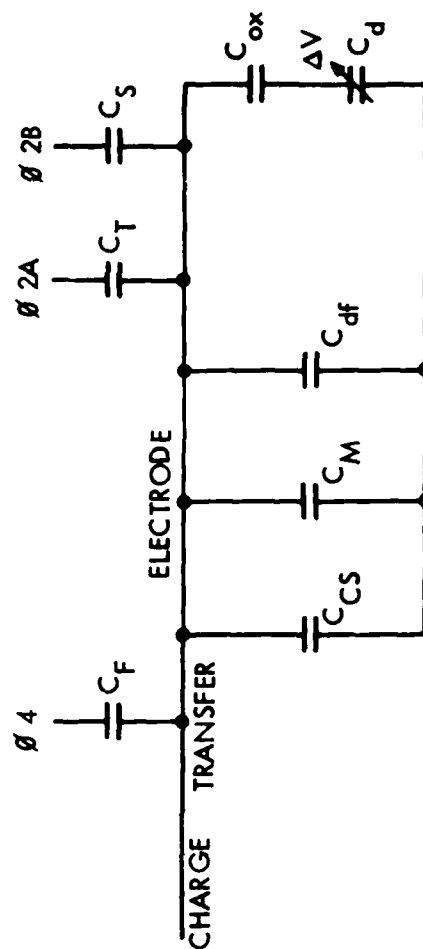


Figure 3-12. Capacitor Model of the Charge Transfer Electrode.

Table 3-2. Process Shrink/Growth Factors.

PARAMETER	MIN	NOM	MAX
X(1) Poly 1 Shrinkage	.024	.029	.034
X(2) Poly 2 Shrinkage	.014	.019	.024
X(3) N+ Lateral Diff.	.026	.03	.034
X(4) P+ Lateral Diff.	.045	.05	.055
X(5) Metal Shrinkage	.025	.03	.035
X(6) N+ Overetch	.004	.0045	.005
X(7) Threshold Variation	0	.05	.1
X(8) P+ Overetch	.02	.024	.028

The change in charge transfer electrode surface potential ( $\Delta\phi_s$ ) is given by:

$$\Delta\phi_s = \Delta V_G' + V_\phi - (2\Delta V_G' V_\phi + V_\phi^2)^{1/2}$$

$$= \alpha \Delta V_G$$

where

$$\Delta V_G' = \Delta V_G - V_{FB}$$

$$V_\phi = \frac{qN_A \epsilon_0 K_{SiO_2}}{C_{OX}^2}$$

Thus

$$\Delta\phi_s = \frac{\alpha \Delta Q}{C_F}$$

Figure 3-13 shows the surface potential diagram for the T cell - Charge Transfer electrode system.

Where:

$\phi_R$  = The preset surface potential of the charge transfer electrode as set by the FET.

$\phi_N$  = When the two charge packets into the "D" cell are a full binary "one" ( $Q_0$ ) and a "fat zero" ( $Q_N$ ), or two "fat zero" charge packets in the case of a three input port full-adder. The full binary one charge packet will transfer onto the "T" gate and the fat zero(s) packet(s) will spill across the barrier to the charge transfer electrode, causing the surface potential to change to  $\phi_N$ .

$\phi_T$  = When the two charge packets into the "D" cell are "thin" (attenuated) binary "ones" ( $2Q_T$ ) a full binary "one" charge, ( $Q_0$ ), will transfer into the "T" gate and the remainder of the two "thin" packets, ( $2Q_T - Q_0$ ), transfers across the barrier to the charge transfer electrode causing the surface potential to change to  $\phi_T$ . ( $2Q_T - Q_0$ ) =  $Q_J$ .

$\phi_0$  = The surface potential on the charge transfer electrode when a full binary "one" charge packet, ( $Q_0$ ), transfers across the barrier onto the charge transfer electrode.

$\phi_p$  = The initial surface potential of an empty "T" cell as set by the most positive voltage level of the clock signal.

$\phi_J$  = The surface potential of the "T" cell when a full binary "one" charge packet ( $Q_0$ ), is transferred into it.

It can be seen that the amount of blocked charge ( $\Delta Q_b$ ) is expressed as:

$$\Delta Q_b = C_T(\Delta\phi_T - (\phi_J - \phi_N))$$

$$\Delta Q_b = \frac{C_T}{C_F} \alpha \Delta Q_J - A C_T \quad 3.1$$

Where

$$A = \phi_J - \phi_N \quad \& \quad \Delta\phi_T = \frac{\alpha \Delta Q_J}{C_F}$$

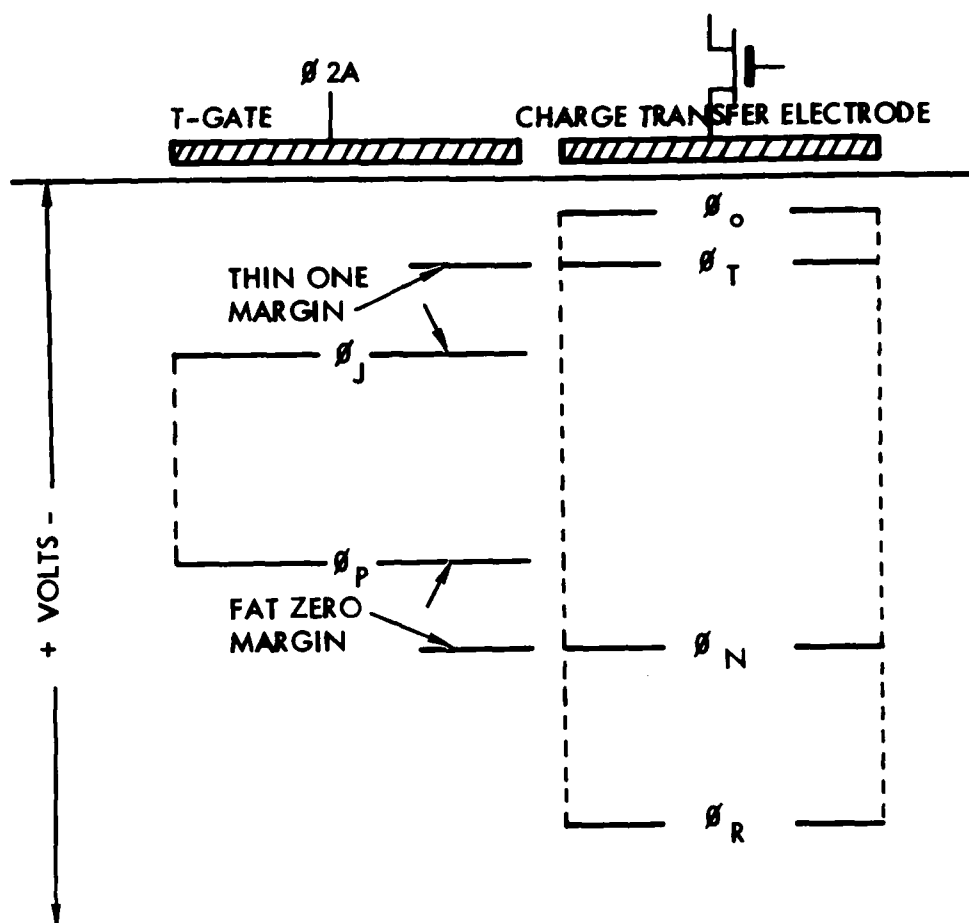


Figure 3-13. Surface Potential Diagram of the T-Cell to Charge Transfer Electrode Interface.

The desired result is: to provide value for  $\Delta Q$  that is approximately the same as (but less than)  $Q_0$ ; also provide a value for  $\Delta Q_b = 0$ , that is  $\phi_J - \phi_T > 0$ ; provide a value for  $\Delta Q$  that is nearly the same (but greater than)  $Q_0$ ; and provide a value for  $\Delta Q_b = 0$ , thereby retaining the margin  $\phi_N - \phi_P > 0$ .

Mathematically,  $Q_b \leq 0$ , (when  $\Delta Q = Q_N$ ) when the charge transfer node does not present a barrier. The largest swing in the charge transfer node (that allows  $\Delta Q_b \leq 0$ ) occurs when  $\Delta Q_b = 0$ . The amount of charge on the charge transfer electrode required to do this is:

$$\Delta Q = \frac{AC_F}{\alpha} \leq Q_0 \quad . \quad 3.2$$

Mathematically,  $\Delta Q \geq Q_0$  (when  $\Delta Q = Q_0$ ), when the charge transfer electrode presents a total barrier. The smallest swing in the charge transfer electrode occurs when  $\Delta Q = Q_0$ . The amount of charge on the charge transfer node required to do this is:

$$\Delta Q = (Q_0 + AC_T) \frac{C_T}{C_F \alpha} \geq Q_0$$

$$\Delta Q = \frac{Q_0 C_F}{\alpha C_T} + \frac{AC_F}{\alpha} \quad 3.3$$

To maximize the switching margin of the "T" cell minus the charge transfer electrode system,  $\frac{Q_0 C_F}{\alpha C_T}$  must be at a minimum.

The computer program calculates the size of the  $Q_1$  full packet from the area of the "D" cell, the maximum clock voltage applied to the D cell and the potential of the barrier gate.

The computer program also calculates the total noise charge packet ( $Q_N$ ), by summing three separate components: the first of these noise components is the residual charge that remains after a full charge packet has been attenuated. The second component is the charge packet that crosses the potential barrier of a previous arithmetic cell, due to low threshold voltage. The third component is due to accumulation of dark current.

For the DP5 full-adder, the full charge packet was calculated to be 3.2 million electrons and the noise charge packet was calculated to be one million electrons.

The computer program successively adjusts the preset surface level of the charge transfer electrode so that the  $\phi_N - \phi_P$  margin equals the  $\phi_J - \phi_T$  margin. The computer RSS program for the DP5 full-adder calculated both margins as 213 mV.

### 3.3.4 Advantages of Full-Adder Over Dual Half-Adder Implementations

#### 3.3.4.1 Power Dissipation

The power consumed in a DCCL is only that power required to charge the gate capacitance to each clock voltage level. The capacitance of the  $\phi 1$  clock line to the full-adder is approximately 1.8 times that of a half-adder; with the exception of that clock line, all other capacitances are identical. This additional capacitance causes a full-adder to dissipate 20% more power than a single half-adder. However, when dual half-adders are used to implement a full-adder function, this configuration requires two one-bit shift-registers and an OR gate. These additional elements, added to the two half-adders, result in an overall power dissipation that is 2.5 times that of a single full-adder.

#### 3.3.4.2 Transfer Efficiency

It is not feasible to use a "fat-zero" in implementing arithmetic functions with DCCL's. As a result, transfer efficiencies of only 0.998 per transfer are achievable. There are two transfers through a full adder, resulting in a transfer efficiency of 0.996. In a dual half-adder configuration there are four transfers producing a transfer efficiency of 0.992. In the layout of a large pipeline arithmetic array it will therefore be necessary to insert a level of charge refresh cells twice as frequently when dual half-adder configurations are used.

#### 3.3.4.3 Pipeline Delays

Both full-adders and half-adders perform a single mathematical function in one clock cycle. Therefore, a full-adder implemented from two cascaded half-adders requires two clock cycles to perform the full-adder function. An adder or multiplier designed from full-adders will impose half as many pipeline delays on the system as the same adder or multiplier designed from cascaded dual half adders. This is significant where maximum circuit density is of primary importance.

### 3.4 HALF-ADDER DESIGNS AND RESULTS

A basic description of the half adder and how it performs arithmetic functions has been previously provided in Section 3.1. For reference, the

truth table for a half adder is shown in Table 3-3. The half-adder can be used for other functions besides addition. As illustrated in Table 3-3, sum output performs the "exclusive-OR" function and the carry output performs an "AND" function.

Table 3-3. Half-Adder Truth Table

Inputs		Outputs	
$A_1$	$B_1$	Sum "Exclusive-OR"	Carry or ("AND")
0	0	0	0
0	1	1	0
1	0	1	0
1	1	0	1

The first half-adder was implemented in August 1975, on the DP-0 evaluation mask. A schematic diagram of this half-adder is shown in Figure 3-14. A description of its method of operation was published<sup>3-4</sup> in March 1976.

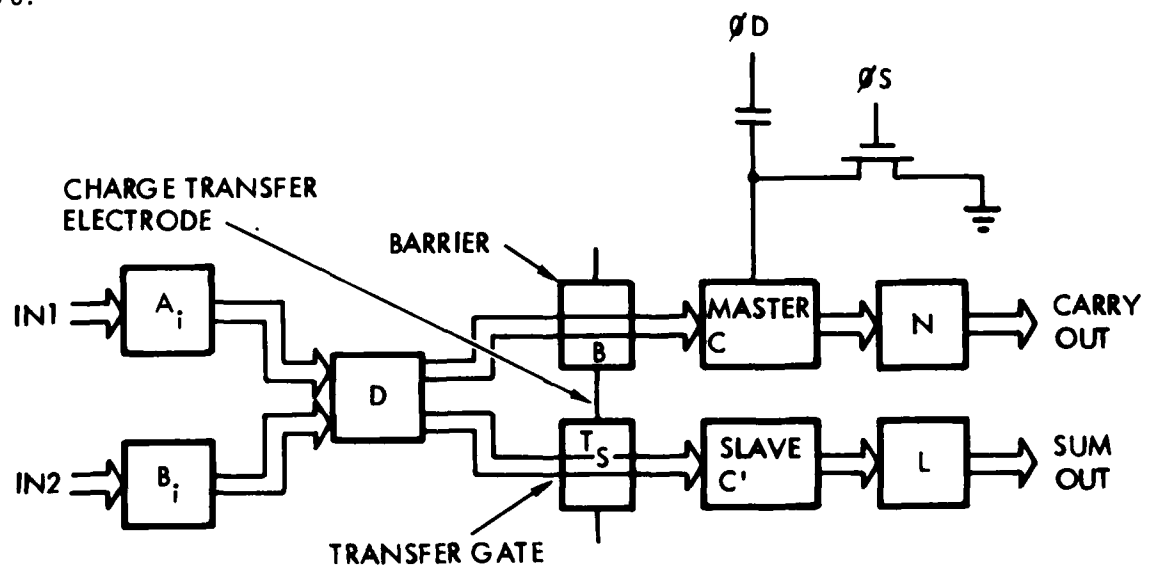


Figure 3-14. Schematic of the 1975 DP0 Half-Adder.

The DP-0 wafer used metal gates over a 2000 Å gate oxide, a single polysilicon gate level over 1000 Å gate, P-channel technology, and a 15000 Å field oxide. The DP-0 half-adder design did not provide useful devices due to metal line breakage resulting from inadequate metal step coverage layout constraints.

The layout problems of the DPO half-adder was corrected (to eliminate the cause of metal breaks) on the DP1 design. The half-adder was subsequently used as a standard cell to form a 4 + 4 adder and a 3 x 3 (magnitude only) multiplier.

Analytical results provided by computer modeling of the full and half-adders made it apparent that the size of the T-gate should be 2.8 to 3.0 times the area of the D-gate in order to enhance the functional performance of the charge sense electrode. It also became apparent that the area under the master end, M, of the charge sense electrode should be as small as possible so as to make the voltage change transmitted to the charge transfer electrode as large as possible.

There were two different half-adder layouts used on the DP1 mask. The first was used in the multiplier and adder along with the full-adder and was identical in design to the full-adder except that one input and the intermediate gate, I, were removed. These half-adder and full-adder combinations all had the large T-gate, small M-gate combinations and the arrays containing them function extremely well.

The second half-adder was a completely different design and did not utilize a large T-gate. This half-adder design was used in the 3 x 3 and 4 + 4 arrays that used the half-adder exclusively. After developing special three level clocks, these half-adders and the multiplier and adder arrays containing them were made to function.

In the next design (the DP2 mask), we used the cascaded half-adder to form a full-adder as shown previously in Figure 3-8. The half-adder design was simplified by eliminating the precharge capacitance and using the FET to preset the charge transfer electrode to the transfer surface potential as well as remove any initial charges.

As mentioned previously in Section 3.3 (regarding DP2 full adders), difficulties were experienced in using a slip-mask approach and the development of the DP3 designs were well underway before we received any DP2 devices. Consequently, very little testing was carried out on the DP2 half-adders.

It was at this time that we discovered by changing the location of the carry output from the master side of the charge sensing electrode to the D input storage gate, we were guaranteed of generating a full charge packet each time there were two or more binary "1" inputs (full-charge packets) into the D input area. Thus, we had an automatic charge refresh capability at the carry-out port of all half-adders on the DP3 and subsequent designs.

Another major improvement on the DP-3 half-adder was to change from using a floating-gate capacitance at the master-side of the charge sense element to the use of the precharge FET source as a floating diffusion.

Both the  $16 + 16$  adder and the  $8 \times 8$  multiplier on the DP3 chip were designed from cascaded half-adders and OR gates. Tests were performed on both the floating-gate and floating-diffusion half-adders and it was shown that the floating-diffusion half-adder had greater sensitivity and better transfer efficiency.

In December 1977, in response to a desire for higher clock speeds, we changed from the two-phase, p-channel structure to a three-phase n-channel structure. The channel was defined by an implanted p+ channel stop.

The first N-channel evaluation mask was designated NE-1 and contained a half-adder as a test device. A schematic diagram of the NE-1 half-adder is shown in Figure 3-15. This half-adder was shown to function correctly in February 1978, and was used as one of the test vehicles for the radiation tests (see Section 5.0).

During the radiation testing of the NE-1 half-adder it was found that the surface potential shift of the charge sense gate did not track well with the surface potential shift of the other CCD gates in the half adder. The

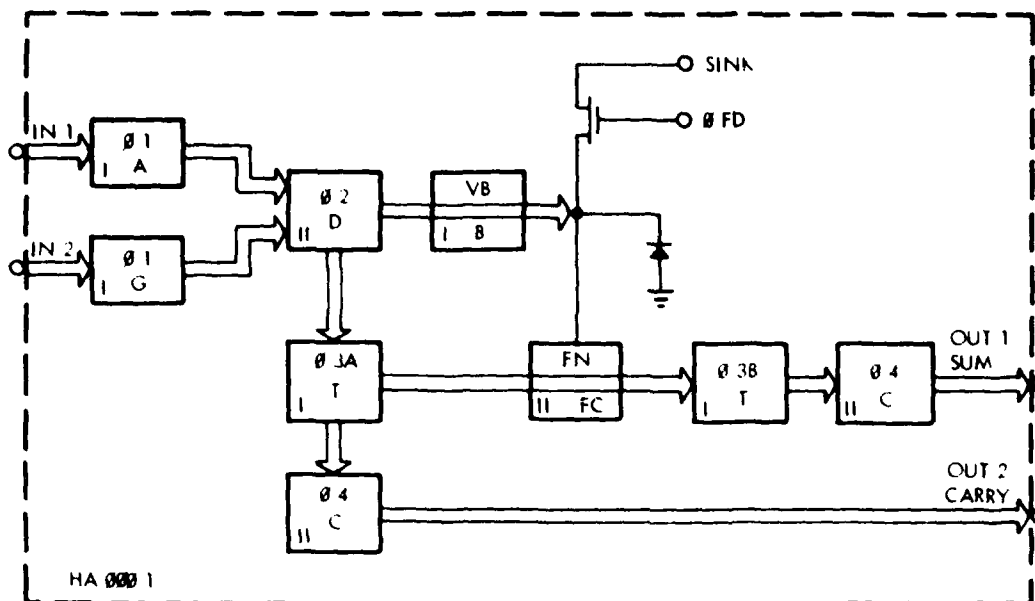


Figure 3-15. Schematic of the NE-1 Half-Adder.

reason for this is that with the drain of the precharge FET connected to its gate, there are two threshold voltage drops involved with the charge sense gate as compared to one between the CCD gates and their surface potentials. Thus as the threshold voltages changed with radiation exposure, the surface potential did not track between the charge sense gate and the other half-adder gates.

This was corrected in the NE-2 half-adder and the exclusive OR-gate used on the DP5 arithmetic array by connecting the FET drain and gate electrodes to separate pads. The trade-off was additional silicon area and an additional bonding pad.

One problem that we found with all of the digital logic and arithmetic cells on the NE-1 design was the incompatibility between the even number of gates in a double polysilicon structure and the odd number of clocks in a 3-phase clocking system. This made contiguous interconnection of identical cells very difficult. Our first approach was to make one storage area from two overlapping polysilicon gates. This seemed a good approach since both

gates have the same oxide thickness, however we found in practice that there was a surface potential bump under the first gate in the overlap structure. This bump caused some charge to be trapped, resulting in an excessive transfer loss.

On the NE-2 and DP-5 designs, instead of connecting both halves of the overlapped gate pair to the same clock line, they were taken to two different clock lines. Both clock lines had the same phase relationship but the second gate clock was larger, producing a deeper potential well. The length of the first gate was reduced making it a transfer gate and the length of the second half series gate was increased so that it would store the whole charge. This proved very satisfactory and the half-adder test device on DP5 proved to have excellent transfer efficiency.

The next half-adder to be designed was for the ACD project (see Section 9.3). There were two new requirements for this device. The first was that it should operate at clock speeds up to 3.5 MHz and second it should operate with the same 4 phase clocks required by our current SPS memory designs.

The first requirement was met by reducing the transfer length of all the gates, and taking special care that the transfer length of the T-gate (the largest gate in the half-adder) was kept to a minimum. The even number of 4 clock phases fell naturally in line with the even number of two polysilicon levels so that the ACD half adder was easier to implement than the NE1/DP5 3-phase half-adders.

In parallel with the design of the ACD half-adder was an earlier version designed for the FHT projects (see Section 9.2). Although this half-adder is similar to the NE-1 design in that it is also N-channel, 3-phase clock, and uses a floating-diffusion for charge sensing; it had one significant difference. The slave-end of the charge transfer electrode is of second level polysilicon, whereas the NE1/DP5/ACD half adders used first level polysilicon for the slave-end. The result of this was that the effective length of the channel under the slave-end of the charge sense electrode was shorter than the later half-adder designs and performance was degraded by fringing-fields from adjacent gates.

The last half-adder designed to date is the ACD-2. This is a further evolution of the NE1-NE2-DP5-ACD series. The newer half-adder has a larger storage well to store the sum-bit and also a wider barrier electrode between the D-gate and the master-end of the charge transfer electrode.

#### 3.4.1 Half-Adder Gain and Operating Margins

The same mathematical and computer models described in Section 3.3.3 for a full-adder can be modified and used to calculate the operating margins of the half-adder. The only modification necessary is to reduce the inputs from three to two and to remove the second barrier overlap capacitance from the floating-diffusion node of the charge transfer electrode.

We define the gain (G), of a half-adder (or a full-adder) as

$$G = \frac{\Delta Q_b}{\Delta Q} \quad 3.4$$

where  $\Delta Q_b$  is the amount of charge blocked and  $\Delta Q$  is the amount of charge transferred to the floating diffusion node of the charge sense electrode. The gain can be calculated from Equation 3.1 (see Section 3.3.3 for Equations 3.1 through 3.3):

$$G = \frac{\Delta Q_b}{\Delta Q} = \frac{C_T}{C_F} \alpha \frac{\Delta Q_J}{\Delta Q} - \frac{AC_T}{\Delta Q} \quad 3.5$$

From Equation 3.2 when  $\Delta Q = Q_J$ :

$$G = \frac{C_T}{C_F} \alpha - \frac{AC_T}{Q_J} \quad 3.6$$

$Q_J$  is the amount of charge that transfers across the barrier to the charge sense electrode when two thin (attenuated) binary ones ( $2Q_T$ ) are transferred into the D cell and a full binary one charge, ( $Q_0$ ) is retained by the barrier.  $Q_J = 2Q_T - Q_0$ .

A test procedure was developed for measuring the half-adder switching margins expressed as a percentage of a binary "one."

In order to carry out this measurement, a 700 Hz triangular waveform is applied to the inject source diode, thus increasing the amplitude of both input charge packets at a linear rate.

A digital input pattern at a 400 kHz rate is applied to both input control gates to the half-adder. The input sequence to one control gate (IN1) is 11101010 and the input to the other control gate (IN2) is 10111010.

The output charge packets from the sum and carry channels from the half-adder are converted to voltages and displayed on an oscilloscope.

The SUM output displays two traces, the main trace is painted at each alternate combination of the input pattern when IN1 and IN2 are both binary one, it therefore paints the trace at 200 kHz. The second trace occurs twice per pattern cycle when either (but not both) inputs are binary one, this ghost trace is painted at 100 kHz.

To calibrate the test set-up correctly, the amplitude of the input triangular waveform must be adjusted so that the slope of the curve 1 (ghost trace) as shown on Figure 3-16 intersects the flat portion of curve 3 at one point (a).

Curve 1 is the SUM output of a single binary one input when its charge is less than required to fill the half-adder D input storage well. The apex of this curve is where the single one charge packet is large enough to exactly fill the D storage well.

If a flat period exists at the apex of curve 1 it indicates that the triangular waveform is too great and the single binary one is overflowing across the barrier, it therefore should be reduced until the apex is a single point.

Curve 2 is the SUM output resulting from two ramped inputs. Segment d-c of curve 2 represents the sum output. The total charge of the two ramped inputs is greater than that required to fill the half-adder D input storage area. During this portion of the curve, the amount of charge transferred across the barrier is insufficient to fully change the potential of the charge sense node from a transfer state to a barrier state.

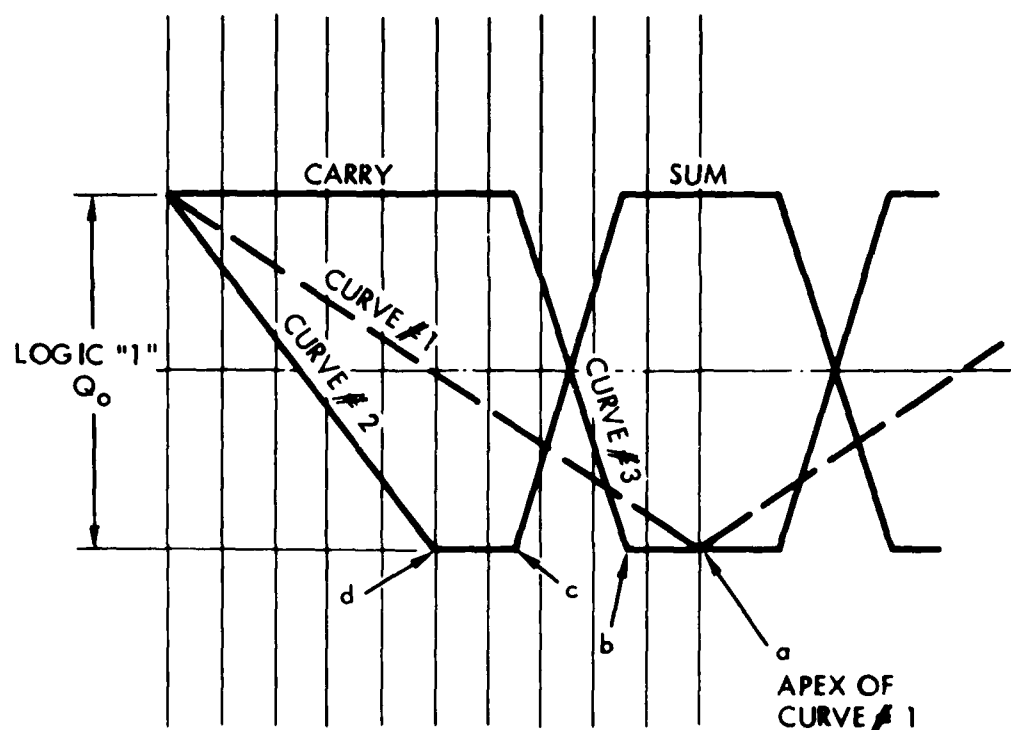


Figure 3-16. Oscilloscope Display of Sum and Carry Outputs of a Half-Adder During Margin Testing.

Curve 3 reflects the carry output from two increasing inputs. As the charge transferred onto the charge sense electrode increases, the carry output increases and the sum output decreases until the inputs reach full ( $Q_0$ ) value.

The timebase of the CRT is adjusted so that curve 1 completely fills ten spaces of the graticule, that is, a binary one fills 100% of the graticule. Each space on the graticule is therefore 20% of the sum output for two binary one inputs displayed on curve 2.

The thin one margin is the flat portion of curve 3 from a to b and the fat zero margin is the flat portion of the curve 2 from c to d. In most cases the two margins should be of equal amplitude, they can be made equal by adjusting the preset transfer level of the charge transfer electrode.

A photograph of the DP5 full-adder output curves is shown in Figure 3-17. Due to the non-linearity of the sum output for a single ramped input (curve a), the test set up was calibrated so that a linear projection of curve a intersects the center of the graticule. The photograph shows a fat zero margin of 25% and a thin one margin of 70%.

#### 3.4.2 Other Uses of Half-Adders

A half-adder can be used for several other applications in addition to the exclusive-OR and the AND functions described previously.

##### 3.4.2.1 Refresh and Invert

By connecting one of the inputs of a half-adder to a constant binary one, the truth table is reduced to that shown in Table 3-4. The functions provided by Table 3-4 provide both a refresh and a binary logic interter.

Table 3-4. Half Adder Truth Table with one Input Always a Binary One.

Inputs			Outputs
A1	B1	Sum/A1	Carry/A1 Restored
0	1	1	0
1	1	0	1

##### 3.4.2.2 Fan-Out

The fan-out generator is similar to the charge refresh cell described above, the only difference is that instead of transferring in a charge packet equal to a binary one at each clock phase (constant binary one input) we transfer in a charge packet that is two to three times the size of a binary one. Care must be taken in the design of the T-gate and multiple output ports of the fan-out generator to ensure that the transfer lengths are exactly the same or differences in charge packet size will be encountered.

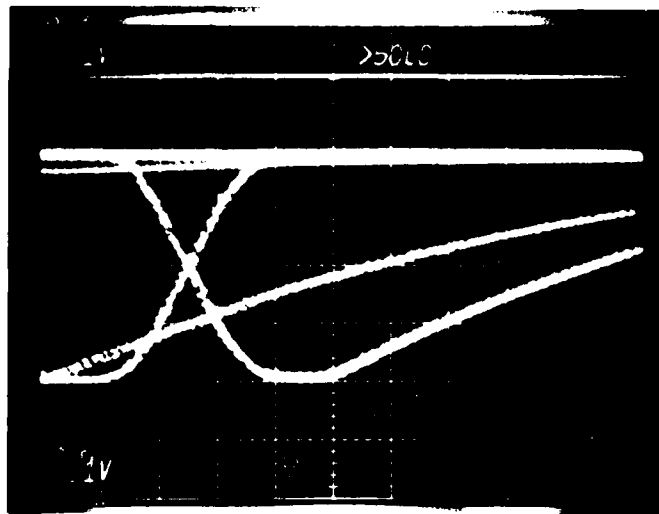


Figure 3-17. Sum and Carry Outputs of a DP5 Full-Adder Showing a 25% Fat Zero Margin and a 70% Thin Binary One Margin.

#### 3.4.2.3 Frequency Divider

A clock frequency can be divided down by any even integer with a half-adder by connecting the SUM output, through a shift-register delay, back to one of the inputs. The input clock is applied to either the source inject diode or the C1 control gate. If no delay is inserted in the feedback path between the SUM output and the input, there is one clock period delay through the half-adder and the output from the carry port will be a pulse train at half the clock frequency.

If a one-bit delay is inserted in the feedback path then the clock frequency will be divided by 4. The output frequency is  $f_c / 2^{(\tau+1)}$  where  $f_c$  is the clock frequency, and  $\tau$  is the number of stage delays inserted in the feedback path.

#### 3.4.3 Advantages of Half-Adders over Full-Adders

##### 3.4.3.1 Clock Frequency

For the large charge packets used in DCCL's, the transfer of charges is dominated by self-induced drift. In a half-adder, the  $\phi_1$  clock is applied

to the D gate. The time duration of the  $\phi 1$  clock is determined by the time necessary for an input of  $2Q_0$  charges to fill the input storage area D, transfer over the barrier and fill the floating diffusion well of the charge sense electrode.

The time required for the initial  $2Q_0$  charge to settle to within one thermal voltage ( $KT/q$ ) has been shown to be

$$t_{HA} = \frac{\pi L^3}{4\mu} \frac{W_{C_{ox}}}{Q_0} \quad 3-7$$

where:  $L$  is the total length of the electrodes over the input gate, the D storage gate, the barrier, and the floating diffusion;  $W$  is the channel width;  $C_{ox}$  is the oxide capacitance per unit area;  $\mu$ , is the mobility of the carriers; and  $(\phi 1 - \phi 2) = 2Q_0 / (L^2 W C_{ox})$  is the input charge. The potential difference  $\phi 1 - \phi 2$  is the difference in surface potentials between an empty well and a well with a full charge packet  $Q_0$ .

At the end of the self-induced drift period, the remaining input charge has a surface potential of  $\sim 26$  mV (at room temperature) and is swept out by the fringing fields.

The full-adder has an additional transfer area and storage gate that has to fill when the initial input charge is  $3Q_0$ . The self-induced drift period for the full adder is

$$t_{FA} = \frac{\pi L^3}{6\mu} \frac{W_{C_{ox}}}{Q_0} \quad 3-8$$

The ratio in self-induced drift time between a half-adder and a full-adder is

$$\frac{t_{FA}}{t_{HA}} = \frac{2}{3} \left( \frac{L_{FA}}{L_{HA}} \right)^3 \quad 3-9$$

For the specific designs described here,  $L_{HA} = 1.4$  mil and  $L_{FA} = 2.6$  mil. Consequently, the  $\phi 1$  period for the full-adder will be 2.1 times that required for the half-adder.

The clock period for 3 phase full-adders and half-adders can be divided into two periods, the period that the charges are equilibrizing while the  $\phi_1$  clock is negative and the period when the  $\phi_1$  clock is positive and the other clocks are controlling the charges. In a half-adder, the first period is approximately 40% or  $0.4t$  and the second period is 60% or  $0.6t$ . In a full-adder the first period is  $2.1 \times 0.4t = 0.84t$  so that the total time for a full adder is  $1.44t$ , compared to  $t$  for a half-adder.

#### 3.4.3.2 Signal-to-Noise Ratio

A half-adder requires one input port to the floating diffusion on the master side of the charge sense electrode.

The additional channel to the intermediate storage area in a full-adder requires that a output port be added to the floating-diffusion node of the charge transfer electrode.

The additional polysilicon-diffusion capacitance due to this output port is added to the charge sense electrode parasitic capacitance, thereby reducing the sensitivity and gain of the full adder as compared to the half adder.

### 3.5 I/O CIRCUITRY

#### 3.5.1 Input Circuits

##### 3.5.1.1 DCCD Input Charge Generation

The basic scuppering (also known as "fill and spill" or "potential equilibration") input scheme is depicted schematically in Figure 3-18. The timing shown is for a 3-phase CCD structure. There are two variations of this scheme; one with the data input on the  $C_1$  electrode, and the other with the data input on the inject diffusion. Both versions use the same voltage timing.

The generation of a DCCD logic one charge packet can be explained from Figure 3-18. At time sector 0, the  $C_1$  surface potential is brought to 4 volts and the  $\phi_1$  clock assumes a blocking level of 1 volt. At sector 1 the inject diffusion lies at 2 volts, and  $C_2$  surface potential goes to 8 volts. The inject diffusion is now forward biased and electrons (holes in the case of

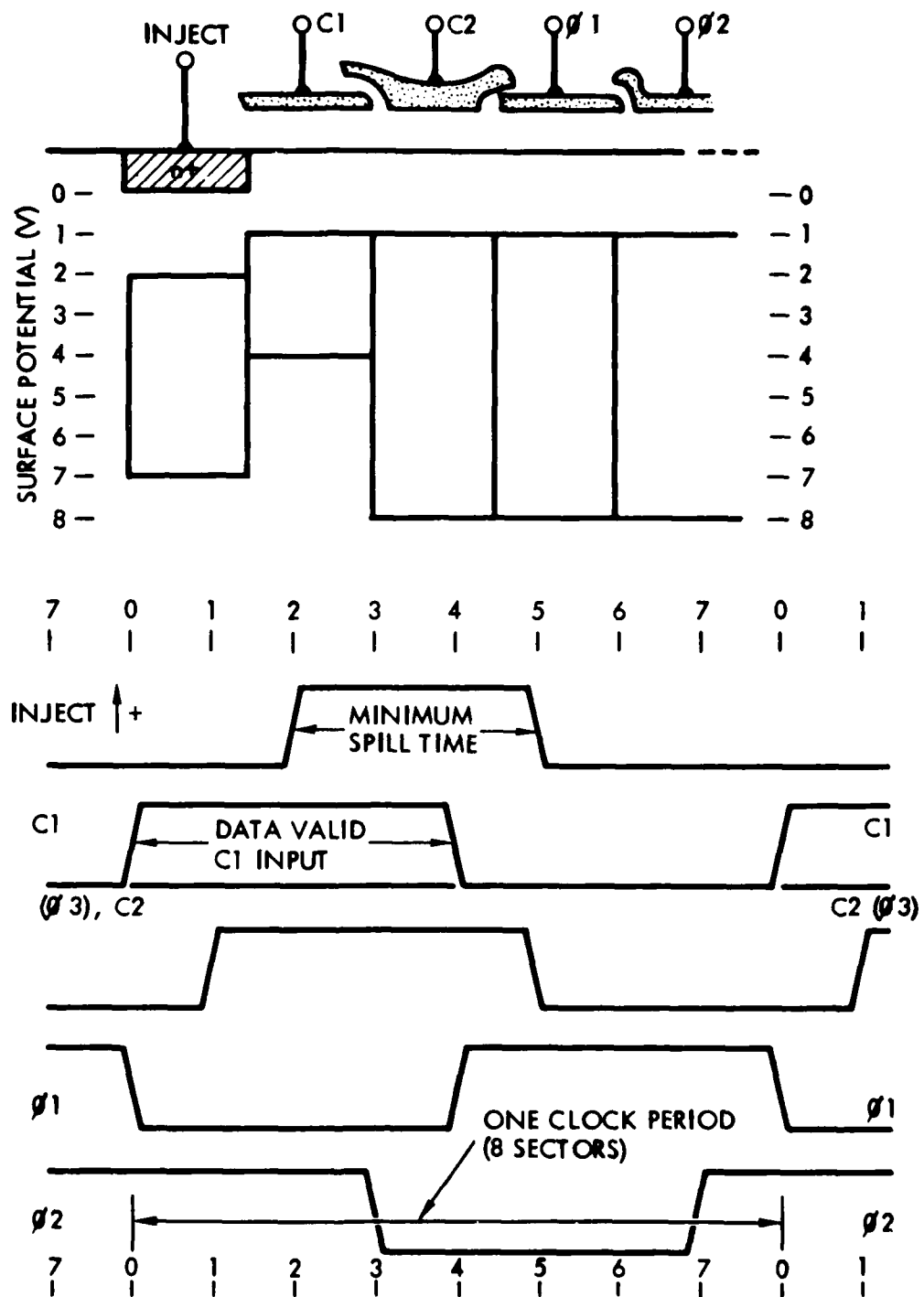


Figure 3-18. Schematic Diagram showing the basic charge input generation technique.

p-channel devices) are injected across the surface under C1 and C2 until those surface potentials reach 2 volts. At sector 2, the inject diffusion is taken back to 7 volts. Electrons in the C1, C2 well, now spill back into the inject diffusion across the 4 volt barrier of C1. This scuppering process is allowed to continue up to sector 4. By this point in time the surface potential under C1 and C2 will be approximately 4 volts. This leaves a packet of electrons trapped in the C2 potential well. The size of this packet can be readily determined by integrating the C2 well capacity with respect to surface potential from 4 to 8 volts. At sector 4 the C1 surface potential is switched back to 1 volt and the  $\phi_1$  surface is brought to 8 volts. Now the charge packed under C2 redistributes itself equally between C2 and  $\phi_1$ . At sector 5 the C2 surface potential returns to 1 volt. During this transition the complement of the charge packet is moved under  $\phi_1$ . Thus a charge packet, representing a DCCD logic one, is generated and shifted out of the input structure. In the case of a logic zero, no charge is captured in C2 as C1 remains at 1 volt during sectors 1 through 4.

#### 3.5.1.2 Input Buffers

A TTL receiver has been developed for the DCCL logic family. It is designed to operate the C1 electrode of the standard input circuit shown in Figure 3-18. Figure 3-19 shows a schematic of the TTL receiver with its output tied to the standard input structure (labeled C11000). This receiver is designed to operate with low power schottky TTL. Q1 of this circuit provides dynamic pull up for the TTL. A single receiver is capable of driving 3 DCCL inputs at a 5 MHz clockrate.

In the second scheme mentioned above, where the inject diffusion is used as the data input port, the formation of logic ones is identical to the one described above with the exception that, to form a logic zero, the inject diffusion must be kept at 7 volts throughout the clock period. In contrast to the first input scheme, C1 is cycled between 1 and 4 volts every clock period and the polarity of the input is reversed (i.e. for the C1 input, the most positive level yields a logic one; for the inject input, the most negative level yields a logic one).

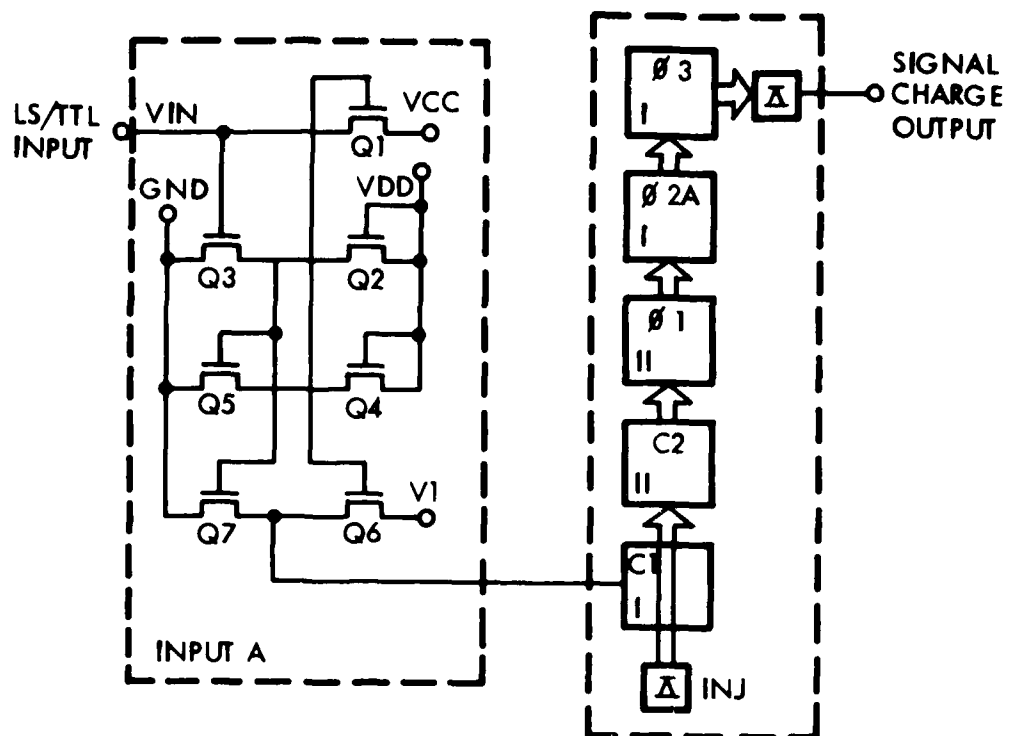


Figure 3-19. Schematic of the TTL to DCCD input circuit.

### 3.5.2 Output Circuits

There are three main output buffers used for DCCL; the simple source follower, the two stage source follower with self biasing, and the TTL transmitter which converts DCCL into TTL inputs.

#### 3.5.2.1 Source Follower Output Circuit

A schematic of the simple source follower is shown in Figure 3-20. This is the most general purpose output buffer for research applications as it is composed of only three transistors and all circuit nodes are independently accessible for biasing flexibility. A functional description of this interface circuit is given below.

At sector 5 (see Figure 3-20 timing diagram) the collapsing  $\phi 3$  surface potential pushes its charge packet across of semiconductor surface and over the  $V_B$  potential barrier to the  $n^+$  output diffusion. This changes the potential of the diffusion from its reset level of  $V_0$ , to a less positive level. A

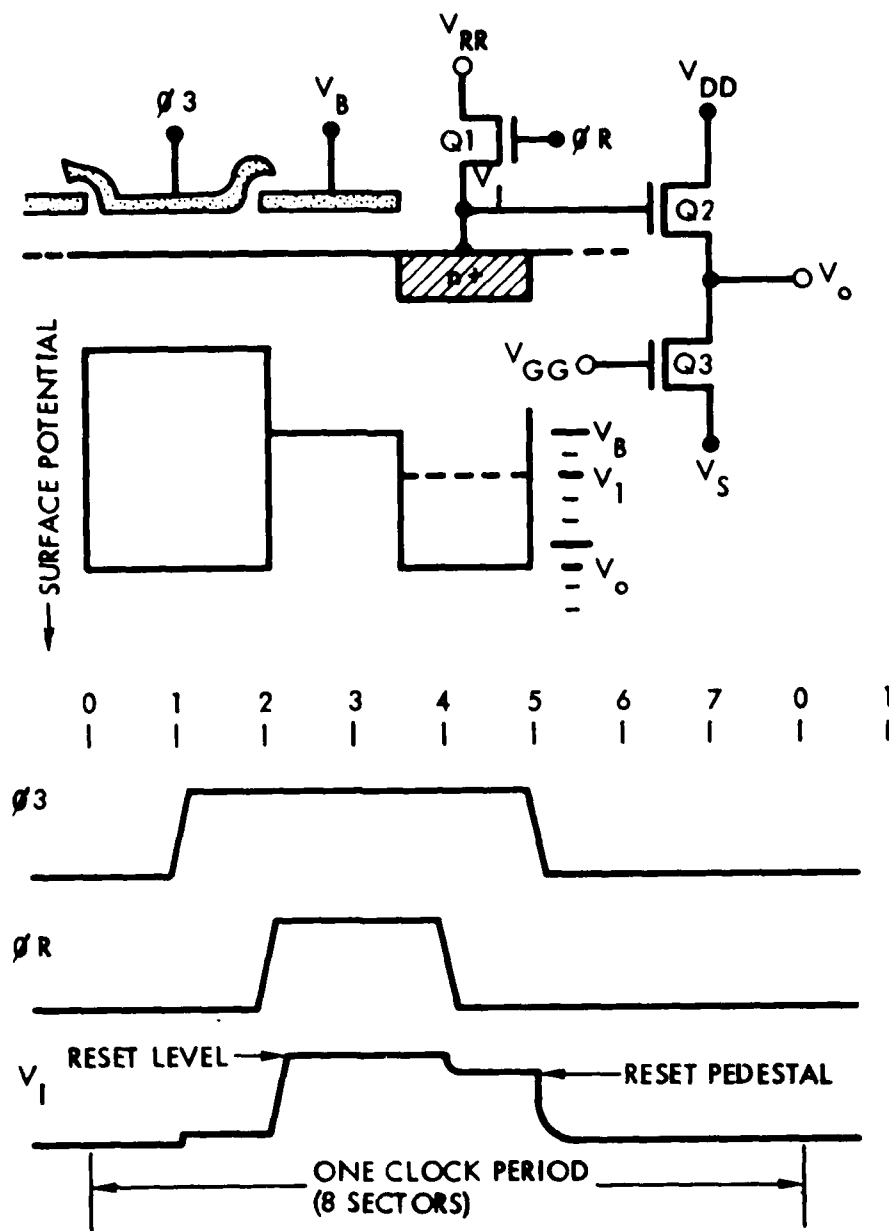


Figure 3-20. Schematic of a simple source follower CCD output circuit.

logic one charge packet brings the diffusion potential to  $V_1$ . This potential will persist until sector 1 where  $\phi_3$  takes a positive transition in voltage. This transition capacitively couples onto the output diffusion to some extent depending on layout. At sector 2 the  $\phi_R$  electrode is strobed to a positive potential such that  $V_0 = V_{RR} - V_{THQ2}$ . By sector 4 the reset condition is stable and  $\phi_R$  is switched to its negative level, thus turning  $Q_1$  off. This negative transition is capacitively coupled to the output diffusion and is typically quite pronounced; it is commonly referred to as the reset pedestal. At this point the output diffusion is ready to accept another signal charge packet from the CCD channel.

### 3.5.2.2 Two Stage Source Follower Output Circuit

In the course of technology development the interface circuits must meet the demands of higher frequency operation. To this end, the two stage source follower shown in Figure 3-21 has been used throughout the development of n-channel CCD. This buffer operates in the same manner as the simple source follower described above with regard to the acceptance and resetting of signal charge. The second follower stage,  $Q_4$  and  $Q_5$  provide additional buffering to the external probe capacitance placed on the  $V_0$  node.  $Q_6$  and  $Q_7$  form a voltage divider which is used to bias the load devices  $Q_3$  and  $Q_5$ . This buffer will drive a 7 pf load with a small signal gain of 0.9 up to a frequency of 5 MHz.

### 3.5.2.3 DCCD to TTL Tri-State Output Circuit

For the purpose of interfacing between DCCL and TTL, a tri-state output buffer has been developed. Figure 3-22 shows a schematic of this type of buffer which is currently slated for use on the fast Hadamard transform device FHT-1. This circuit is composed of a source follower input stage ( $Q_1$  through  $Q_4$ ). The output of this stage is capacitively coupled through  $C_1$  to the input of the inverter stage  $Q_6$  and  $Q_7$ . The inverter stage is dynamically biased by  $\phi_A$  through  $Q_5$ . The inverter output is sampled into the next stage by  $\phi_5$  through  $Q_8$ . The next stage,  $Q_9$  through  $Q_{14}$ , forms

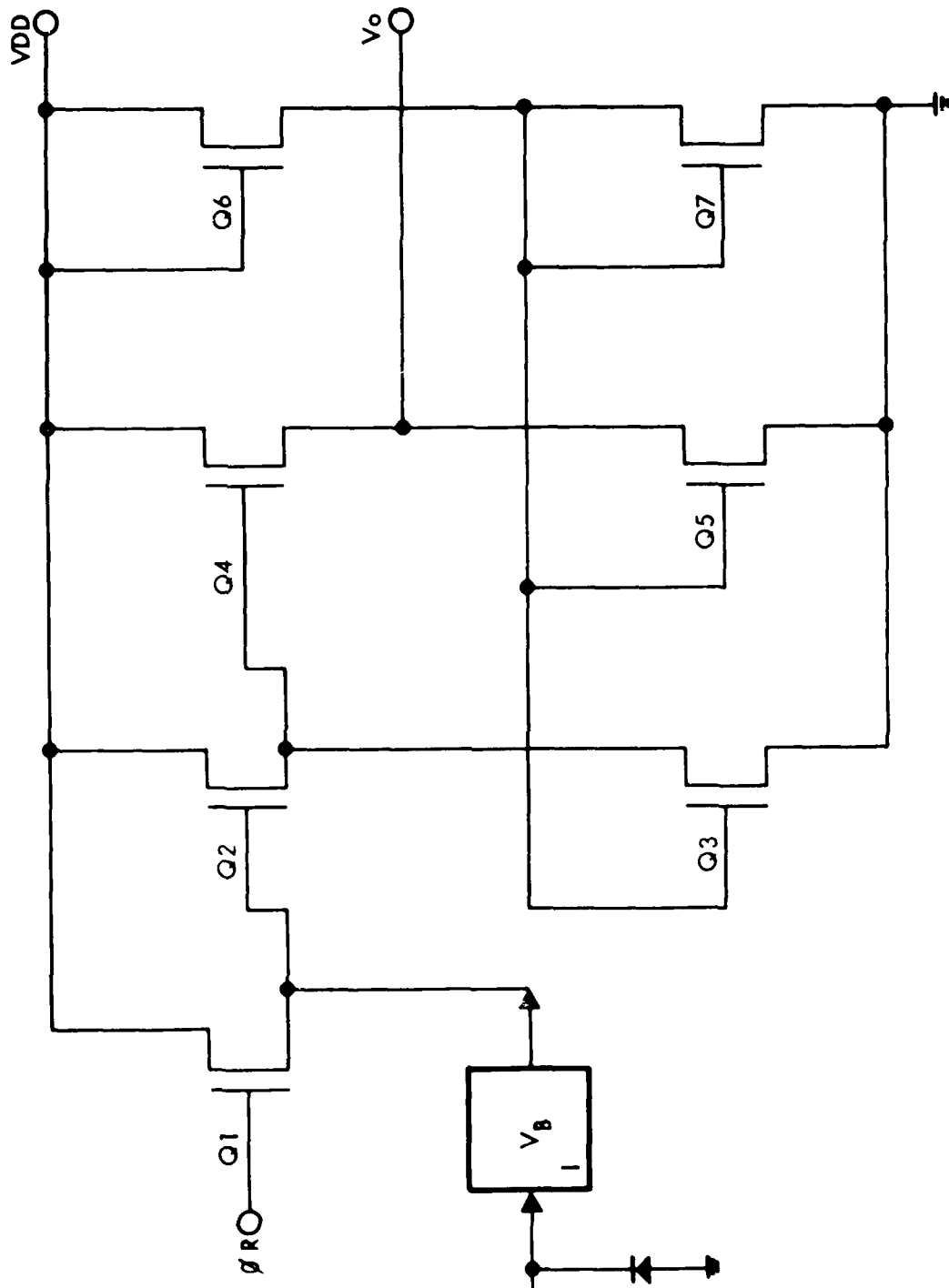


Figure 3-21. Schematic of the two stage source follower.



a cross coupled inverter pair which switch the output transistors  $Q_{15}$  and  $Q_{16}$  in a complementary fashion. In the tri-state mode  $EN1$  is low and the inverter, composed of  $Q_{18}$  and  $Q_{17}$ , turns both output transistors off through  $Q_{11}$  and  $Q_{14}$ . The load devices  $Q_9$  and  $Q_{12}$  are also turned off through  $Q_{20}$ . This was done in order to minimize the static current drawn in the tri-state mode and thus minimize the power dissipation.

The tri-state impedance is greater than 1 M $\Omega$ . The maximum operating frequency is 5.0 MHz driving a single low power schottky TTL input.

### 3.6 MEMORY CELLS

One of the most significant advantages of DCCD technology is the ability to integrate high density, large scale memories with high density digital logic circuits. A study of CCD memory applications indicated that a gap existed between existing high speed - high power bipolar and MOS memories and slower, high density magnetic memories; it was thought that this gap could be filled by CCD memories that combined the advantages of very high density, moderate speed and extremely low power requirements. Although CCD memories are significantly slower than the fastest bipolar memories, they are significantly faster than disc and bubble memory storage systems. The extremely high density of CCD memories permit their use for bulk storage applications. They can also be used effectively for both comparator and correlation functions, in addition to accumulation functions.

During the course of the memory development program, it became evident that the complex offset gate geometry (to be discussed later in this section) would have a significant impact on memory cell yields. The advantages of much higher bit density were offset by potential yield losses, due to a factor of two (2) increase in processing complexity. Combining a large number of offset gate memory cells for bulk storage applications appeared infeasible due to potential yield losses.

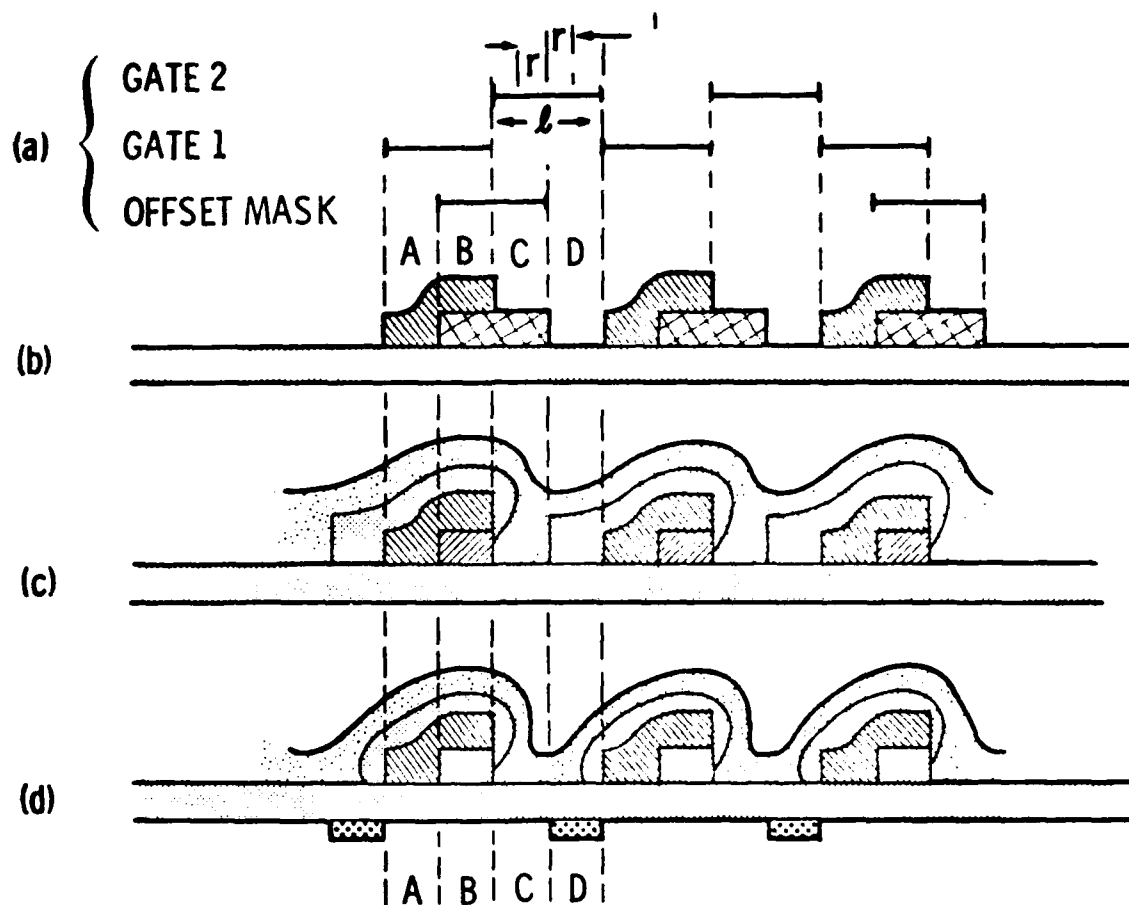
During 1975 and 1976, processing capabilities improved sufficiently to insure fabrication of conventional SPS memory blocks that employed 5 micron spacing. Memory block density therefore improved sufficiently to compete with offset gate device density; this was accompanied by yields that indicated the feasibility of interconnecting 2-kilobit memory blocks into 128 kilobit or 256-kilobit (large scale) memory arrays.

### 3.6.1 The Offset Gate Device Configuration

The initial design of the offset gate device consisted of two adjoining transfer-storage (t-s) regions, as shown in Figure 3-23. One t-s pair was connected to the Phase I clock, while another t-s pair was connected to the Phase II clock. The t-s regions were formed by electrically connecting adjacent pairs of overlapping gate structures. The properties of the two types of gates were chosen to create a transfer and storage region for the clocked charge packets, when connected to the same clock phase. Each pair of transfer and storage regions provided one minimum geometry unit,  $\ell_{\min}$ , equivalent to one-half of a bit length.

The offset gate device was formed with either one or two additional mask layers than required by a conventional two-phase overlapping-gate structure. Compared to conventionally configured devices, the offset gate geometry has a significant bit packing density advantage of 2x for both linear and parallel arrays, while the advantages of the offset gate structure over conventional serpentine and series-parallel arrays can be as great as a factor of four. Since each polygate electrode pair was connected to the same clock phase, short-circuits did not create functional problems when occasional strands of polysilicon shorted adjacent polygate structures together. Additionally, the two-phase clocking arrangement had a significant effect on the total number of contacts necessary for a given memory block. The conventional structure requires a minimum of two contacts per bit, along any shift register that cannot be accessed from both sides; the offset gate device required contacts only to the initial clock line inputs.

The concept of the offset gate device is shown in Figure 3-23. The first mask step is used to define the offset steps in the gate insulator, along the length of the CCD channel. The first gate electrode structure, comprised of polysilicon, is then aligned to the partially covered regions of thin dielectric (region A) which in this instance, is thermally-grown oxide. The polygate electrode also covered the thick dielectric (region B) as well. The step in the insulator beneath this gate created the t-s pair within each element of the gate structure. A step in the insulator also existed in the regions not covered by the gate electrodes, indicated in the diagrams as regions C and D; these regions had to be modified to produce a t-s pair for the subsequently deposited and defined metal gate electrode.



- a) Alignment considerations of offset masks with respect to the gate masks
- b) Use of an offset mask to produce a change in insulator thickness beneath a gate structure
- c), d) Illustration of the use of  $\text{Si}_3\text{N}_4$  and ion implantation respectively to produce the desired asymmetry for two phase operation

Figure 3-23. Offset gate device.

When an insulator step was used to define the t-s region, only one offset mask was required. After forming the first gate electrode structure, the gates were used as a mask to selectively remove and regrow the exposed dielectric in the channel region. A second offset mask could then be used to define a properly oriented t-s pair beneath the overlapping gate structure, to insure that the charge packets would be permitted to flow in the correct direction.

Figure 3-23 (a) shows in cross-section two of the masks necessary to make the offset gate structure and Figure 3-23(b) shows the two gate masks necessary for a standard (or conventional) overlapping gate two phase CCD. In Figure 3-23 the basic geometry unit is designated  $\ell$ , while  $r$  represents the mask alignment tolerance. Table 3-5 contains some comparisons for the two structures.

The design of the conventional two-phase overlapping gate CCD makes it independent of any mask misalignment  $m$ , that is less than the maximum tolerance,  $r$ . The column of values listed in Table 3-5 reflects this fact. The offset gate device is, however, dependent upon the accuracy of mask-to-mask alignment. One column in Table 3-5 gives the nominal values when  $m = 0$ ; the other column lists the appropriate values for  $m < r$ . Since  $m$  can be positive or negative, the sign associated with the worst-case situation is shown. In the nominal case, the offset gate device had more than a factor of two improvement in power dissipation, more than a factor of four improvement in maximum operating frequency, and more than a square root of two degradation in signal-to-noise ratio. The variations are direct consequences of the storage length reduction in the offset gate device. There is no change in the parallel edge effect, since both device configurations are assumed to have the same channel width. It is worth noting that loss in the signal-to-noise ratio can be regained by allowing wider channels for the offset gate device. This will produce signal-to-noise ratios equal to, or better than those for the conventional device, while maintaining a bit area advantage for the offset gate device.

CCD-1 was the designation of the mask set that was in use when this program was initiated. The mask set was designed to allow production of conventional two or four phase CCD shift registers in both serial and serpentine organizations. Offset gate devices could also be produced with both serial and serpentine organizations. Table 3-6 summarizes the shift register devices that appeared on mask set CCD-1. The table includes the bit length of the serial devices

Table 3-5. Implementation comparison for Equal Channel Widths.

Parameter	Standard Two Phase Overlapping Gate	Offset Gate	
		Nominal Value	Value for Misalignment $m$
Total Length/Bit	$4(\ell + r)$	$2\ell$	$2\ell$
Storage Length/Bit	$(\ell + 2r)$	$\ell/2$	$\ell/2 + m$
Transfer Length/Bit Area/Bit Parallel	$\ell$	$\ell/2$	$\ell/2 + m$
Series-Parallel-Series Serpentine	$8\ell(\ell + r)$	$4\ell^2$	$4\ell^2$
	$8(\ell + r)^2$ **	$4\ell^2$	$4\ell^2$
	$(8 + 4\sqrt{2})\ell^2 + 4\sqrt{2}\ell r$	$4\ell^2$	$4\ell^2$
On Chip Power/Bit	$P_D$	$\frac{P_D}{2}(1 + 2r/\ell)$	$\frac{P_D}{2}(1 + 2m/\ell)/(1 + 2r/\ell)$
Maximum Frequency	$f_m$	$4f_m(1 + 2r/\ell)^2$	$4f_m(1 + 2r/\ell)^2/(1 + 2m/\ell)^2$
Signal to Noise Ratio*	SN	$SN/(2 + 4r/\ell)^{1/2}$	$SN(1 - 2m/\ell) \left[ \frac{1}{2 + 4r/\ell} \right]^{1/2}$
Parallel Edge Effect Loss	$\epsilon_{pE}$	$\epsilon_{pE}$	$\epsilon_{pE}$

\* Assuming fast surface state noise is the dominant component

\*\* Assuming a clocking scheme that allows interleaving data; no such interleaving is required in the offset gate device.

Table 3-6. CCD-1 shift register devices.

Device Type	Device Length (Bits)	Serial Bit Length (Microns) Or Serpentine Bit Density	Device Organization
		(Microns <sup>2</sup> /Bit)	
Standard	8	86.4	Serial
Standard	8	43.2	Serial
Standard	64	43.2	Serial
Standard	128	1187.	Serpentine
Standard	128	1187.	Serpentine with Refresh
Offset Gate	8	20.3	Serial
Offset Gate	24	309.7	Serpentine
Offset Gate	72	309.7	Serpentine

and the bit density of the serpentine devices. In all cases, the CCD channel width was 7.5 microns. In addition to producing offset gate devices, CCD-1 allowed evaluation of the effects of turning corners, as is required by serpentine organizations. An examination of the results obtained by testing these devices indicated that the offset gate geometry was producible and operated as expected, when compared to conventional shift register-type device configurations. Tests also indicated that the serpentine devices suffered no degradation in performance as a result of corner-turning. The success of CCD-1 was used as a basis for the generation of a second mask set, designated LSM-1.

The LSM-1 mask set was devoted primarily to the production of offset gate devices. The mask set was designed to allow further evaluation of these devices, particularly the serpentine organization. In addition, refresh circuits were designed and included on this mask set for the first time. These refresh circuits were specifically designated to fit within the space of two serpentine shift registers; this restriction necessitated the use of several untested circuit concepts. While the LSM-1 mask set did provide additional experience producing offset gate devices, the main impact on the program was the experimental results, indicating that the use of silicon nitride in the gate structure was undesirable. This conclusion was based upon processing difficulties caused by the  $\text{Si}_3\text{N}_4$ , rather than by high fast surface state density ( $N_{ss}$ ) levels. It was discovered that the refresh circuit designs included on the LSM-1 chip did not function in the required manner. While a fix of this problem was devised, the continuing evaluation of overall system trade-offs indicated that an SPS structure was far more useful than a serpentine structure. The net result was that the refresh circuit design for the serpentine structure was set aside. Consequently, a new mask set design that concentrated on the SPS memory was begun and was designated CCD-2.

The serial-to-parallel-to-serial (SPS) shift register design concept has been known for some time. Figure 3-24 illustrates the organization of such a shift register as well as the lines of data flow. The data comes in serially, is then clocked along the parallel registers and finally shifted out of the memory cell serially.

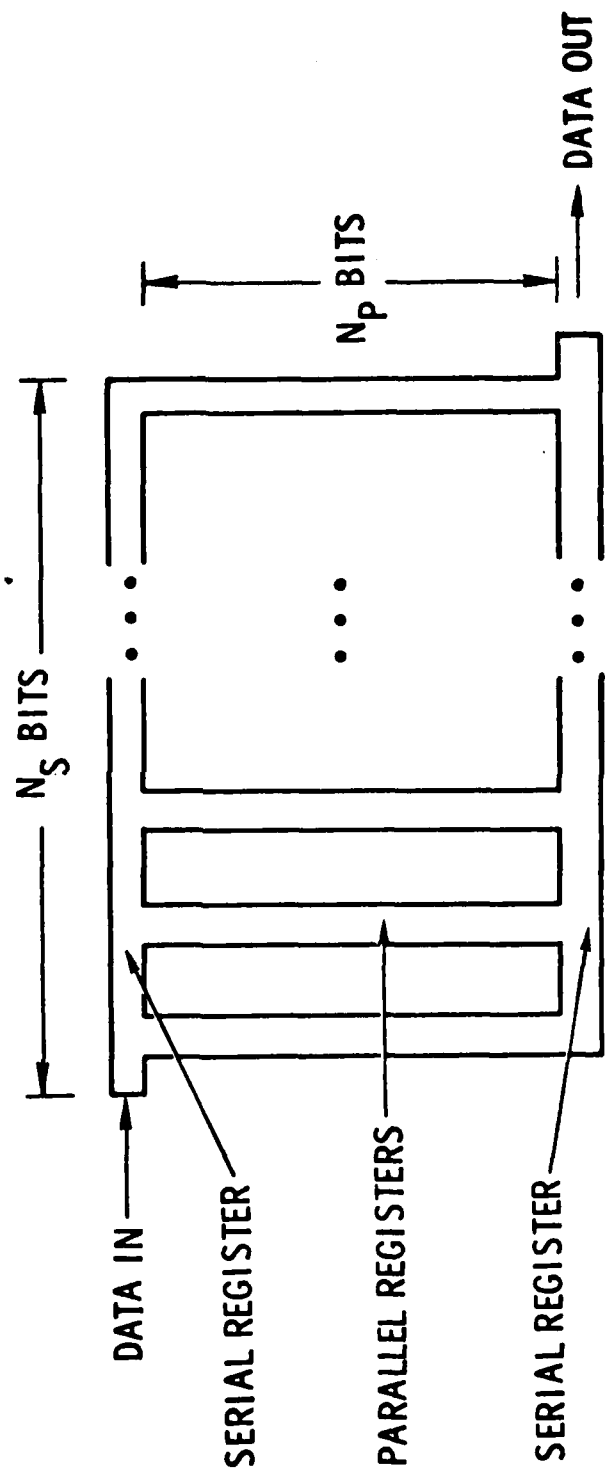


Figure 3-24. Organization of a serial-parallel-serial shift register.

Operation of an SPS register was different for the offset gate device than for the standard or conventional two phase device. The difference arises from the fact that maximum bit density is dependent upon the spacing between the parallel shift registers. Thus, the optimum spacing of parallel channels corresponds exactly to the spacing of the clock phases in the offset gate serial register, whereas, it corresponds to a distance equal to one-half the spacing of the phases in the standard serial register, as shown in Figures 3-25, 3-26, 3-27, and 3-28. Consequently, to achieve maximum density with an SPS memory built from a conventional structure, it is necessary to interleave the parallel registers in the following manner:

The input serial register is loaded until all data resides under Phase III serial gates; then a parallel transfer of data occurs. This event is followed by a reloading of the input serial register, such that all data now resides under Phase I serial gate structures. Parallel transfer of the data again occurs, thereby insuring that all data is stored in the first location of the interleaved parallel shift registers. The parallel register is clocked one bit and the serial load procedure is repeated. A similar procedure is used again as a means of unloading the data through the output serial register. In order to achieve maximum bit density with a conventional or standard SPS structure, it is necessary to provide a special clock waveform for the strobe lines that allow data to enter and leave the parallel registers. The strobe occurrence must be synched to the Phase I clock for one-half of the cycle; then, synched to the Phase III clock for the following half cycle. The high density structure permits a simpler clocking scheme for the strobe lines, as a result of the fact that only one serial load per parallel clock is required instead of two as described above for the conventional structure.

To appreciate the implications of the two types of CCD organizations, consider Figure 3-29. The minimum geometry dimension permitted by the mask design rules was designated by  $\ell$ ; the minimum mask overlap required was labeled  $r$ . Part a) of Figure 3-29 shows the well-known result that a total length of  $4(r + \ell)$  is required for each bit of a standard structure CCD. Similarly, part c) shows that a length of  $4\ell$  is required to build a high density CCD, starting with the structural design. Part b) of Figure 3-29 shows what can be done if a standard structure design is implemented using the high density technique. Note that there is a factor of two improvement in required bit length in comparison to the structure of part a) and the best improvement is obtained

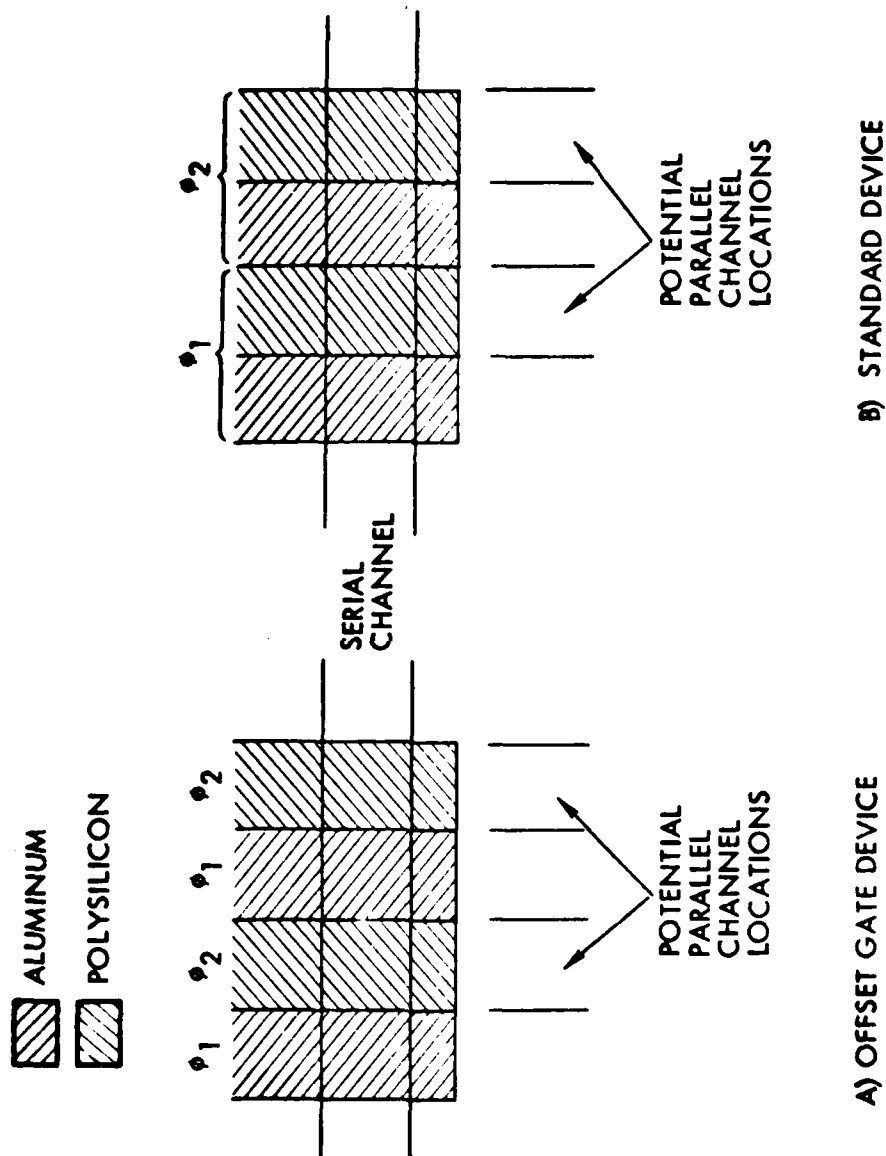


Figure 3-25. Location of parallel channels for maximum density.

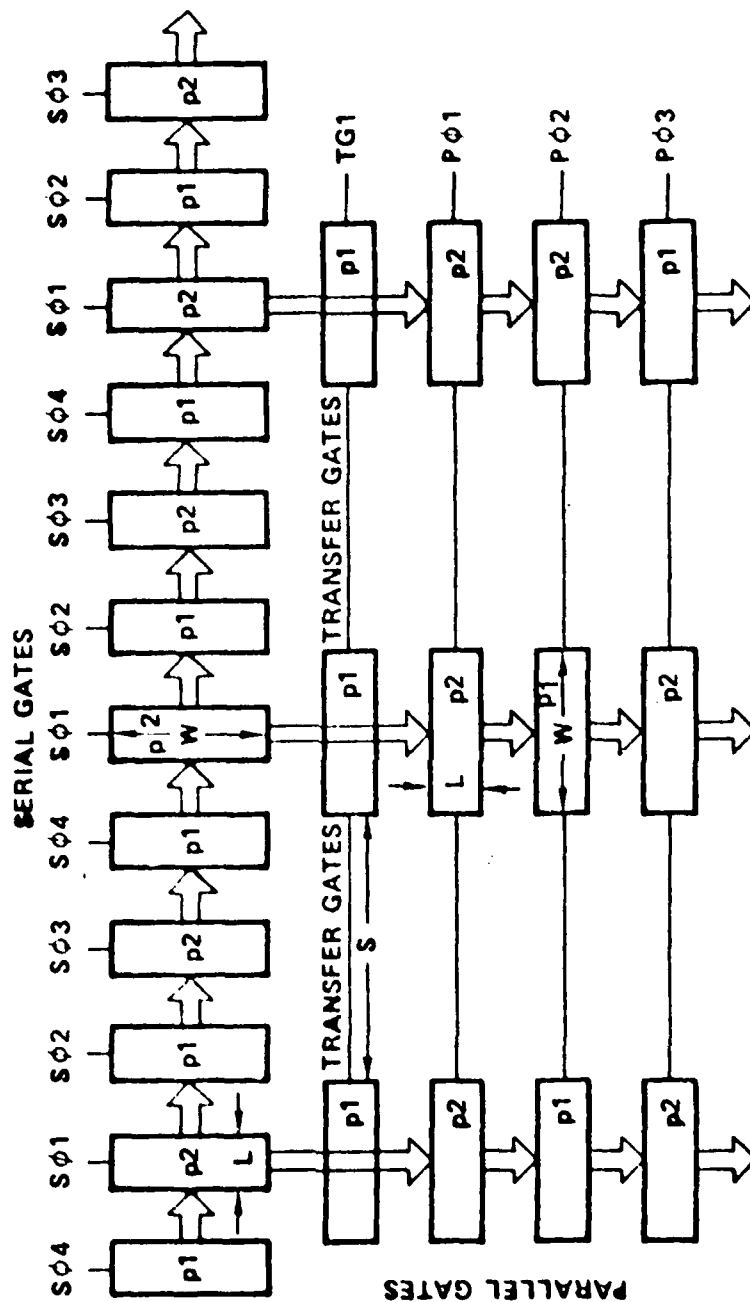


Figure 3-26. A Typical SPS Structure.

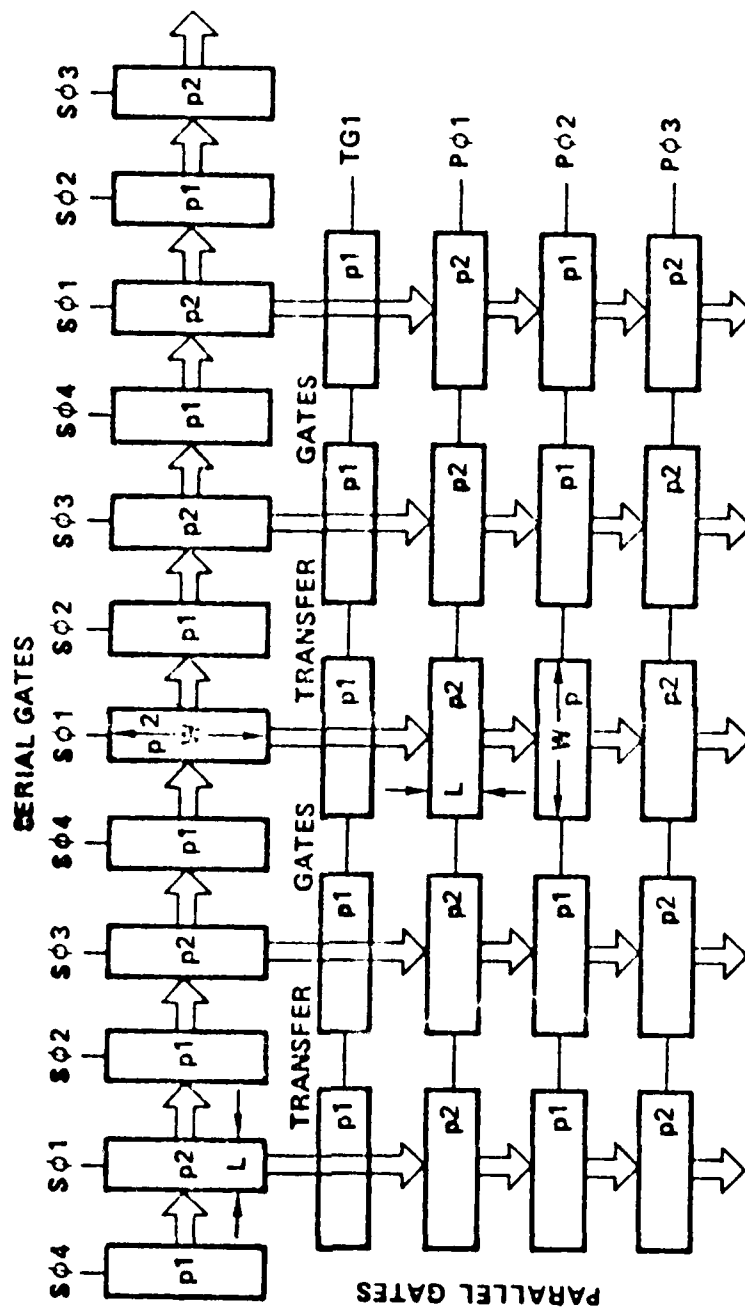


Figure 3-27. Serial to parallel interlaced SPS structure.

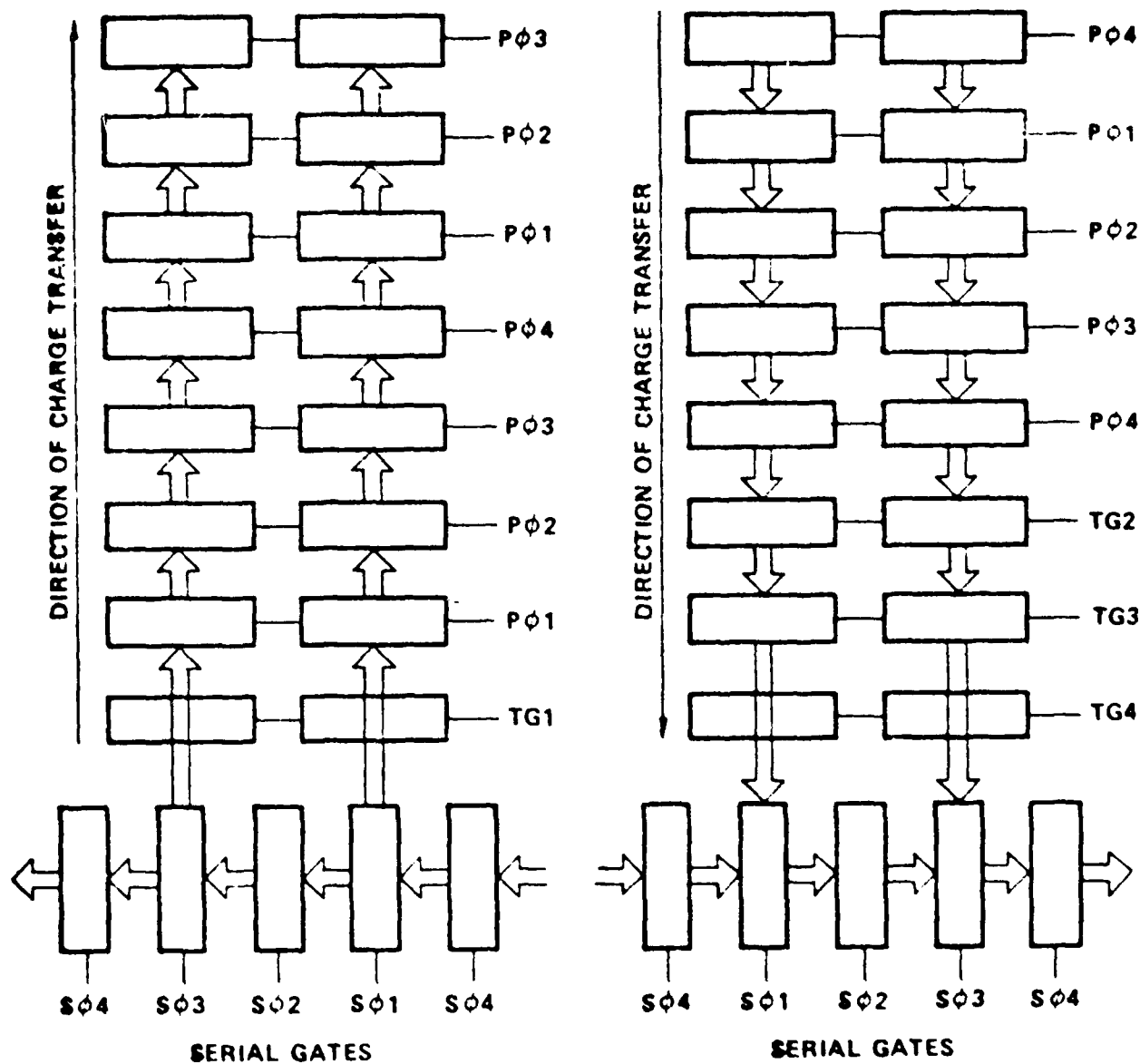


Figure 3-28. Clocking system required to change from LIFO read-out to read-in.

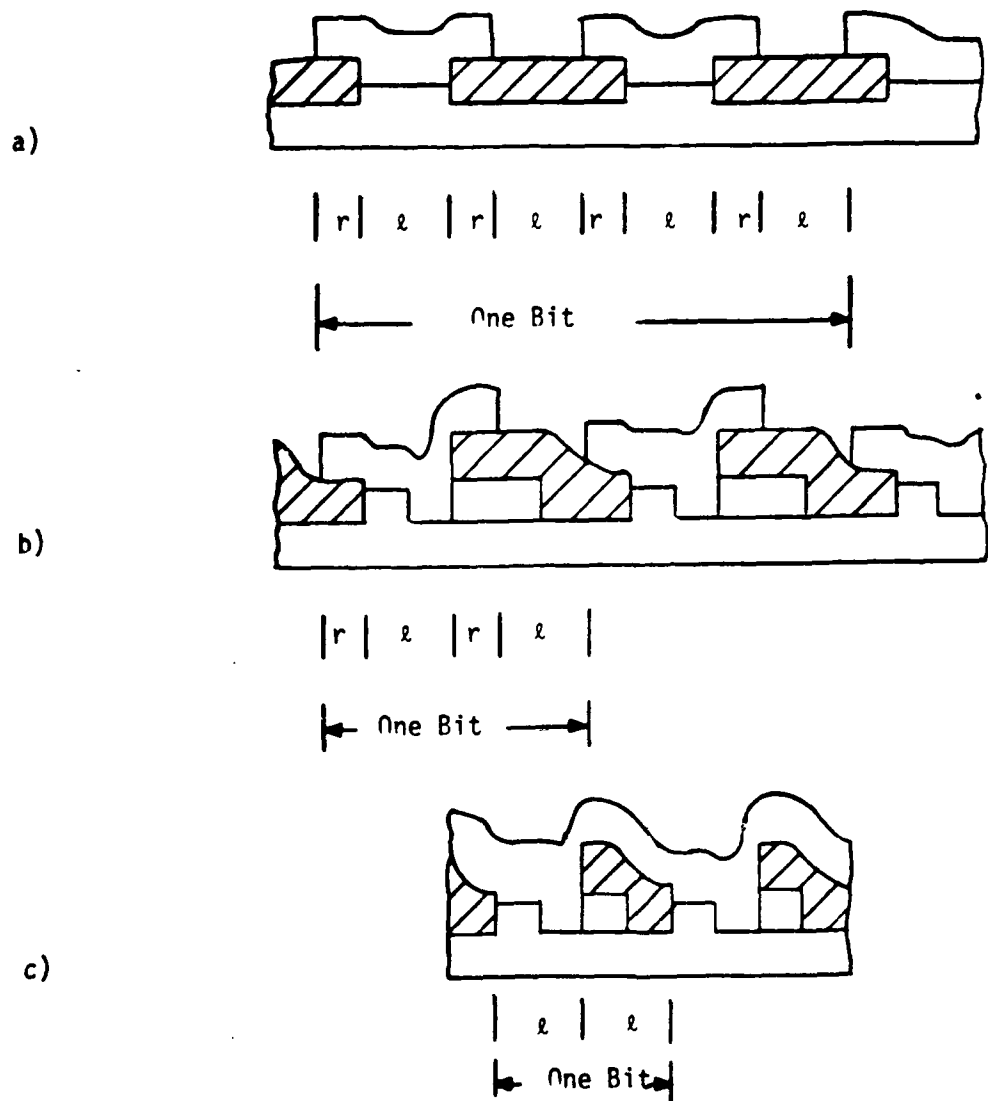


Figure 3-29. Comparison of device structures  
 (a) Standard device structure  
 (b) High density device built with original standard structure design  
 (c) High density device built with original high density structure design

by the structure of part c). Figure 3-30 quantifies this statement, by showing the required bit length as a function of  $(r/l)$ .

Examination of the parallel section of an SPS memory can provide information as to the required area per bit. This is provided in Table 3-7, where data interleaving is assumed to exist for the standard structure.

Figure 3-31 provides the required area per bit as a function of the  $(r/l)$  ratio. Thus, it is seen that for any SPS memory, the high density (offset gate) approach will always have an area advantage of at least a factor of two. In essence, the high density approach will produce at least twice as many bits for a given chip size as the standard approach.

Assuming the implementation of an SPS organization, there are several methods of optimizing the structure. The two most important approaches are: (a) minimize the total number of transfers,  $N_T$ , necessary to move a data bit from input to output, and (b) minimize the total power,  $P$ , required to operate the SPS device.

In performing these minimizations, it is reasonable to assume that the total storage capacity,  $S$ , and the input frequency,  $f_s$ , are dictated by other system requirements and therefore are fixed. Table 3-8 lists the basic structure.  $C_{BIT}$  is the capacitance per bit (including both Phase I and Phase II components) and is assumed proportional to the total storage area per bit. Table 3-9 shows the parameter values for the two optimization approaches while Table 3-10 compares these two approaches. Note that as  $S$  becomes large, the ratios in Table 3-10 approach limiting values. The offset gate structure ratios both approaches and indicates a value of 1.06; this indicates that for a large storage capacity,  $S$ , a design that is optimized for minimum power will in fact require only 6% more transfers than a design that is optimized for minimum transfers. The same is true for power required by a design optimized with respect to transfers. In actuality, the two optimum conditions are quite similar. The standard structure, on the other hand, shows a limiting value of 25% between the two design approaches. It is evident that the offset gate structure can achieve near optimum operation with respect to both  $N_T$  and  $P$  with one design, while the standard structure cannot. (Unfortunately, when ease of fabrication and yields are taken into consideration, the ability to build the standard memory cell outweighs the offset gate configuration in every respect.)

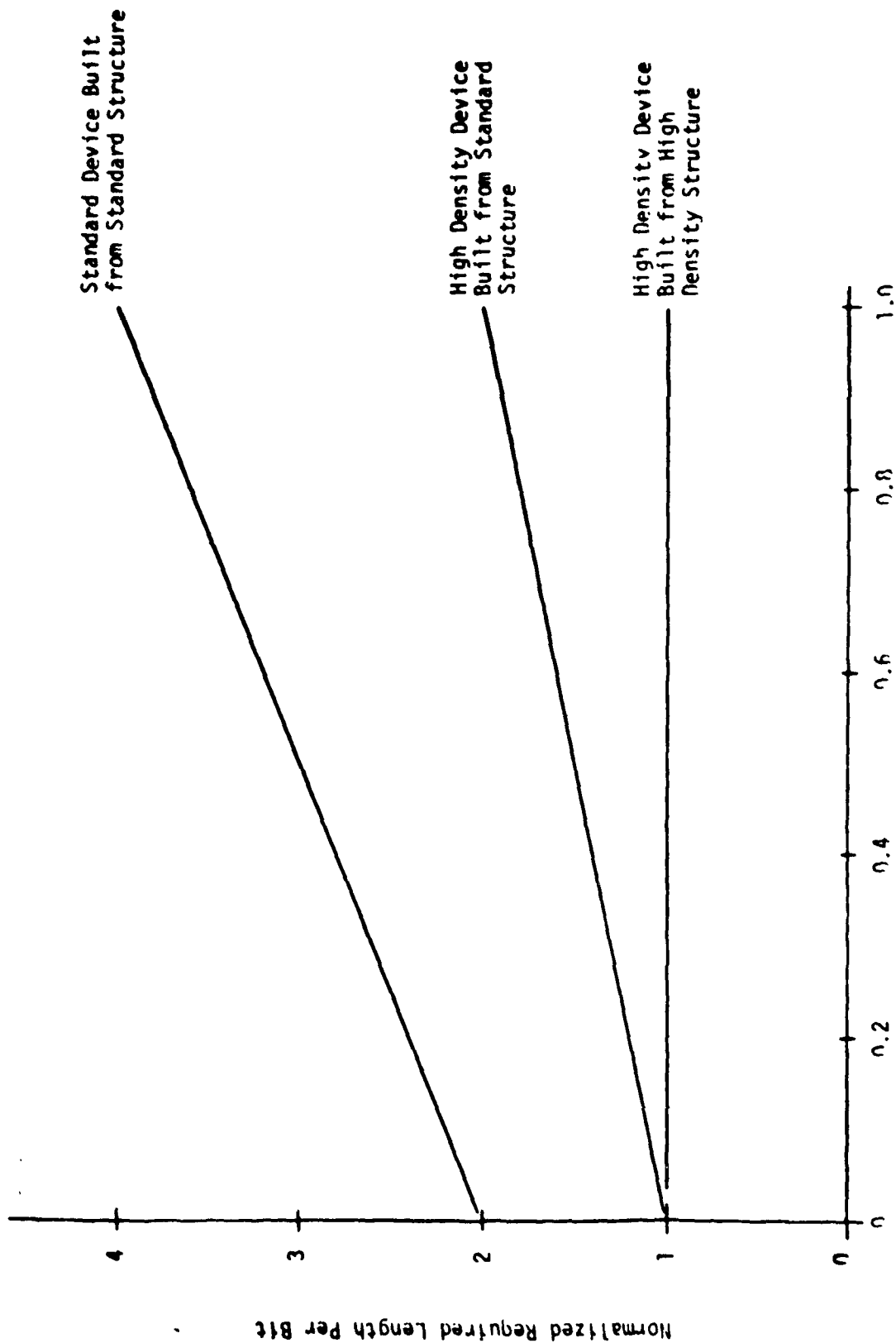


Figure 3-30. Normalized required length per bit as a function of the ratio of mask misalignment tolerance,  $r$ , to minimum geometry length,  $\lambda$ .

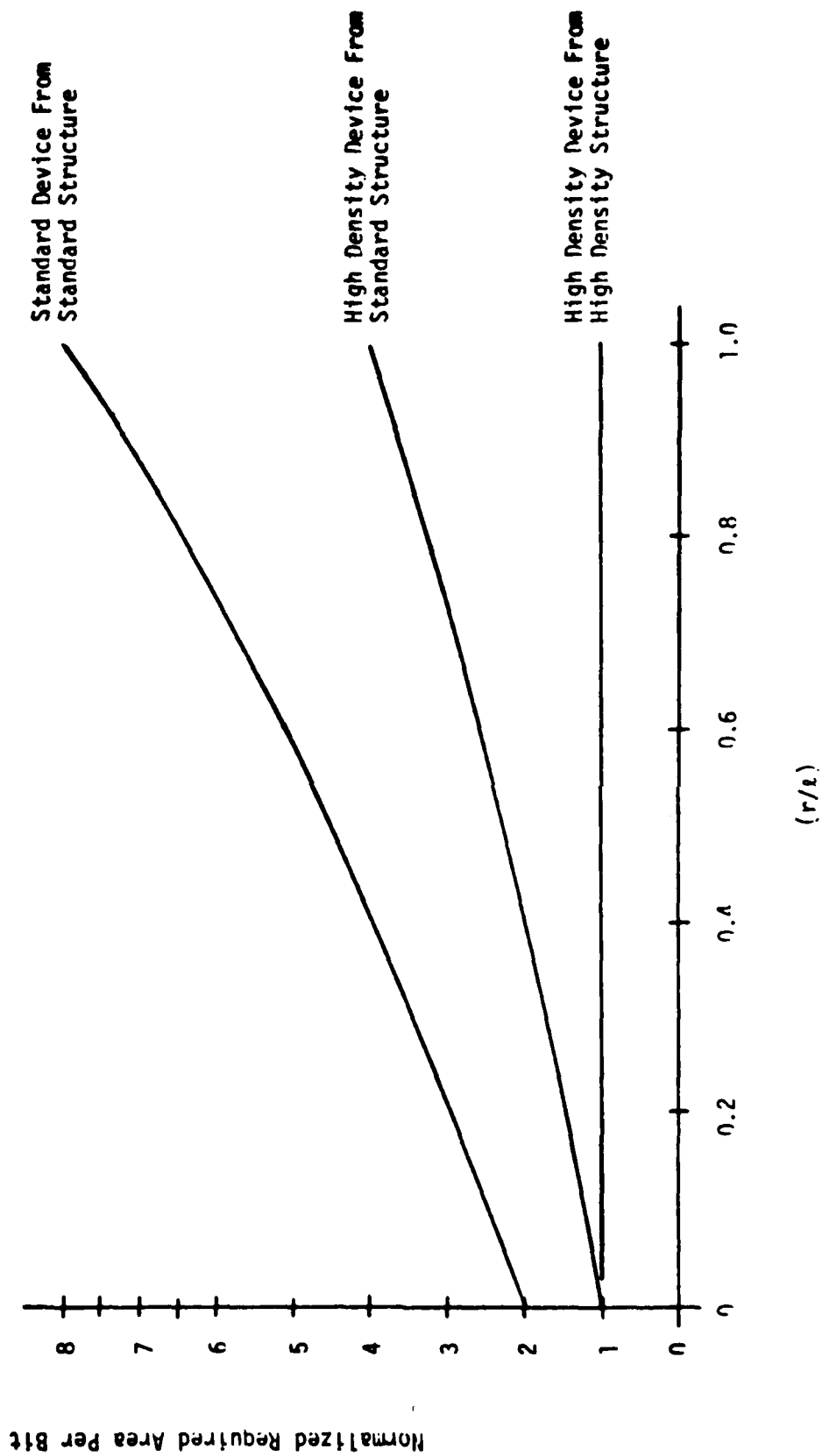


Figure 3-31. Normalized required area per bit as a function of the ratio of mask misalignment tolerance,  $r$ , to minimum geometry length,  $l$ .

Table 3-7. Required area per bit for the devices of Figure 3-29.

<u>Device Type</u>	<u>Area per Bit</u>
Standard Device From Standard Structure	$8(l + r)^2$
High Density Device From Standard Structure	$4(l + r)^2$
High Density Device From High Density Structure	$4l^2$

Table 3-8. Basic SPS relationships.

Item	Symbol	Interrelationship	
		Offset Gate	Standard
Serial Shift Register Length (Bits)	$N_s$	$N_s$	$N_s$
Parallel Shift Register Length (Bits)	$N_p$	$N_p$	$N_p$
Storage Capacity (Bits)	$S$	$N_s N_p + N_s$	$2 N_s N_p + N_s$
Total Number of Transfers	$N_T$	$2 (N_s + N_p)$	$2 (N_s + N_p)$
Serial (Input/Output) Frequency (Hz)	$f_s$	$f_s$	$f_s$
Parallel Frequency (W2)	$f_p$	$f_s / N_s$	$f_s / (2 N_s)$
Capacitance Per Bit (forads)	$C_{Bit}^*$	$K(e^2)$	$K(2e[\lambda + ]r])$
Power Per Bit (watts)	$P$	$V^2 C_{Bit} f_s [2 N_s + N_p]$	$V^2 C_{Bit} f_s [2 N_s + N_p / 2]$

\*K is the proportionality factor relating area to capacitance.

Table 3-9. Optimized SPS parameter values.

Parameter	Offset Gate	Standard
$\left. \begin{array}{l} N_s \\ N_p \\ P \\ N_T \end{array} \right\}$ Minimum $N_T$	$\sqrt{S}$	$\sqrt{S/2}$
	$\sqrt{S} - 1$	$\sqrt{S/2} - 1/2$
	$C_{Bit} f_s [3\sqrt{S} - 1]$	$C_{Bit} f_s [5\sqrt{S/2} - 1/2]/2$
	$4\sqrt{S} - 2$	$2\sqrt{2S} - 1$
$\left. \begin{array}{l} N_s \\ N_p \\ P \\ N_T \end{array} \right\}$ Minimum $P$	$\sqrt{S/2}$	$\sqrt{S/2} / 2$
	$\sqrt{2S} - 1$	$\sqrt{2S} - 1/2$
	$v^2 C_{Bit} f_s [2\sqrt{2S} - 1]$	$v^2 C_{Bit} f_s [\sqrt{2S} - 1/4]$
	$3\sqrt{2S} - 2$	$5\sqrt{2S} / 2 - 1$

Table 3-10. Comparison of the minimum number of transfers and minimum power optimizations for SPS units.

	Offset Gate	Standard
$\frac{N_T (\text{Min } P)}{N_T (\text{Min } N_T)}$	$\frac{3\sqrt{2S} - 2}{4\sqrt{S} - 2} \approx \frac{3\sqrt{2}}{4} = 1.06$	$\frac{5\sqrt{2S} / 2 - 1}{2\sqrt{2S} - 1} \approx \frac{5\sqrt{2} / 2}{2\sqrt{2}} = 1.25$
$\frac{P (\text{Min } N_T)}{P (\text{Min } P)}$	$\frac{3\sqrt{S} - 1}{2\sqrt{2S} - 1} \approx \frac{3}{2\sqrt{2}} = 1.06$	$\frac{(5\sqrt{S} / 2 - 1/2) / 2}{\sqrt{2S} - 1/4} \approx \frac{5/(2\sqrt{2})}{\sqrt{2}} = 1.25$

Table 3-11 compares the offset gate and standard structures for both of the optimizations. The table indicates that the number of transfers in the standard structure is less than those provided by the offset gate structure, when both are designed for minimum  $N_T$ . On the other hand, the offset gate structure will require less power when both are designed for minimum  $P$ ; the actual value of the power ratio depends upon the value of  $(r/l)$ , as expected. Assuming a photolithographic capability of 7.5 microns and an optimistic misalignment tolerance of one micron, Table 3-11 predicts that the standard structure requires 27% more power. If a 5 micron photolithographic capability is assumed, a power increase of 40% can be expected. This fact holds true as the misalignment tolerance does not scale down with an improvement in photolithographic capabilities. The implications are clear; as technology improvements permit greater device density, the advantages of implementing the offset gate geometry would seem to increase. Factors that limit the use of the offset gate device technology below 5 microns will be covered in a subsequent discussion.

One additional advantage of the offset gate structure should be noted here. The ability to use a single level of metal or polygate structures, covering both storage and transfer regions, permitted the offset gate configuration to use significantly fewer contacts per SPS memory cell than standard two-phase designs. It was shown that the standard structure required  $4N_S$  clock line contacts per SPS, while the offset gate configuration required only the initial pair. This fact alone should have provided a decided improvement in offset gate device yields and corresponding reliability, if not counterbalanced by substantial processing complications that severely limited device yields and reliability.

The CCD-2 mask set was designed using a minimum geometry gate length of 7.6 microns and a mask misalignment tolerance of 2.54 microns. The basic element used on CCD-2 was an SPS memory that stored 2048 bits as a standard device, or 4098 bits as a high density device. (One of the original purposes of this mask set was to produce standard or conventional shift register memory as well as SPS memory and use both types of memory building blocks for structural and electrical comparisons. The mask set did not maximize each of the two structures for bit density, as the ability to do a one-on-one comparison of the conventional versus the SPS structure would have been lost. As a matter of

Table 3-11. Comparison of offset gate and standard structure  
SPS units for both optimizations.

$N_T$ (Min $N_T$ , Standard)	$\frac{2\sqrt{2S} - 1}{4\sqrt{S} - 2} = \frac{2\sqrt{2}}{4} = 0.707$
$N_T$ (Min $N_T$ , Offset Gate)	
$\frac{P}{P} \left( \frac{\text{Min } P, \text{ Standard}}{\text{Min } P, \text{ Offset Gate}} \right)$	$\frac{C_{\text{Bit}_{\text{STD}}} f_s (\sqrt{2S} - 1/4)}{C_{\text{Bit}_{\text{OG}}} f_s (2\sqrt{2S} - 1)} = \frac{C_{\text{Bit}_{\text{STD}}}}{2 C_{\text{Bit}_{\text{OG}}}} = (1 + \frac{2r}{x})$

convenience, it was decided to put four SPS memories on each chip; thus each chip contained a total of  $8192 \times 2$ , or 16,384 bits. This particular chip design was also viewed as an excellent vehicle to determine SPS yields, that were affected by area related factors (i.e., oxide pin holes; random crystallographic defects; polysilicon and metal pattern- related shorts and opens; and step coverage).

Table 3-12 lists all of the mask levels designed into the CCD-2 mask set. This mask set permitted several variations of the basic design; the mask set had the capability of producing a double poly CCD structure, in which all gates were formed from either the first polysilicon layer (Poly I) or the second polysilicon layer (Poly II); no aluminum gate structures were employed in the double polygate configuration.

Table 3-13 summarizes some of the pertinent factors of the standard CCD as well as the high density designs included on CCD-2. It is worth mentioning that the standard SPS was designed to give the highest bit density possible for the photolithographic capability available at that time (this included minimum dimensions for line widths of 7.6 microns and maximum misalignment tolerance of 2.54 microns). The high density SPS was designed to be mask compatible with the standard SPS structure; thus, the high density SPS structure's bit density is not the absolute highest density achievable at that time.

Figure 3-32 is a photomicrograph (SEM) of an SPS memory block taken from a CCD-2 chip. There are 64 bits in the parallel and serial registers of the offset gate version; there are 32 bits in each register for the standard version. Test results from the CCD-2 mask set were encouraging. It was felt at the time that 4 kilobits were not sufficient as a demonstration device and a larger SPS structure was needed. Consequently, the 16 kilobit structures used on the LSM-2 mask set were designed and fabricated.

The mask set designated LSM-2 was used as a test vehicle for the 16 kilobit SPS structures. The overall layout is shown in Figure 3-33, which is a photomicrograph of a typical LSM-2 chip. The circuits of primary concern are the two 16 kilobit SPS blocks (one designed for 7.5 micron photolithography and shown in Figure 3-34 and the other designed for 5.0 microns, as shown in Figure 3-35).

Table 3-12. CCD-2 Mask levels.

Level Numbers	Function	Standard Version	High Density Version	Double Poly Version
1	Defines all p+ regions	X	X	
2	Defines CCD and FET channel	X	X	
3	Defines offset gate region		X	
4	Defines all polysilicon	X	X	
5	Defines contact holes	X	X	
6	Defines aluminum	X	X	
7	Defines passivation	X	X	
8	Defines protected region during channel etch	X	X	
9	Defines polysilicon			X
10	Defines contacts			X
11	Defines aluminum			X
12	Defines guard ring	X	X	
13	Defines pre-contact			X
14	Defines contact			X

Table 3-13. Comparative SPS layout values  
of CCD-2.

	High Density SPS	Standard SPS
Bits/SPS	4096	2048
Microns <sup>2</sup> /Bit/SPS	413.	826.
SPS/Wafer	300	300
Bits/Wafer	$1.2 \times 10^6$	$6.1 \times 10^5$
Micron <sup>2</sup> /Bit/Wafer	$1.7 \times 10^3$	$3.3 \times 10^3$

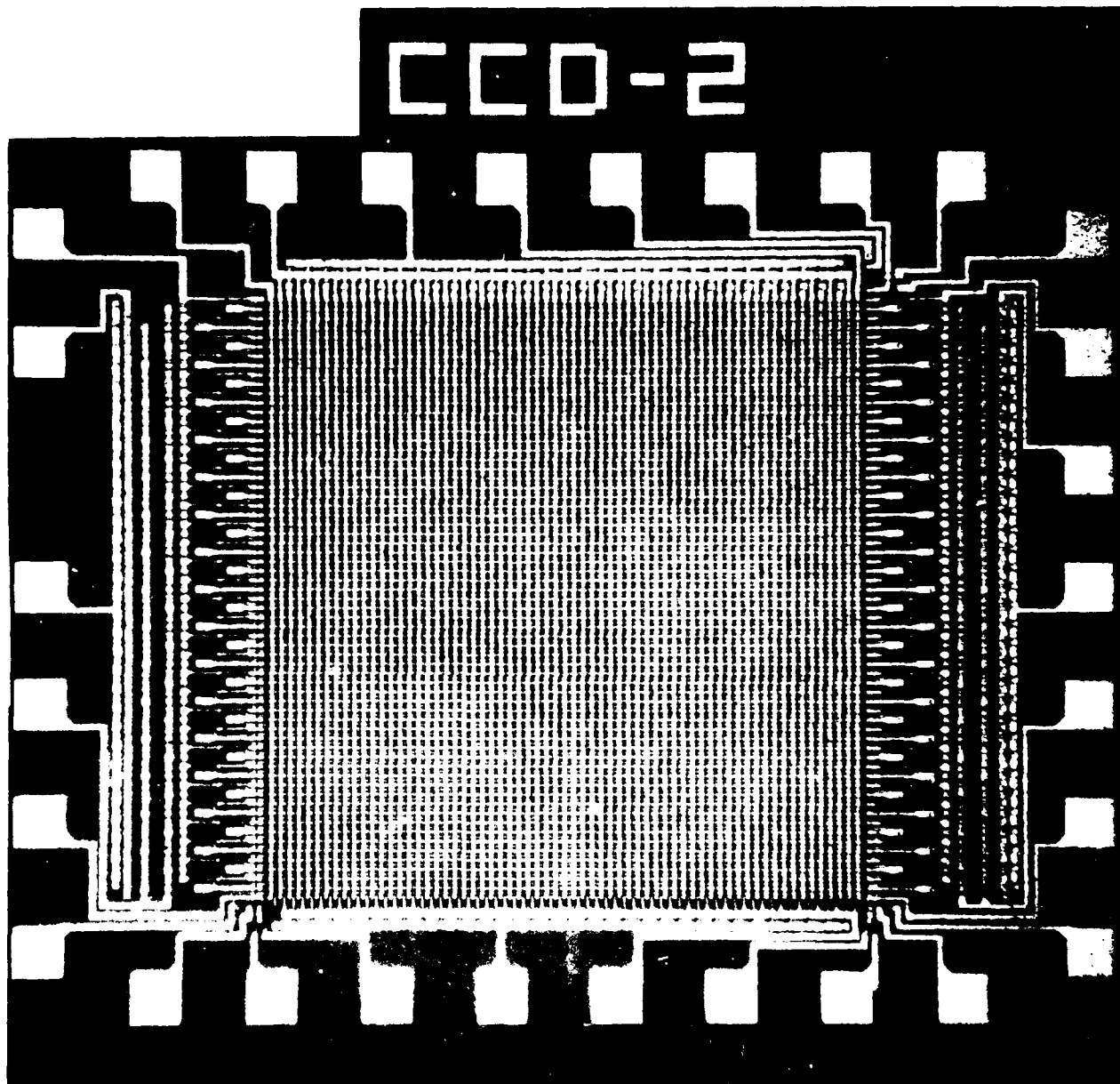


Figure 3-32. CCD-2 SPS memory device.

AD-A084 829

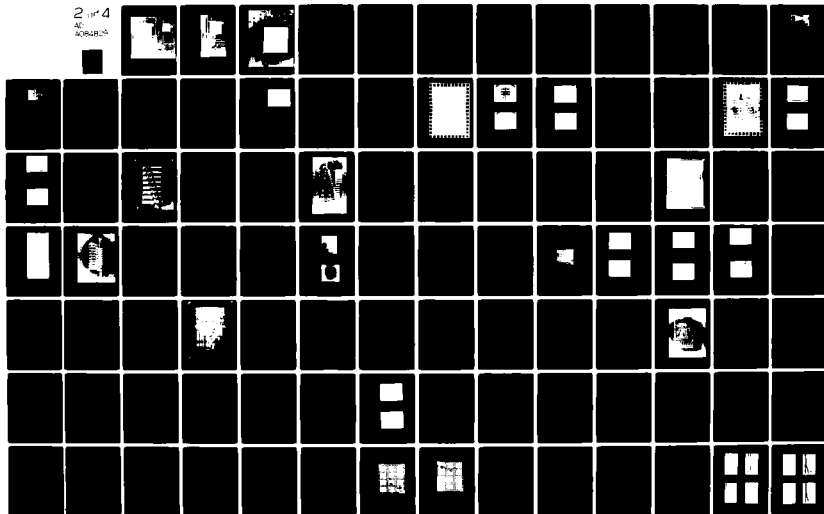
TRW DEFENSE AND SPACE SYSTEMS GROUP REDONDO BEACH CA F/G 9/1  
CHARGE COUPLED DEVICES IN SIGNAL PROCESSING SYSTEMS. VOLUME V. --ETC(U)  
DEC 79 R A ALLEN; J M ANDERSON; F G HAMILTON N00014-74-C-0068

UNCLASSIFIED

NL

2 of 4

AD-A084 829



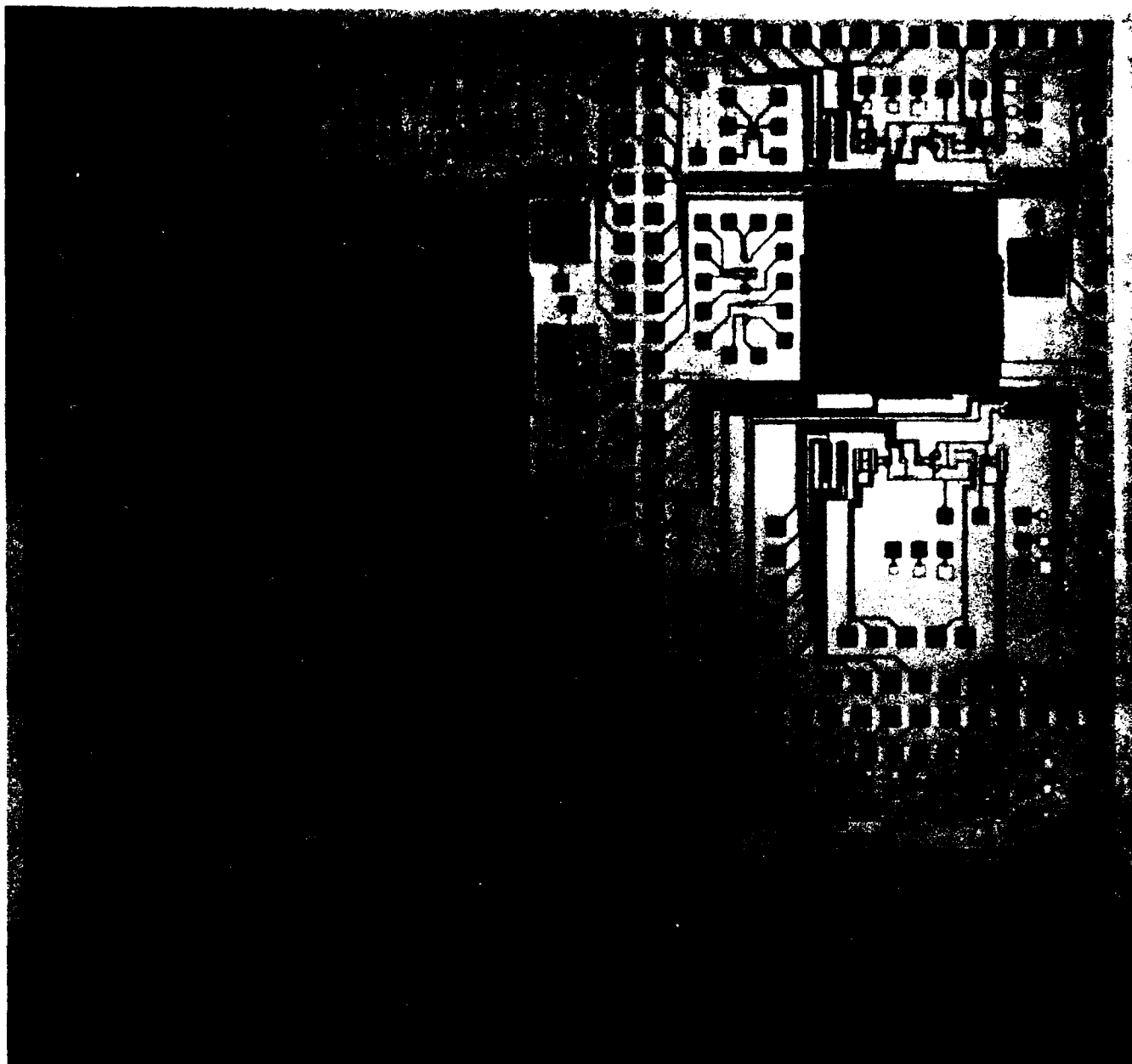


Figure 3-33. Photomicrograph of a typical LSM-2 chip.



Figure 3-34. 16 K-bit SPS unit designed for 7.5 micron photolithography.

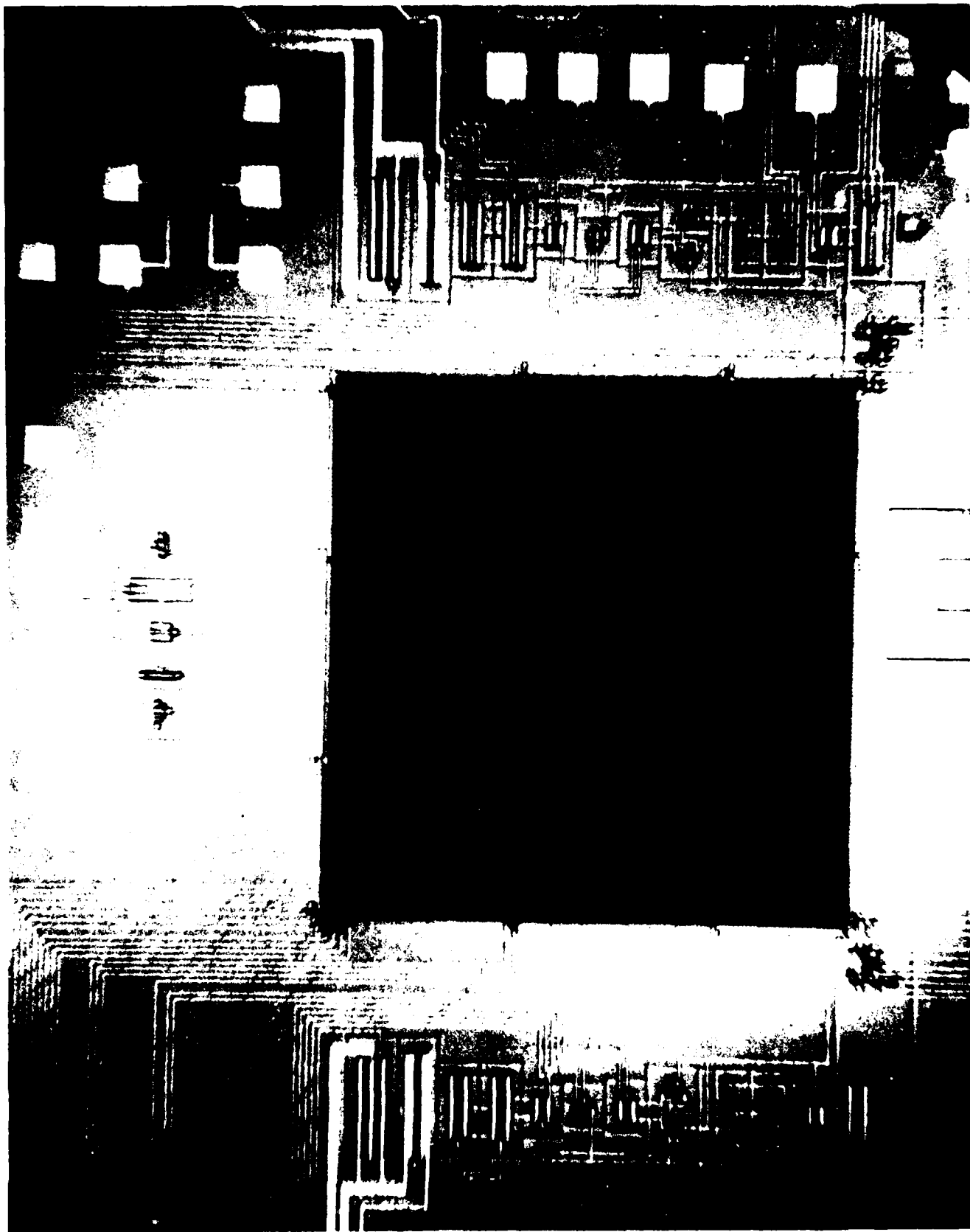


Figure 3-35. 16 K-bit SPS unit designed for 5.0 micron photolithography.

The design of the two SPS blocks are quite similar; both have  $N_s = N_p = 128$ . This particular choice was dictated by ease of testing rather than by a desire to achieve any particular design criteria. Choosing a binary number for  $N_s$  and  $N_p$  permits the use of simple, available test equipment and control logic. All of the parameters of interest, such as transfer loss, dark current and surface state density, can be measured on such a device. A summary of some of the pertinent design parameters is given in Table 3-13.

Figure 3-36 contains a general schematic plan view of the LSM-2 SPS layout, showing the overall organization. The dual output circuits are identified; they allow testing of the serial input register alone. Also shown are the two input circuits, one for providing a "fat zero" charge and the other for providing the signal charge. The cross-sections show the general make-up of the gate structures and indicate some typical oxide thickness (approximately 1000Å). Those gates that could be controlled independently and those that were bussed together are so indicated.

It is worth noting that a total of 19 LSM-2 device lots were fabricated, including five single polysilicon lots, as well as 14 double polysilicon lots. Table 3-14 is a compilation of the results that were obtained from the LSM-2 and LSM-3 mask sets.

#### 3.6.1.1 LSM-3 Device Test Results

Two lots, totaling six wafers, were processed using the LSM-3 processing sequence. The transfer inefficiency of the memory input serial registers was .003 - .004 for the 7.5 micron geometry devices and .005 for the 5 micron devices. The cause of this relatively poor transfer inefficiency was subsequently attributed to the intergate barrier or "bump" problem, discussed elsewhere in this report. The dynamic range of the offset memory devices was found to be in the range of 30 to 190 millivolts for the 7.5 micron devices and 40 to 90 millivolts for the 5 micron devices. The low dynamic range of the devices made with the LSM-3 mask set (as compared to the 400 to 600 millivolts of the LSM-2 devices) was unexpected and probably due to dark current leakage originating from etch pits at the  $\text{SiO}_2$ /Silicon interface.

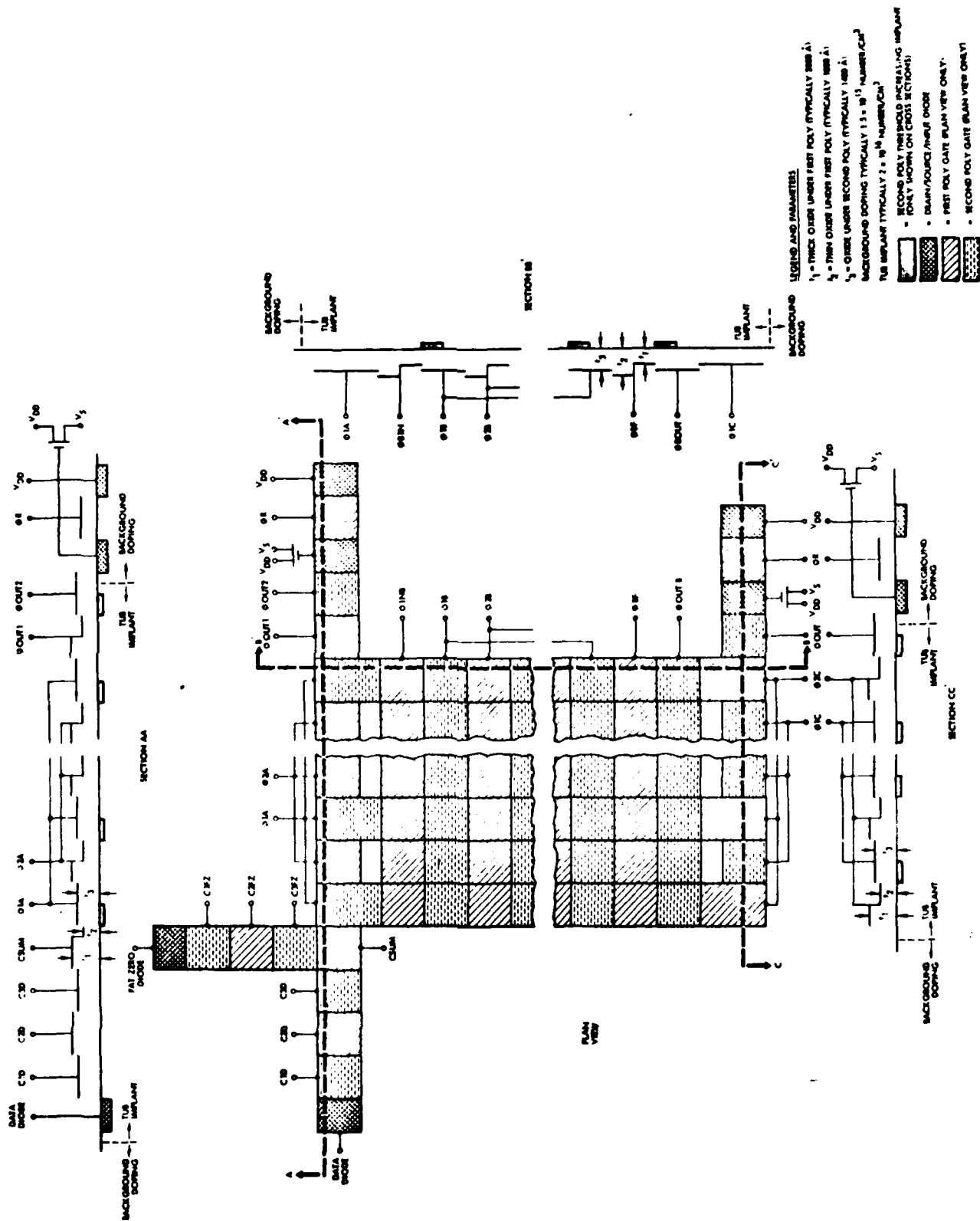


Figure 3-36. LSM-2 plan view and cross sectional diagrams.

Table 3-13. Comparative SPS layout values of  
CCD-2.

	High Density SPS	Standard SPS
Bits/SPS	4096	2048
Microns <sup>2</sup> /Bit/SPS	413.	826.
SPS/Wafer	300	300
Bits/Wafer	$1.2 \times 10^6$	$6.1 \times 10^5$
Micron <sup>2</sup> /Bit/Wafer	$1.7 \times 10^3$	$3.3 \times 10^3$

Table 3-14. Summary of LSM-2 and LSM-3 lots processed.

Lot No.	Description	Results
LSM2-1	Regular lot	Poly/metal Shorts
-2	TEOS for step coverage	
-3	Used mask 6 & 3 to measure test FETS	
-4	Used AZ 2400 P.R. for step coverage	
-5	Used various postbake conditions	
-6	Regular lot	Accidental implantation of both Boron and Phosphorous into barrier
-7	Regular lot	Evaluated
-8	2nd polysilicon nitride left on	Poly 1/Poly 2 low breakdown voltage
-9	Modified Barrier drive-in conditions	Evaluated
-10	Variations in processing: (1) phosphorous gettering of storage gate oxide (2) thicker storage gate oxide (3) plasma etched vs chemically etched polysilicon	Evaluated
-11	Change in process sequence to eliminate nitride remaining between polysilicon 1 & 2	Evaluated
-12		
-17		
-18	20' & 40' barrier anneals	Evaluated
-19	40' & 100' barrier anneals	Evaluated
-20	10,000 field oxide	Completed non-evaluated
-21	Only FETS 1400/2800 oxide ratio	Completed non-evaluated
-22	No tub, no guard	Completed non-evaluated
-23	Field oxide grown at 1200°C	Evaluated
-23A	Oxide ratio 1400/2800	Completed non-evaluated
-23A	Only FETS 14/00/2800 implant doses 4.5, 5 and $5.5 \times 10^{12} \text{P}^{32}/\text{cm}^2$	Evaluated
2020	Aligned in Cobilt 2020 machine	Evaluated
LSM3-1	Using streamlined process. As channel stops. Revised levels 4, 5 & 7	1 and 2 evaluated 3 and 4 in process
-2		
-3		
-4		

Yield data taken from both 7.5 micron and 5 micron 16 kilobit memory devices was significantly higher than expected. The memories were considered good, or functionally acceptable if the proper delay between input and output data was achieved. A functional yield of 86% was obtained for the 7.5 micron devices; a yield of 70% was obtained for the 5 micron devices. Non-functional devices were generally found in die locations near the edge of the wafers, which was expected. Though the efforts to produce high density offset gate memories were generally considered to be successful, the processing complexity and difficult device topography indicated a memory technology that would receive limited acceptance, despite high bit storage density. Inspection of Figure 3-37 provides an accurate indication of the complex device geometry involved in producing offset gate memories.

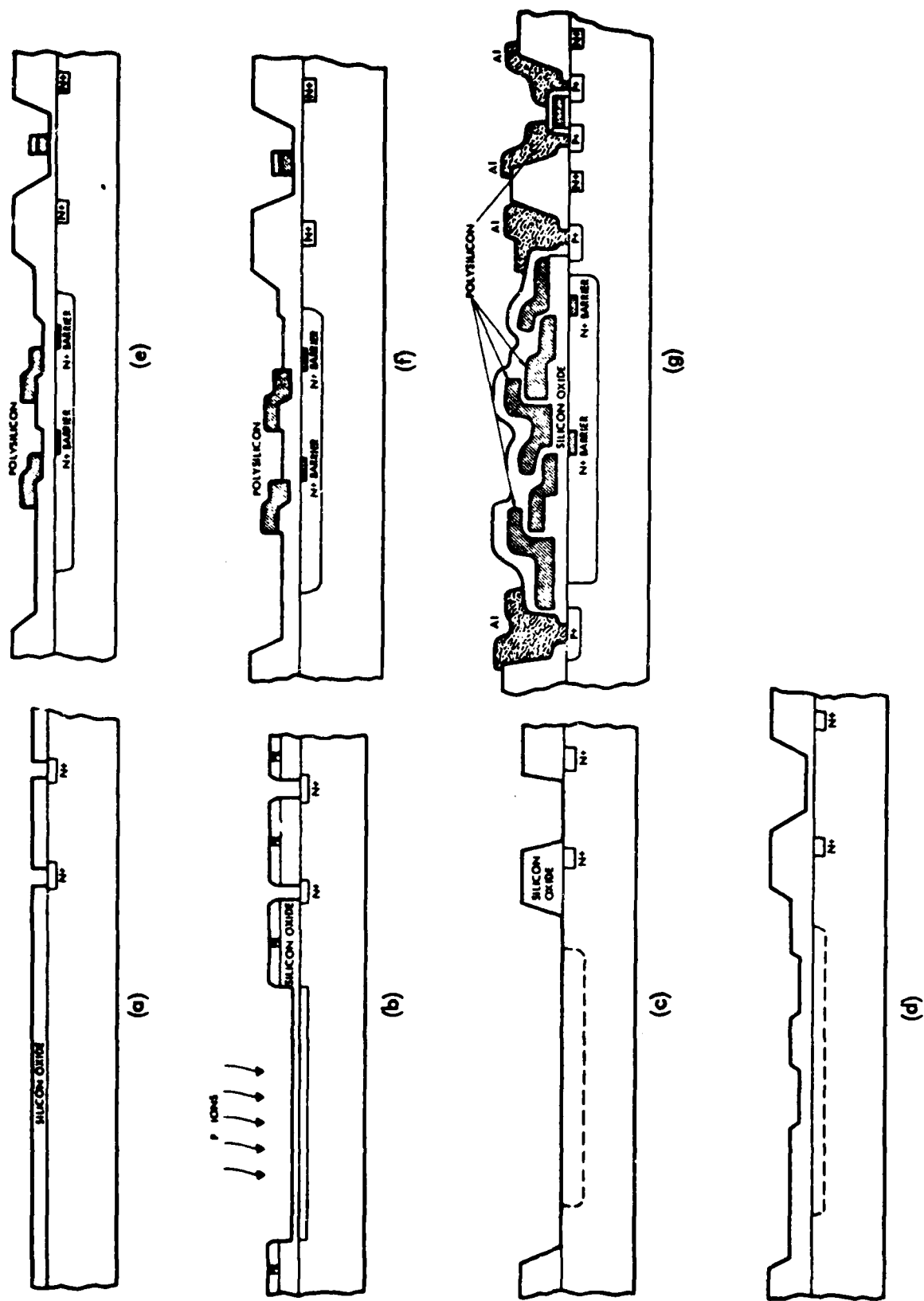


Figure 3-37. LSM-2 process for CCD device fabrication.

## 4.0 LARGE SCALE INTEGRATION (LSI) DEVELOPMENT

### 4.1 INTRODUCTION

In Section 1.1 we discussed, in general, the need for pipelined arithmetic when using DCCL building blocks. As an introduction the discussion of such functions as multiplication, addition, and subtraction some specific examples will be of value. If we want to add or subtract two binary words,  $a_1, a_2, \dots, a_n$  and  $b_1, b_2, \dots, b_n$ , we can proceed in the following straightforward manner.

$$\begin{array}{rcl}
 \text{First word} & a_n \dots a_3 & a_2 \ a_1 \\
 \text{Second word} & b_n \dots b_3 & b_2 \ b_1 \\
 \text{Carry bit} & c_n \dots c_3 & c_2 \\
 \hline
 \text{Sum} \quad c_n + 1 & s_n \dots s_3 & s_2 \ s_1
 \end{array}$$

A block diagram of a 2-word, 16-bit adder is shown in Figure 4-1 and a chip photograph of a DP3 16-bit adder is shown in Figure 4-2. There is a one clock period delay between the input charge to a full-adder and the generation of the sum and carry output charges. It will be seen that delay stages have been added to the input signals of the most significant input channels in order that the input bits arrive synchronously with the carry bits. If an unskewed output is desired, it is also necessary to include corresponding delays to all of the sum output lines except the most significant output bits. Two levels of charge refresh are included in the layout of the 16-bit adder of Figure 4-22 and a large MOS output driver buffers the output signals from the bonding pads.

A parallel DCCD multiplier uses a much more random interconnect pattern than the adder array. A random pattern becomes difficult to layout using DCCL cells if channel crossings must be avoided. Parallel multipliers involve the use of AND functions as well as a combinational network of half-and full-adders. The multiplication of two 4-bit binary numbers,  $a_1 - a_4$  and  $b_1 - b_4$ , is performed in the following straightforward manner;

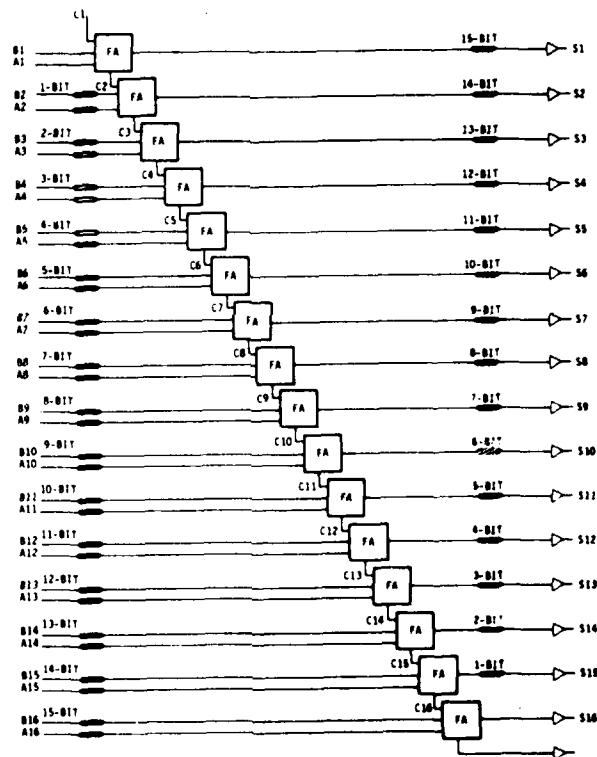
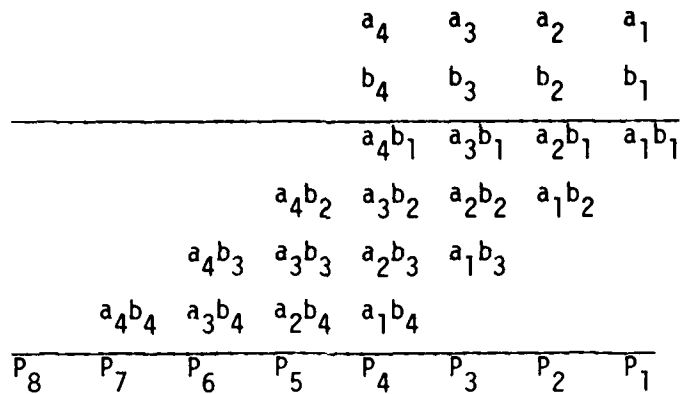


Figure 4-1. Block diagram of 2-word, 16-bit adder.

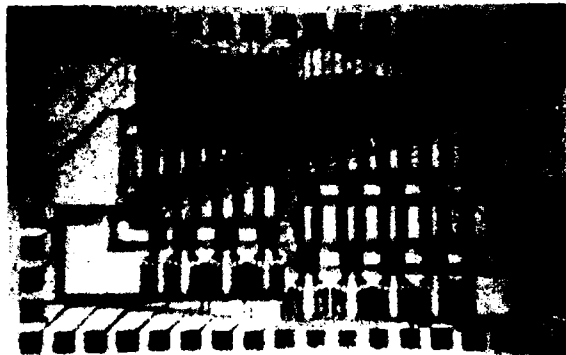


Figure 4-2. A 2-word, 16-bit adder array of digital charge-coupled devices.

Delays are also required in the multiplier in order that the summands proceed synchronously through the array. In a similar manner to the adder, additional delays are required in the multiplier output channels if a deskewed product is required.

The block diagram of a 4 x 4 multiplier is shown in Figure 4-3, for example, and a chip photograph of a DP3 8 x 8 multiplier array is shown in Figure 4-4.

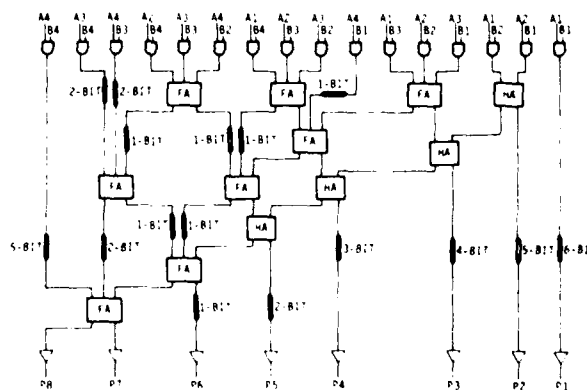


Figure 4-3. A block diagram of a 4-bit x 4-bit parallel multiplier array.



Figure 4-4. An 8-bit x 8-bit multiplier array of digital charge-coupled devices.

#### 4.2 EVOLUTION OF DCCD ADDER/SUBTRACTOR DESIGNS

This section describes the evolution of the adder and subtractor array designs implemented on the DP mask series and the Azimuth Correlator Device (ACD) mask.

##### 4.2.1 DP1 Adder Array

The first digital CCD adders were designed on the DP1 mask in November 1975. There were two versions of 4 + 4 bit adders on the DP1 mask. One adder was designed from ten half-adders as shown in Figure 4-5 and the other designed from three full-adders and a single half-adder as shown in Figure 4-6.

The addition of two 4-bit binary numbers  $a_0, a_1, a_2, a_3$ , and  $b_0, b_1, b_2, b_3$  in which  $a_0$  and  $b_0$  are the least significant bits, is performed with DCCL in the following manner;

First Word	$a_3$	$a_2$	$a_1$	$a_0$	
Second Word	$b_3$	$b_2$	$b_1$	$b_0$	
Carry Bits	$c_4$	$c_3$	$c_2$	$c_1$	
SUM	$s_4$	$s_3$	$s_2$	$s_1$	$s_0$

(Carry bit  $c_n$  is generated by column  $n-1$ .)

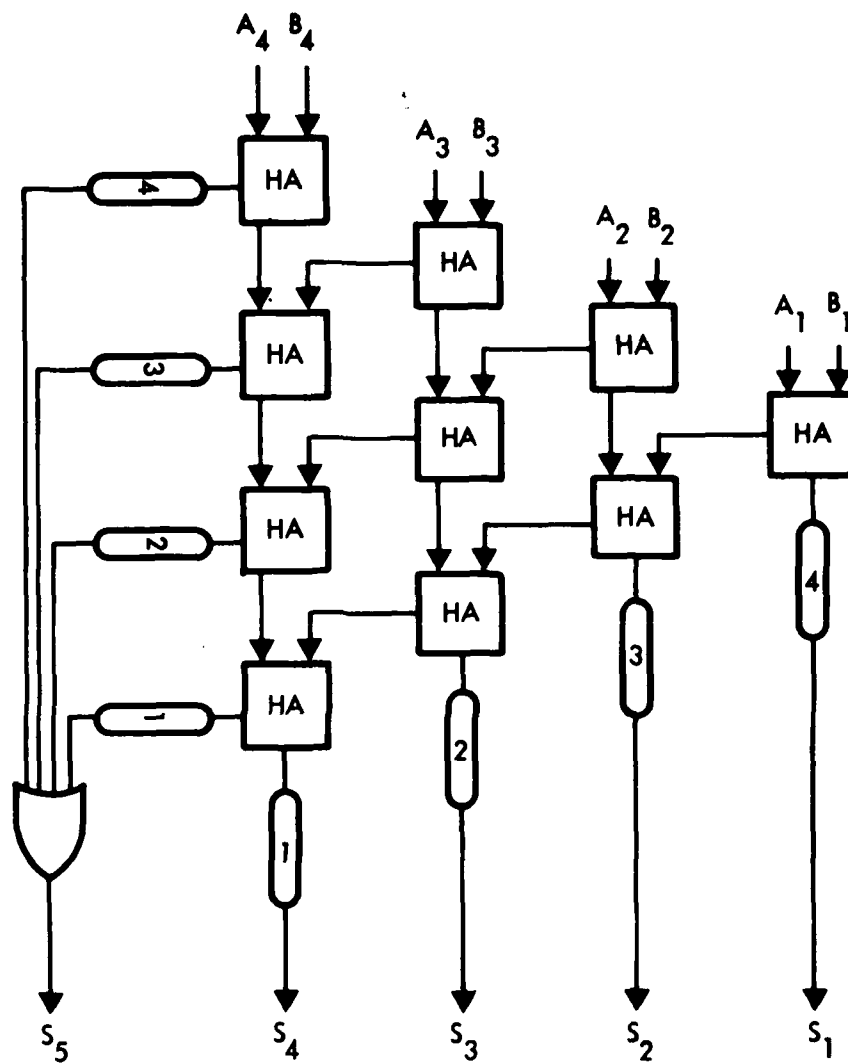


Figure 4-5. Schematic diagram of the DP1 4-Bit + 4-Bit adder array using half-adders.

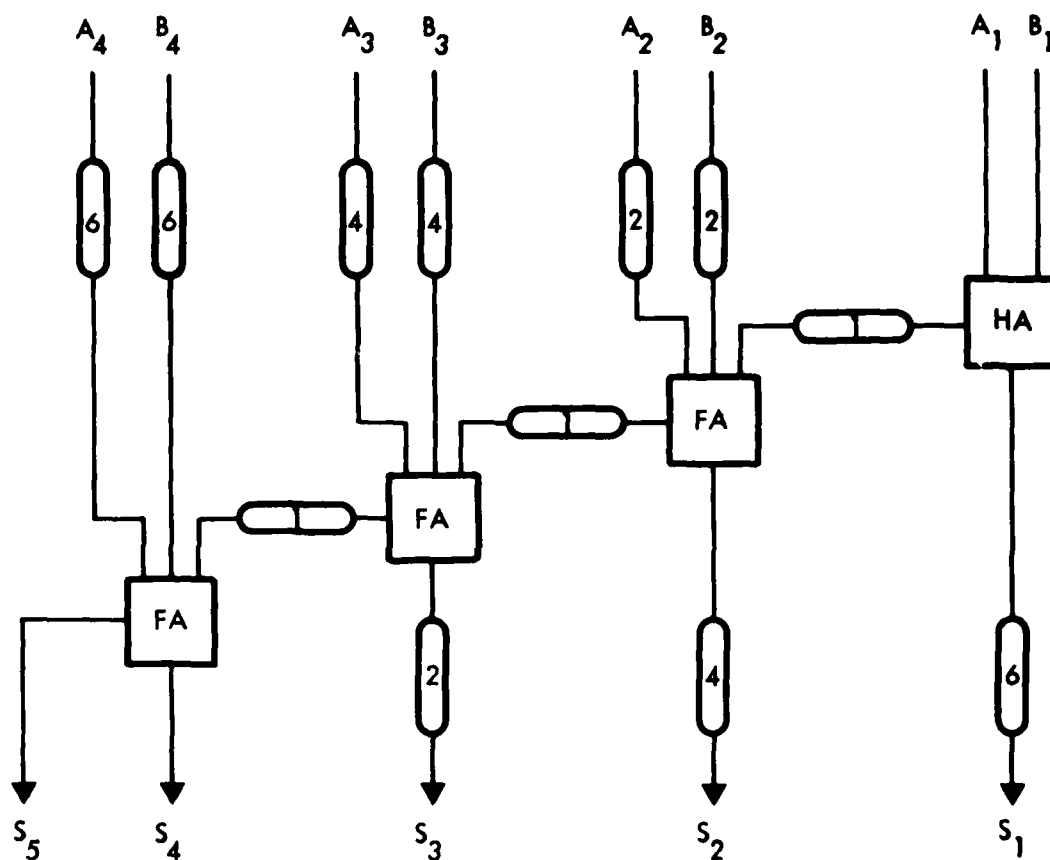


Figure 4-6. Schematic diagram of the DP1 4-Bit + 4-Bit adder array using full-adders.

Testing of the 4-Bit adder designed exclusively from half-adders, two problems emerged that made a successful demonstration very difficult. The first problem was the large transfer loss incurred through the three to four cascaded half-adders associated with the most significant bits. This loss resulted in very small sum and carry charge packets that were too small to switch the charge transfer electrodes. The second problem was the accumulation of a very large fat-zero where the five most significant carry channels were "OR'd."

It also proved difficult to exercise this adder because of the different number of CCD transfers in each column.

None of these problems occurred in the 4+4 bit adder array that was designed using full-adders. This array was demonstrated successfully in February 1976 and the test results were published,<sup>(6)</sup> the following September.

Testing was initially carried out at room temperature (25°C) and at a clock frequency of 10 kHz. The clock frequency was divided down by 16 to produce a 625 Hz word rate so that only one output word was displayed on the monitoring CRT at one time. By using this technique we could check that the pipeline delay shift register stages were functioning correctly (all output bits should be coincidental in time). The photograph of Figure 4-7 shows the 4 most significant bits of the output sum when input word-a is 1110 and input word-b is 0000.

Output patterns for different input conditions were photographed at clock frequencies of 100 kHz and 175 kHz. The logic "1" output levels do not attenuate significantly as the frequency is increased; however, they become obscured as the logic "0" output levels (fat-zero) grow larger. By switching the  $b_3$  input and observing the output patterns on the oscilloscope, it was observed that the adder array performed the correct arithmetic functions up to 200 kHz, but with a deteriorated signal-to-noise level.

The operating temperature range was determined by functional testing in a temperature controlled chamber. The clock voltages were adjusted at a frequency of 11 kHz and at 25°C so that the 3 most significant output bits from the adder array were performing correctly for each input combination and with a maximum signal-to-noise ratio. The temperature was increased in 10°

[Not shown,  $S_1 = 0$ ]

Output bit  $S_2 = 1$

Output bit  $S_3 = 1$

Output bit  $S_4 = 1$

Output bit  $S_5 = 0$

(Decimal 28)

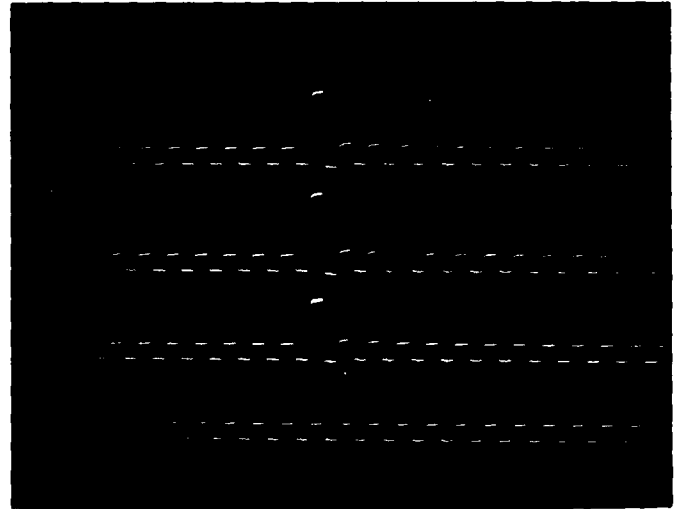


Figure 4-7. Output Signals from the 2-word, 4-bit Adder Array  
When a-word = 1110 and the b-word = 0000.

increments while the inputs were switched and the outputs monitored. At  $65^{\circ}\text{C}$ , the MSB of the array ceased to function. The  $S_4$  sum-bit output remained at "0", and the  $S_5$  carry-bit output remained at "1". The  $S_3$  sum-bit output continued to function correctly. At  $110^{\circ}\text{C}$  the fat-zero level of all outputs had increased sufficiently such that no bits were operable. It should be noted that the combination of high temperature and low frequency is the most difficult operating condition from the standpoint of thermal leakage. Proper operation at  $125^{\circ}\text{C}$  could be assured simply by operating the existing device at a frequency above 500 kHz.

The temperature was then reduced to  $25^{\circ}\text{C}$  and all outputs resumed operating correctly. The temperature was then lowered in  $10^{\circ}$  steps, the inputs switched and again the 3 most significant output bits monitored. At  $-15^{\circ}\text{C}$  the fat-zero level was reduced, but no further change in arithmetic performance. The temperature was then reduced to  $-65^{\circ}\text{C}$  and the  $C_2$  control line adjusted so that all channels performed correctly with a maximum signal-to-noise ratio.

#### 4.2.2 The DP2 4 + 4 Bit Adder Array

The DP2 adder arrays incorporated several significant improvements over the DP1 designs. One of these was the change from metal-polysilicon gates to double polysilicon gates. This change provided us with three levels of interconnect, metal and two polysilicon layers insulated from each other by a layer of oxide. Advantage was taken of the additional interconnecting level by increasing the density of the layout, resulting in the ability to directly interconnect full-adder or half-adder cells without any intercell delay stages. Another improvement was achieved by changing the CARRY out port from the master node of the charge transfer electrode to the storage area now referred to as the T-gate. This change provided the capability of obtaining a fully restored CARRY output charge packet.

There were three adder arrays on the DP2 chip; a 4 + 4 bit that used cascaded half-adders, 8 + 8 bit that used cascaded half-adders and a 8 + 8 bit that used full-adders. Both of the arrays using cascaded half-adders also used the fully restored CARRY output packets. However, the adder designed with full-adders used the concepts that were employed previously on the DP1. The reason for retaining the original full adder array design was based on the success of the 4 + 4 bit adder on DP1. A block diagram of the DP2, 4 + 4 bit adder array using the dual cascaded half-adders is shown in Figure 4-8. A photograph of a processed array is shown in Figure 4-9. This 4 + 4 bit adder array consists of seven half-adders, three OR-gates, fifteen single-bit shift-registers and five output buffers. The 4 + 4 bit array processes the data in parallel, thus the two 4-bit numbers are applied synchronously and the outputs are also available synchronously following a pipeline delay of four clock periods.

Testing of the DP2 4 bit adder array verified full functional operation. The eight input lines of the adder array were exercised through all possible sixteen combinations and the output from the array was observed on an oscilloscope. It was observed that the five array lines produced the correct output data for each input combination.

Photographs of the 4 + 4 adder array outputs for various input data combinations are shown in Figures 4-10, 4-11, 4-12, 4-13.

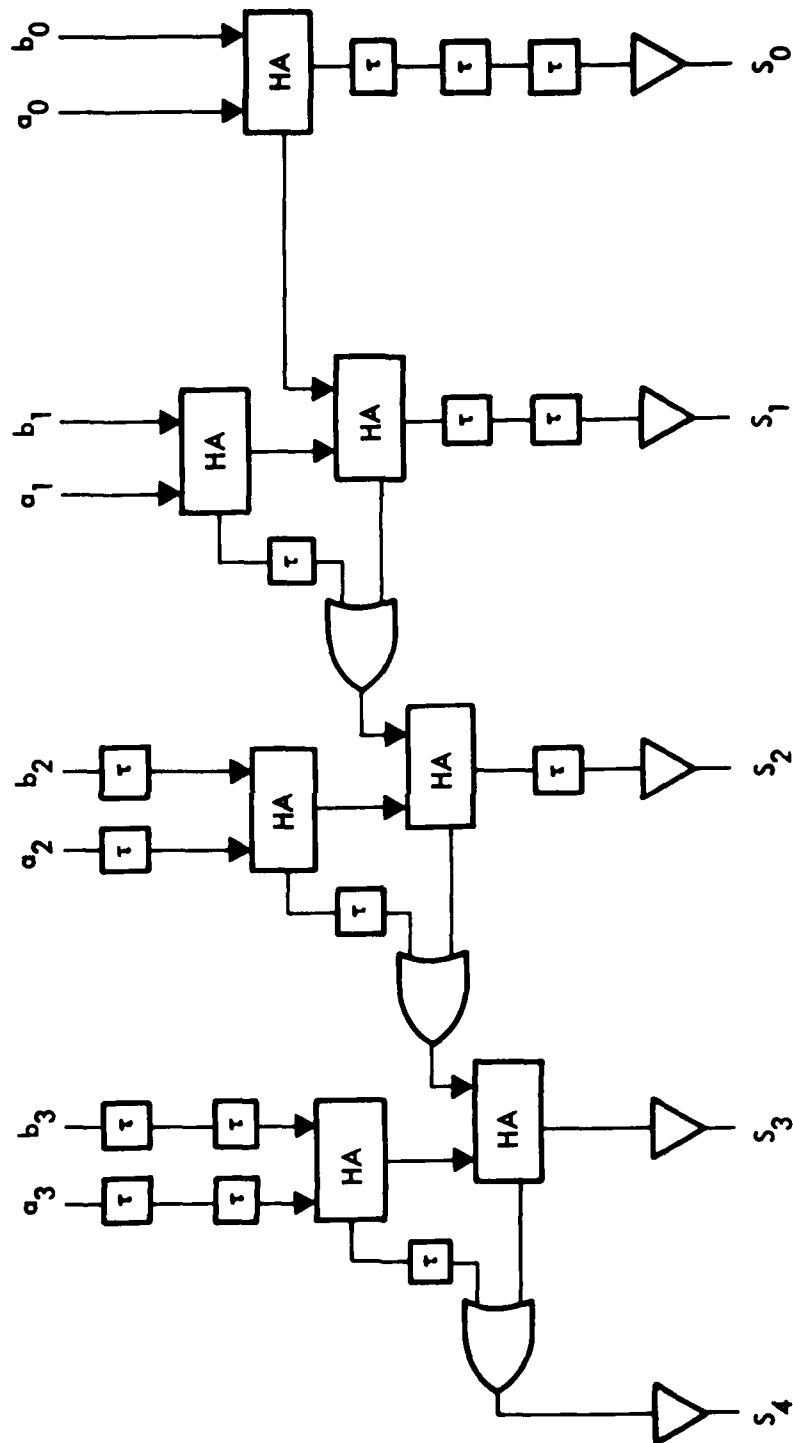


Figure 4-8. 4 + 4 Bit Adder Array Utilizing Dual Half-Adders.

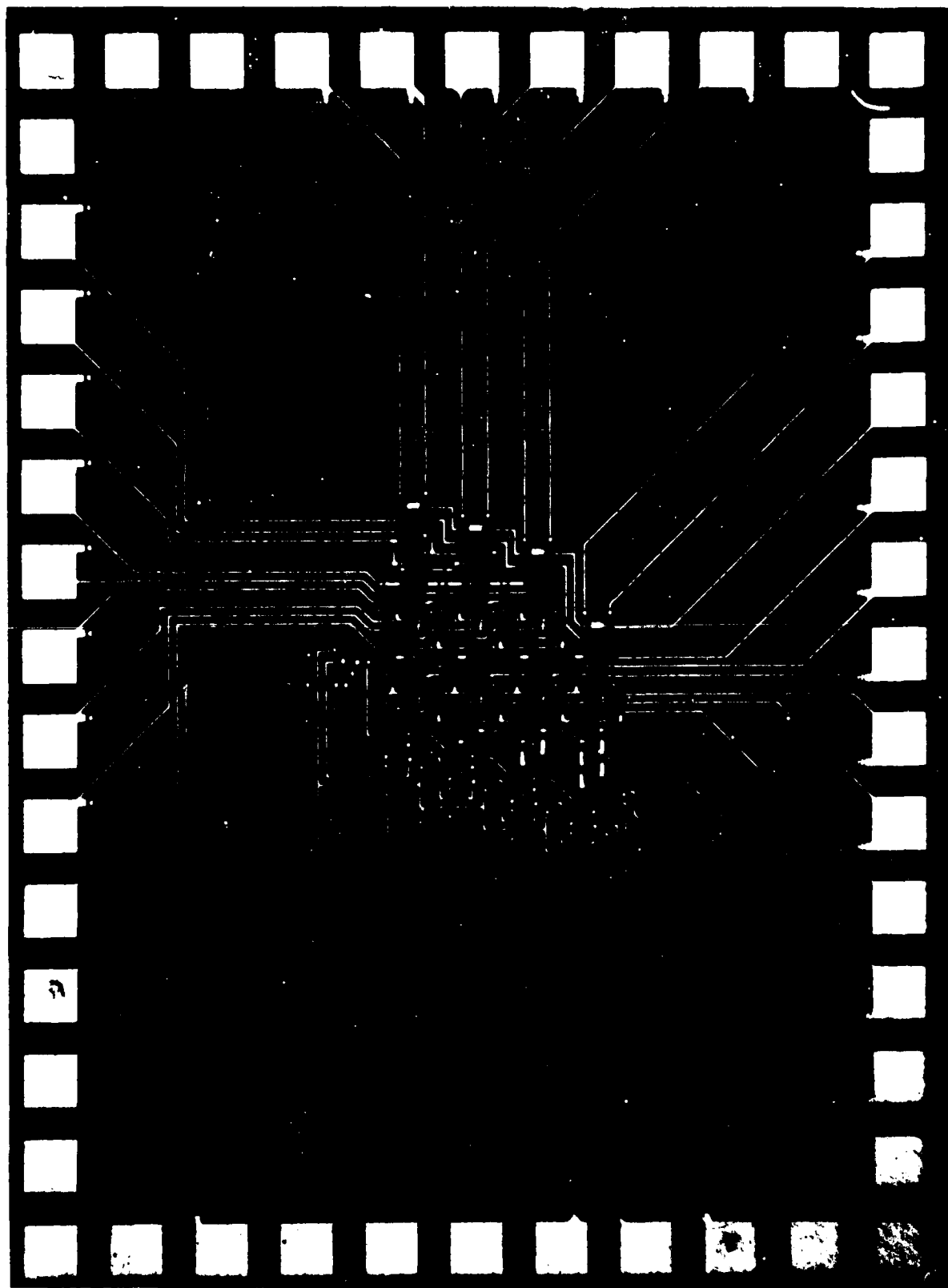
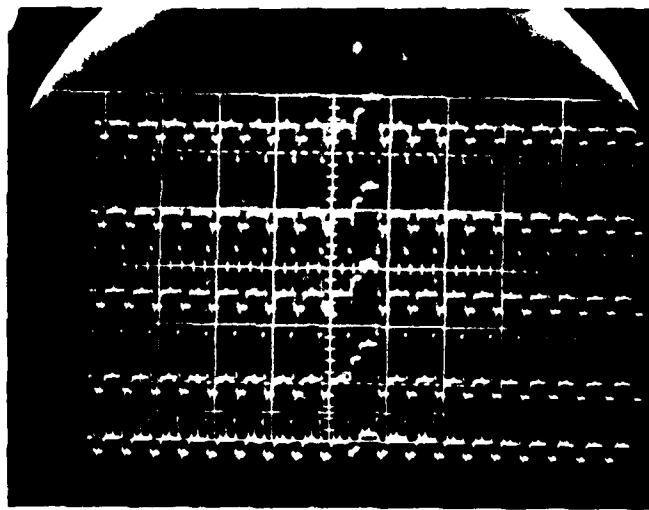


Figure 4-9. DP2 4 + 4 Adder Array Utilizing Three Cascaded Half-Adders and a Single Half-Adder.

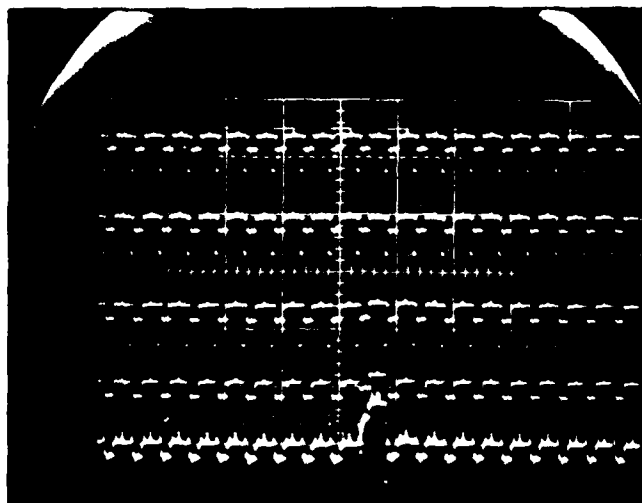


$\leftarrow S_0$   
 $\leftarrow S_1$   
 $\leftarrow S_2$   
 $\leftarrow S_3$   
 $\leftarrow S_4$

2V/cm

Figure 4-10. Input to 2-Word 4-Bit Adder

$$\begin{array}{rcl}
 a_i & = & 1 \ 1 \ 1 \ 1 \\
 b_i & = & 0 \ 0 \ 0 \ 0 \\
 \hline
 s_i = \text{Sum} & = & 0 \ 1 \ 1 \ 1 \ 1
 \end{array}
 \left. \begin{array}{l} \\ \\ \end{array} \right\} \begin{array}{l} \text{1V Inputs} \\ \\ \text{Carry} \end{array}$$

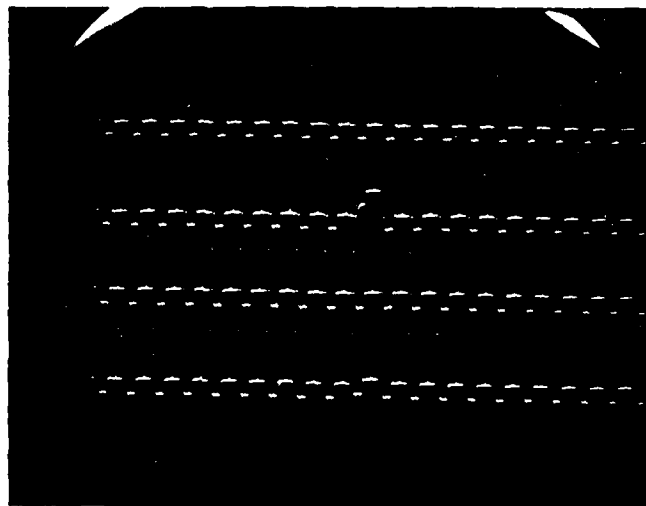


$\leftarrow S_0$   
 $\leftarrow S_1$   
 $\leftarrow S_2$   
 $\leftarrow S_3$   
 $\leftarrow S_4$

2V/cm

Figure 4-11. Input to 2-Word 4-Bit Adder

$$\begin{array}{rcl}
 a_i & = & 1 \ 1 \ 1 \ 1 \\
 b_i & = & 0 \ 0 \ 0 \ 1 \\
 \hline
 s_i = \text{Sum} & = & 0 \ 0 \ 0 \ 0
 \end{array}
 \left. \begin{array}{l} \\ \\ \end{array} \right\} \begin{array}{l} \text{1V Inputs} \\ \\ \text{Carry} \end{array}$$



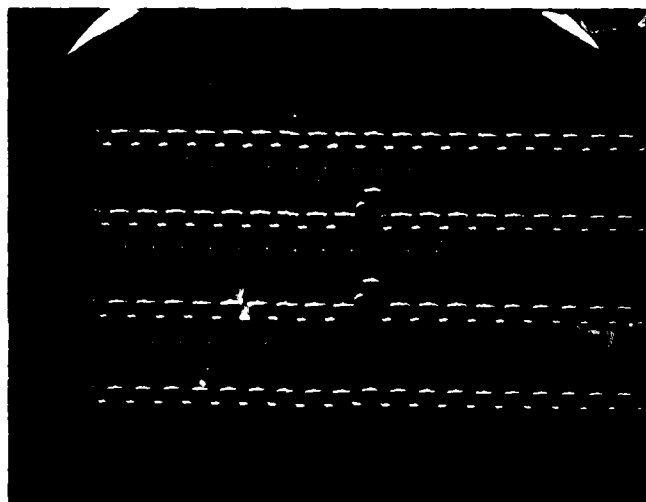
$s_0$   
 $s_1$   
 $s_2$   
 $s_3$

2V/cm

Figure 4-12. Input to 2-Word, 4-Bit Adder

$$\begin{array}{rcl}
 a_i & = & 1 \ 1 \ 1 \ 1 \\
 b_i & = & 0 \ 0 \ 1 \ 1 \\
 \hline
 s_i = \text{Sum} & = & 1 \ 0 \ 0 \ 1 \ 0
 \end{array}
 \quad \left. \vphantom{\begin{array}{rcl} a_i \\ b_i \end{array}} \right\} \text{1V Inputs}$$

Carry (not shown)



$s_0$   
 $s_1$   
 $s_2$   
 $s_3$

2V/cm

Figure 4-13. Input to 2-Word, 4-Bit Adder

$$\begin{array}{rcl}
 a_i & = & 1 \ 1 \ 1 \ 1 \\
 b_i & = & 0 \ 1 \ 1 \ 1 \\
 \hline
 s_i = \text{Sum} & = & 1 \ 0 \ 1 \ 1 \ 0
 \end{array}
 \quad \left. \vphantom{\begin{array}{rcl} a_i \\ b_i \end{array}} \right\} \text{1V Inputs}$$

Carry (not shown)

#### 4.2.3 The DP2 8 + 8 Bit Adder Arrays

##### 4.2.3.1 The Cascaded Dual Half Adder Design

In this adder array the arithmetic is performed using cascaded dual half-adders. This 8 + 8 bit adder array is an extension of the 4 + 4 bit array discussed in Section 4.2.2. The addition of two 8-bit binary numbers  $a_0 - a_7$  and  $b_0 - b_7$  is performed with DCCL in the same manner as described for the 4 + 4 bit array.

First Word	$a_7$	$a_6$	$a_5$	$a_4$	$a_3$	$a_2$	$a_1$	$a_0$
Second Word	$b_7$	$b_6$	$b_5$	$b_4$	$b_3$	$b_2$	$b_1$	$b_0$
Carry Bits	$c_8$	$c_7$	$c_6$	$c_5$	$c_4$	$c_3$	$c_2$	$c_1$
SUM	$s_8$	$s_7$	$s_6$	$s_5$	$s_4$	$s_3$	$s_2$	$s_1$
	$s_0$							

A block diagram of this 8 + 8 bit adder array is shown in Figure 4-14. The array utilizes fifteen half-adders, seven OR gates, seventy-seven bits of shift register and eight output buffers. There is a propagation delay of eight clock periods through this version of the 8 + 8 bit array. A photograph of a processed array is shown in Figure 4-15.

The 8 + 8 bit adder arrays were operated with the same clock voltages used for the 4 + 4 bit arrays described previously. All nine output channels responded correctly to the input signals as verified by the oscilloscope photographs of Figures 4-16, 4-17, 4-18, and 4-19. In these figures,  $a_i$  and  $b_i$  are the input bits, where  $a_0$  and  $b_0$  represent the least significant bits and  $s_i$  represents the array outputs.

##### 4.2.3.2 Full Adder Design

The 8 + 8 bit full adder version of the array performs the addition of two 8-bit numbers in the same manner as described in Section 4.2.3.1. A block diagram of this adder array is shown in Figure 4-20. This array utilizes one half-adder, seven full-adders, eighty-four single bits of shift register and eight output buffers. There is a propagation delay of eight clock phases through this version of the 8 + 8 bit adder array. A photograph of a processed array is shown in Figure 4-21.

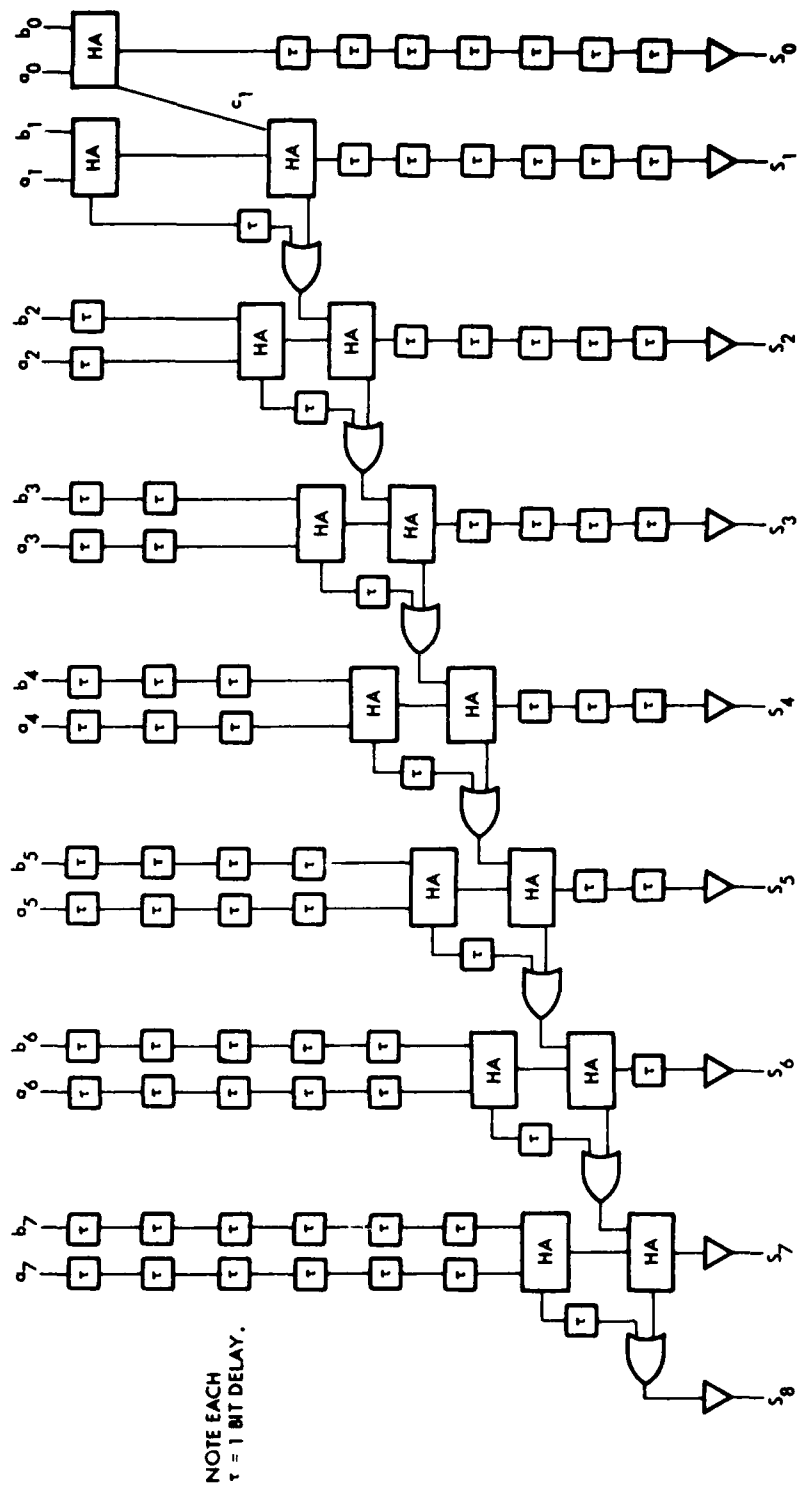


Figure 4-14. 8 + 8 Bit Adder Array Utilizing Cascaded Dual Half-Adders.

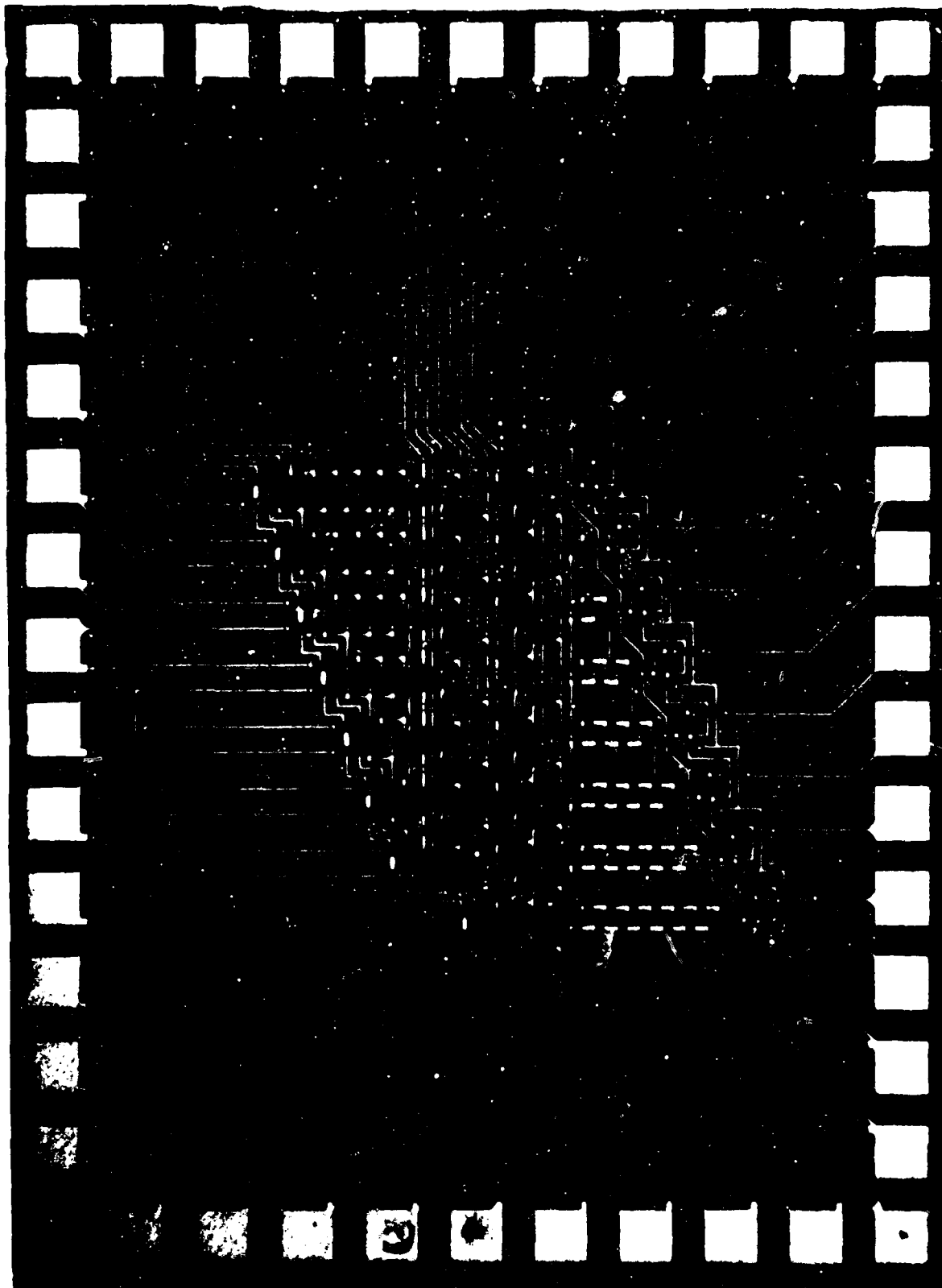
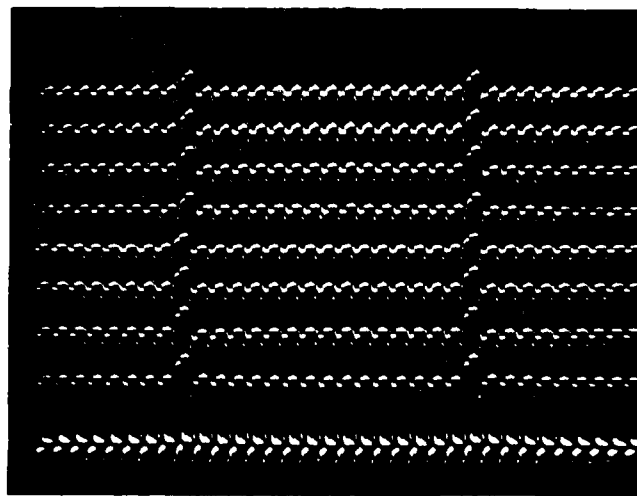


Figure 4-15. DP2 8 x 8 Adder Array Utilizing Seven Cascaded Half-Adders and a Single Half-Adder.



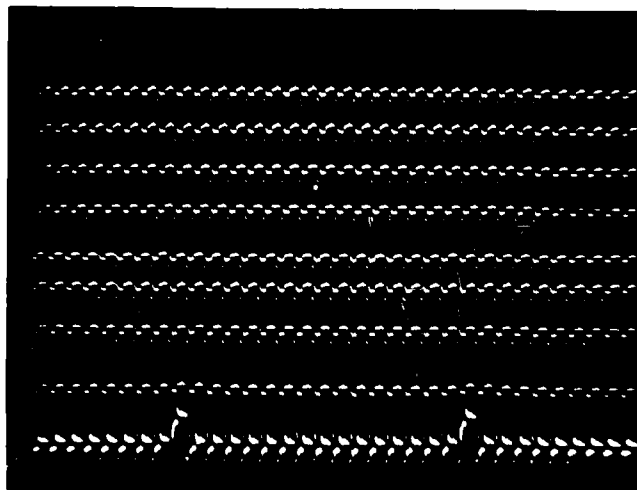
$s_0$   
 $s_1$   
 $s_2$   
 $s_3$   
 $s_4$   
 $s_5$   
 $s_6$   
 $s_7$   
 $s_8$  Carry

5 V/cm

Figure 4-16. Input to 2-Word, 8 Bit Adder

$a_i = 11111111$   
 $b_i = 00000000$   
 $s_i = 01111111$

↑ Carry



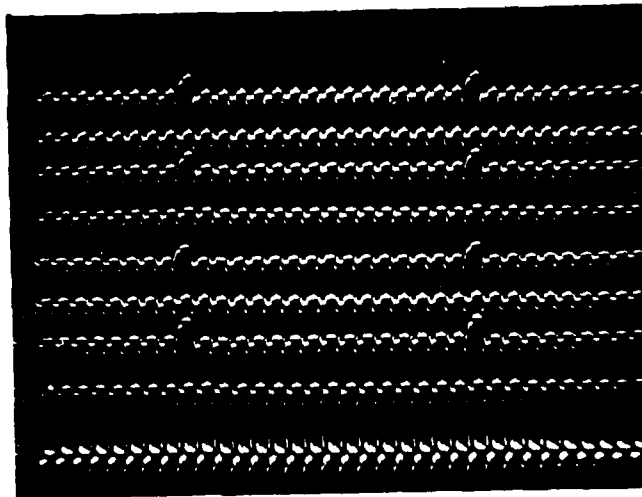
$s_0$   
 $s_1$   
 $s_2$   
 $s_3$   
 $s_4$   
 $s_5$   
 $s_6$   
 $s_7$   
 $s_8$  Carry

5 V/cm

Figure 4-17. Input to 2-Word, 8 Bit Adder

$a_i = 11111111$   
 $b_i = 00000001$   
 $10000000$

↑ Carry



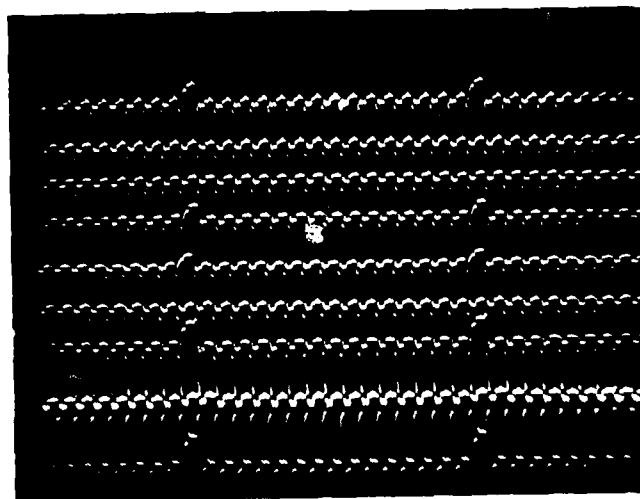
-  $5S_0$   
 -  $S_1$   
 -  $S_2$   
 -  $S_3$   
 -  $S_4$   
 -  $S_5$   
 -  $S_6$   
 -  $S_7$   
 -  $S_8$

5 V/cm

Carry

Figure 4-18. Input to 2-Word, 8 Bit Adder

$a_i = 00101011$   
 $b_i = 00101010$   
 $s_i = 001101010$   
 ↑ Carry



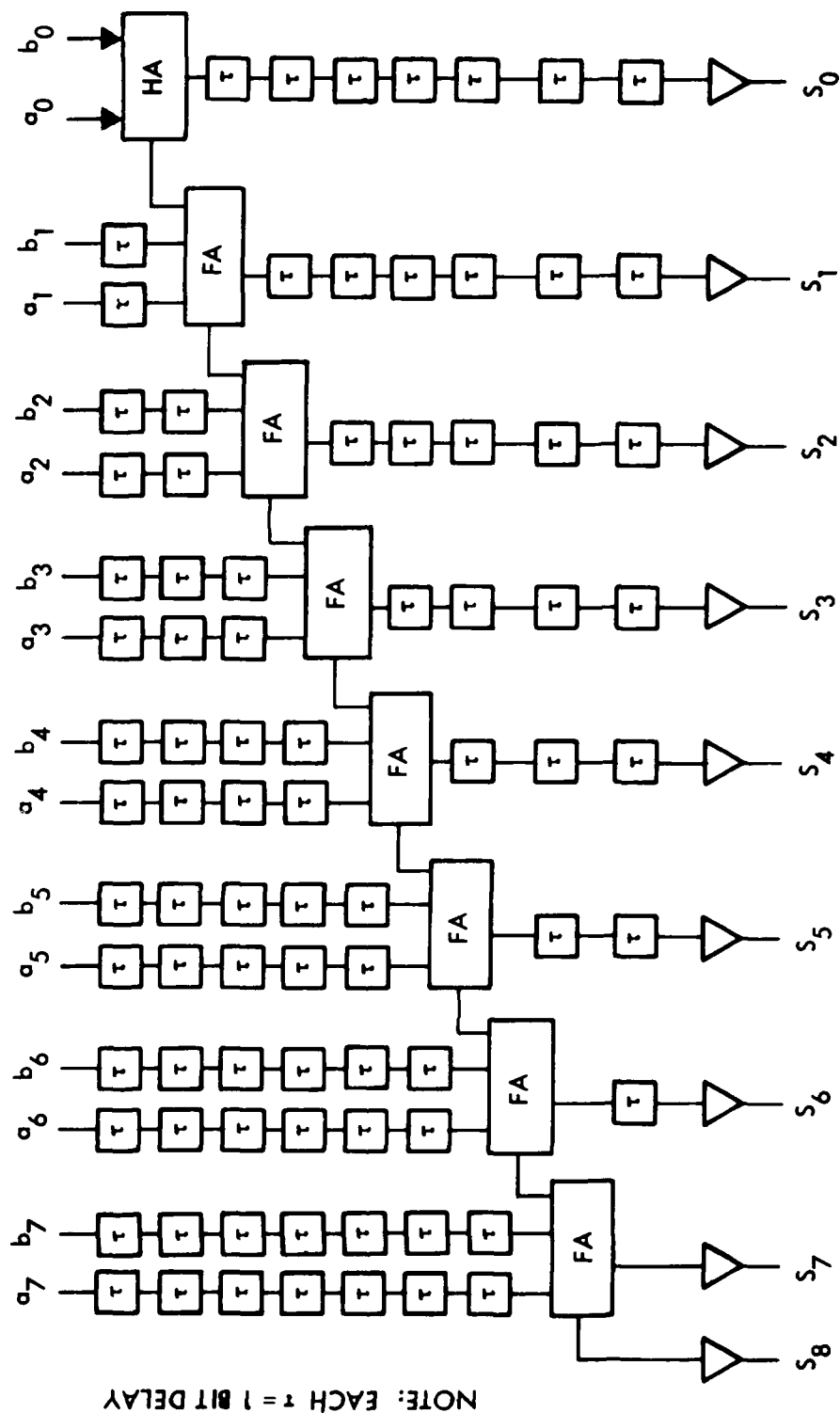
-  $5S_0$   
 -  $S_1$   
 -  $S_2$   
 -  $S_3$   
 -  $S_4$   
 -  $S_5$   
 -  $S_6$   
 -  $S_7$   
 -  $S_8$

5 V/cm

Carry

Figure 4-19. Input to 2-Word, 8 Bit Adder

$a_i = 11010101$   
 $b_i = 10000100$   
 $s_i = 101011001$   
 ↑ Carry



NOTE: EACH  $\tau = 1$  BIT DELAY

Figure 4-20. 8 + 8 Bit Adder Array Utilizing Full-Adders.

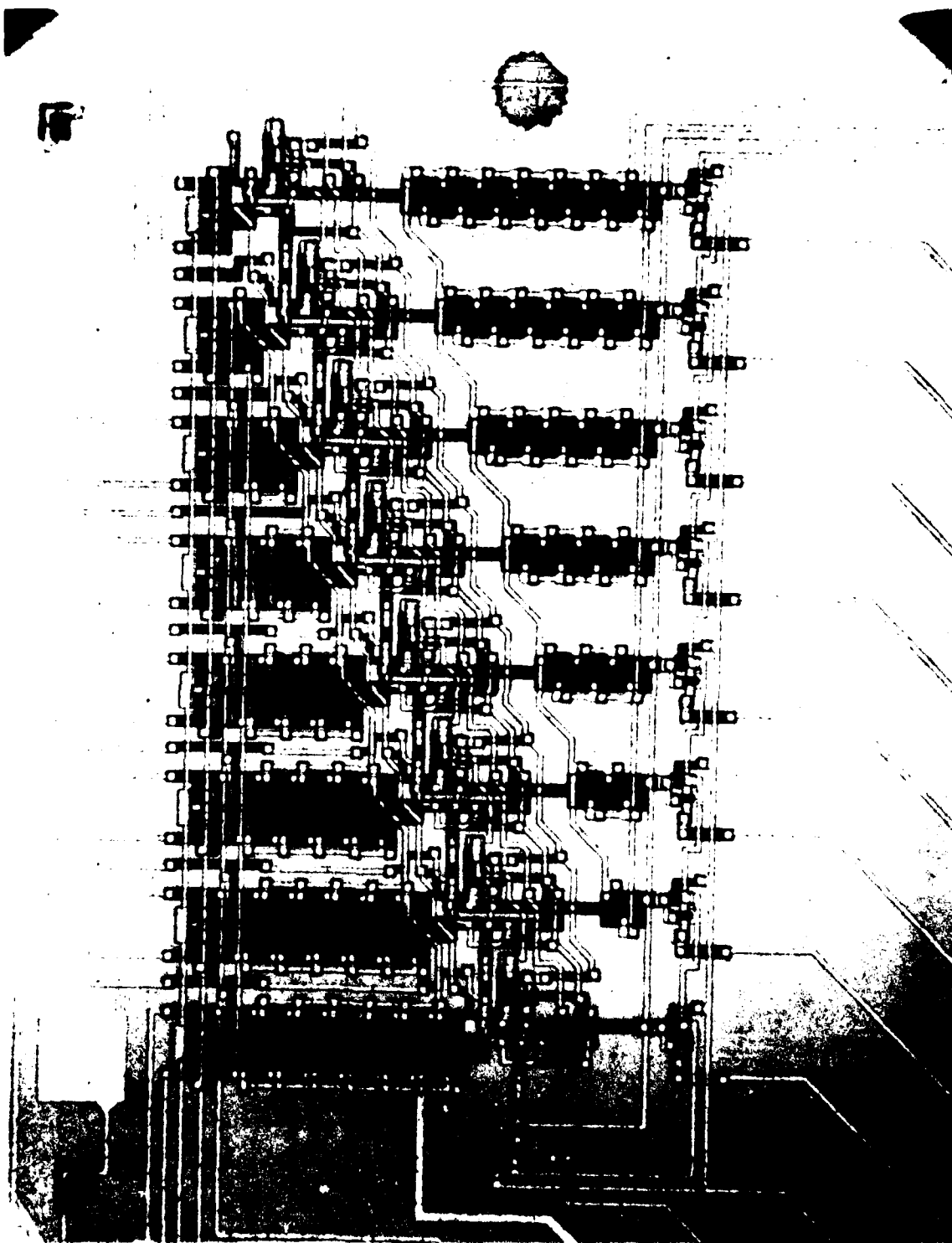


Figure 4-21. DP2 8 + 8 Adder Array Utilizing a Half-Adder and Seven Full-Adders.

Several mask errors were discovered on the full-adder version which prevented it from functioning. Since the DP3 mask set (using the cascaded dual half adder approach) was soon to be completed, we decided not to procure a corrected version of the DP2 mask set.

#### 4.2.4 The DP3 Adder Array

The DP2 and DP3 designs differ in both geometry and wafer processing. With respect to geometry, the DP2 design utilized a  $7.6\ \mu$  minimum geometry whereas the DP3 design utilized a  $5.1\ \mu$  geometry.

The DP3  $16 + 16$  bit adder array performs the addition of two 16-bit binary numbers in the same manner described for the  $8 + 8$  bit adder array described in Section 4.2.3.1. A block diagram of the  $16 + 16$  bit adder array is shown in Figure 4-22. The full adder blocks shown in Figure 4-22 are composed of dual cascaded half adders and an OR gate as described in Section 3.3. A change was made to the basic design by utilizing a full adder for the least significant bit (LSB) rather than a half-adder. The additional input allowed us to cascade arrays up to any number of bit length words by using the "carry-in" feature on the LSB.

The packets of charge propagating through this array undergo seventeen transfers. Due to the low transfer efficiencies observed on the DP2 arithmetic arrays, two levels of charge refresh cells were incorporated in the  $16 + 16$  bit DP3 array.

The first level of charge refresh was inserted after nine or ten transfers and the second level after the seventeenth transfer (immediately before the charge packet is converted to a voltage signal by the output buffer). The  $16 + 16$  bit array utilizes thirty-two half-adders, sixteen OR gates, forty charge refresh cells, three hundred and forty-one single stage shift-register bits and seventeen output buffers.

There is a pipeline delay of seventeen clock periods through the  $16 + 16$  bit adder array. A photograph of a processed array is shown in Figure 4-23.



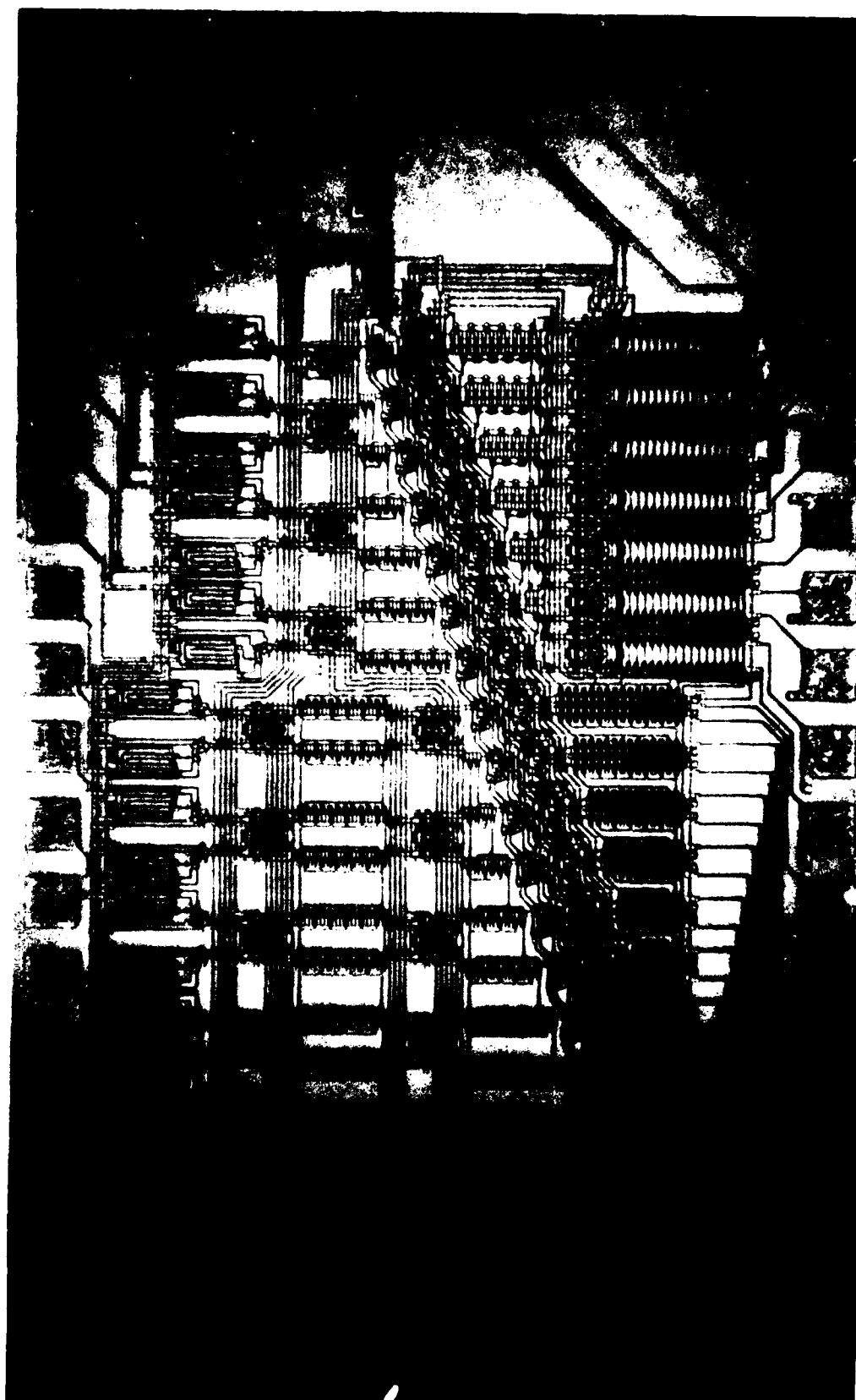


Figure 4-23. The DP3 16 + 16 Adder Array.

In an effort to reduce the number of clock lines required by the adder designs, analytical calculations and empirical testing on DP2 single half-adder test cells indicated that the dual half-adder would function correctly with only five clock lines (plus the inject diode and the OR reset clock). The DP3, 16 + 16 bit adder array design was based on this five clock scheme. Unfortunately, due to several gates being tied to the same clock line, race conditions were encountered which prevented meaningful evaluation of the 16 + 16 bit adder array.

#### 4.2.5 The DP5, Adder/Subtractor Array

In July 1977, work began on the design of a 32 + 32 bit adder array designated as DP5. At the same time, the requirement for clock speeds of 5 MHz and above developed in response to near term voice processing applications since a maximum clock speed of 2 MHz was projected for our current P-channel designs, a decision was made to pursue an n-channel design for the 32 + 32 bit adder.

A n-channel process was devised, design rules drawn up and a n-channel evaluation mask set, designated NE-1, designed. The successful demonstration of n-channel full-adders and half-adders on the NE-1 mask, encouraged the continuation of the n-channel 32 + 32 bit adder array.

In an attempt to satisfy the needs of a near term voice processing application, it was decided that the DP5 array should be able to add, subtract and perform the exclusive-OR function. This array was to have three control lines (J, K, and D) and perform eight different functions as shown in Table 4-1.

Table 4-1. Selectable Functions of the DP5 Array.

J	K	D	
1	0	0	(A+B) Add
1	1	1	(A-B) Subtract
1	0	1	(A+B+1) Increment
1	1	0	(A+B) Add complement
0	0	0	(A ⊕ B) Exclusive-OR
0	1	0	(A ⊕ B) Equivalence
0	0	1	Not required in this application
0	1	1	Not required in this application

In pipeline DCCL arithmetic, where it is required to begin processing a new word each successive clock cycle, the 2's complement number system is ideal for addition and subtraction. For this reason, 2's complement was chosen as the number system for the DP5 32-bit array.

The following paragraphs provide a description of the signal flow and control line functions of the final DP5 array design. Two 32-bit 2's complement numbers synchronously enter the array and are appropriately skewed by CCD shift registers. One of the input words (the subtrahend in the case of the subtract mode) is transferred into one of the two input ports of each of the 32 exclusive-OR gates.

The control line, K, determines the binary value of the input to the other input port of the exclusive-OR gates as shown in Figure 4-24. When control line K is switched so that a binary zero is entered into the exclusive-OR gates, the data is transferred through the exclusive-OR without being changed. However, when the control line K is switched so that a binary one is entered into the exclusive-OR gates, the data is complemented. The control line K, is also transferred into one input terminal of a half-adder and a binary one input packet is transferred into the other half-adder input during each clock period. The half-adder will generate a binary-one charge packet from its carry-out port each clock period when  $K = 1$  and a binary-zero charge packet from the carry-out port when  $K = 0$ . The carry-out port of the half-adder is connected to the carry-in port of the least-significant-bit full-adder in the array. Thus when  $K = 1$ , the input data (the subtrahend) is complemented and the difference is incremented by one.

The output from the 32 exclusive-OR gates and the other 32-bit input data are transferred into two of the three inputs of each of the 32 full-adders as shown in Figure 4-25. The carry-out port of each full-adder is connected to the carry-in port of the next more significant full-adder. Each pair of bits are added (or subtracted) in turn, at each subsequent clock phase. Therefore the most significant pair are acted upon, 32 clock phases after the least significant pair.

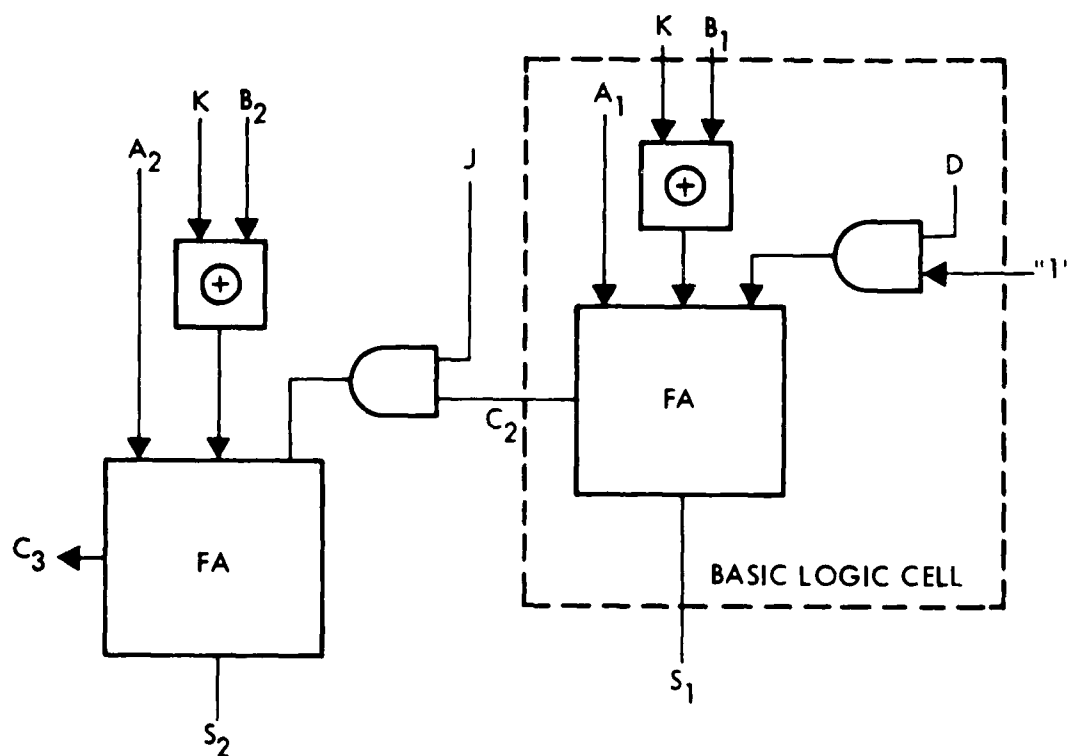


Figure 4-24. Logic Diagram of the two least significant bit logic cells of the 32-Bit DP5 Array.

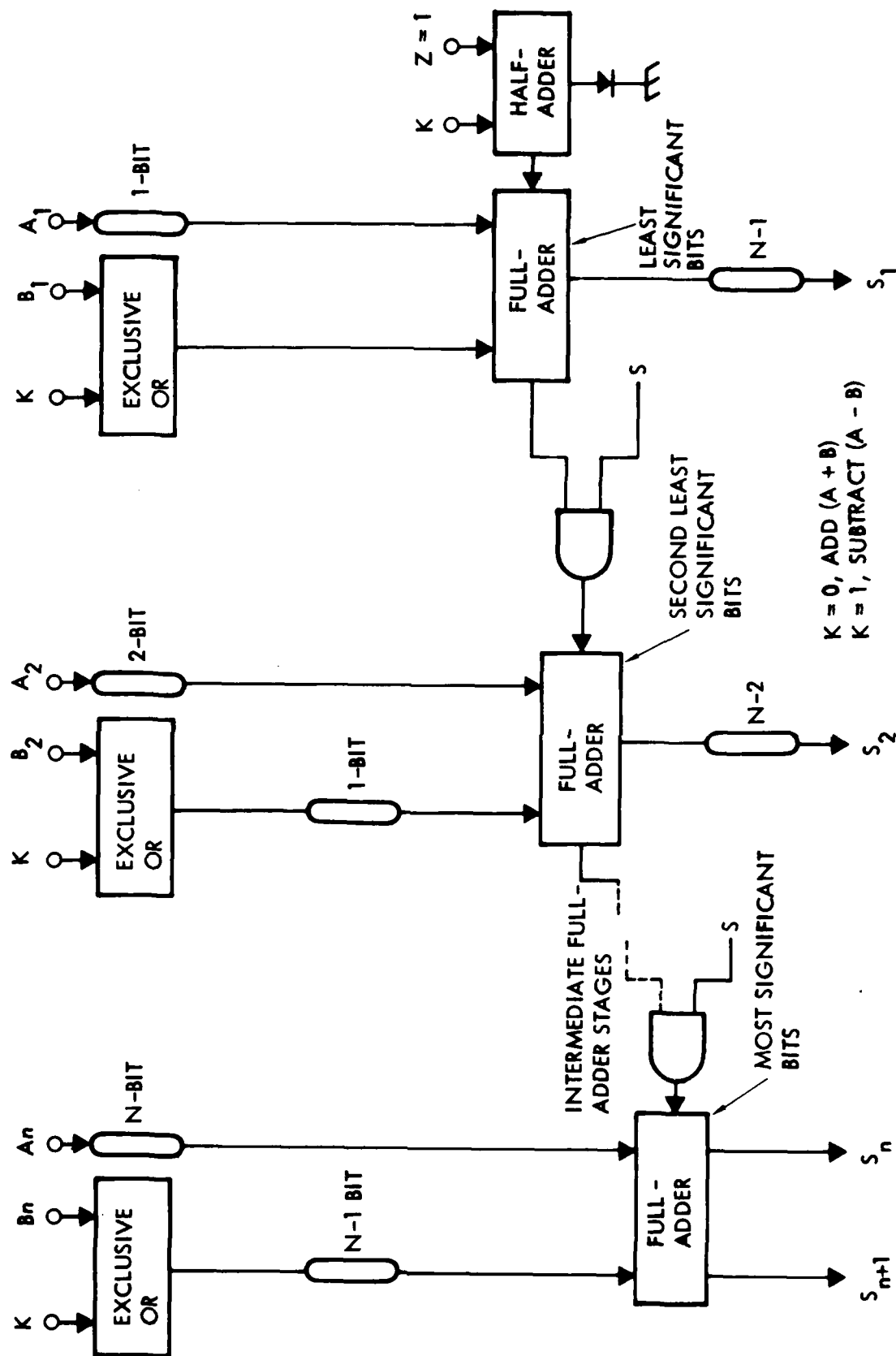


Figure 4-25. Block diagram of the DP5 adder/subtractor exclusive-OR array.

In order to be able to switch the function of the array from add/subtract to exclusive-OR, two input AND gates are inserted between the carry-out and carry-in ports of each full-adder. A control line S controls the value of the binary input to the other input port of the AND gates. When S is at the binary zero value, the carry channel is inhibited, and the array output is the exclusive-OR. When S is at the binary-one value, the carry-bits are enabled and the array output is the add/subtract. There are no clock phase delays through a DCCL AND gate, so this extra functional capability does not require more skewing.

Layout of the DP5 array was completed in September 1978 and a device lot was fabricated. Due to the size and complexity of the DP5 array, many gates, and contacts were later found to be missing from the layout making it impossible to test the array. Since the original voice processing application for this 32-bit DP5 array had disappeared by this time, no corrections to the DP5 masks were pursued. A photograph of the DP5 chip is shown in Figure 4-26.

#### 4.2.6 Azimuth Correlator Device (ACD) 10 + 10 Bit Adder

The 10 + 10 bit adder, required for the ACD project, utilized dual cascaded half-adders to perform the full-adder function. The design of this adder was nearly identical to the DP2 8-bit adder, with the exception that no skewing or de-skewing delays were included. The first version of this adder was incorporated onto the ACDO test mask.

The outputs on the ACDO 10 bit array were transferred into charge-comparator latches. Due to design problems in these comparator circuits, it was impossible to get two of them to function at the same bias voltages which made it impossible to get meaningful test data on the adder array.

The identical adder was placed on the revised (ACD2) mask with the troublesome charge-comparator latch circuit replaced with NMOS analog source follower output buffers.

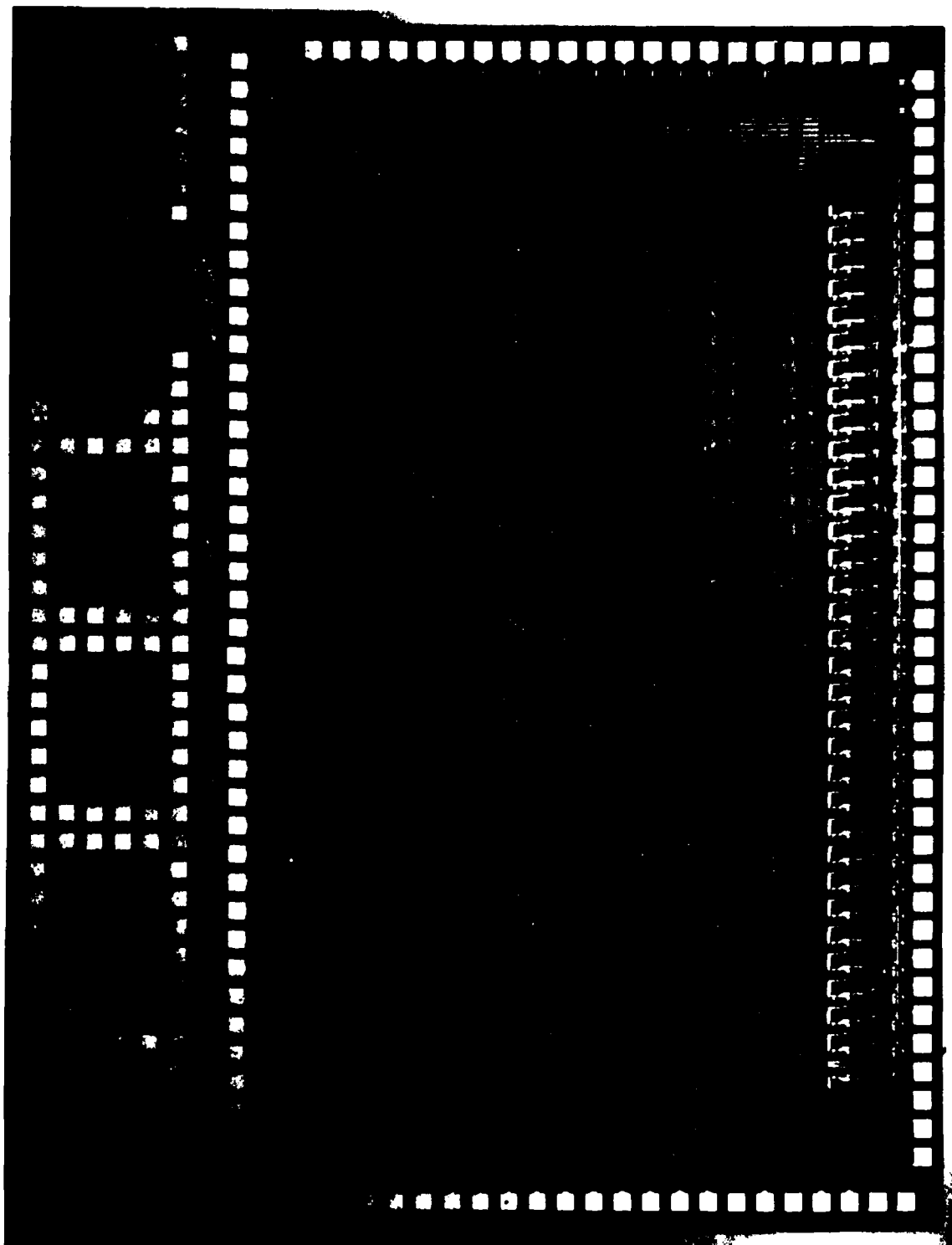


Figure 4-26. DP5 32-bit adder/subtractor/exclusive-OR chip

Sufficient testing of the 10 + 10 bit adder was performed to verify that the layout was correct and that the carry charge packet would propagate through all ten stages. The ACD2 10-bit adder consists of 10 full-adders formed from dual cascaded half-adders as shown in Figure 4-27.

Functional testing was performed by making one input word all "1"'s, the second input word all "0"'s, and varying the input carry-bit between a "1" and a "0". Setting the input carry-bit to a "1" results in the output word's most significant bit becoming a "1" and the other bits a "0", while setting the input carry bit to a "0" results in the output word's most significant bit becoming a "0" and the other bits a "1". This data pattern exercises the full scale of the adder. This result is graphically seen in the photographs of Figure 4-28. The top trace of the photograph is the input carry bit alternating between a "0" (low level) for 14 cycles and a "1" (high level) for two cycles. Seven cycles later the least significant bit (S1) of the output word switches between a "1" and a "0" in response to the input signals. The output of each successive bit is delayed by 1 cycle to account for the propagation of the carry bit through the adder, until 17 cycles after the initial input signal, the two most significant bits (S10 and S11) of the output word switch to their correct positions. Thus the 10 bit adder is demonstrated as working successfully. Tests were performed over a frequency range of 50 kHz to the 1.5 MHz upper limit imposed by the probe station and available test equipment. A photograph of the 10-Bit + 10-Bit adder is shown in Figure 4-29.

#### 4.3 EVOLUTION OF MULTIPLIERS

The following sections describe the evolution of the DCCD multiplier development effort from the first DPl designs to the latest ACD designs.

##### 4.3.1 The DPl Multiplier Arrays

All of the multipliers described in this section are parallel multipliers that operate in the manner described<sup>(7)</sup> by C. S. Wallace.

The DCCD operations used to multiply two 3-bit binary numbers are performed in the following manner.

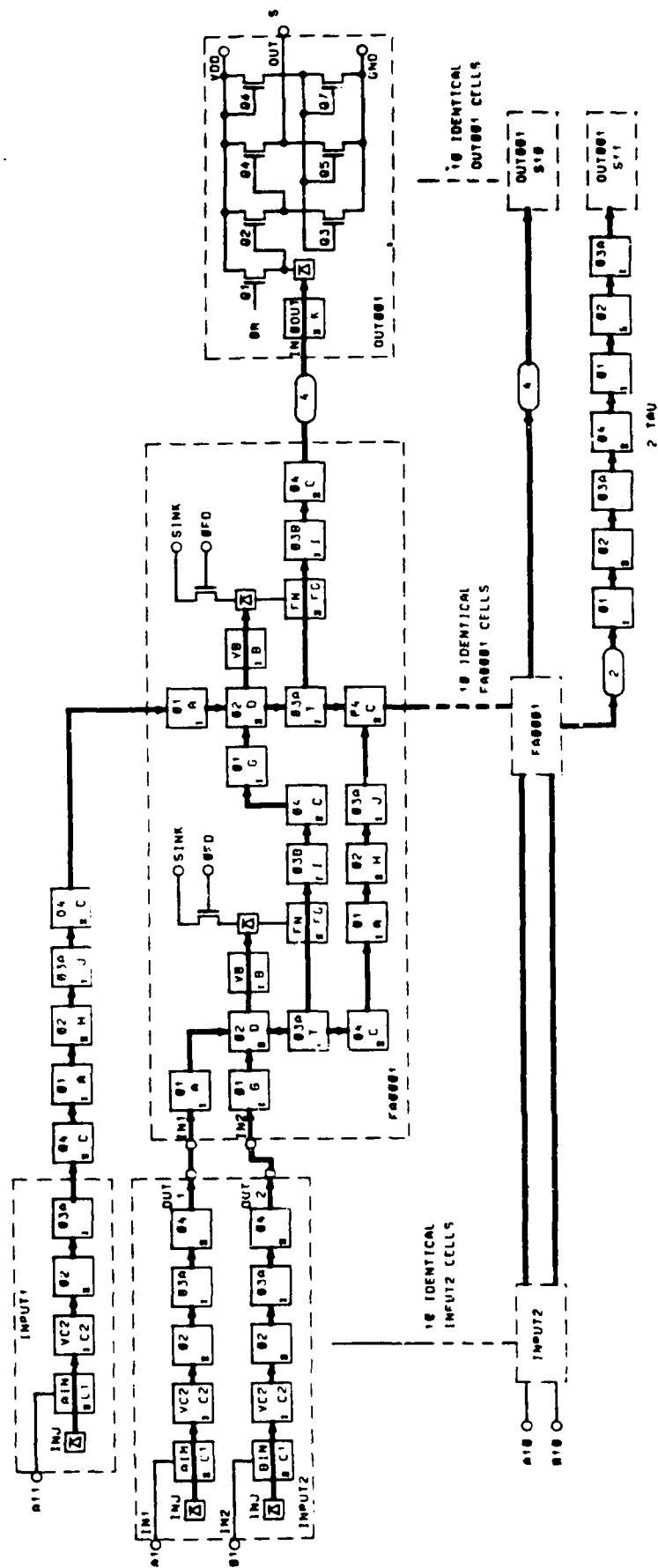


Figure 4-27. ACD2 10-Bit + 10-Bit Adder Array.

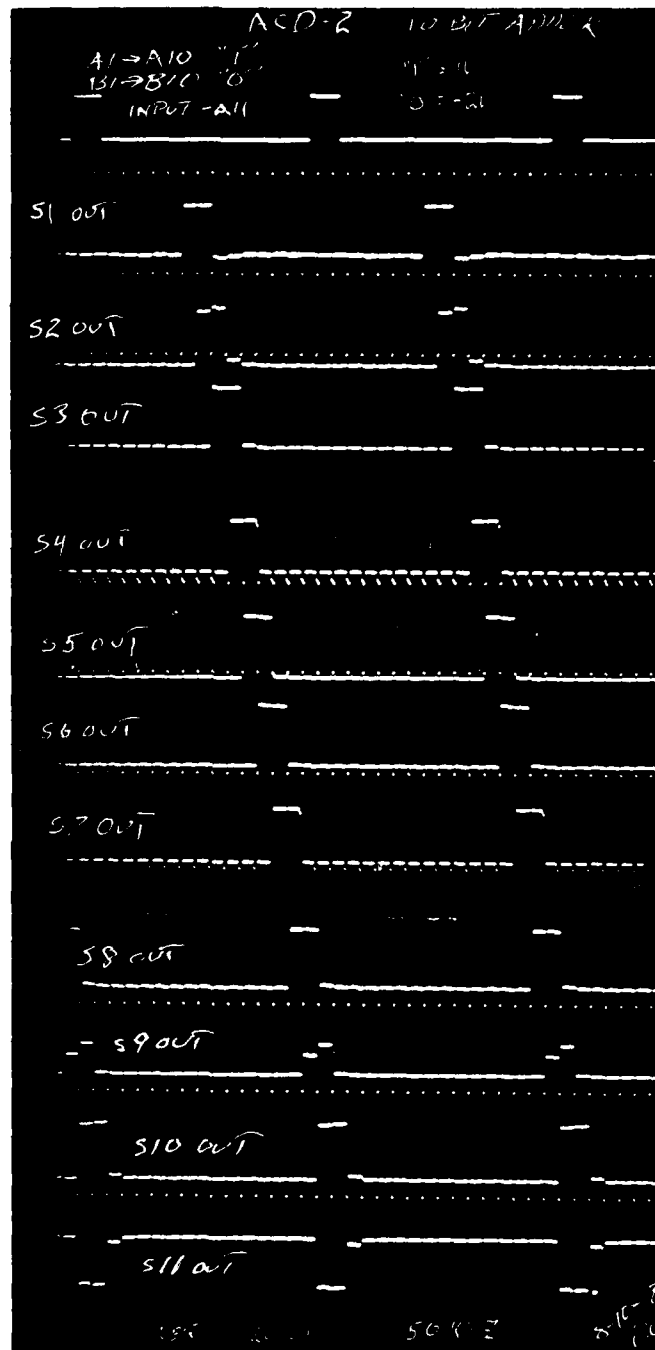


Figure 4-28. Photos of carry input and 11 output bits of the 10 bit adder.

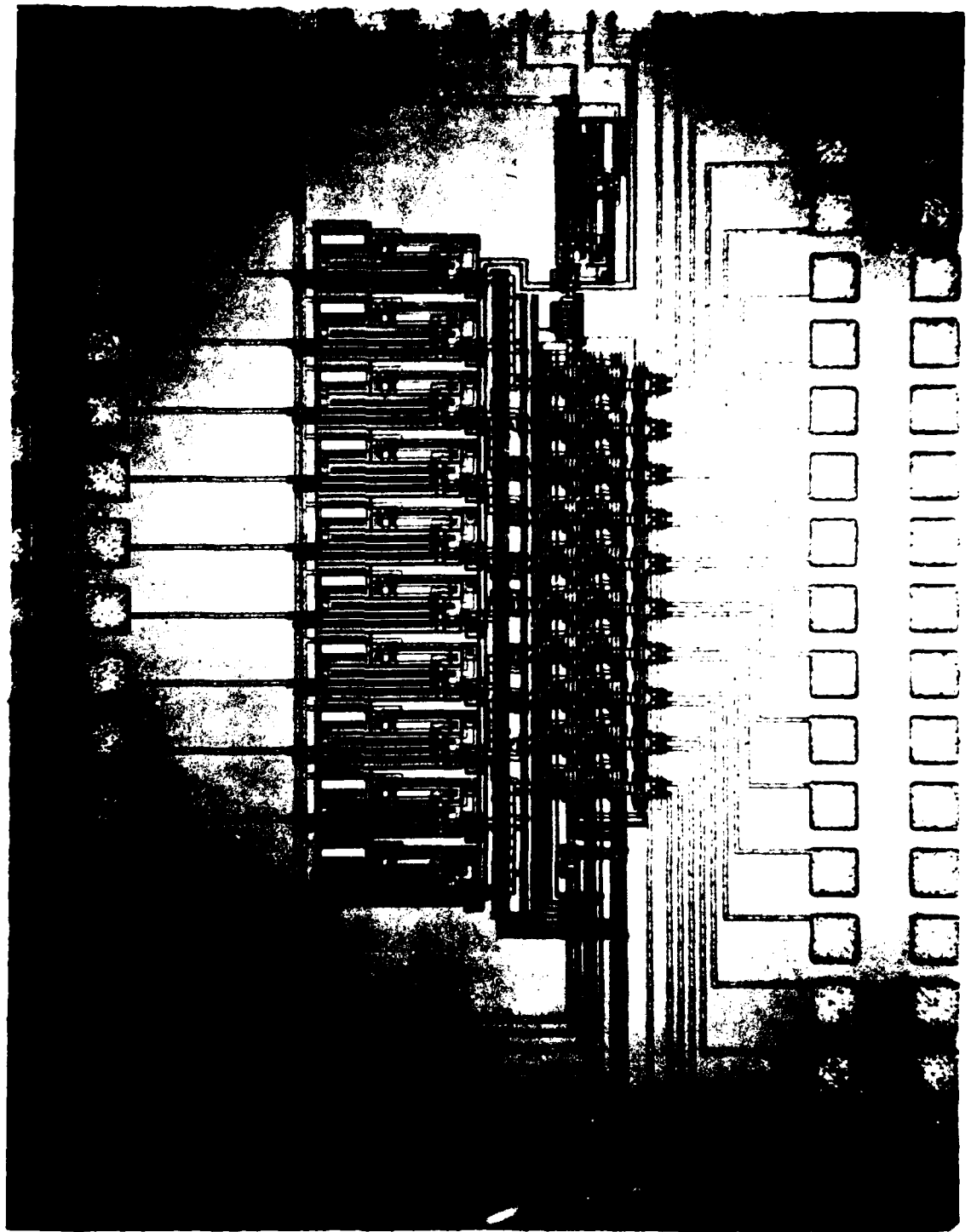


Figure 4-29. 10-Bit + 10-Bit Adder.

			$a_3$	$a_2$	$a_1$
			$b_3$	$b_2$	$b_1$
			$a_3b_1$	$a_2b_1$	$a_1b_1$
	$a_3b_2$	$a_2b_2$	$a_1b_2$		
	$a_2b_3$	$a_1b_3$			
	$a_3b_3$	$a_2b_3$	$a_1b_3$		
$p_6$	$p_5$	$p_4$	$p_3$	$p_2$	$p_1$

The nine summands must be formed with logic AND gates and then added by columns (with carries) to form the product  $p_6$  ---  $p_2, p_1$ .

The DPL 3 x 3 bit multipliers, designed in November 1975, were p-channel, metal polysilicon gate, 7.6  $\mu$  geometry devices. A block diagram of a 3 x 3 bit multiplier designed using AND gates and half-adders is shown in Figure 4-30. Also, a block diagram of the same multiplier implemented using AND gates and a mixture of half-adders and full-adders is shown in Figure 4-31. Photographs of these multipliers are shown in Figure 4-32 (half adder version) and Figure 4-33 (half adder and full adder mixture).

In February 1976 testing began on the 3 x 3 bit multiplier designed from a mixture of half-adders and full-adders. Two mask errors were found which limited the operation of the multiplier array. One error was a very narrow break in the metal connection to an input injection diode which prevented the  $a_1$  input (LSB) from operating. The second error was at missing contact to a polysilicon gate in the sum channel of the most significant full adder. However, since the most significant bit carry output functioned correctly it was possible to infer proper logic operation of all cells in the array. Correct logic operation of the entire multiplier array was demonstrated by keeping the  $a_1$  input constant at binary "0" and exercising the other five inputs through all possible combinations.

There are six parallel outputs from the multiplier array, so that obtaining a meaningful photograph showing simultaneous outputs is quite difficult. For simple input combinations where only four outputs are required,

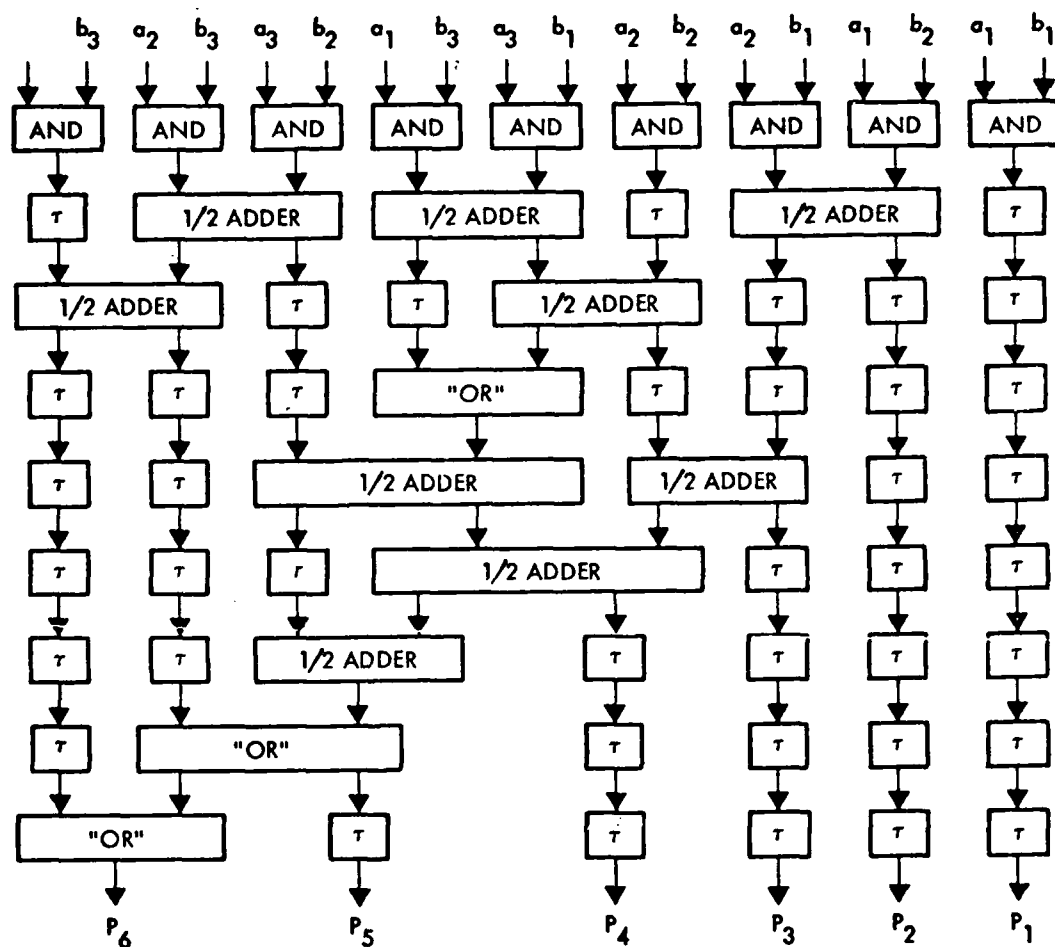


Figure 4-30. 3 x 3 Bit Multiplier using half adders and "or" circuits.

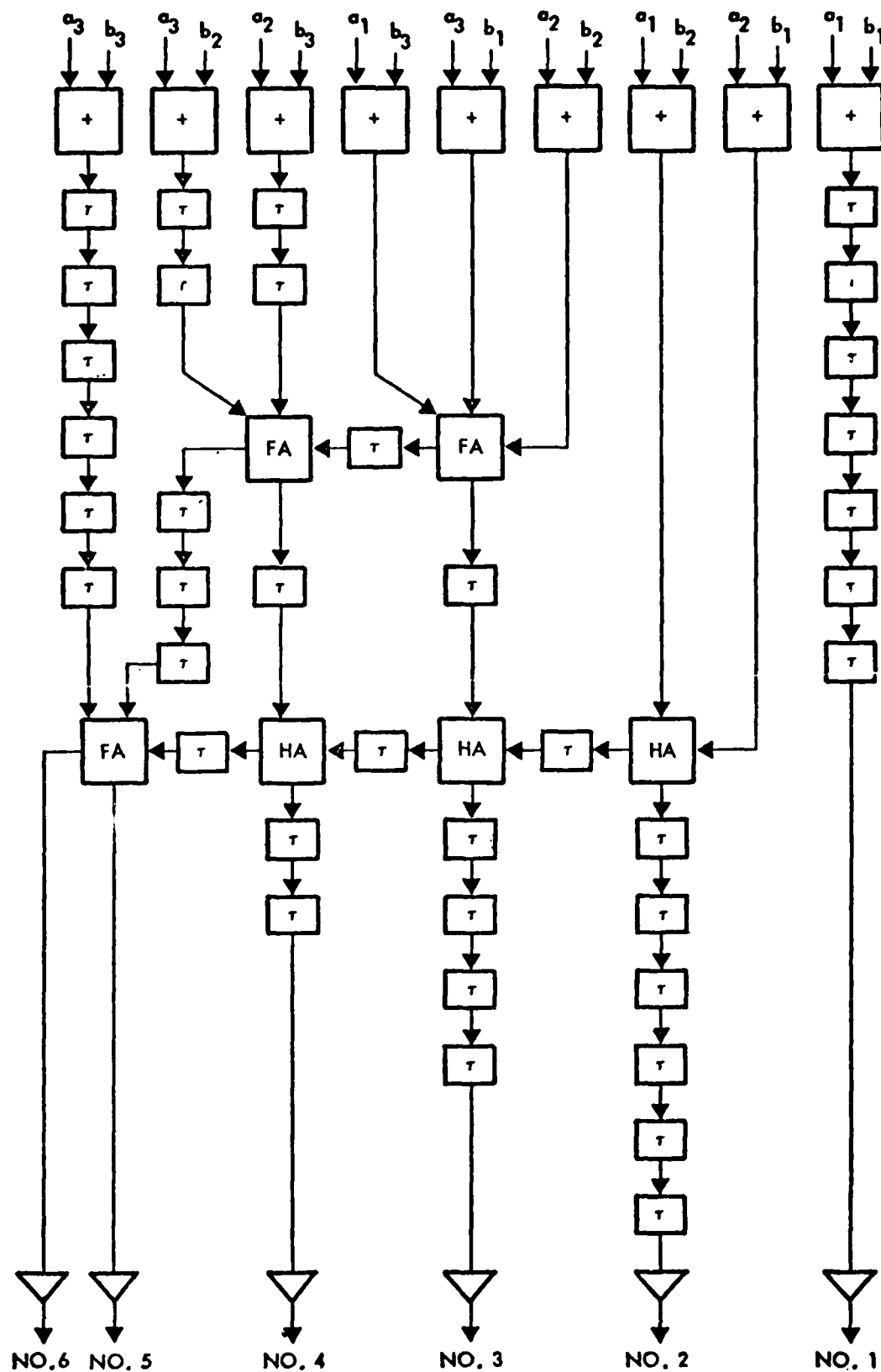


Figure 4-31. 3 x 3 bit multiplier using full adders and half adders.

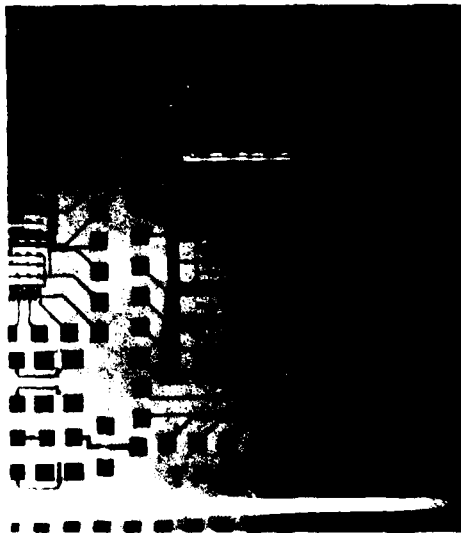


Figure 4-32. Half Adders.

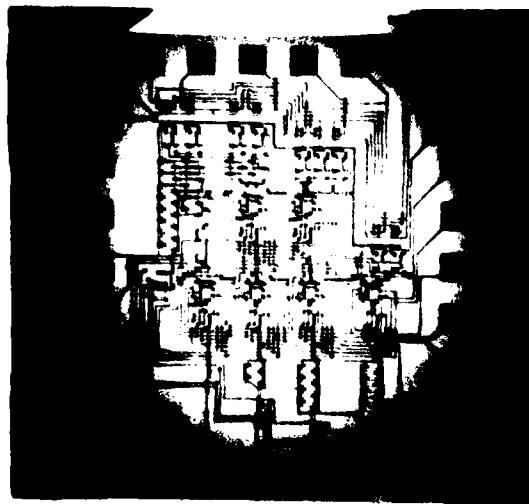


Figure 4-33. Full and Half Adders.

the output pulses wave forms are very similar to those shown previously for adder arrays. However, when all logic cells are operational and charges have to propagate through the MSB chain of full adder cells, there is some deterioration of the charge and a noticeable difference in the output pulse amplitudes depending upon bit position. Nevertheless, complete functional operational was achieved. Full, test results on this multiplier were published,<sup>(6)</sup> in September 1976.

The 3 x 3 bit multiplier designed entirely from half-adders was never successfully demonstrated. This was due to the additional number of charge transfers required by this approach, the large number of channels OR'd for the most significant bit, and some design errors discovered in the deskewing logic clocking scheme.

#### 4.3.2 The DP2 Multiplier Arrays

In April 1976 we started on the design of the DP2 test matrix. In this design, a change from a metal-polysilicon gate structure to a double-polysilicon structure was made.

In a similar manner as for the DP1 designs, the DP2 mask contained two versions of 3 x 3 bit multiplier. One multiplier employed cascaded dual half-adders as shown in Figure 4-34 had contained automatic carry refresh capabilities. The other multiplier, designed from full-adders and half-adders as shown in Figure 4-35, was designed without the refresh capability. Figure 4-34 shows that the generation of  $p_1$  (LSB) only requires an AND gate, the generation of  $p_2$  requires a half-adder, and the generation of  $p_3$  and  $p_4$ , both require three half-adders. This version of the 3 x 3 bit array utilizes nine AND gates, nine half-adders, three OR gates, seventeen 1-bit shift registers and six output buffers. There is a pipeline delay of four clock phases through this 3 x 3 bit multiplier. A photograph of the DP2 3 x 3 bit multiplier designed from cascaded half-adders is shown in Figure 4-36.

Testing performed on the cascaded half adder version of the DP2 3 x 3 bit multiplier verified correct operation for all combinations of input states. Oscilloscope photographs of the multiplier output for several different input data combinations are shown in Figures 4-37, 4-38, 4-39, 4-40, 4-41 and 4-42. In these figures,  $a_i$  and  $b_i$  represent the input bits and  $p_i$  represents the bits of the output product.

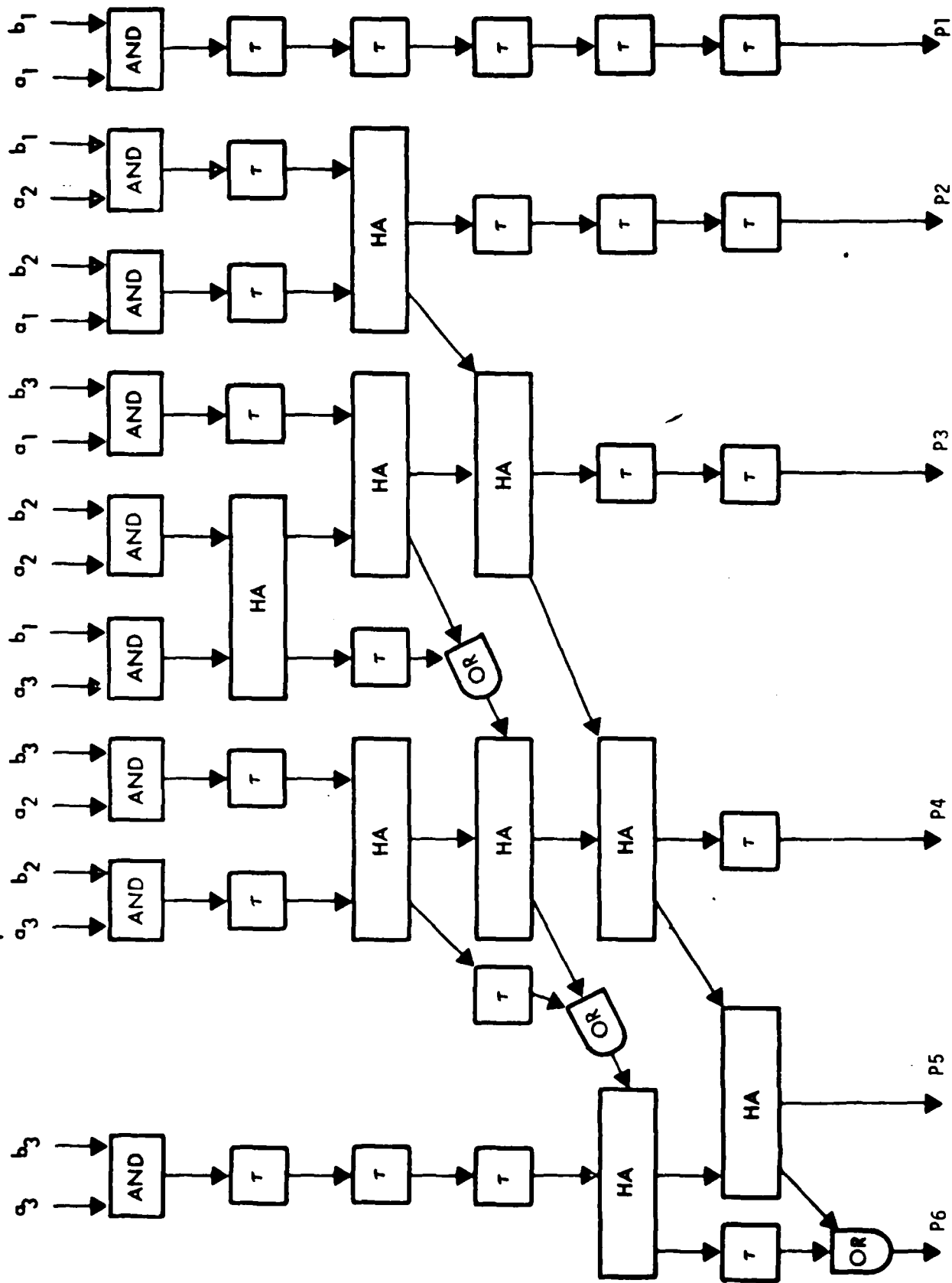


Figure 4-34. 3 x 3 bit multiplier utilizing half adder.

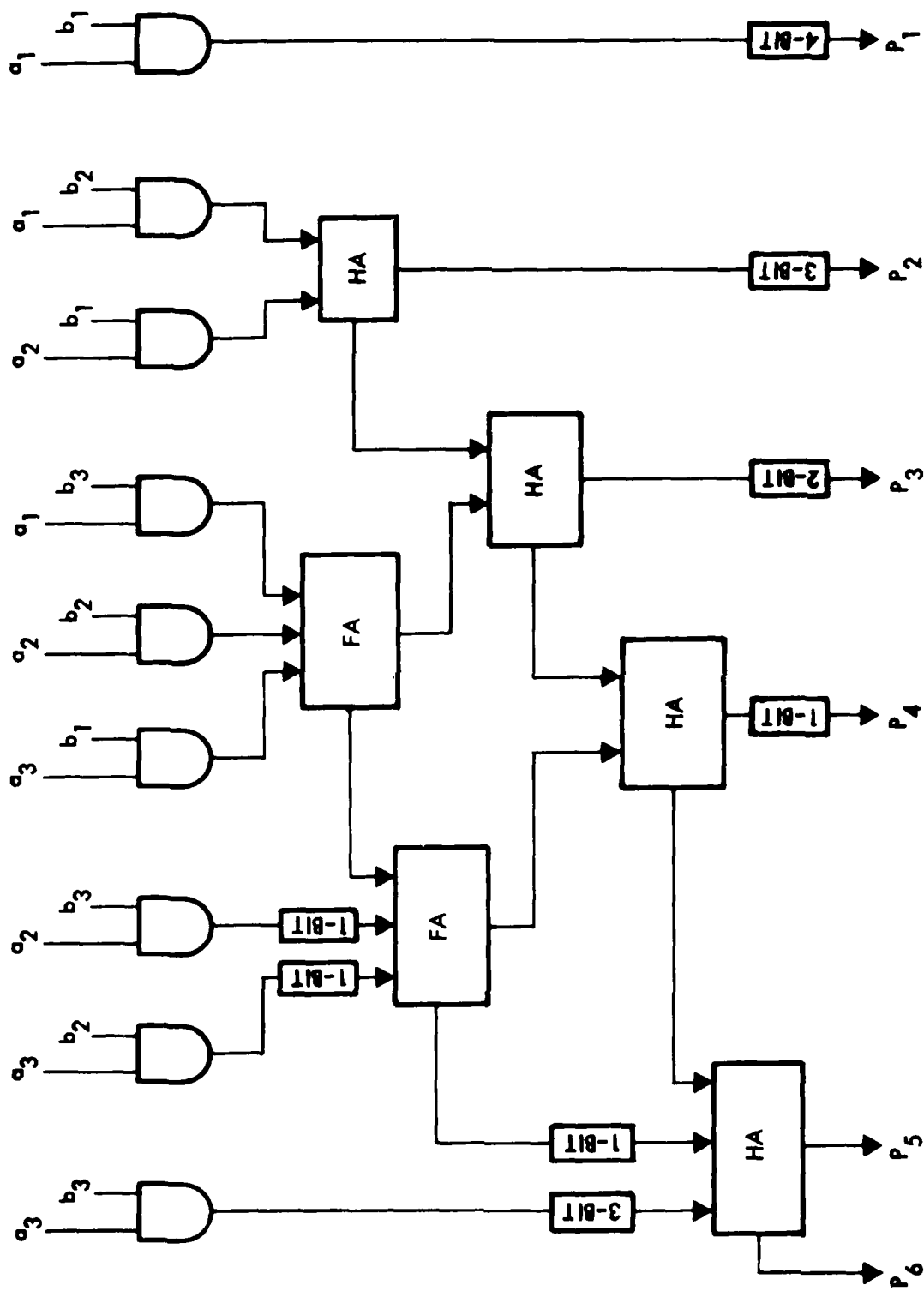


Figure 4-35. 3 x 3 bit multiplier utilizing full adders.

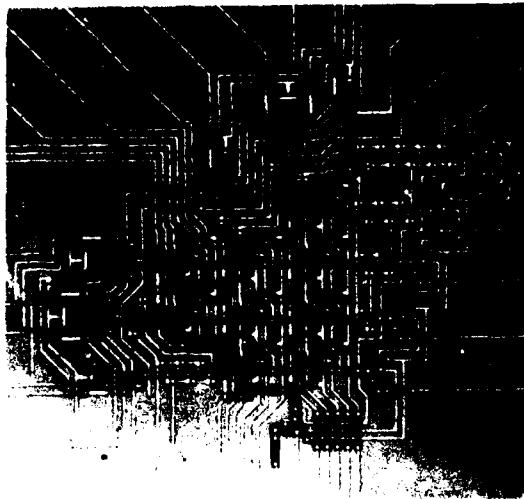


Figure 4-36. DP2.

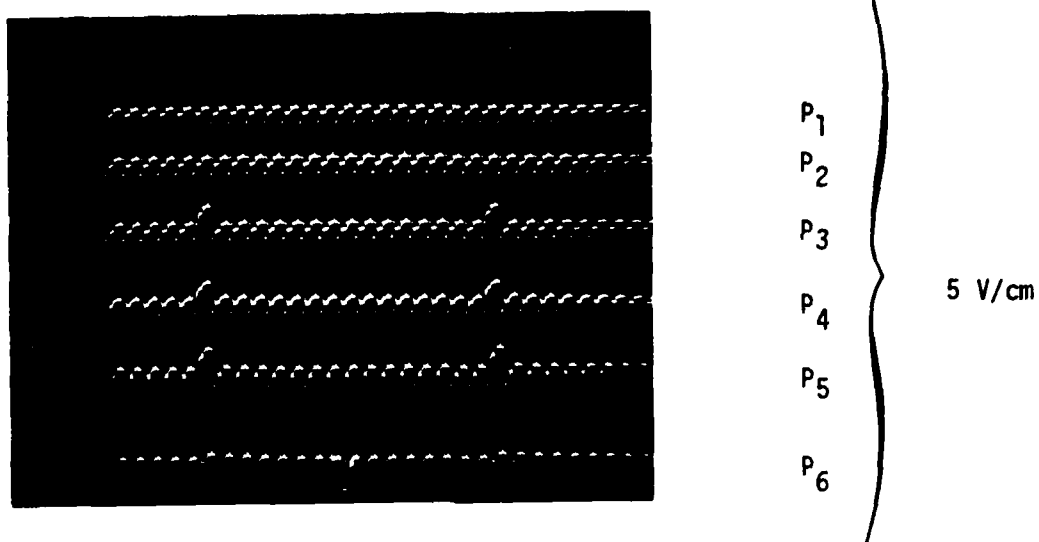


Figure 4-37. Input to the 2-Word, 3-Bit Multiplier

$a_i = 111$   
 $b_i = 100$  } 1.5 V/cm  
 $p_i = 011100$

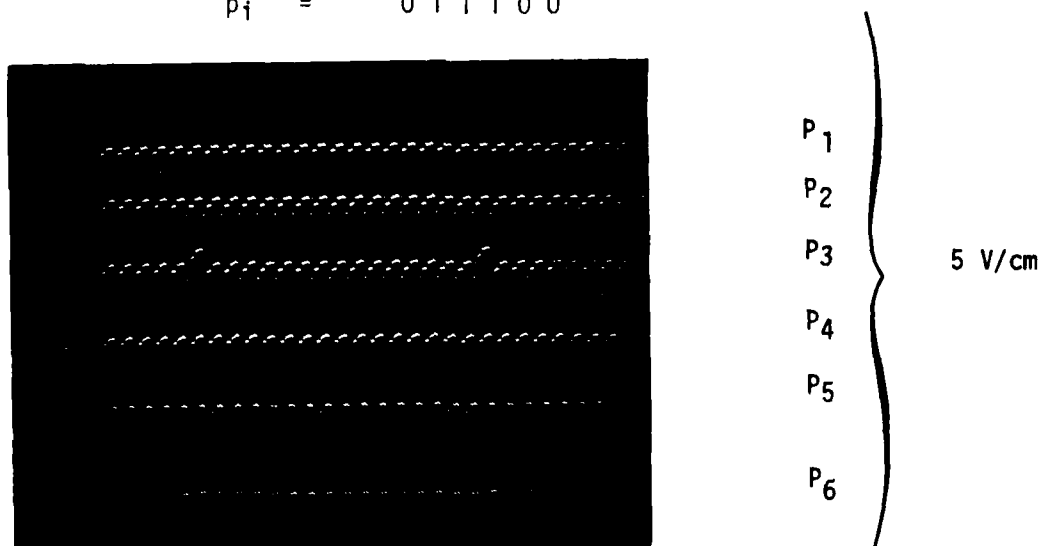
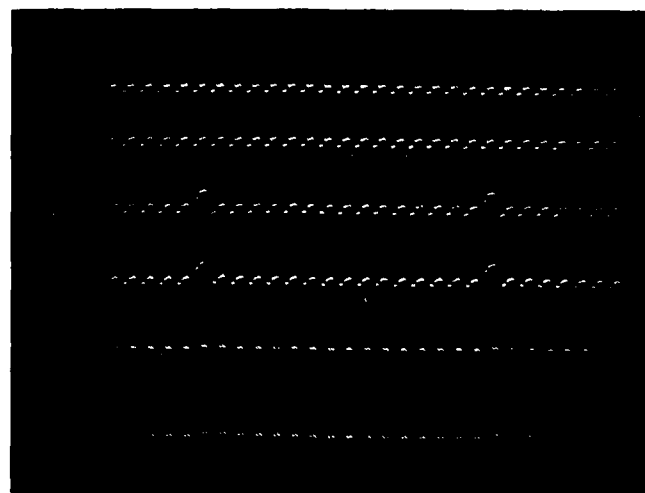


Figure 4-38. Input to the 2-Word, 3-Bit Multiplier

$a_i = 010$   
 $b_i = 010$  } 1.5 V/cm  
 $p_i = 000100$



P<sub>1</sub>

P<sub>2</sub>

P<sub>3</sub>

P<sub>4</sub>

P<sub>5</sub>

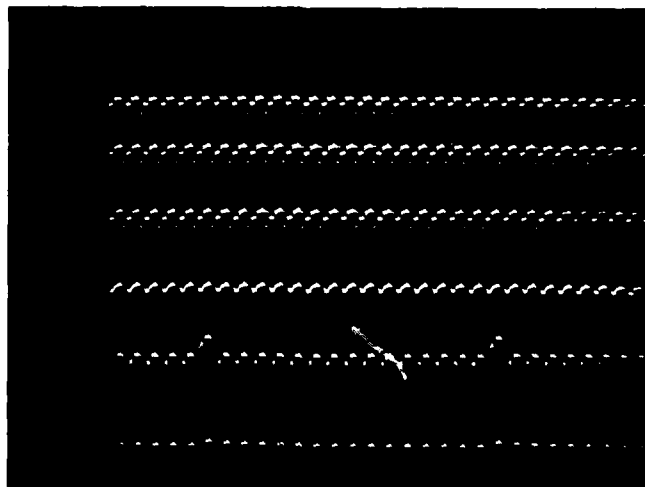
P<sub>6</sub>

5 V/cm

Figure 4-39. Input to the 2-Word, 3 Bit Multiplier

$a_i = 110$   
 $b_i = 010$   
 $p_i = 001100$

1.5 V/cm



P<sub>1</sub>

P<sub>2</sub>

P<sub>3</sub>

P<sub>4</sub>

P<sub>5</sub>

P<sub>6</sub>

5 V/cm

Figure 4-40. Input to the 2-Word, 3 Bit Multiplier

$a_i = 100$   
 $b_i = 100$   
 $p_i = 010000$

1.5 V/cm

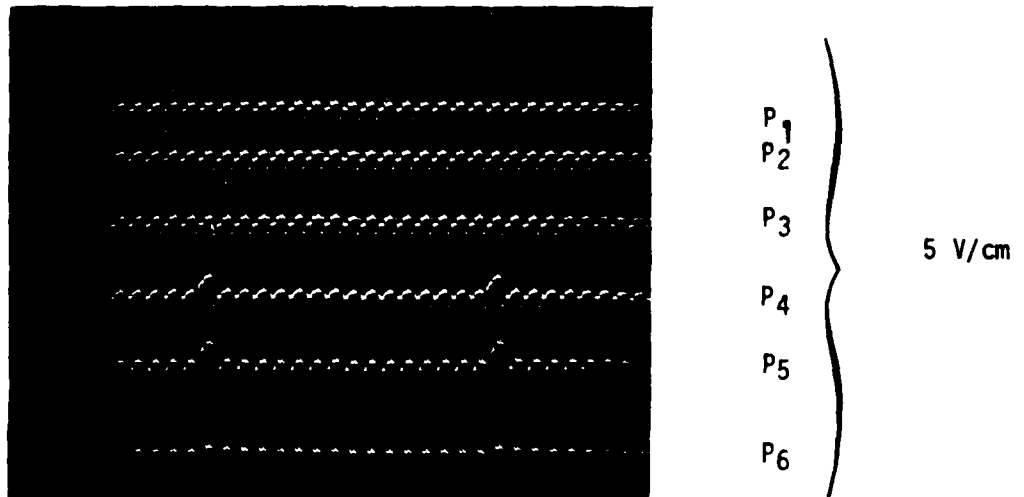


Figure 4-41. Input to the 2-Word, 3 Bit Multiplier

$a_i$	=	1 1 0	} 1.5 V/cm
$b_i$	=	1 0 0	
$p_i$	=	0 1 1 0 0 0	

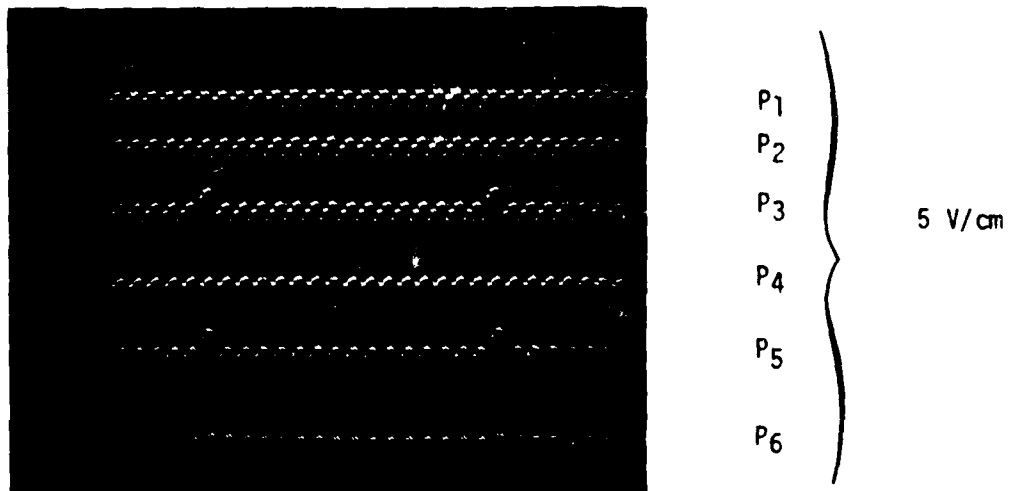


Figure 4-42. Input to the 2-Word, 3 Bit Multiplier

$a_i$	=	1 0 1	} 1.5 V/cm
$b_i$	=	1 0 0	
$p_i$	=	0 1 0 1 0 0	

The multiplier designed from a mixture of single binary level full-adders and half-adders was never successfully demonstrated.

#### 4.3.3 The DP3 Multiplier Array

The design and layout of a 8 x 8 bit multiplier for the DP3 test mask was begun in July 1976. The 8 x 8 multiplier requires many more operations than its DP2 3 x 3 bit predecessor as shown in Table 4-2.

The 64 summands are formed by 64 AND gates and then added by columns (with carries) to form the products  $p_{16}$  ---  $p_2, p_1$ . Note: for example, that if all inputs are a binary "1" then two carries are formed in the generation of  $p_3$  so that a total of six entries must be added to generate  $p_4$ . This increase in entries continues until we reach  $p_9$ ; this column has seven summands plus four carries resulting in a total of eleven entries. Thus, column  $p_9$  requires five cascaded half-adders or ten half-adders for implementation.

A block diagram of the DP3 8 x 8 bit multiplier is shown in Figure 4-43. This array requires 64 AND gates, 111 half-adders, 48 OR gates, 154 charge refresh cells, 466 single-bit shift-registers and 16 output buffers. This 8 x 8 bit multiplier exhibits a pipeline delay of 32 clock periods. A photograph of the DP3 8 x 8 bit multiplier is shown in Figure 4-44.

Although the carry output charge packet of the DP3 full-adder design contained the automatic refresh feature, the sum outputs remain attenuated by transfer losses. In the longest column of the DP3 multiplier array, a sum charge packet bit propagates through seven adders with each full-adder requiring four transfers. Prior test results from the DP-1 arrays showed that when a charge packet is reduced by more than eight transfers, it causes the arithmetic functions to become unreliable. Based on this data, the decision was made to restore the sum output charge packet after two levels of binary addition and restore the sum bit three times in each column.

Table 4-2. Algorithm for a 8 x 8 Bit Multiplier.

a <sub>8</sub>	a <sub>7</sub>	a <sub>6</sub>	a <sub>5</sub>	a <sub>4</sub>	a <sub>3</sub>	a <sub>2</sub>	a <sub>1</sub>								
b <sub>8</sub>	b <sub>7</sub>	b <sub>6</sub>	b <sub>5</sub>	b <sub>4</sub>	b <sub>3</sub>	b <sub>2</sub>	b <sub>1</sub>								
a <sub>8</sub> <sup>b</sup> <sub>1</sub>	a <sub>7</sub> <sup>b</sup> <sub>1</sub>	a <sub>6</sub> <sup>b</sup> <sub>1</sub>	a <sub>5</sub> <sup>b</sup> <sub>1</sub>	a <sub>4</sub> <sup>b</sup> <sub>1</sub>	a <sub>3</sub> <sup>b</sup> <sub>1</sub>	a <sub>2</sub> <sup>b</sup> <sub>1</sub>	a <sub>1</sub> <sup>b</sup> <sub>1</sub>								
a <sub>8</sub> <sup>b</sup> <sub>2</sub>	a <sub>7</sub> <sup>b</sup> <sub>2</sub>	a <sub>6</sub> <sup>b</sup> <sub>2</sub>	a <sub>5</sub> <sup>b</sup> <sub>2</sub>	a <sub>4</sub> <sup>b</sup> <sub>2</sub>	a <sub>3</sub> <sup>b</sup> <sub>2</sub>	a <sub>2</sub> <sup>b</sup> <sub>2</sub>	a <sub>1</sub> <sup>b</sup> <sub>2</sub>								
a <sub>8</sub> <sup>b</sup> <sub>3</sub>	a <sub>7</sub> <sup>b</sup> <sub>3</sub>	a <sub>6</sub> <sup>b</sup> <sub>3</sub>	a <sub>5</sub> <sup>b</sup> <sub>3</sub>	a <sub>4</sub> <sup>b</sup> <sub>3</sub>	a <sub>3</sub> <sup>b</sup> <sub>3</sub>	a <sub>2</sub> <sup>b</sup> <sub>3</sub>	a <sub>1</sub> <sup>b</sup> <sub>3</sub>								
a <sub>8</sub> <sup>b</sup> <sub>4</sub>	a <sub>7</sub> <sup>b</sup> <sub>4</sub>	a <sub>6</sub> <sup>b</sup> <sub>4</sub>	a <sub>5</sub> <sup>b</sup> <sub>4</sub>	a <sub>4</sub> <sup>b</sup> <sub>4</sub>	a <sub>3</sub> <sup>b</sup> <sub>4</sub>	a <sub>2</sub> <sup>b</sup> <sub>4</sub>	a <sub>1</sub> <sup>b</sup> <sub>4</sub>								
a <sub>8</sub> <sup>b</sup> <sub>5</sub>	a <sub>7</sub> <sup>b</sup> <sub>5</sub>	a <sub>6</sub> <sup>b</sup> <sub>5</sub>	a <sub>5</sub> <sup>b</sup> <sub>5</sub>	a <sub>4</sub> <sup>b</sup> <sub>5</sub>	a <sub>3</sub> <sup>b</sup> <sub>5</sub>	a <sub>2</sub> <sup>b</sup> <sub>5</sub>	a <sub>1</sub> <sup>b</sup> <sub>5</sub>								
a <sub>8</sub> <sup>b</sup> <sub>6</sub>	a <sub>7</sub> <sup>b</sup> <sub>6</sub>	a <sub>6</sub> <sup>b</sup> <sub>6</sub>	a <sub>5</sub> <sup>b</sup> <sub>6</sub>	a <sub>4</sub> <sup>b</sup> <sub>6</sub>	a <sub>3</sub> <sup>b</sup> <sub>6</sub>	a <sub>2</sub> <sup>b</sup> <sub>6</sub>	a <sub>1</sub> <sup>b</sup> <sub>6</sub>								
a <sub>8</sub> <sup>b</sup> <sub>7</sub>	a <sub>7</sub> <sup>b</sup> <sub>7</sub>	a <sub>6</sub> <sup>b</sup> <sub>7</sub>	a <sub>5</sub> <sup>b</sup> <sub>7</sub>	a <sub>4</sub> <sup>b</sup> <sub>7</sub>	a <sub>3</sub> <sup>b</sup> <sub>7</sub>	a <sub>2</sub> <sup>b</sup> <sub>7</sub>	a <sub>1</sub> <sup>b</sup> <sub>7</sub>								
a <sub>8</sub> <sup>b</sup> <sub>8</sub>	a <sub>7</sub> <sup>b</sup> <sub>8</sub>	a <sub>6</sub> <sup>b</sup> <sub>8</sub>	a <sub>5</sub> <sup>b</sup> <sub>8</sub>	a <sub>4</sub> <sup>b</sup> <sub>8</sub>	a <sub>3</sub> <sup>b</sup> <sub>8</sub>	a <sub>2</sub> <sup>b</sup> <sub>8</sub>	a <sub>1</sub> <sup>b</sup> <sub>8</sub>								
P <sub>16</sub>	P <sub>15</sub>	P <sub>14</sub>	P <sub>13</sub>	P <sub>12</sub>	P <sub>11</sub>	P <sub>10</sub>	P <sub>9</sub>	P <sub>8</sub>	P <sub>7</sub>	P <sub>6</sub>	P <sub>5</sub>	P <sub>4</sub>	P <sub>3</sub>	P <sub>2</sub>	P <sub>1</sub>
0	1	2	3	4	5	6	7	8	7	6	5	4	3	2	1
1	2	2	3	3	4	4	4	4	4	3	2	2	1	0	0
0	1	2	2	3	3	4	4	4	4	4	3	2	2	1	0
SUMMANDS'															
CARRIES ADDED															
CARRIES FORMED															

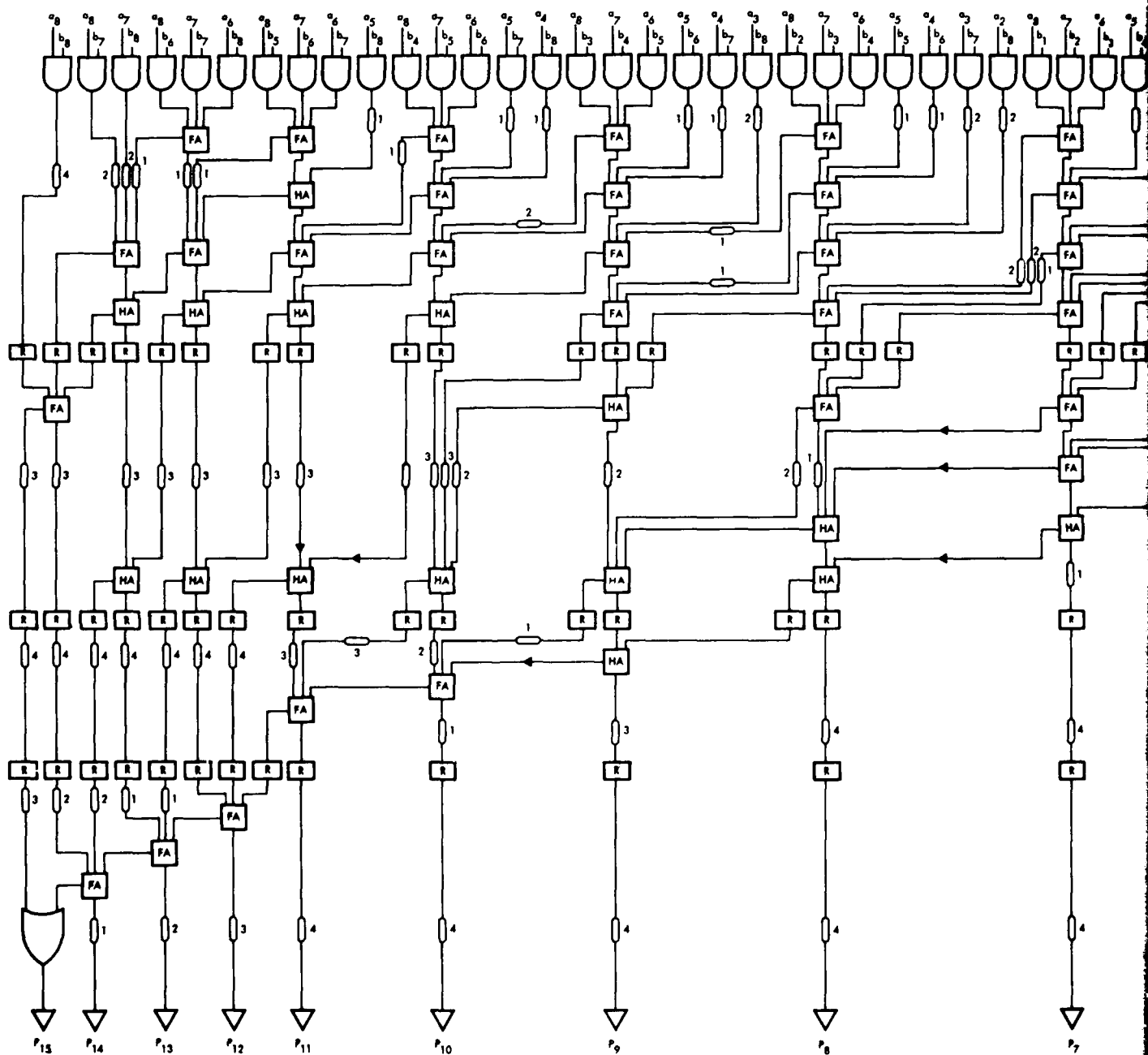


Figure 4-43. Schematic diagram of the 8-bit x 8-bit multiplier.

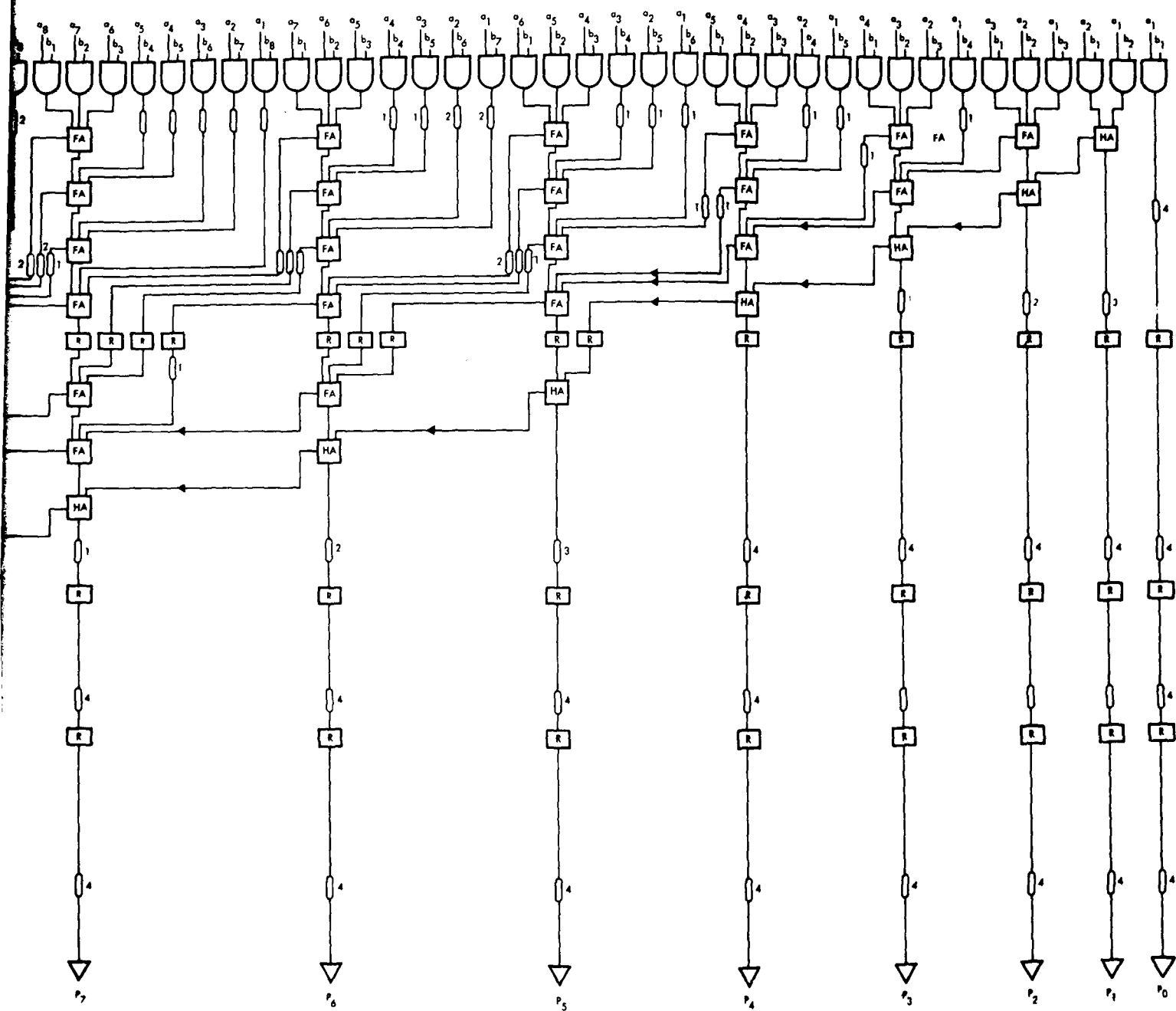




Figure 4-44. DP3 8 x 8 Multiplier Array.

A half-adder cell was modified to form a charge refresh cell by connecting one input to a constant logic "1" value. When a degraded (from transfer loss effects) charge packet is transferred into the other half-adder input, the carry out port of the half adder provide a fully restored charge level. This simple charge restoring cell measures 5.4 x 2.1 mils. In this version of the restoring cell, the usual half-adder sum output is connected to a sink diode. However, in more complex layout, the sum output can be taken to an output FET source-follower to provide a " $\bar{A}$ -out" test point. This logic cell measures 7.9 x 3.9 mils and introduces two extra transfers. It was used in the array after four levels of addition where the column density is reduced from 43 at the first level of restoration to 29 at the second level.

Since the design of the DP3 8 x 8 bit array used the same logic cells as the 16 + 16 bit adder previously described in Section 4.2.4, it also had the identical race condition and was untestable. Due to the tight development schedule, the decision was made not to correct the design in order to proceed with the design of the DP4 test mask.

#### 4.3.4 The DP4 Multiplier Array

The design of the DP4 16 x 16 multiplier began in May 1977. The DP4 multiplier was a 3-phase, n-channel, double-polysilicon overlapping gate structure. Up until this design, all previous DP series multipliers had been 2-phase, p-channel. The complexity of the 61 x 16 bit multiplier can be seen from Table 4-3.

A considerable amount of time was spent in digitizing large standard building blocks from four levels of full-adders and attempting to interconnect the cells without adding extra pipeline delays. A refresh cell imposes two additional pipeline delays on the throughput of the multiplier. It was calculated that, at the system speed requirements of 5 MHz clock rate, we would have to refresh the SUM channels between each level of 4 cascaded full-adders. Thus, there would be six levels of refresh required corresponding to a total pipeline delay of thirty nine clock periods.

Layout of the cells and interconnection of the DP4 16-bit x 16-bit multiplier continued until September 1977 when it became evident that the DP4

[illegible]

		a <sub>16</sub>	a <sub>15</sub>	a <sub>14</sub>	a <sub>13</sub>	a <sub>12</sub>	a <sub>11</sub>	a <sub>10</sub>	a <sub>9</sub>	a <sub>8</sub>	a <sub>7</sub>	a <sub>6</sub>	a <sub>5</sub>	a <sub>4</sub>	a <sub>3</sub>	a <sub>2</sub>	a <sub>1</sub>
		b <sub>16</sub>	b <sub>15</sub>	b <sub>14</sub>	b <sub>13</sub>	b <sub>12</sub>	b <sub>11</sub>	b <sub>10</sub>	b <sub>9</sub>	b <sub>8</sub>	b <sub>7</sub>	b <sub>6</sub>	b <sub>5</sub>	b <sub>4</sub>	b <sub>3</sub>	b <sub>2</sub>	b <sub>1</sub>
		a <sub>16</sub> b <sub>1</sub>	a <sub>15</sub> b <sub>1</sub>	a <sub>14</sub> b <sub>1</sub>	a <sub>13</sub> b <sub>1</sub>	a <sub>12</sub> b <sub>1</sub>	a <sub>11</sub> b <sub>1</sub>	a <sub>10</sub> b <sub>1</sub>	a <sub>9</sub> b <sub>1</sub>	a <sub>8</sub> b <sub>1</sub>	a <sub>7</sub> b <sub>1</sub>	a <sub>6</sub> b <sub>1</sub>	a <sub>5</sub> b <sub>1</sub>	a <sub>4</sub> b <sub>1</sub>	a <sub>3</sub> b <sub>1</sub>	a <sub>2</sub> b <sub>1</sub>	a <sub>1</sub> b <sub>1</sub>
	a <sub>16</sub> b <sub>2</sub>	a <sub>15</sub> b <sub>2</sub>	a <sub>14</sub> b <sub>2</sub>	a <sub>13</sub> b <sub>2</sub>	a <sub>12</sub> b <sub>2</sub>	a <sub>11</sub> b <sub>2</sub>	a <sub>10</sub> b <sub>2</sub>	a <sub>9</sub> b <sub>2</sub>	a <sub>8</sub> b <sub>2</sub>	a <sub>7</sub> b <sub>2</sub>	a <sub>6</sub> b <sub>2</sub>	a <sub>5</sub> b <sub>2</sub>	a <sub>4</sub> b <sub>2</sub>	a <sub>3</sub> b <sub>2</sub>	a <sub>2</sub> b <sub>2</sub>	a <sub>1</sub> b <sub>2</sub>	
a <sub>16</sub> b <sub>3</sub>	a <sub>15</sub> b <sub>3</sub>	a <sub>14</sub> b <sub>3</sub>	a <sub>13</sub> b <sub>3</sub>	a <sub>12</sub> b <sub>3</sub>	a <sub>11</sub> b <sub>3</sub>	a <sub>10</sub> b <sub>3</sub>	a <sub>9</sub> b <sub>3</sub>	a <sub>8</sub> b <sub>3</sub>	a <sub>7</sub> b <sub>3</sub>	a <sub>6</sub> b <sub>3</sub>	a <sub>5</sub> b <sub>3</sub>	a <sub>4</sub> b <sub>3</sub>	a <sub>3</sub> b <sub>3</sub>	a <sub>2</sub> b <sub>3</sub>	a <sub>1</sub> b <sub>3</sub>	3 X 3 ARRAY	
a <sub>15</sub> b <sub>4</sub>	a <sub>14</sub> b <sub>4</sub>	a <sub>13</sub> b <sub>4</sub>	a <sub>12</sub> b <sub>4</sub>	a <sub>11</sub> b <sub>4</sub>	a <sub>10</sub> b <sub>4</sub>	a <sub>9</sub> b <sub>4</sub>	a <sub>8</sub> b <sub>4</sub>	a <sub>7</sub> b <sub>4</sub>	a <sub>6</sub> b <sub>4</sub>	a <sub>5</sub> b <sub>4</sub>	a <sub>4</sub> b <sub>4</sub>	a <sub>3</sub> b <sub>4</sub>	a <sub>2</sub> b <sub>4</sub>	a <sub>1</sub> b <sub>4</sub>			
a <sub>14</sub> b <sub>5</sub>	a <sub>13</sub> b <sub>5</sub>	a <sub>12</sub> b <sub>5</sub>	a <sub>11</sub> b <sub>5</sub>	a <sub>10</sub> b <sub>5</sub>	a <sub>9</sub> b <sub>5</sub>	a <sub>8</sub> b <sub>5</sub>	a <sub>7</sub> b <sub>5</sub>	a <sub>6</sub> b <sub>5</sub>	a <sub>5</sub> b <sub>5</sub>	a <sub>4</sub> b <sub>5</sub>	a <sub>3</sub> b <sub>5</sub>	a <sub>2</sub> b <sub>5</sub>	a <sub>1</sub> b <sub>5</sub>				
a <sub>13</sub> b <sub>6</sub>	a <sub>12</sub> b <sub>6</sub>	a <sub>11</sub> b <sub>6</sub>	a <sub>10</sub> b <sub>6</sub>	a <sub>9</sub> b <sub>6</sub>	a <sub>8</sub> b <sub>6</sub>	a <sub>7</sub> b <sub>6</sub>	a <sub>6</sub> b <sub>6</sub>	a <sub>5</sub> b <sub>6</sub>	a <sub>4</sub> b <sub>6</sub>	a <sub>3</sub> b <sub>6</sub>	a <sub>2</sub> b <sub>6</sub>	a <sub>1</sub> b <sub>6</sub>					
a <sub>12</sub> b <sub>7</sub>	a <sub>11</sub> b <sub>7</sub>	a <sub>10</sub> b <sub>7</sub>	a <sub>9</sub> b <sub>7</sub>	a <sub>8</sub> b <sub>7</sub>	a <sub>7</sub> b <sub>7</sub>	a <sub>6</sub> b <sub>7</sub>	a <sub>5</sub> b <sub>7</sub>	a <sub>4</sub> b <sub>7</sub>	a <sub>3</sub> b <sub>7</sub>	a <sub>2</sub> b <sub>7</sub>	a <sub>1</sub> b <sub>7</sub>						
a <sub>11</sub> b <sub>8</sub>	a <sub>10</sub> b <sub>8</sub>	a <sub>9</sub> b <sub>8</sub>	a <sub>8</sub> b <sub>8</sub>	a <sub>7</sub> b <sub>8</sub>	a <sub>6</sub> b <sub>8</sub>	a <sub>5</sub> b <sub>8</sub>	a <sub>4</sub> b <sub>8</sub>	a <sub>3</sub> b <sub>8</sub>	a <sub>2</sub> b <sub>8</sub>	a <sub>1</sub> b <sub>8</sub>				8 X 8 ARRAY			
a <sub>10</sub> b <sub>9</sub>	a <sub>9</sub> b <sub>9</sub>	a <sub>8</sub> b <sub>9</sub>	a <sub>7</sub> b <sub>9</sub>	a <sub>6</sub> b <sub>9</sub>	a <sub>5</sub> b <sub>9</sub>	a <sub>4</sub> b <sub>9</sub>	a <sub>3</sub> b <sub>9</sub>	a <sub>2</sub> b <sub>9</sub>	a <sub>1</sub> b <sub>9</sub>								
a <sub>9</sub> b <sub>10</sub>	a <sub>8</sub> b <sub>10</sub>	a <sub>7</sub> b <sub>10</sub>	a <sub>6</sub> b <sub>10</sub>	a <sub>5</sub> b <sub>10</sub>	a <sub>4</sub> b <sub>10</sub>	a <sub>3</sub> b <sub>10</sub>	a <sub>2</sub> b <sub>10</sub>	a <sub>1</sub> b <sub>10</sub>									
a <sub>8</sub> b <sub>11</sub>	a <sub>7</sub> b <sub>11</sub>	a <sub>6</sub> b <sub>11</sub>	a <sub>5</sub> b <sub>11</sub>	a <sub>4</sub> b <sub>11</sub>	a <sub>3</sub> b <sub>11</sub>	a <sub>2</sub> b <sub>11</sub>	a <sub>1</sub> b <sub>11</sub>										
a <sub>7</sub> b <sub>12</sub>	a <sub>6</sub> b <sub>12</sub>	a <sub>5</sub> b <sub>12</sub>	a <sub>4</sub> b <sub>12</sub>	a <sub>3</sub> b <sub>12</sub>	a <sub>2</sub> b <sub>12</sub>	a <sub>1</sub> b <sub>12</sub>		12 X 12 ARRAY									
a <sub>6</sub> b <sub>13</sub>	a <sub>5</sub> b <sub>13</sub>	a <sub>4</sub> b <sub>13</sub>	a <sub>3</sub> b <sub>13</sub>	a <sub>2</sub> b <sub>13</sub>	a <sub>1</sub> b <sub>13</sub>												
a <sub>5</sub> b <sub>14</sub>	a <sub>4</sub> b <sub>14</sub>	a <sub>3</sub> b <sub>14</sub>	a <sub>2</sub> b <sub>14</sub>	a <sub>1</sub> b <sub>14</sub>													
a <sub>4</sub> b <sub>15</sub>	a <sub>3</sub> b <sub>15</sub>	a <sub>2</sub> b <sub>15</sub>	a <sub>1</sub> b <sub>15</sub>														
a <sub>3</sub> b <sub>16</sub>	a <sub>2</sub> b <sub>16</sub>	a <sub>1</sub> b <sub>16</sub>		16 X 16 ARRAY													
P <sub>18</sub>	P <sub>17</sub>	P <sub>16</sub>	P <sub>15</sub>	P <sub>14</sub>	P <sub>13</sub>	P <sub>12</sub>	P <sub>11</sub>	P <sub>10</sub>	P <sub>9</sub>	P <sub>8</sub>	P <sub>7</sub>	P <sub>6</sub>	P <sub>5</sub>	P <sub>4</sub>	P <sub>3</sub>	P <sub>2</sub>	P <sub>1</sub>
15	15	14	13	12	11	10	9	8	7	6	5	4	3	2	1	0	0
14	14	14	13	12	11	10	9	8	7	6	5	4	3	2	1	0	0
0	1	1	1	1	1	1	1	1	1	1	1	1	1	1	0	0	0

Table 4-3. Algorithm for a 16-bit x 16-bit multiplier.

design was much more complex than originally envisioned. Work on DP4 mask was stopped when it was concluded that the probability of successfully completing the layout within the program cost and schedule constraints was very small.

In retrospect it appears that although the Wallace algorithm as shown in Tables 4-1 and 4-3 may be suitable for implementation in digital CCD logic up to 8-bits x 8-bits it becomes too complex to implement for larger numbers. Possibly the algorithm proposed,<sup>(8)</sup> by Robert Logan, in which high-speed multiplication by summing squares is described could be more simply implemented.

#### 4.3.5 The Azimuth Correlator Device (ACD) Multiplier Array

A complex multiplication was required for the ACD project (described in Section 9.3). This requirement was implemented with 4 separate, but identical, multipliers. All of the previous multiplier designs performed a magnitude only product. The ACD system required a 6 x 4 bit 2's complement multiplier. The algorithm for performing this multiplication is shown in Table 4-4.

Table 4-4. Multiplication of 6 x 4, 2's Complement Numbers  
Producing a Positive Product

$2^0$	$2^{-1}$	$2^{-2}$	$2^{-3}$	$2^{-4}$	$2^{-5}$	$2^{-6}$	$2^{-7}$	$2^{-8}$
$(A_0+B_9)$	$A_0\bar{B}_1$	$A_0\bar{B}_2$	$A_0\bar{B}_3$					
	$B_0\bar{A}_1$	$B_0\bar{A}_2$	$B_0\bar{A}_3$	$B_0\bar{A}_4$	$B_0\bar{A}_5$			
		$A_0$			$B_0$			
		$A_1B_1$	$A_2B_1$	$A_3B_1$	$A_3B_1$	$A_5B_1$		
			$A_1B_2$	$A_2B_2$	$A_3B_2$	$A_4B_2$	$A_5B_2$	
				$A_1B_3$	$A_2B_3$	$A_3B_3$	$A_4B_3$	$A_5B_3$
$P_0$	$P_1$	$P_2$	$P_3$	$P_4$	$P_5$	$P_6$	$P_7$	$P_8$

The 3-phase, n-channel half-adder designed for the NE-1 chip was modified for 4-phase clocks and the transfer lengths of the gates reduced to meet the 3.5 MHz ACD clock speed requirement.

The ACDO (first test mask) multiplier was implemented entirely from half-adders in a nearly identical manner to the 3 x 3 bit multiplier described in Section 4.3.1. The single half-adder was chosen as the basic building block of the multiplier because of the speed with which the cell could be step-and-repeated into an array in the CAD system. In practice we found that the attendant custom skewing delay layout required more time and effort than that saved by the cell step and repeat procedure.

A schematic diagram of the ACDO 6 x 4 bit multiplier is shown in Figure 4-45. As seen from this diagram, there are four refresh levels required in this multiplier and a pipeline delay of twenty-six clock periods for the most significant output product. This multiplier uses 21 AND gates, 37 charge refresh cells, 85 half-adders, and measures 100 x 82 mils. Deskewing of the output product bits was not performed. The output products are transferred directly into charge-comparator latches. Design problems in these charge comparator amplifiers made it impossible to get two of them to function from the same voltage clock lines. This made it impossible to meaningfully test the ACDO multiplier.

#### 4.3.6 The ACD2 Multiplier Array

The revised version (ACD2) of the 6-bit x 4-bit 2's complement multiplier utilized dual cascaded half-adders as shown in the schematic diagram of Figure 4-46. As can be seen from this diagram, only one level of charge refresh is required and only 10 pipeline delays are required for the most significant product. This multiplier contains 21 AND gates, 6 charge refresh cells, 35 half-adders and measures 54 x 52 mils and requires only one third the area of the ACDO multiplier. Deskewing of the product was still not performed. However, to avoid the ACDO charge comparator amplifier problem, the output product charge packets were transferred into NMOS analog source follower output buffers. This multiplier was tested in September 1979 and performed correctly over the frequency range 50 kHz to 500 kHz. Higher frequency operation is expected from packaged devices. A photograph of the ACD2 6 x 4 bit multiplier is shown in Figure 4-47.

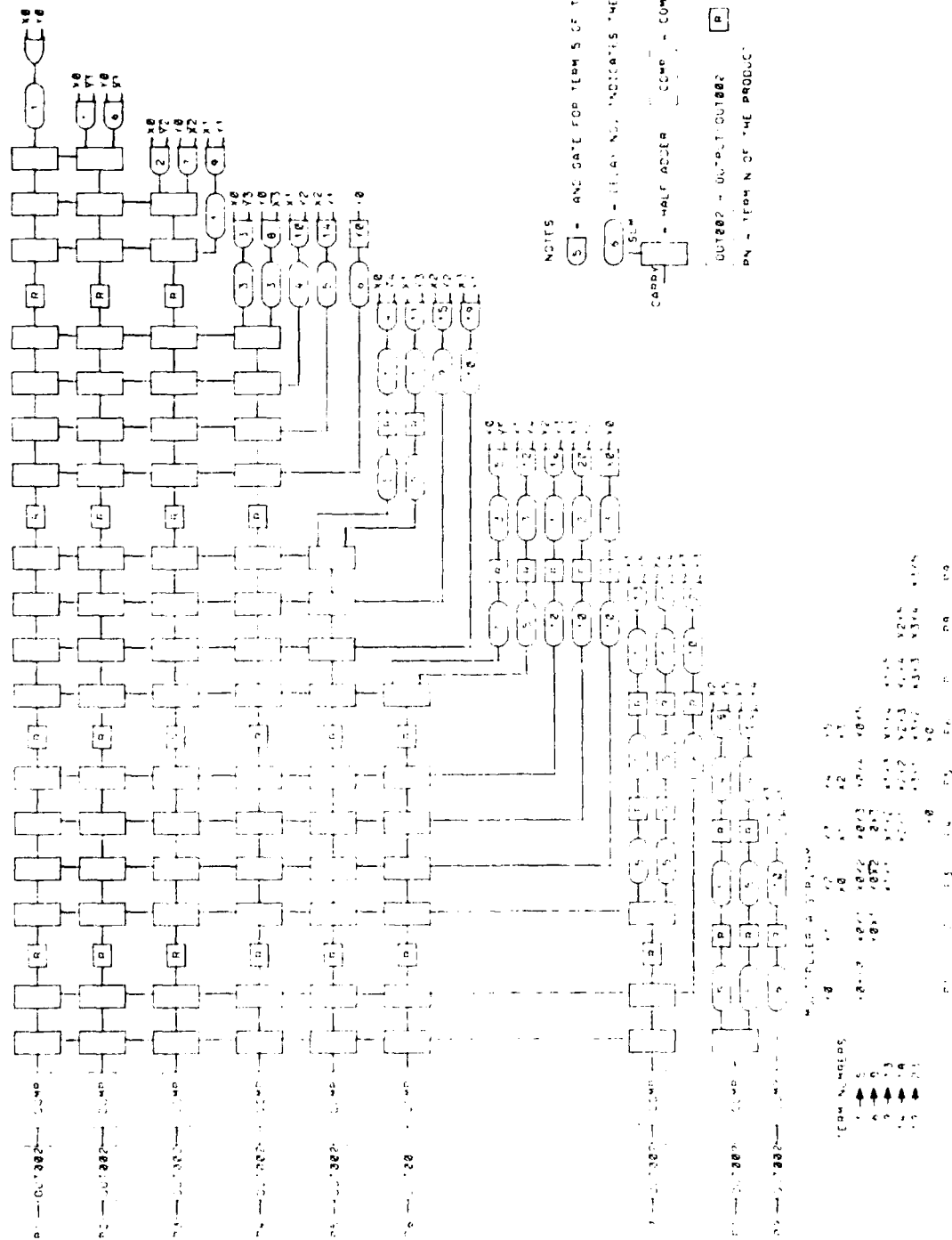


Figure 4-45. ACD0 2' Complement 4 x 6 Bit Multiplier.



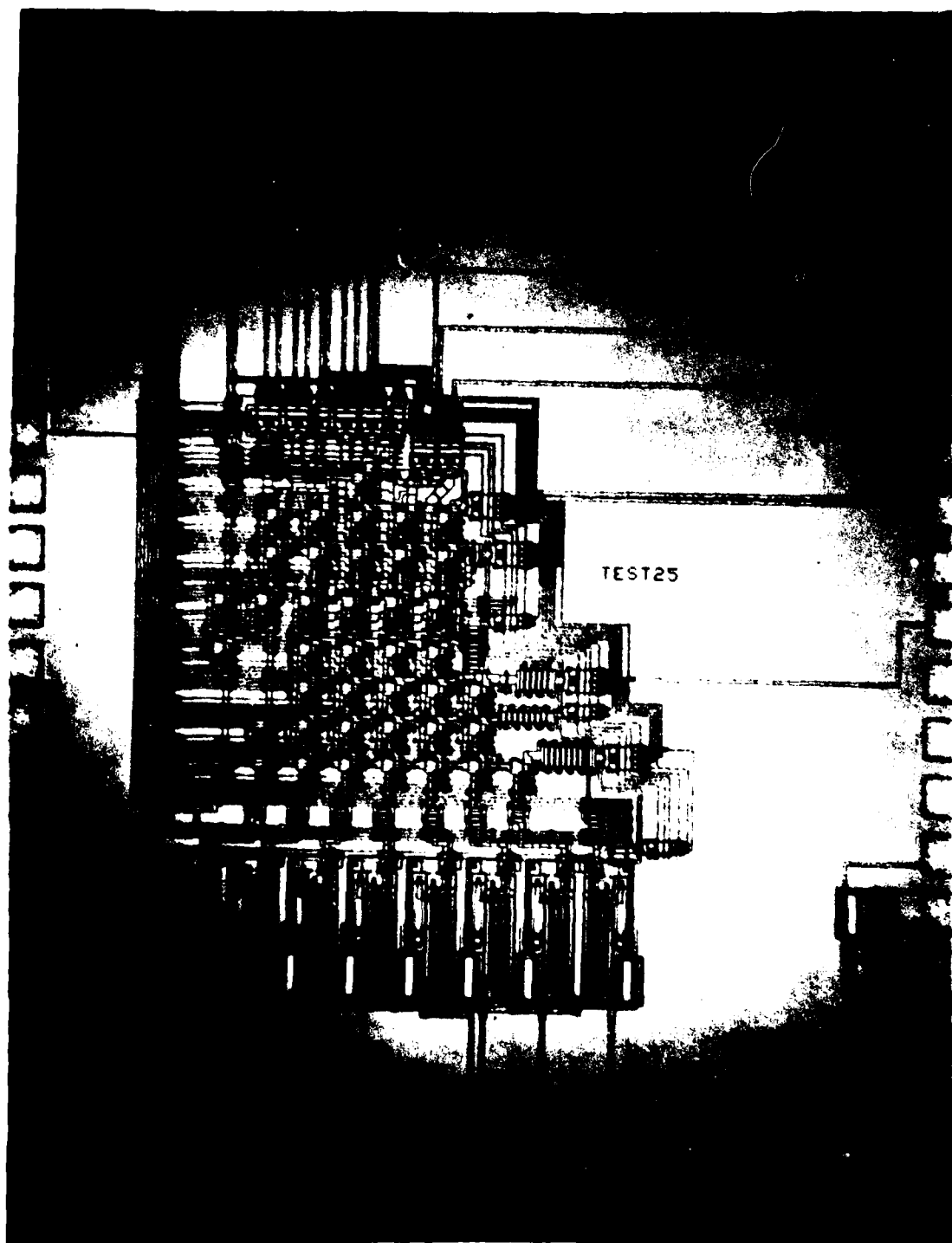


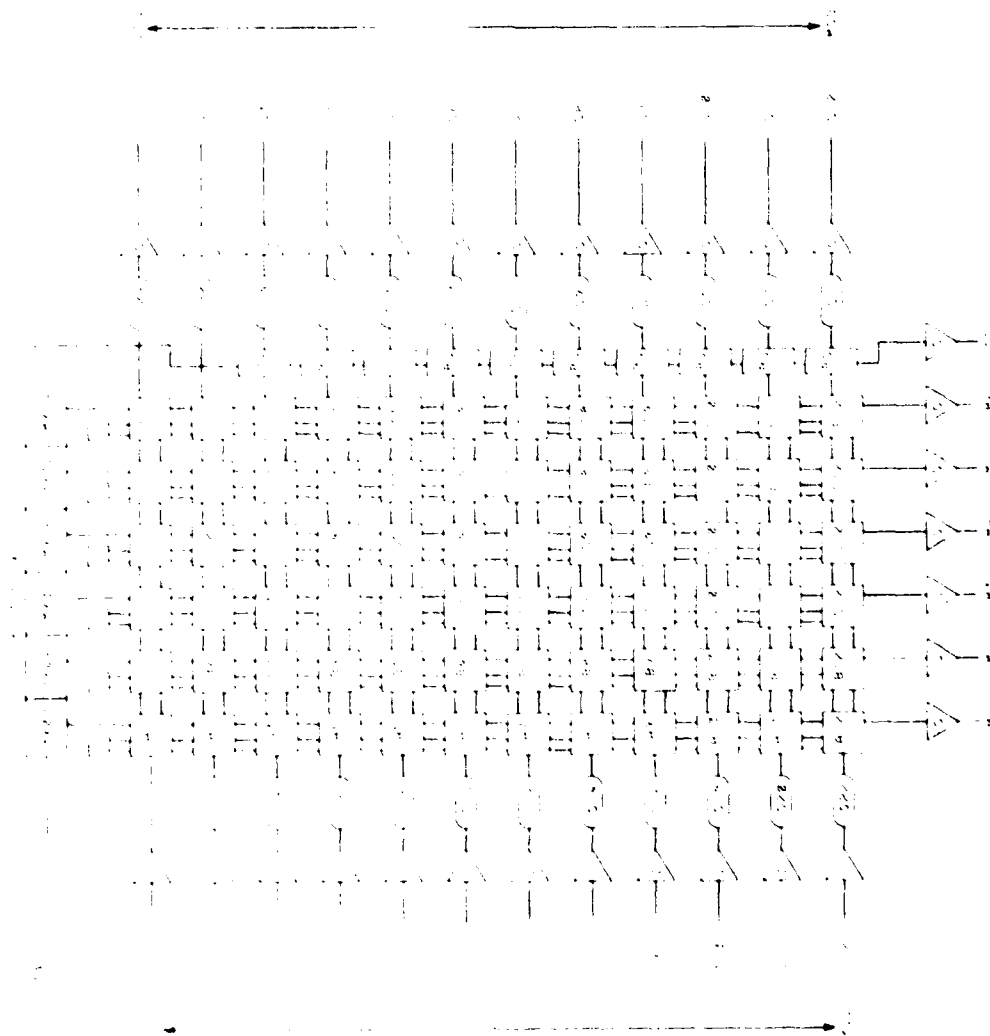
Figure 4-47. ACD2 6 x 4 Multiplier.

#### 4.4 FAST HADAMARD TRANSFORM (FHT) CELL

An interconnect diagram of the full up FHT chip (FHT-1), is shown in Figure 4-48. The blocks labeled A1-12 through F 1-12 are the Hadamard functional blocks. All A blocks are identical as is the case with the B, C, D, E, and F blocks. The interconnect within the A-block is shown in Figure 4-49 along with a listing of the fundamental circuits comprising the block. Note that the following four basic circuits make up the A-FHT block; shift register, half adder, charge fan-out (CFO) and charge transfer node (CTN). A more complete description of the CTN is provided later in this section. The CFO is a device similar in structure to the half adder but different in function in that it generates two logical replicas from a single logic input. Figure 4-50 shows a signal timing diagram for the A1 block. This is the simplest as it produces the sums and differences of the input data, i.e.,  $a + b$ ,  $a - b$ ,  $c + d$ ,  $c - d$ , etc. The B blocks take this information and produce more complex results,  $(a + b) + (c + d)$ ,  $(a + b) - (c + d)$ ,  $(a - b) + (c - d)$ ,  $(a - b) - (c - d)$ , etc. This sequence of sums and differences is controlled by the distributed multiplexer, denoted C1B000, in Figure 4-49. This is called distributed because it appears in each functional block. The multiplexing is done with signal charge allowing it to propagate through the array synchronously with the data that it controls.

The CFO is an important device in the general scheme of DCCL since a logic one charge packet cannot be divided up without destroying the logical significance of the signal. In other words, a logic one charge packet by itself has a fan-out of one. The CFO takes care of the situation where a fan-out of two is needed and accomplishes this task in one clock period.

The CTN is a single transistor device that was developed to transfer signal charge efficiently over distances and geometry that prohibit the use of CCD shift register. A CTN can be described as a diffused region terminating the typical CCD channel with a metal line attaching it to another diffusion some distance away (typically several mils.). The latter diffusion has an adjoining gate electrode typically biased with a D.C. voltage, which begins the next DCCL device. Figure 4-51 shows a schematic timing diagram and surface potential diagram for the CTN structure. Signal charge is



- 1. 64-POINT FAST HADAMARD TRANSFORM
- 2. 64-POINT FAST HADAMARD TRANSFORM
- 3. 64-POINT FAST HADAMARD TRANSFORM
- 4. 64-POINT FAST HADAMARD TRANSFORM
- 5. 64-POINT FAST HADAMARD TRANSFORM
- 6. 64-POINT FAST HADAMARD TRANSFORM
- 7. 64-POINT FAST HADAMARD TRANSFORM
- 8. 64-POINT FAST HADAMARD TRANSFORM
- 9. 64-POINT FAST HADAMARD TRANSFORM
- 10. 64-POINT FAST HADAMARD TRANSFORM
- 11. 64-POINT FAST HADAMARD TRANSFORM
- 12. 64-POINT FAST HADAMARD TRANSFORM
- 13. 64-POINT FAST HADAMARD TRANSFORM
- 14. 64-POINT FAST HADAMARD TRANSFORM
- 15. 64-POINT FAST HADAMARD TRANSFORM
- 16. 64-POINT FAST HADAMARD TRANSFORM
- 17. 64-POINT FAST HADAMARD TRANSFORM
- 18. 64-POINT FAST HADAMARD TRANSFORM
- 19. 64-POINT FAST HADAMARD TRANSFORM
- 20. 64-POINT FAST HADAMARD TRANSFORM
- 21. 64-POINT FAST HADAMARD TRANSFORM
- 22. 64-POINT FAST HADAMARD TRANSFORM
- 23. 64-POINT FAST HADAMARD TRANSFORM
- 24. 64-POINT FAST HADAMARD TRANSFORM
- 25. 64-POINT FAST HADAMARD TRANSFORM
- 26. 64-POINT FAST HADAMARD TRANSFORM
- 27. 64-POINT FAST HADAMARD TRANSFORM
- 28. 64-POINT FAST HADAMARD TRANSFORM
- 29. 64-POINT FAST HADAMARD TRANSFORM
- 30. 64-POINT FAST HADAMARD TRANSFORM
- 31. 64-POINT FAST HADAMARD TRANSFORM
- 32. 64-POINT FAST HADAMARD TRANSFORM
- 33. 64-POINT FAST HADAMARD TRANSFORM
- 34. 64-POINT FAST HADAMARD TRANSFORM
- 35. 64-POINT FAST HADAMARD TRANSFORM
- 36. 64-POINT FAST HADAMARD TRANSFORM
- 37. 64-POINT FAST HADAMARD TRANSFORM
- 38. 64-POINT FAST HADAMARD TRANSFORM
- 39. 64-POINT FAST HADAMARD TRANSFORM
- 40. 64-POINT FAST HADAMARD TRANSFORM
- 41. 64-POINT FAST HADAMARD TRANSFORM
- 42. 64-POINT FAST HADAMARD TRANSFORM
- 43. 64-POINT FAST HADAMARD TRANSFORM
- 44. 64-POINT FAST HADAMARD TRANSFORM
- 45. 64-POINT FAST HADAMARD TRANSFORM
- 46. 64-POINT FAST HADAMARD TRANSFORM
- 47. 64-POINT FAST HADAMARD TRANSFORM
- 48. 64-POINT FAST HADAMARD TRANSFORM
- 49. 64-POINT FAST HADAMARD TRANSFORM
- 50. 64-POINT FAST HADAMARD TRANSFORM
- 51. 64-POINT FAST HADAMARD TRANSFORM
- 52. 64-POINT FAST HADAMARD TRANSFORM
- 53. 64-POINT FAST HADAMARD TRANSFORM
- 54. 64-POINT FAST HADAMARD TRANSFORM
- 55. 64-POINT FAST HADAMARD TRANSFORM
- 56. 64-POINT FAST HADAMARD TRANSFORM
- 57. 64-POINT FAST HADAMARD TRANSFORM
- 58. 64-POINT FAST HADAMARD TRANSFORM
- 59. 64-POINT FAST HADAMARD TRANSFORM
- 60. 64-POINT FAST HADAMARD TRANSFORM
- 61. 64-POINT FAST HADAMARD TRANSFORM
- 62. 64-POINT FAST HADAMARD TRANSFORM
- 63. 64-POINT FAST HADAMARD TRANSFORM
- 64. 64-POINT FAST HADAMARD TRANSFORM

Figure 4-48. Block diagram of the 64 point fast Hadamard Transform Chip.

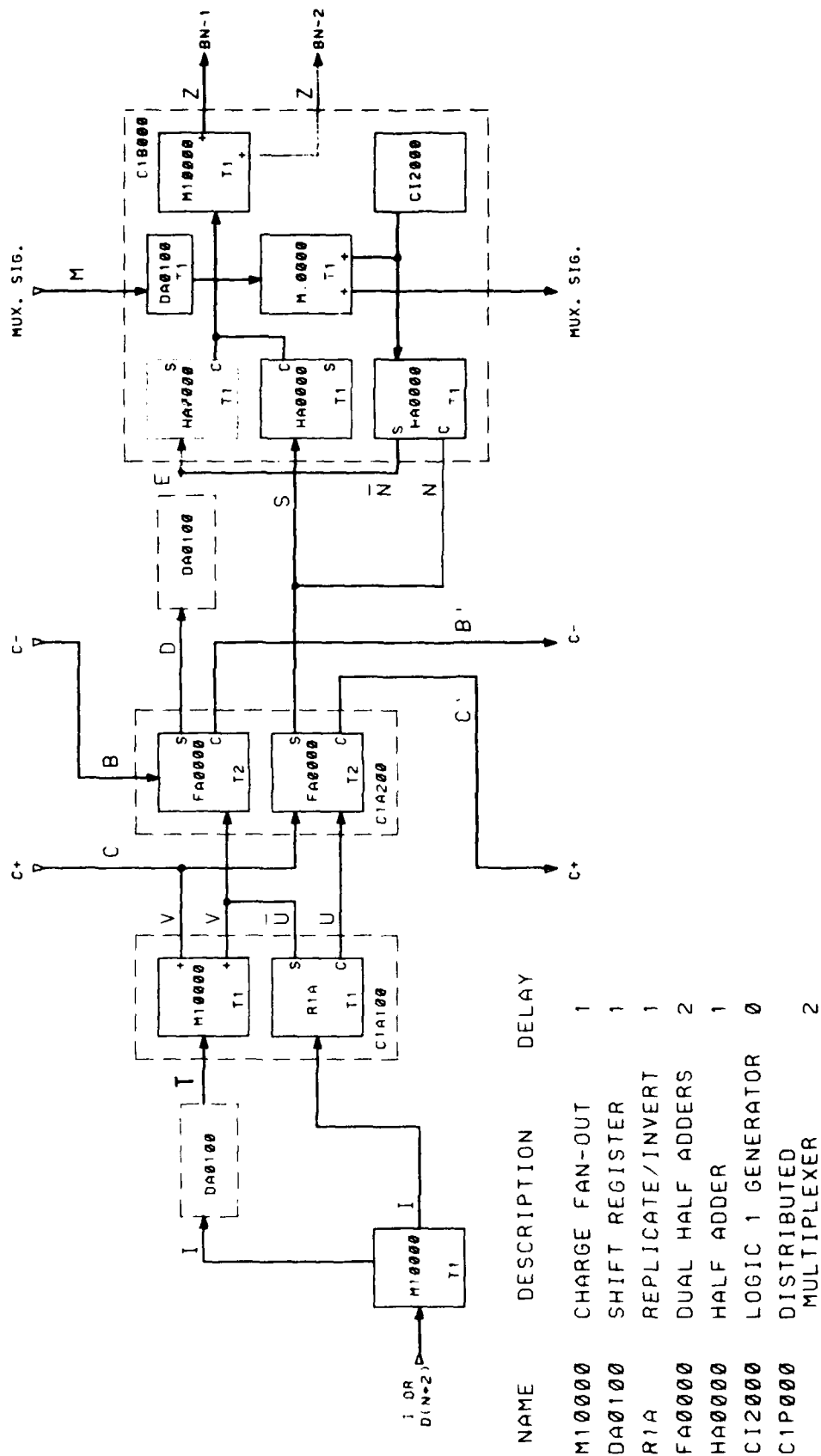


Figure 4-49. Block diagram of A1 through A12 functional block.

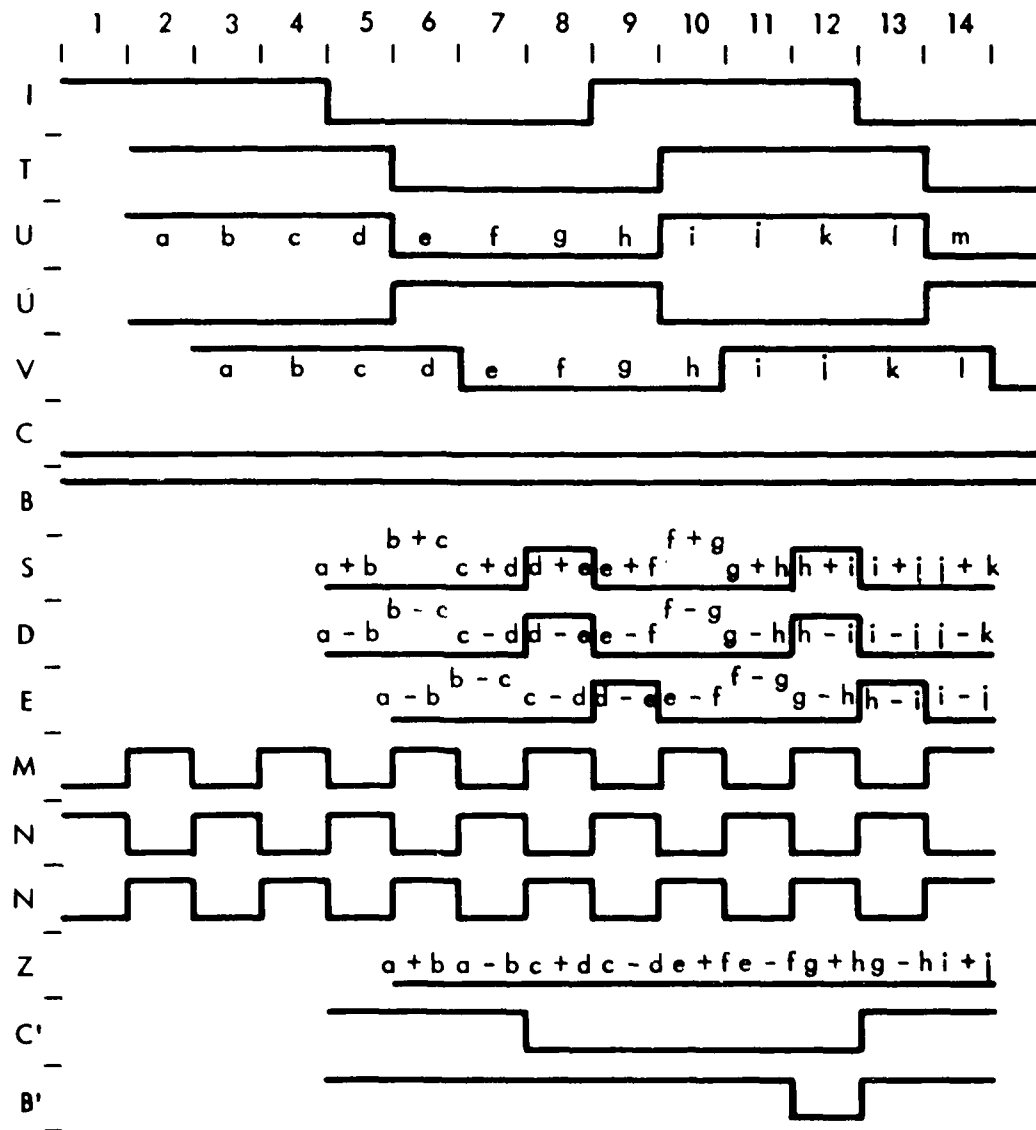


Figure 4-50. 8-point Hadamard transform block timing diagram.

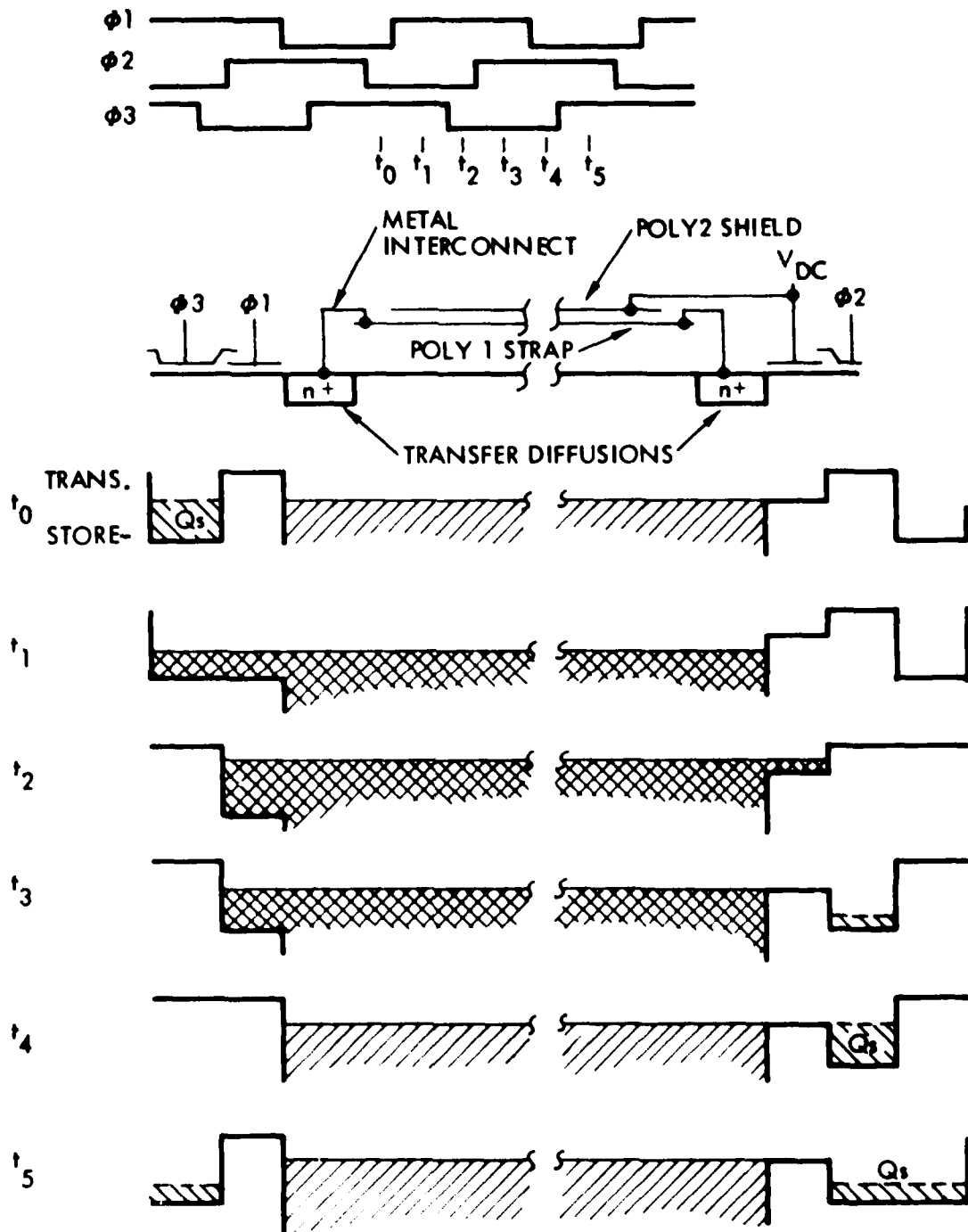


Figure 4-51. Schematic and operational diagram of the charge transfer node (CTN)

pushed into the first diffusion by the collapsing surface potentials of its adjacent gates. This charge effectively transfers across the interconnect, out through the latter diffusion and across the silicon surface under the adjoining D.C. gate. This transfer cycle repeats each clock period as the CTN is driven by the very gates that form the signal paths it is interconnecting. Since the CTN consists primarily of metal, and in some cases diffused tunnel (for passing signal charge under metal lines), it provides a serviceable and simple signal transmission system for DCCL devices. CTN's are serviceable because they permit a wide range of chip layout configurations that would otherwise be impracticable (if not impossible). CTN's are simple because they permit DCCL devices to be interconnected virtually in the same manner as MOS transistors.

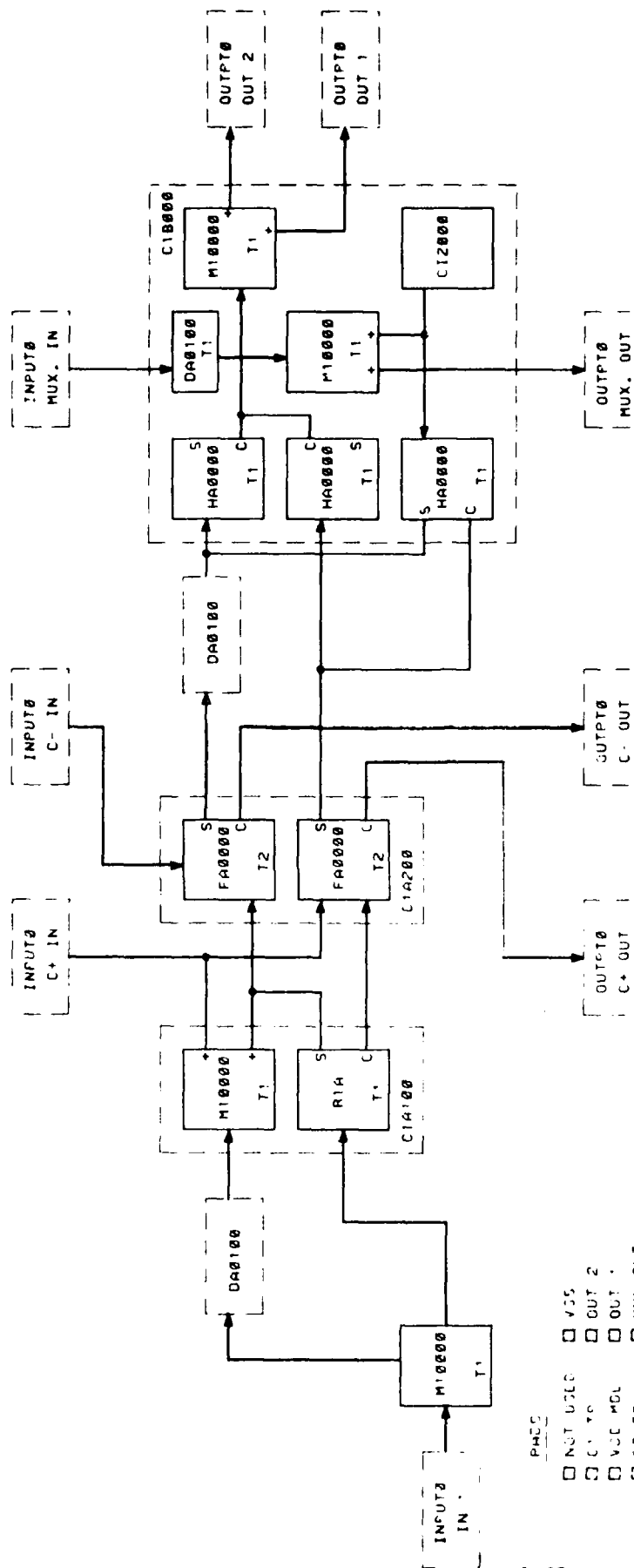
#### 4.4.1 FHT-0 Test Chip

A test chip for the FHT-1 has been designed and is called FHT-0. The purpose of this chip is to take all the functional blocks that compose the FHT-1 and configure a test interface around them. This way, the functional blocks can be thoroughly tested and characterized before attempting to characterize the full-up chip. The test configuration which is of primary interest is the A1 FHT functional blocks. The test configuration for this is called the A-FHT.

#### 4.4.2 A-Hadamard Functional Block

The shortest functional block (A-FHT) has been operated at the lowest frame rate and found to be completely functional. Figure 4-52 shows a functional block diagram of the A-FHT test arrangement.

Figure 4-53 shows a state variable timing diagram used in testing for the A-FHT. The IN1 pattern shown there is part of one actually used in testing and was picked as one that would exercise all the signal paths within the A-FHT cell. Figure 4-54 and 4-55 show photos of the output signals of the A-FHT. Figure 4-54 has the actual input data pattern on the lower trace and was taken with all zeros on the MUX.IN. The patterns shown as C+, C- and OUT2 are correct except that the signal amplitude at OUT2 is quite low. The output at OUT2 is just what the subtractor F2A is developing at its sum output node.



# PADS

- ☐ NOT USED
- ☐ C1 Y0
- ☐ VCC M0L
- ☐ C2 TP
- ☐ C1 IN
- ☐ C1 IN
- ☐ MUX IN
- ☐ NOT USED
- ☐ C1
- ☐ VCC
- ☐ NOT USED
- ☐ VSS
- ☐ NOT USED
- ☐ C1 BUS
- ☐ 2 BUS
- ☐ IN0 TS
- ☐ 0P
- ☐ C OUT
- ☐ VCC
- ☐ NOT USED
- ☐ VCC
- ☐ GND
- ☐ VSS
- ☐ OUT 2
- ☐ OUT
- ☐ MUX OUT
- ☐ C OUT
- ☐ C OUT
- ☐ V4
- ☐ VB
- ☐ 04
- ☐ 03P
- ☐ 03
- ☐ NOT USED
- ☐ 02B
- ☐ 02A
- ☐ 01
- ☐ VCC
- ☐ IN 1
- ☐ NOT USED
- ☐ NOT USED
- ☐ NOT USED
- ☐ MUX IN2

## NOTES

1. PADS ARE LISTED CLOCKWISE FROM THE UPPER LEFT PAD

Figure 4-52. Functional block diagram of the A-FHT cell test arrangement.

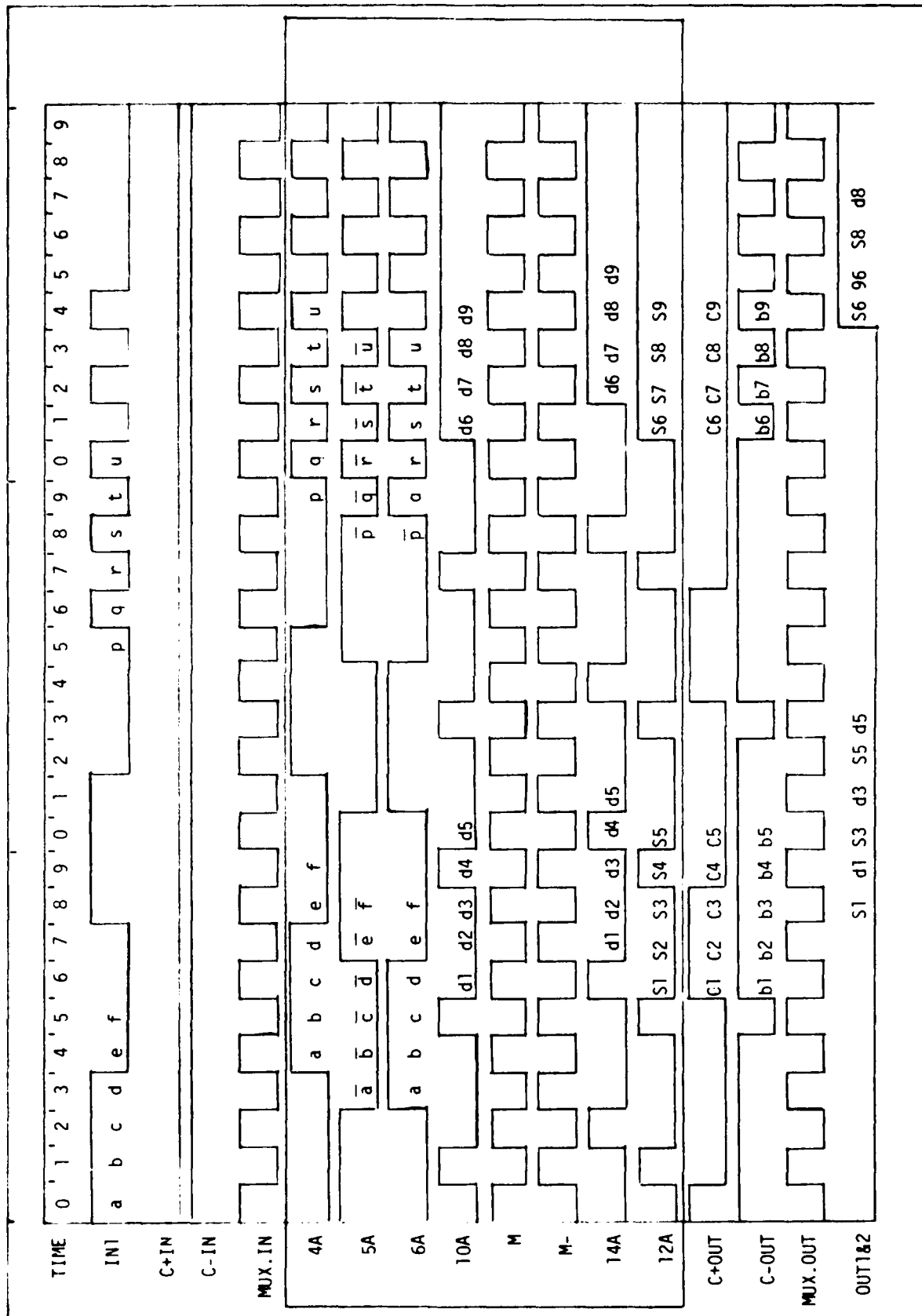


Figure 4-53. A-FHT functional block state variable timing diagram. The data output (OUT1&2) can be algebraically expressed in terms of the input (IN1) in the interest of compact notation:  
 $a+b+c = C1, S1, a+b+c- = b1, d1, c+d+c+ = C3, S3, c+d+c = b3, d3$ , where  $S = \text{sum}$ ,  $C = \text{carry}$ ,  
 $d = \text{difference}$ ,  $b = \text{borrow}$ .

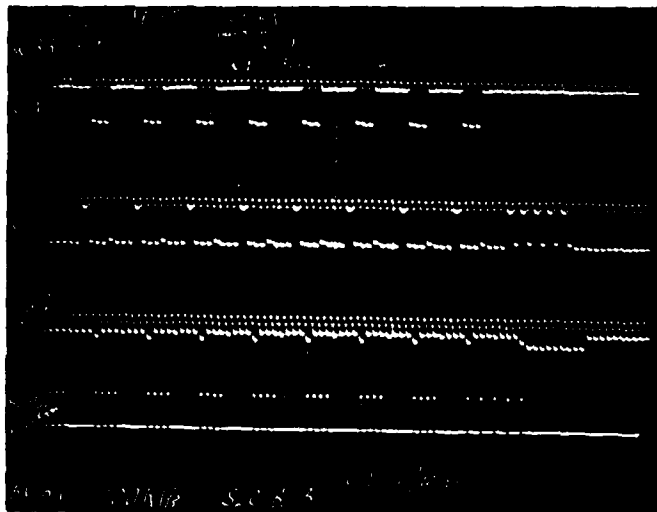


Figure 4-54. A-FHT outputs with MUX.IN equal to all zeros.

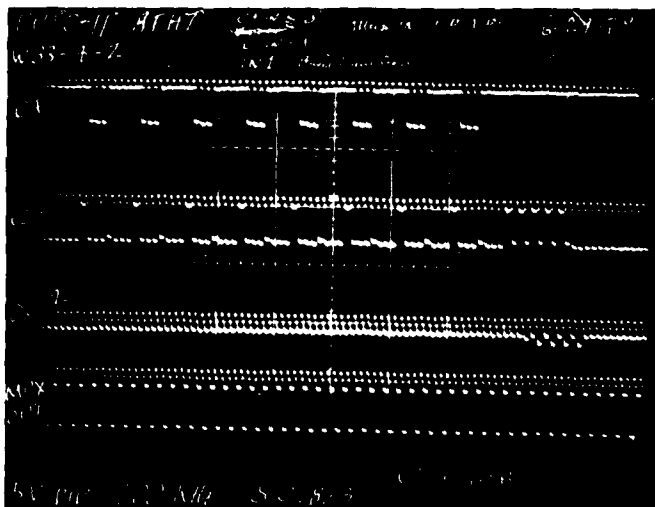


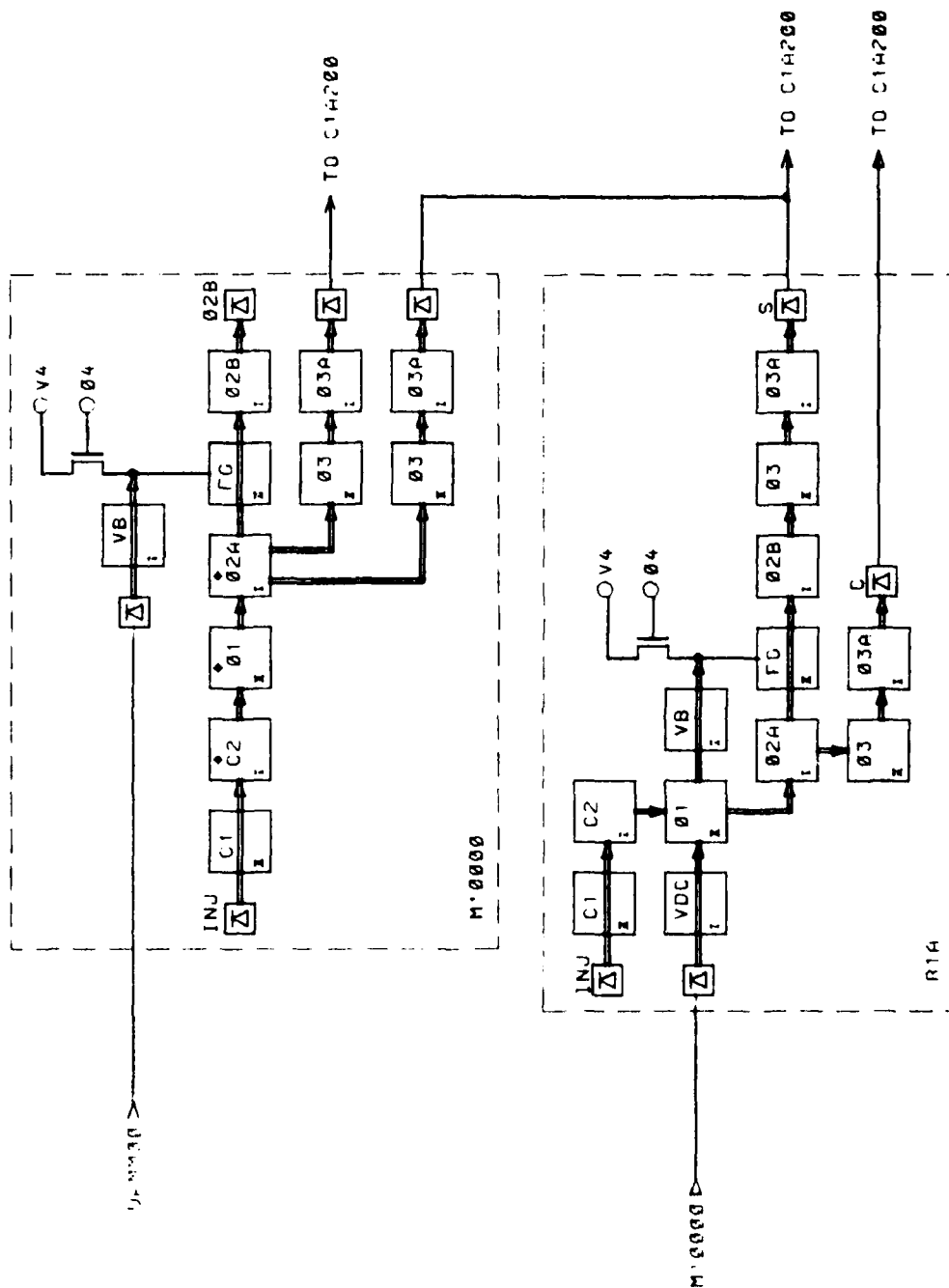
Figure 4-55. A-FHT outputs the proper one-zero pattern on MUX.IN.

Figure 4-55 shows a case where the MUX.IN is set with an alternating one-zero pattern and in the right half shows the same pattern as those of the state variable diagram (Figure 4-53). The C+, C- and MUX OUT signals in the photo agree very well with the diagram (in the diagram a logic one is a high level and in the photos a logic one is a low pulse). As in Figure 4-54 the signal amplitude is quite low but it essentially agrees with the state variable diagram. The alternating one-zero pattern at the right side of the photo should appear as a string of 10 ones except that AND function degrades these signals below the maximum zero level of the output CFO (M10000). Some adjustment of the FG switching threshold is possible which reveals the presence of the lesser 5 of the 10 ones but this is nonstandard and causes undesirable noise margin shifts in the HA.

Three problems have been identified in the A-FHT functional block. The first problem is that the CFO device develops a considerable bias charge level at its output. The second problem is that the internal transfer efficiency is marginal. The third problem is that AND function needed a logic one charge packet that was 60% larger than for the half adder. Solutions to these problems have been implemented on FHT-OC. Characterization of FHT-OC will precede fabrication and testing of FHT-1. Following is more detailed discussion of these problems and their solutions.

#### 4.4.3 Charge Fan-Out

The signal Charge Fan-Out (FCO) was operated between 0.2 MHz and 2.0 MHz with the clocks and bias which properly operates the half adder (HA). Figure 4-56 shows a schematic of the circuit test arrangement consisting of the CFO, labeled M10000, and the HA, labeled RLA. The mismatch in amplitude of the logic ones of the CFO was found to be typically 6%. This is quite acceptable for performing digital logic. A problem with the logic zeros occurs as operating frequency increases from around 400 kHz where they increase linearly in amplitude until at, around 2.5 MHz, the typical logic zero equals 50% of a logic one. This is an unworkable situation for any logic elements which would follow since the CFO and HA both have fat zero - minimum one input noise margins of around 30%-70%. This situation is due to the impedance of the floating gate



1. ASTERISK (\*) INDICATES TWICE THE STANDARD CHANNEL AREA OF C24  
NOTES

Figure 4-56. Schematic of the test arrangement consisting of the charge fan-out, labeled M10000, and the half adder, labeled R1A.

channel. Since a "two-logic-ones" charge packet is available under the  $\phi 2A$  electrode each clock period, this charge must either, (1) flow past the floating gate (FG) or, (2) flow under the  $\phi 3$  electrodes. If in the (1) case, the charge flow past the FG is sufficiently restricted, some of this charge will be left behind and subsequently be pulled under the  $\phi 3$  electrodes. This charge will then be transferred to the output circuits in the test arrangement. Figure 4-57 shows one of several plots made of the logic one and zero levels vs. frequency. It clearly shows that, although the logic ones remain stable and well matched, the logic zeros level increases linearly with frequency.

There are two possible solutions for this situation that were being considered. One was to widen the floating gate channel just enough to meet the maximum speed criterion but not seriously compromise the existing chip layout. The other was to go to a CFO design using a dynamic N-MOS inverter to switch the formation of the two output charge packets. While the trade-offs of both approaches are being examined, widening the floating gate channel was taken as the best near term solution. Calculations indicate that this will yield about a 7% bias level for logic zeros at 2.5 MHz. This will be quite adequate for the FHT-1.

Figure 4-58 shows a plot of normalized fat zero level vs. clock frequency. The fat zero levels plotted are for FHT-OB measured, FHT-OB calculated by the charge control method,<sup>(9)</sup> FHT-OC calculated by the charge control method, and FHT-OC calculated by a linear region transfer (LRT) model. Test results taken on CFO test configurations of FHT-0 (and others) tends to confirm the charge control model. The LRT model assumes that charge leaving a potential well of dimension  $W$  and  $L$  over a barrier whose dimensions are  $W_B$  and  $L_B$  is governed, to a first order, by linear region current flow in a channel of  $W/L$  where  $W_B/L_B \gg W/L$ . There is not yet any experimental basis that supports the LRT model.

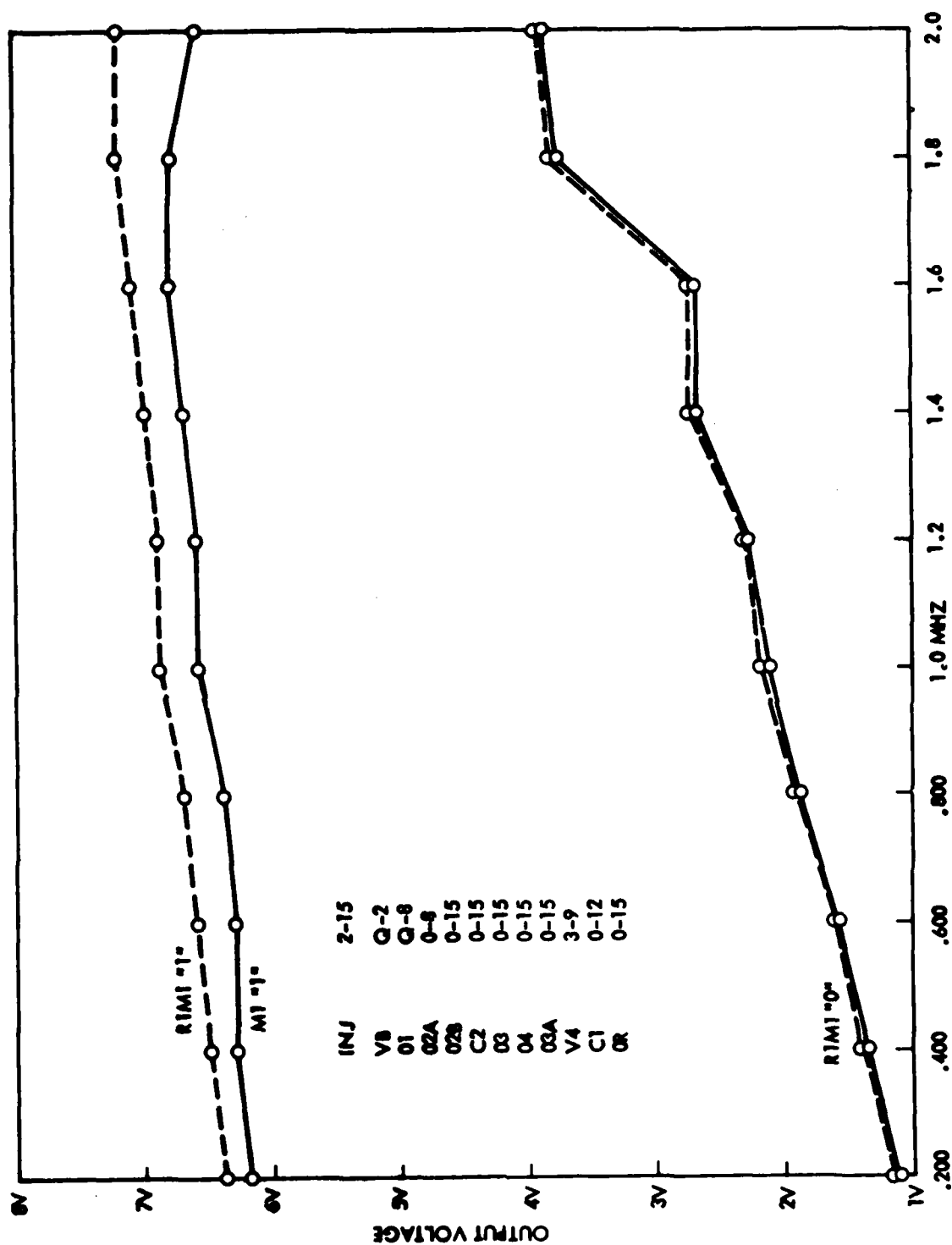


Figure 4-57. Output characteristic curve of the FHT charge fan-out circuit showing how the binary one and zero levels change as a function of frequency.

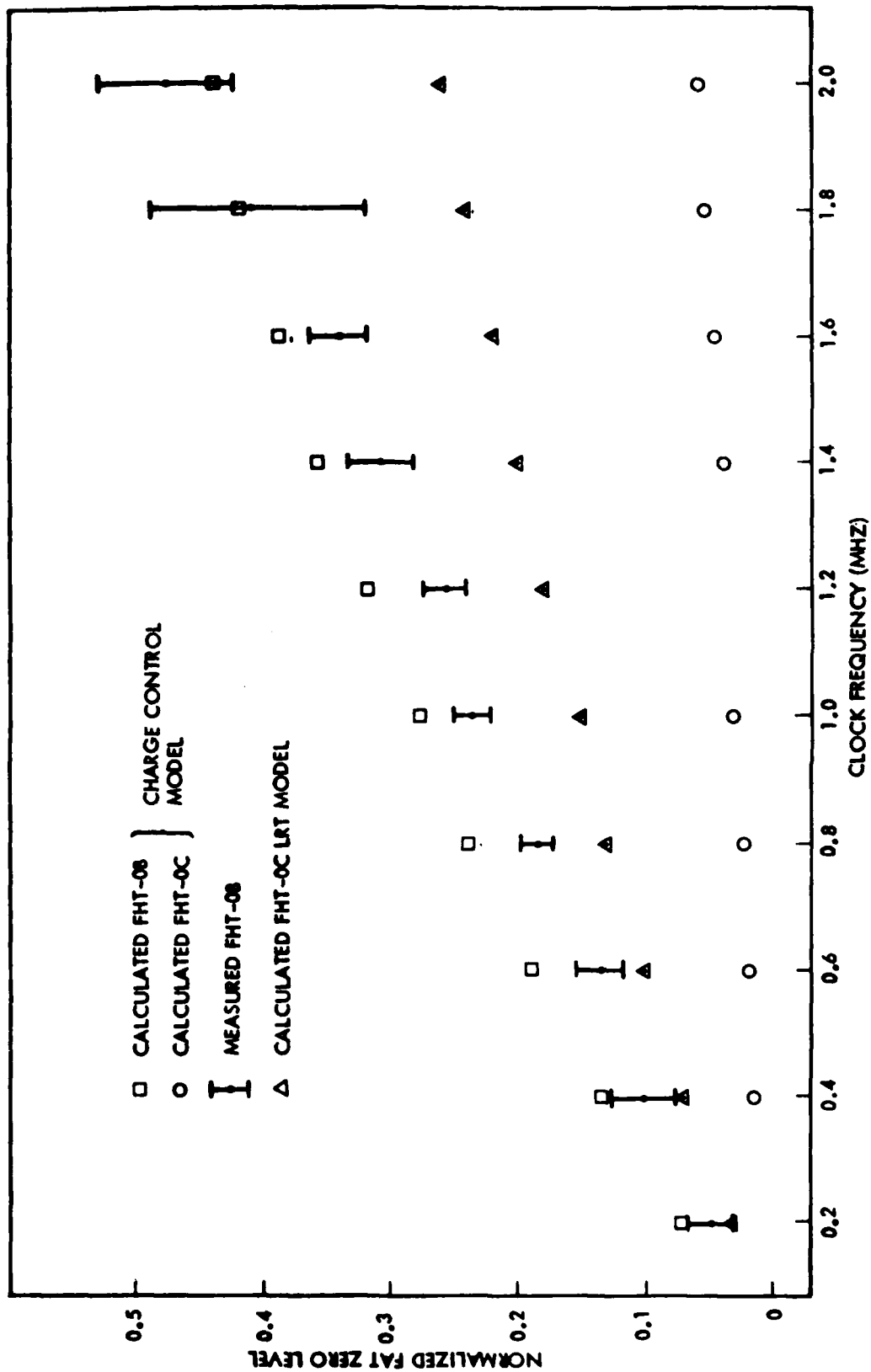


Figure 4-58. A normalized plot of the fat zero level of a FHT-0B charge fan-out circuit vs. clock frequency. The curves show both the measured and the calculated results.

#### 4.4.4 Transfer Efficiency

Output signal patterns revealed marginal efficiency in the transfer paths that lead to the signal inputs of the two AND logic gates contained in the AFHT block shown in Figure 4-52. The solution for this is to minimize the shift register lengths within the dual half adders and change to  $n^+$  diffused tunnels for several of the CTN to lower capacitance and thereby increase operating efficiency. Calculations show that the  $n^+$  tunnel CTN will operate with efficiencies of 80% or better at 2.5 MHz which should be more than adequate.

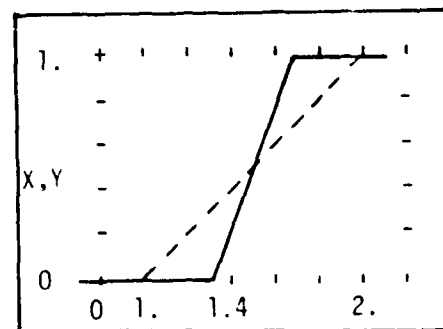
#### 4.4.5 AND Function

The third problem is that the D-Well ( $\phi_1$ -V3 potential well) of the AND function is some 60% larger in charge capacity than the D-Well of the HA. To do the AND operation, two logic charge packets are combined in the D-Well. In the case of two logic ones, one of them, in effect, scuppers across the VB barrier potential into a  $\phi_1$  electrode potential. This is then the output of the AND function. In the case of the AND function, output as a result of two ones will be a 40% logic one (i.e. a degraded logic zero). This, upon input to a CFO, will give outputs that are only about 20% logic one. This is precisely the observed case in the serial outputs of the A-FHT test configuration. Just at the point in time when logic ones should be observed at the output of the CFO the observed ones are 20% or less of their full value. Further testing of the distributed MUX (C1B000) test configuration confirmed this situation.

The tentative solution is to use the HA for performing the AND function by using the carry output and discarding the sum output. There is the disadvantage that the HA requires more area than just the present AND configuration. However, this is more than offset by the fact that the carry output is a refreshed signal i.e. logic ones are full value and logic zeros are empty charge packets. Figure 4-59 shows for comparison the logic level truth tables of the HA AND and the simple AND functions (assuming equivalent D-Well capacities and an input noise margin of 30-70).

(i+j)	X—	Y---
0.0 to 1.0	0	0
1.0 to 1.3	0	0 - .3
1.3 to 1.4	0 - .25	.3 - .4
1.4 to 1.7	.25 - 1	.4 - .7
1.7 to 1.80	1	.7 - .80
1.80 to 2.0	1	.80 - 1

(a)



(b)

Figure 4-59. Comparative logic level truth table (a) and corresponding plot (b) for the half adder AND (output = x) and the simple AND (output = y) functions. Inputs (i+j) and outputs are normalized.

Table 4-5 summarizes the progress in FHT-OB test and characterization. Table 4-6 gives the major design/layout changes contemplated as of this report date for the final test chip (FHT-OC).

Table 4-5. FHT-08 High Level Briefing.

FHT-08 HIGH LEVEL BRIEFING				
	TEST	GOAL	RESULTS	CHANGES
FAN-OUT	INPUT NOISE MARGIN	33-67 150 kHz	UP TO 33-67	WIDEN FLOATING GATE CHANNEL ACCOMODATING CFO
		25-75 2.5 MHz	FORTHCOMING	
	INPUT NOISE MARGIN	33-67 150 kHz	30-70 NOMINAL	WIDEN FLOATING GATE CHANNEL
		25-75 2.5 MHz	FORTHCOMING	
A-FHT	OUTPUT SIGNAL MATCHING	WITHIN 5%	TYPICALLY 6%	
	OUTPUT BIAS LEVEL	< 5% LOGIC ONE	50% AT 2.5 MHz	
F-FHT	FUNCTIONALLY EXERCISE	100%	100% UP TO 200 KHz	NEW CTN
			SERIAL OUTPUTS TO SMALL	NEW AND/OR
MUX. CONTROL	FUNCTIONALLY EXERCISE WITH STANDARD CLOCKS	100% 5%	80% UP TO 200 KHz	LAYOUT + A-FHT
			100% UP TO 200 KHz	
ARRAY	FUNCTIONALLY EXERCISE WITH STANDARD CLOCKS	100%	0%	DONE BY A-F FHT

Table 4-5. FHT-OB Design/Layout Changes, Incorporated in FHT-1 and FHT-OC.

FHT-OB DESIGN/LAYOUT CHANGES	
ID	CHANGE
ADDER-SUBTRACTOR	<ul style="list-style-type: none"> <li>• MINIMIZE ALL TRANSFER LENGTHS</li> <li>• USE N+ TUNNELS FOR CTN</li> <li>• BOTH DUAL HALF ADDERS ARE THE SAME CELL</li> </ul>
AND FUNCTION	<ul style="list-style-type: none"> <li>• USE THE HALF ADDER - USE CARRY DISCARDING SUM</li> </ul>
CHARGE FAN-OUT	<ul style="list-style-type: none"> <li>• WIDEN FLOATING GATE CHANNEL</li> </ul>
N+ TUNNELS	<ul style="list-style-type: none"> <li>• CTN WITH CRITICALLY HIGH CAPACITANCE GET N+ TUNNELS WHERE THIS ENHANCES PERFORMANCE</li> </ul>

#### 4.5 MEMORIES

The Advanced Memory Study was completed in July 1976; this particular program, including the one immediately preceding it, were directed toward investigation of the offset gate CCD memory structure. A detailed description of the offset gate device that includes its theory of operation, basic geometry, topology and topography considerations, operating characteristics and mask set and process evolution are provided in Section 3.6 of this report.

The offset gate device study program included fabrication of shift registers of various sizes and organizations to provide an accurate and direct comparison of the offset gate configuration with a standard or conventional shift register CCD memory. One of the most noteworthy accomplishments of this program was the design and development of a 16 kilobit serial-parallel-serial (SPS) memory building block that was used as the major test element. The LSM-3 mask set included a 7.5 micron design, as well as a 5.0 micron design, that provided bit densities of 225 and 100 microns<sup>2</sup>/bit, exclusive of the area required by the output circuits.

The 7.5 and 5.0 micron offset gate memory blocks were produced and tested under a variety of conditions. Experimental data indicated that the LSM-3 process sequence produced uniform and repeatable SPS memory blocks that gave predictable results. Further evaluation of the offset gate configuration indicated that the complex geometry of this design would have a significant impact on reducing memory cell yields. It was anticipated that further improvements in photolithographic techniques would act as a forcing function toward producing offset gate devices with higher bit densities. Development of an offset gate structure with bit densities greater than that obtained by the 5.0 micron SPS memory block was expected to require significant changes to the processing sequence.

The offset gate memory's internal organization was also re-examined as additional data was accumulated on device operating characteristics. At the beginning of the advanced memory study program, simple serial shift registers were considered as the primary candidates for implementation of large bulk delay memories. It is worth repeating that the ultimate goal of CCD memories was their use as ultra-high density large bulk memories. The initially proposed serial shift register memory organization was considered to be appropriate at that point in time for several reasons:

- (1) System studies indicated that the overall system bit error rate and system reliability could easily be maintained at acceptable levels.
- (2) CCD clocking schemes appeared to be quite simple.
- (3) Very low power, effective bit refreshing circuits appeared to be feasible.

As time elapsed, more experimental data made it clear that the tradeoffs shifted in favor of a serial-parallel-serial (SPS) organization, for the basic memory unit or building block. The SPS organization placed less stringent requirements on the CCD itself, by lessening the need for achieving high transfer efficiency.

The next major innovation in CCD memories occurred during 1979; this involved the design of a 1.2 kilobit and 2 kilobit interleaved SPS memory, that significantly increased bit density. In essence, data was clocked into the serial register, shifted into the "A" parallel stream; this was followed by the input of additional data into the serial register that was then clocked into the "B" parallel stream. With both "A" and "B" data inputs loaded into the interleaved parallel registers, the clocking sequence permitted simultaneous shifting of data through both interleaved parallel registers, with sequentially clocked output of the data through the output serial register.

A number of unique concepts were generated during the course of this memory study program; these concepts included the Yield Enhancement Study (YES), that discussed the possibility of deleting defective memory blocks from a large scale array by means of programmable fuse links. These fuse links can be programmed and blown open to disconnect defective memory cells from the large scale memory array. The fuse link technique suggested is similar in concept and design implementation to that employed by PROM suppliers and users.

An Entire Slice Processing (ESP) concept was also advanced as a method of producing billion-bit memory arrays. In essence, an entire wafer would be comprised of interconnected memory cells that could be tested following fabrication, to determine the row and column location of defective memory cells. The defective cells would then be removed from the array by blowing fusible links of nichrome or Titanium-Tungsten, or blowing diodes inserted into each conductor lead, to insure the removal of unwanted memory cell outputs.

## 5.0 RADIATION TEST RESULTS

### 5.1 INTRODUCTION

The three commonly specified nuclear radiation environments for military and spacecraft applications of semiconductors are (1) prompt-pulse ionizing radiation (2) the total dose of ionizing radiation, and (3) high energy neutron irradiation. The TRW NE1 CCD's were evaluated to the effects of the first two of these environments. It had been intended to test in the neutron environment but test time did not permit.

The very nature of signal flow within CCD's, that is, with packets of charge rather than voltages and currents, makes them probably the most functionally sensitive semiconductor device to prompt-ionizing radiation. A prompt-ionizing dose of as little as 1 Rad (Si) produces sufficient charge in a CCD to swamp out any stored information. Thus, in the prompt pulse tests, the objective was to determine the threshold of data upset in the test devices.

Since CCD's are of metal-oxide-silicon (MOS) construction, they are susceptible to the effects of trapped oxide charge produced by large total doses of ionizing radiation. The predominant effect is the shift in device threshold voltage as observed in other MOS devices. Other effects of concern on the CCD due to total ionizing dose include degradation of the intrinsic parameters such as charge transfer efficiency and dark current.

The test devices used in the radiation tests were a 16-stage shift register and a half-adder. One of each of these devices is contained on an NE1 die. The die were mounted in 40-pin flat packages with the leads bonded to either a shift register or half-adder. Each die also contains several independent MOSFET's which are used for threshold voltage measurements. Three of these FET's were also bonded to package leads in both the shift register and half adder packages. The bonding diagrams for the half-adder and the shift register are shown in Figures 5-1 and 5-2, respectively. The test FET's 3, 4, and 10 use common gate and common drain connections to package pins with separate pins for each source.

A summary of the test results is provided in Table 5-1.

Table 5-1. NE1 Radiation Test Result Summary

Radiation Test	Test Circuit	Criteria	Results
Prompt Ionizing Range: $4 \times 10^4$ to $3 \times 10^7$ RAD (Si)/Sec	16 Bit Shift Register	<ul style="list-style-type: none"> <li>● <u>Upset Threshold</u>: Visual identification of disturbance in the device output waveforms.</li> <li>● <u>Saturation</u>: Dose rate at which test device has all bits at logic "1".</li> <li>● <u>Recovery Time</u>: Time required to restore output waveforms to their undisturbed condition.</li> </ul>	<ul style="list-style-type: none"> <li>● <math>\sim 8 \times 10^4</math> RAD (Si)/Sec</li> <li>● <math>\sim 1 \times 10^7</math> RAD (Si)/Sec</li> <li>● @f = 100 kHz Upset: 160-320 <math>\mu</math>sec</li> <li>● Saturation: 1-4 msec</li> </ul>
Total Ionizing Dose	16 Bit Shift Register  FET's  Half Adder	<ul style="list-style-type: none"> <li>● Charge Transfer Inefficiency Increase</li> <li>● Threshold Voltage</li> <li>● Correct Logic Function</li> </ul>	<ul style="list-style-type: none"> <li>● <math>0.8 \times 10^{-7}</math> to <math>4.2 \times 10^{-7}</math>/RAD(Si)* (<math>10^4</math>-<math>10^5</math> RAD(Si) Range)</li> <li>● -13 <math>\mu</math>V/RAD(Si)</li> <li>● <math>10^4</math> RAD(Si)*</li> </ul>
*With Bias Voltage Readjustments Between Exposures.			

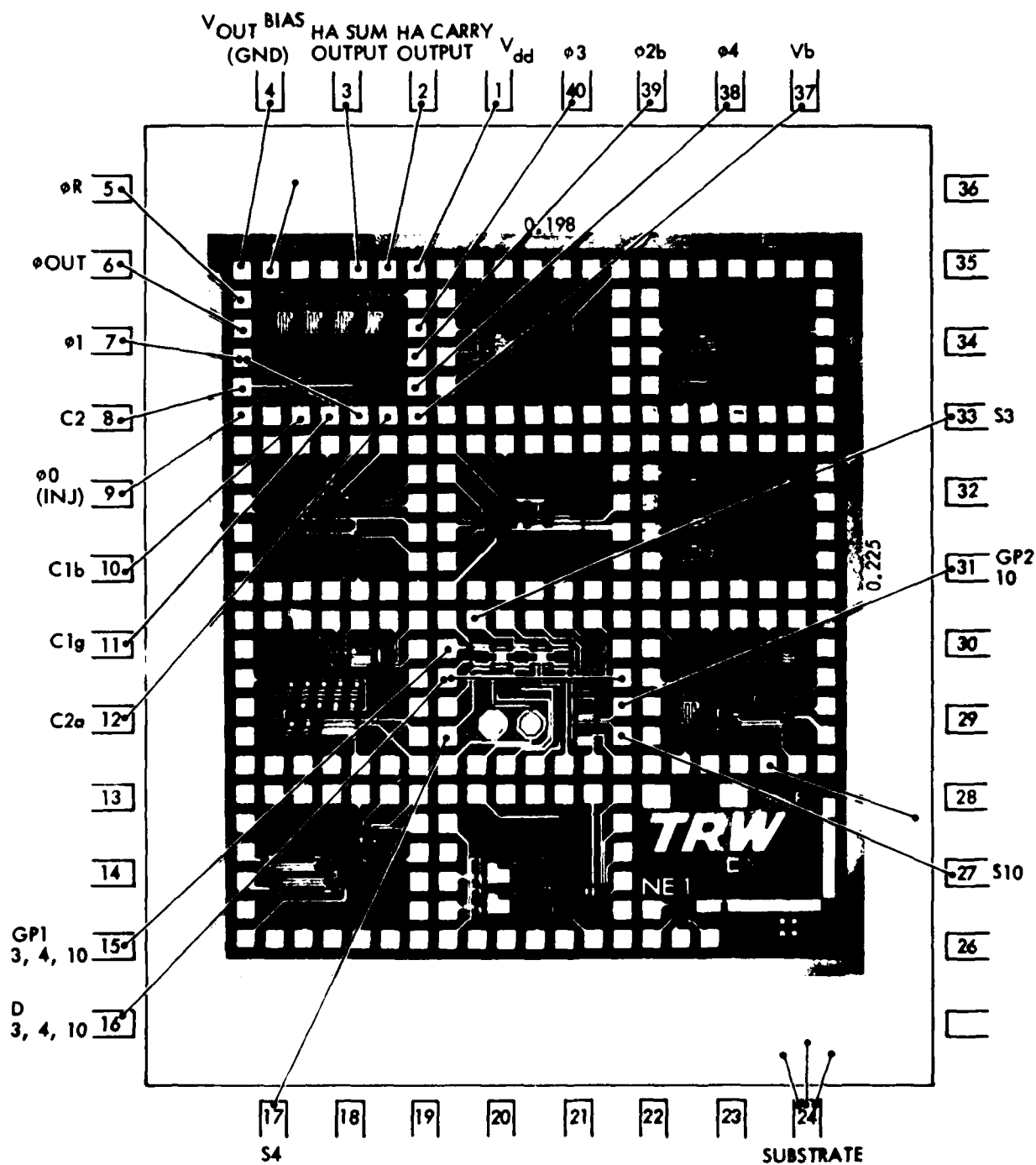


Figure 5-1. Half-adder bonding diagram.

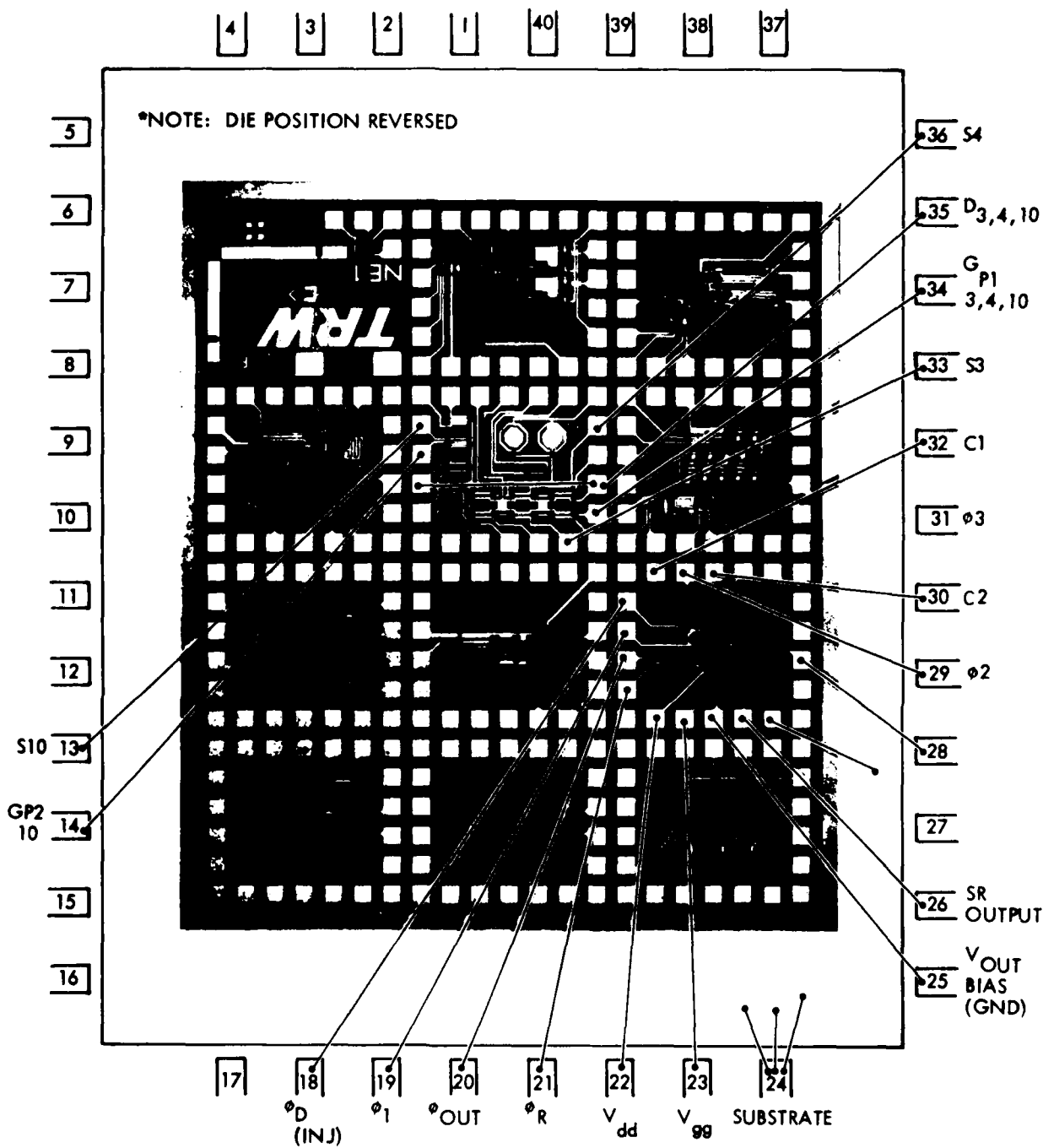


Figure 5-2. Shift register bonding diagram.

## 5.2 PROMPT-IONIZING RADIATION UPSET TESTS

### 5.2.1 Test Setup and Discussion of Results

Five CCD shift registers were tested in the prompt-ionizing radiation environment for observation of any upset to device data inputs. The tests were conducted in the TRW Febetron flash x-ray facility on March 28 through March 30, 1978.

The devices were operated in two modes of data input: (1) all zeros input, and (2) an alternate pattern of ones and zeros. Thus, the objective of these tests was to observe the perturbation of the logical one and zero levels as outputted from the device.

The test set-up used is shown in Figure 5-3. The test sample was inserted into an electromagnetically shielded test fixture which was placed at various distances from the Febetron flash x-ray. The clock generator, data pattern generator, and DC bias supplies were located in the exposure room to minimize cable length to the test fixture. A line driver was used to buffer the device output signal to the oscilloscope in the instrumentation room. All equipment in the exposure room, except the test fixture, was shielded with lead bricks and placed out of the direct field of the Febetron to minimize radiation-induced noise pickup.

Because of the high inherent susceptibility of CCDs to ionizing radiation, it was found necessary to place lead shielding around the test fixture to reduce the dose rate impinging on the device. With the lead shielding and enough distance from the Febetron target, the dose rate level at which upset just occurs could be determined.

The devices were irradiated over a range of  $4 \times 10^4$  to  $3 \times 10^7$  Rads (Si)/sec. Oscilloscope photographs of device output response are presented in Appendix A. The upper trace of each photo shows the long-term response (50 to 200 microseconds/division) and the lower trace shows the short-term response (20 to 50 microseconds/division) of the same output. All the samples were also irradiated with an 8-ones and 8-zeros input pattern.

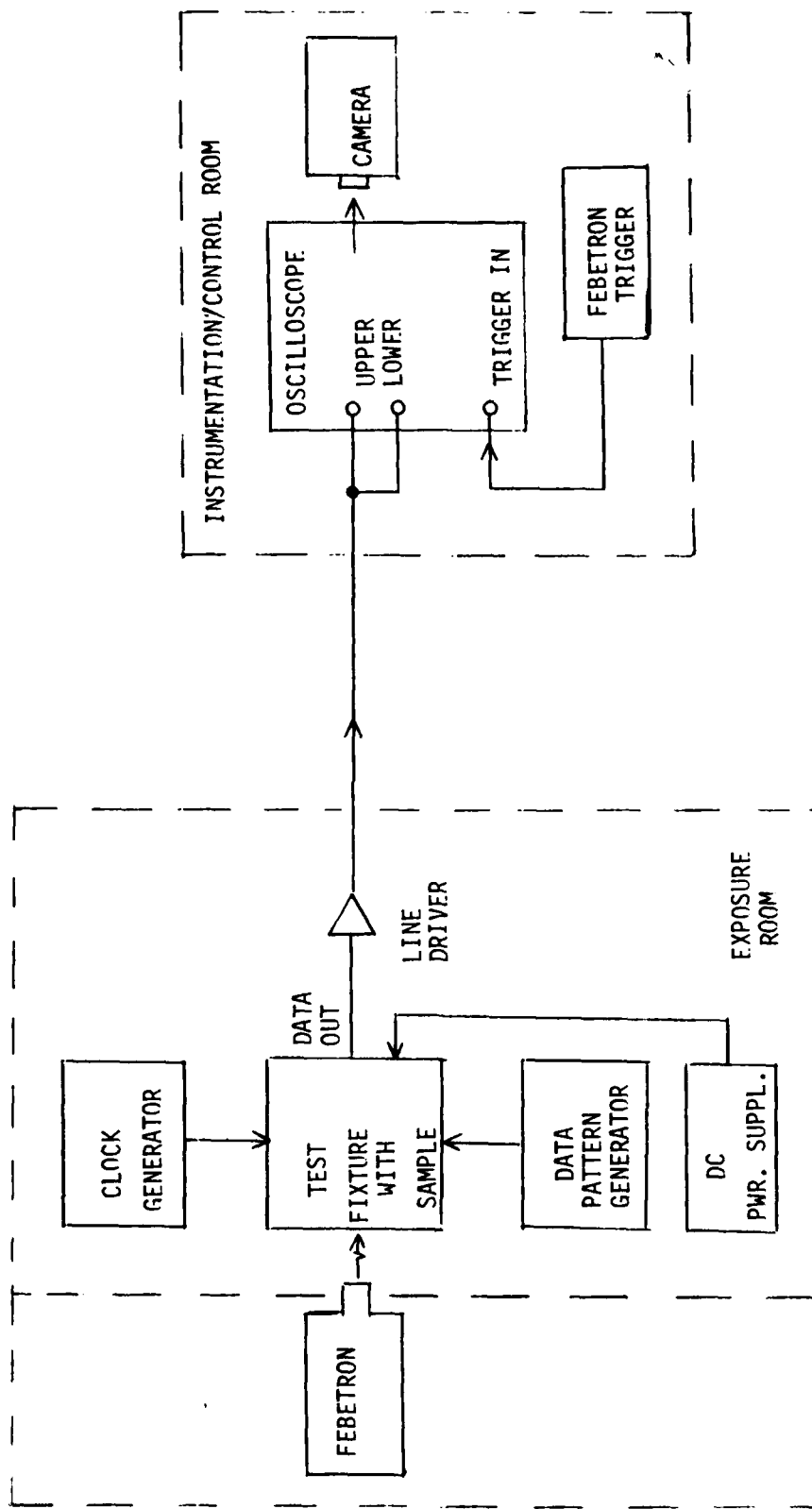


Figure 5-3. Shift Register Upset Test Set-Up

In general, for all samples tested, noticeable deviation of the device output data pattern begins to occur at a dose rate of about  $8 \times 10^4$  Rads (Si)/sec. For most of the sample photos taken at low dose rate, a full one-level pulse is observable in the 15th and/or 16th data bit position. These error pulses cannot be explained completely, but are presumed to be generated by the flash x-ray electromagnetic noise which couples to the data input terminal of the device or by photocurrent produced in the inject diode junction. The true radiation response of the devices is the gradual rise to saturation with dose rate of the logical zero bits in the data pattern. This is the result of free charge generated in the silicon substrate which fills the potential wells which transport the data through the device.

The most pronounced filling of the potential wells by the radiation-induced charge appears to be localized towards the center of the device's length. This is seen in the low dose rate photographs where the middle data bits are raised toward the logical one level more than the beginning and ending bits. This phenomenon can be explained by the higher concentration of excess charge occurring near the center of the silicon substrate as charge near the ends is swept away more rapidly. As dose rate is increased, the output deviation appears to increase linearly until saturation of all the samples tested occurred at approximately  $1 \times 10^7$  Rads(Si)/sec. Dose rates above this level resulted in no significant increase of device recovery time.

On sample number 5, the effect of clock frequency on device recovery time was tested. By switching the clock frequency from the normal 100 kHz to 200 and 300 kHz, the recovery times are reduced by the same multiples. This, of course, is due to the excess charge being swept out faster from the device.

Three of the samples (serial numbers 6, 9, and 15) were also irradiated with an input data pattern consisting of eight ones alternated with eight zeros. The same general effects as observed with an all-zero input pattern were seen here. Sample number 9, which was not operated at full well capacity, is seen to have its logical one level raised as well as the zero level by the ionizing radiation.

No noticeable effect on device operation was observed several seconds after exposure to the Febetron radiation. This is to be expected since the total ionizing dose on each sample did not exceed 1 or 2 Rads(Si).

#### 5.2.2 Prompt-Ionizing Radiation Upset Test Data

Figures 5-4 through 5-12 represent typical oscilloscope photographs of the CCD shift register response to prompt ionizing radiation. The term "response" should be understood to mean the effect on digital data which was in the shift register at the time of the radiation event. The clocking frequency (100 kHz) of the devices is slow compared to the duration of the radiation pulse (25 nanoseconds); thus, the photographs actually show the perturbed digital data and the excess radiation-induced charge which are clocked out of the shift register immediately after the pulse.

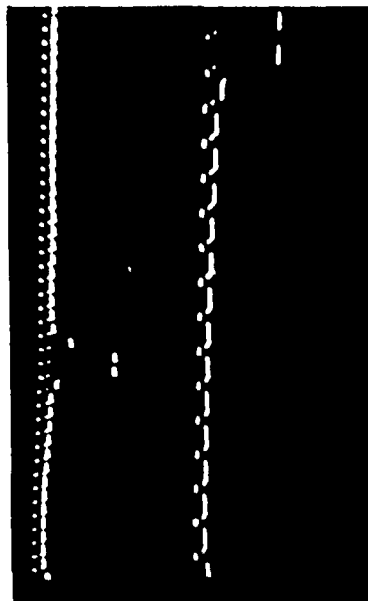
Dual traces are shown on each photograph of the same output. The upper trace shows long-term response and recovery of the device while the lower, faster trace shows more detail of the digital bits just coming out of the device. A logic one is represented by a negative excursion of the waveforms.

### 5.3 TOTAL IONIZING DOSE TESTS

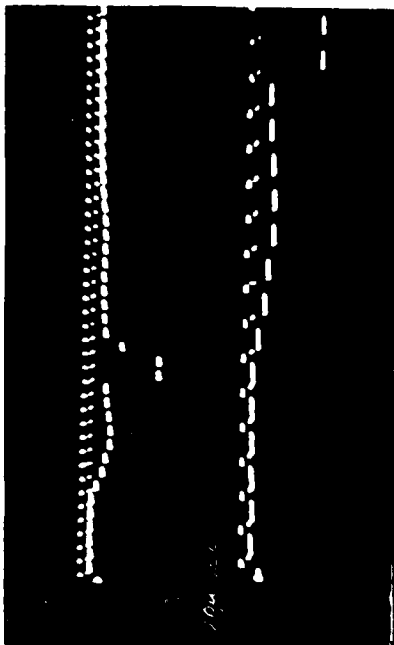
#### 5.3.1 Test Setup and Discussion of Results

Total ionizing dose testing was performed on the NE1 CCD's over the period of April through June, 1978 in TRW's Building 84 test facility. Both shift registers and half-adders were tested. The objective of these tests was to observe the effects of total ionizing dose on intrinsic CCD parameters such as charge transfer inefficiency, threshold voltage, and dark current (these in the shift register) and also to observe the effects on functional operation of a CCD logic device (the half-adder).

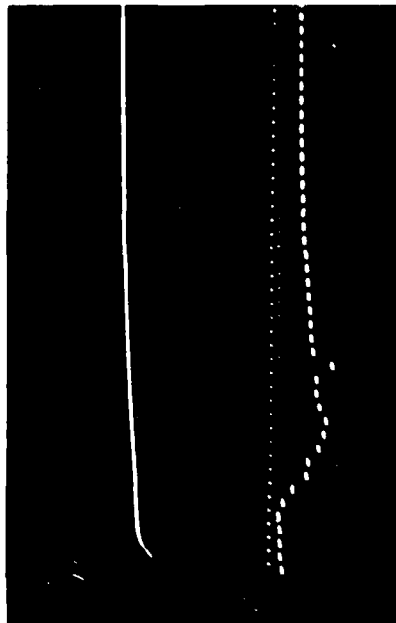
Testing began with four samples of the shift register and two half-adder samples from lot number NE1-1. The same test fixture and instrumentation as in the upset tests were used here with the exception of the line drivers, since the equipment was located close to the radiation source. The radiation source was a Gammacell Co<sup>60</sup> source capable of providing approximately 1000 Rads(Si) per minute to the test sample. The test fixture, a circuit



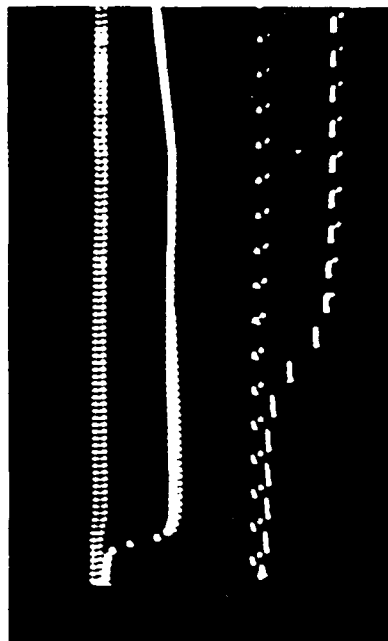
Ser. No. 5 4 x 10<sup>4</sup> R/sec  
 Comments Upper Trace: 2V/DIV; 50  $\mu$ sec  
 Lower Trace: 2V/DIV; 20  $\mu$ sec



Ser. No. 5 2.2 x 10<sup>5</sup> R/sec  
 Comments Upper Trace: 2V/DIV; 50  $\mu$ sec  
 Lower Trace: 2V/DIV; 20  $\mu$ sec

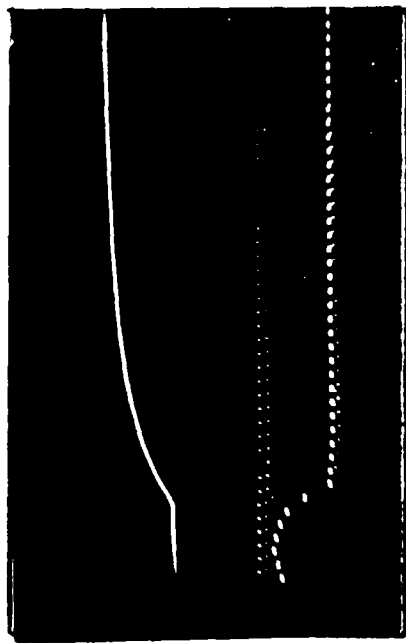


Ser. No. 5 5.5 x 10<sup>5</sup> R/sec  
 Comments Upper Trace: 2V/DIV; .5 msec  
 Lower Trace: 2V/DIV; 50  $\mu$ sec

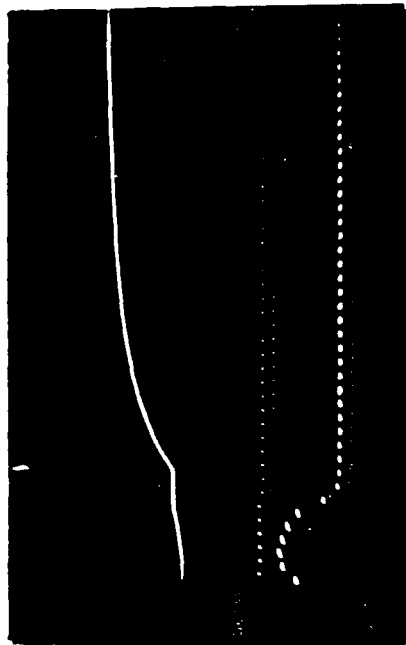


Ser. No. 5 2 x 10<sup>6</sup> R/sec  
 Comments Upper Trace: 2V/DIV; 100  $\mu$ sec  
 Lower Trace: 2V/DIV; 20  $\mu$ sec

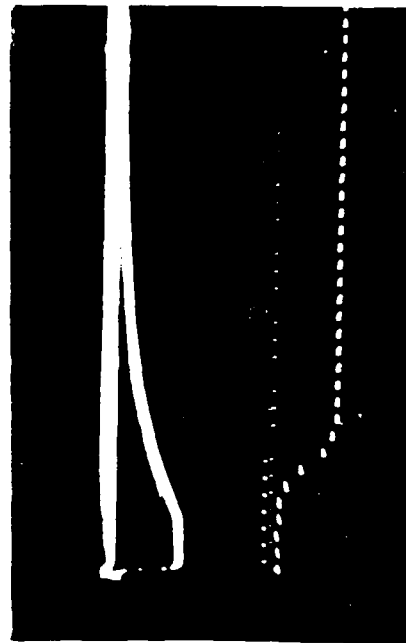
Figure 5-4. CCD shift register, prompt ionizing radiation upset.



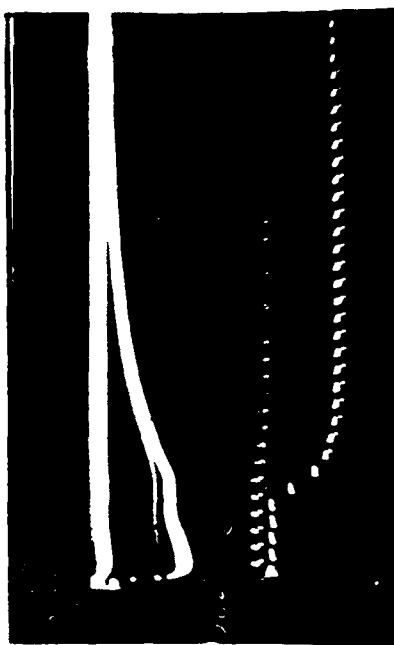
Ser. No. 5  $1.6 \times 10^7$  R/sec  
 Comments Upper Trace: 2V/DIV; .5 msec  
 Lower Trace: 2V/DIV; 50  $\mu$ sec



Ser. No. 5  $2.4 \times 10^7$  R/sec  
 Comments Upper Trace: 2V/DIV; .5 msec  
 Lower Trace: 2V/DIV; 50  $\mu$ sec



Ser. No. 5  $2.7 \times 10^6$  R/sec  
 Comments Clock frequency = 200 kHz  
 Upper Trace: 2V/DIV; 200  $\mu$ sec  
 Lower Trace: 2V/DIV; 20  $\mu$ sec



Ser. No. 5  $4.1 \times 10^6$  R/sec  
 Comments Clock frequency = 200 kHz  
 Upper Trace: 2V/DIV; 200  $\mu$ sec  
 Lower Trace: 2V/DIV; 20  $\mu$ sec

Figure 5-5. CCD shift register, prompt ionizing radiation upset.

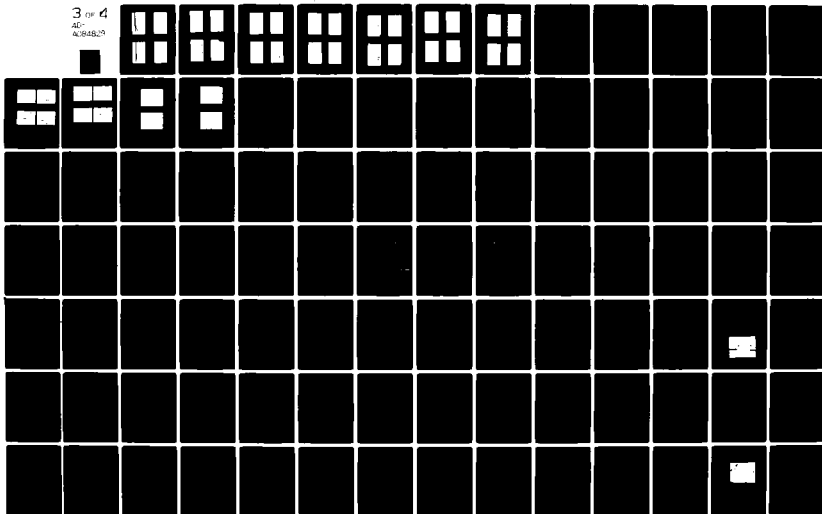
AD-A084 829

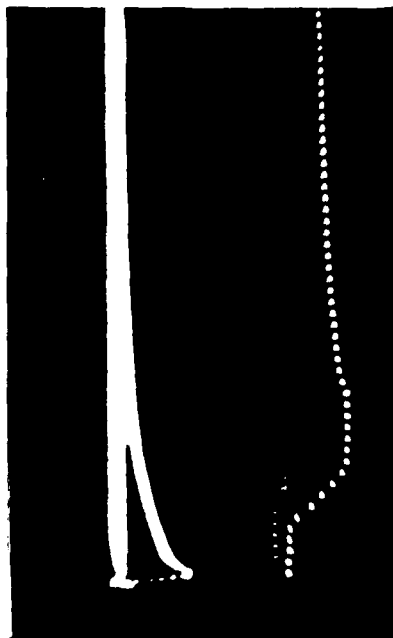
TRW DEFENSE AND SPACE SYSTEMS GROUP REDONDO BEACH CA F/G 9/1  
CHARGE COUPLED DEVICES IN SIGNAL PROCESSING SYSTEMS. VOLUME V. --ETC(U)  
DEC 79 R A ALLEN, J M ANDERSON, F G HAMILTON N00014-74-C-0068

UNCLASSIFIED

3 of 4  
40-  
16/94B/23

NL

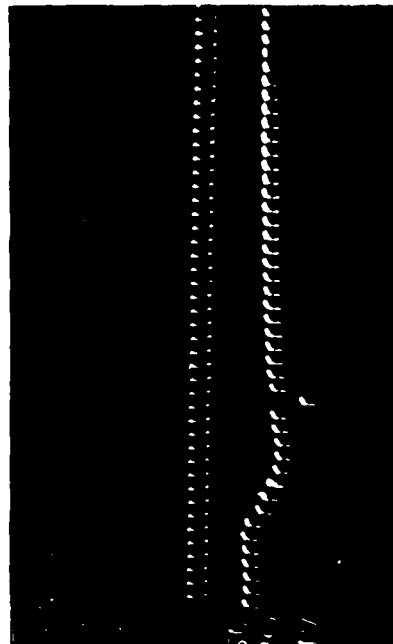




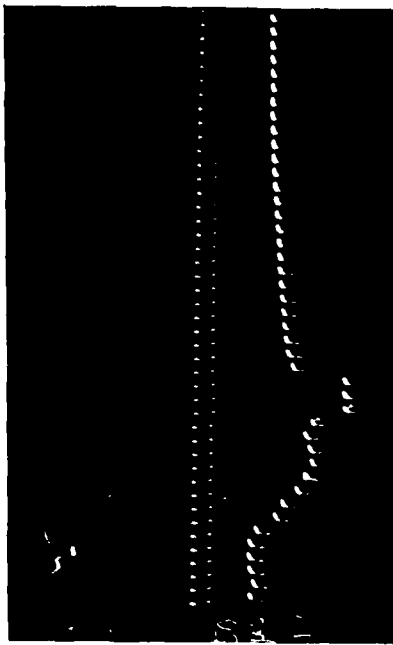
Ser. No. 5  $3.3 \times 10^6$  R/sec  
 Comments Clock frequency = 300 kHz  
 Upper Trace: 2V/DIV; 200  $\mu$ sec  
 Lower Trace: 2V/DIV; 20  $\mu$ sec



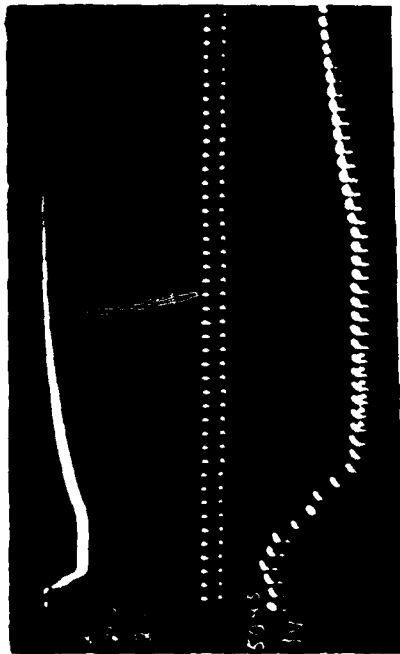
Ser. No. 5  $5.3 \times 10^6$  R/sec  
 Comments Clock frequency = 300 kHz  
 Upper Trace: 2V/DIV; 200  $\mu$ sec  
 Lower Trace: 2V/DIV; 20  $\mu$ sec



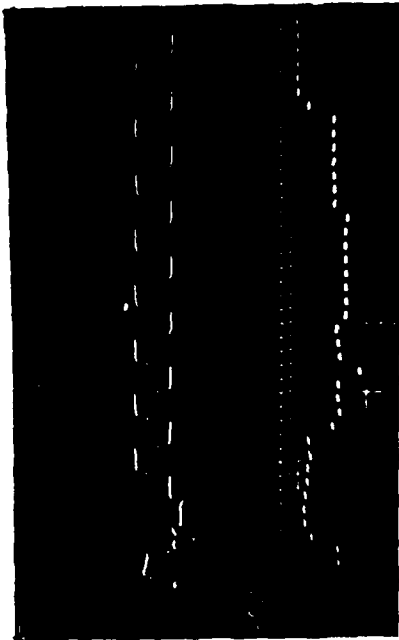
Ser. No. 6  $1.3 \times 10^5$  R/sec  
 Comments Upper Trace: 2V/DIV; 200  $\mu$ sec  
 Lower Trace: 1V/DIV; 50  $\mu$ sec



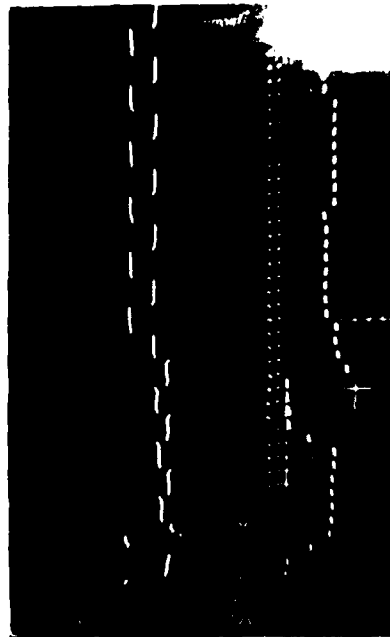
Ser. No. 6  $3.3 \times 10^5$  R/sec  
 Comments Upper Trace: 2V/DIV; 200  $\mu$ sec  
 Lower Trace: 1V/DIV; 50  $\mu$ sec



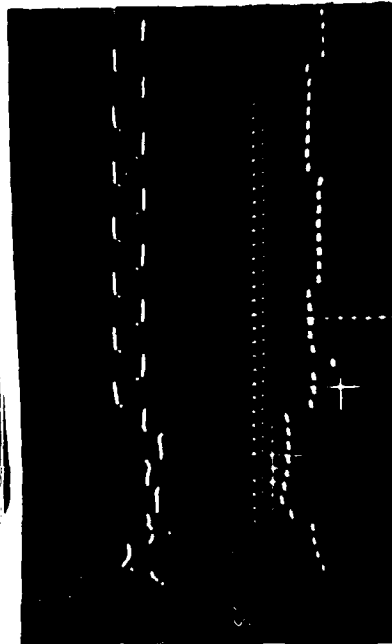
Ser. No. 6 7.2 x 10<sup>5</sup> R/sec  
 Comments Upper Trace: 2V/DIV; 200  $\mu$ sec  
 Lower Trace: 1V/DIV; 50  $\mu$ sec



Ser. No. 9 1.2 x 10<sup>5</sup> R/sec  
 Comments Ones and zeros input  
 Upper Trace: 2V/DIV; 200  $\mu$ sec  
 Lower Trace: 2V/DIV; 50  $\mu$ sec

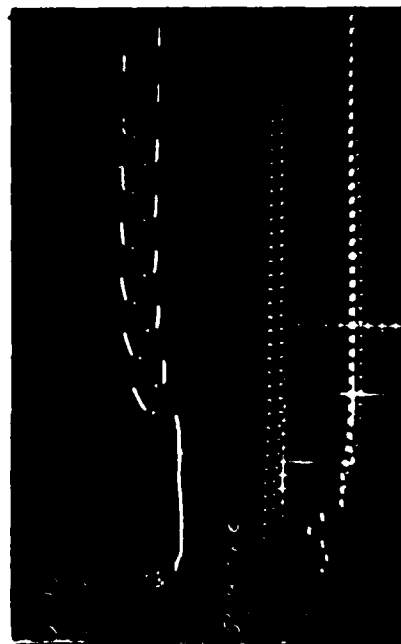


Ser. No. 9 2 x 10<sup>5</sup> R/sec  
 Comments Ones and zeros input  
 Upper Trace: 2V/DIV; 200  $\mu$ sec  
 Lower Trace: 2V/DIV; 50  $\mu$ sec

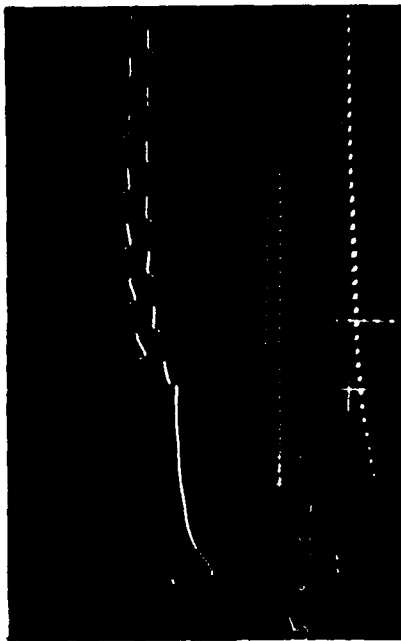


Ser. No. 9 7.2 x 10<sup>5</sup> R/sec  
 Comments Ones and zeros input  
 Upper Trace: 2V/DIV; 200  $\mu$ sec  
 Lower Trace: 2V/DIV; 50  $\mu$ sec

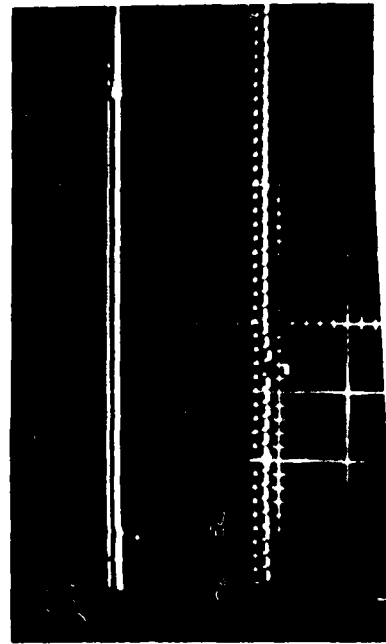
Figure 5-7. CCD shift register, prompt ionizing radiation upset.



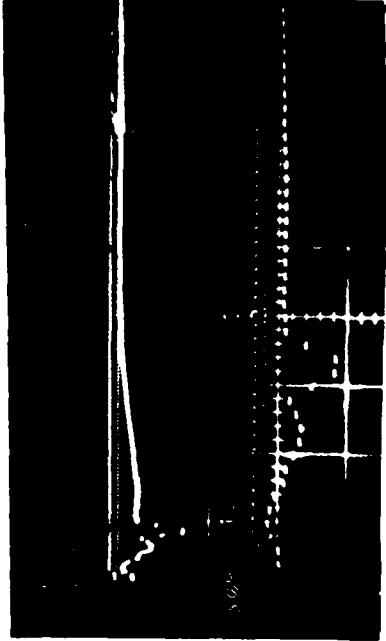
Ser. No. 9 2.1 x 10<sup>6</sup> R/sec  
 Comments Ones and zeros input  
 Upper Trace: 2V/DIV; 200  $\mu$ sec  
 Lower Trace: 2V/DIV; 50  $\mu$ sec



Ser. No. 9 5.1 x 10<sup>6</sup> R/sec  
 Comments Ones and zeros input  
 Upper Trace: 2V/DIV; 200  $\mu$ sec  
 Lower Trace: 2V/DIV; 50  $\mu$ sec

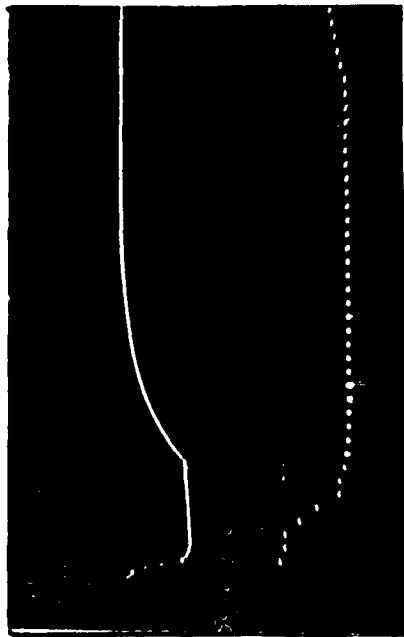


Ser. No. 9 3.6 x 10<sup>3</sup> R/sec  
 Comments Upper Trace: 2V/DIV; 200  $\mu$ sec  
Lower Trace: 2V/DIV; 50  $\mu$ sec

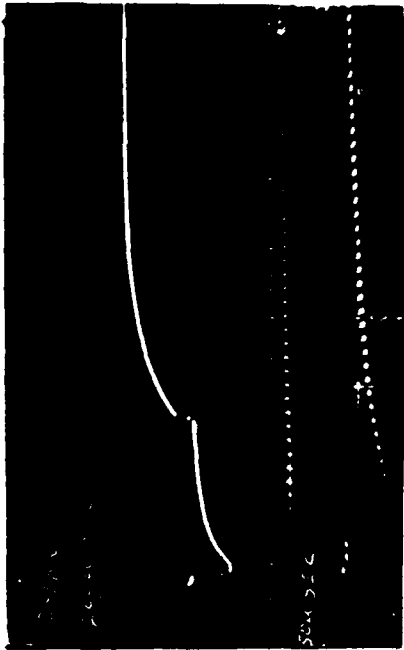


Ser. No. 9 4 x 10<sup>5</sup> R/sec  
 Comments Upper Trace: 2V/DIV; 200  $\mu$ sec  
Lower Trace: 2V/DIV; 50  $\mu$ sec

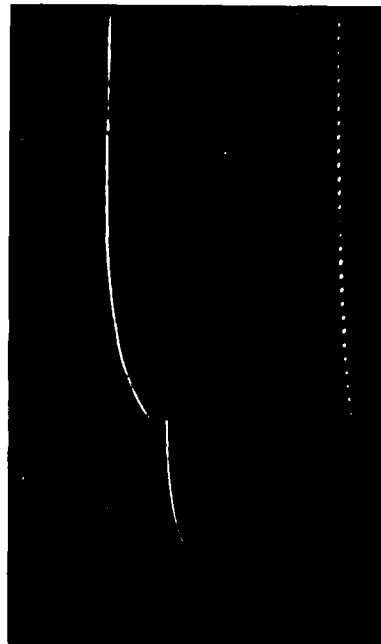
Figure 5-8. CCD shift register, prompt ionizing radiation upset.



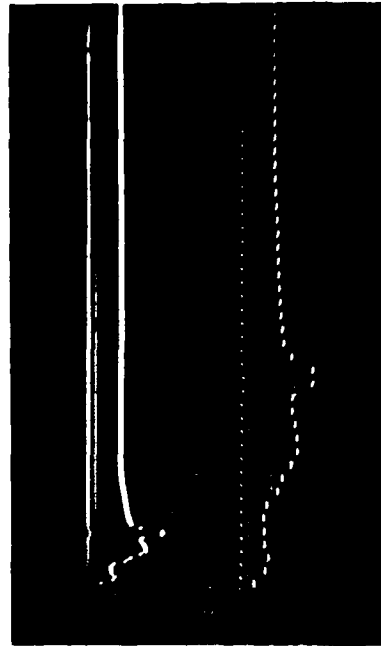
Ser. No. 9  $2.4 \times 10^6$  R/sec  
 Comments Upper Trace: 2V/DIV; 200  $\mu$ sec  
 Lower Trace: 2V/DIV; 50  $\mu$ sec



Ser. No. 9  $5.4 \times 10^6$  R/sec  
 Comments Upper Trace: 2V/DIV; 200  $\mu$ sec  
 Lower Trace: 2V/DIV; 50  $\mu$ sec

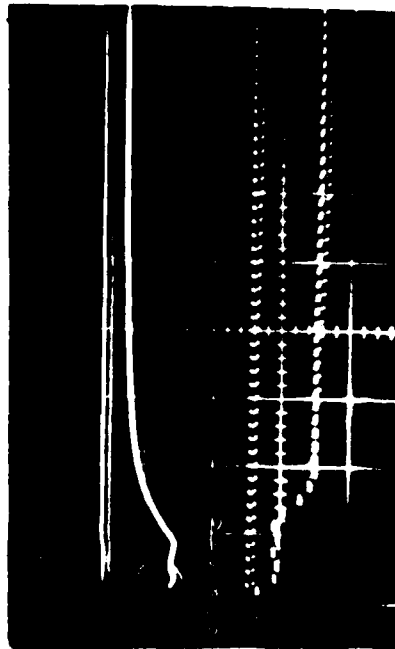


Ser. No. 9  $9.6 \times 10^6$  R/sec  
 Comments Upper Trace: 2V/DIV; 200  $\mu$ sec  
 Lower Trace: 2V/DIV; 50  $\mu$ sec

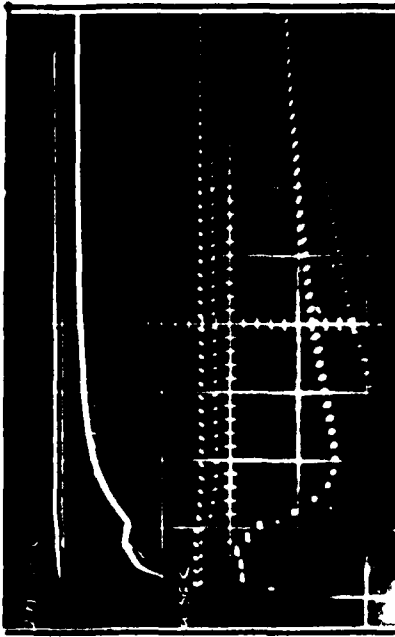


Ser. No. 10  $4 \times 10^5$  R/sec  
 Comments Upper Trace: 2V/DIV; 200  $\mu$ sec  
 Lower Trace: 2V/DIV; 50  $\mu$ sec

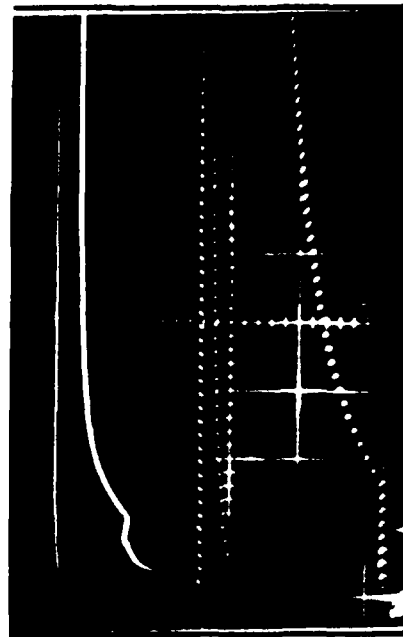
Figure 5-9. CCD shift register, prompt ionizing radiation upset.



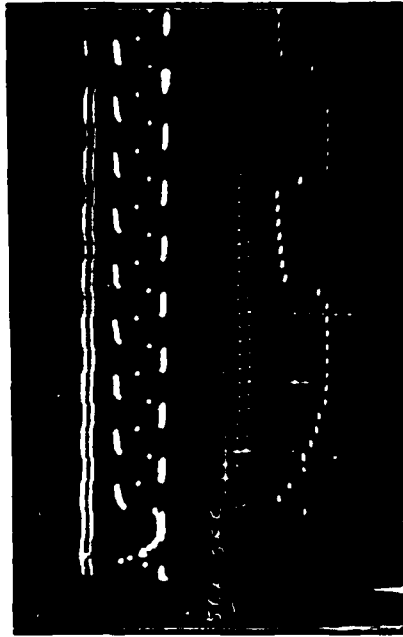
Ser. No. 10  $1.3 \times 10^6$  R/sec  
 Comments Upper Trace: 2V/DIV; 2 msec  
 Lower Trace: 2V/DIV; 50  $\mu$ sec



Ser. No. 10  $5 \times 10^6$  R/sec  
 Comments Upper Trace: 2V/DIV; 2 msec  
 Lower Trace: 2V/DIV; 50  $\mu$ sec

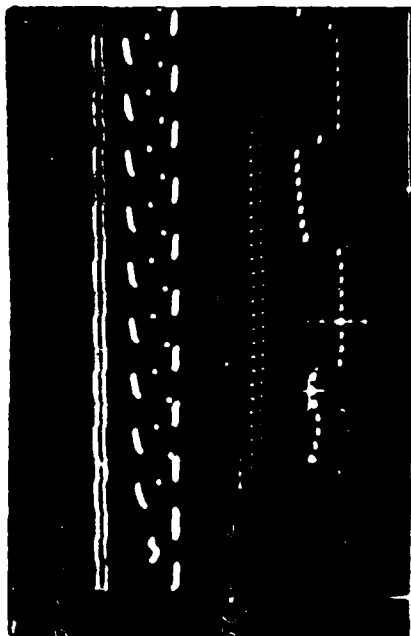


Ser. No. 10  $1.2 \times 10^7$  R/sec  
 Comments Upper Trace: 2V/DIV; 2 msec  
 Lower Trace: 2V/DIV; 50  $\mu$ sec

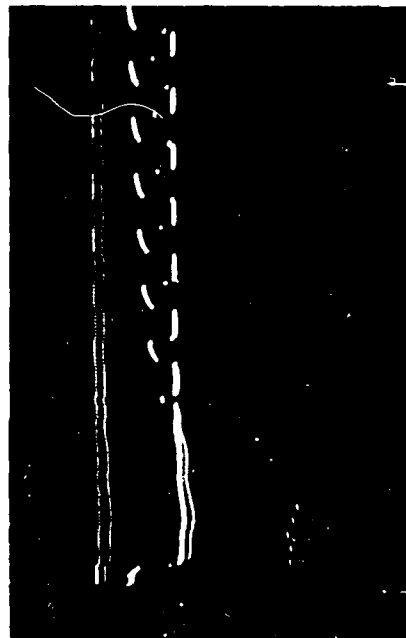


Ser. No. 15  $8 \times 10^4$  R/sec  
 Comments Ones and zeros input  
 Upper Trace: 2V/DIV; 200  $\mu$ sec  
 Lower Trace: 2V/DIV; 50  $\mu$ sec

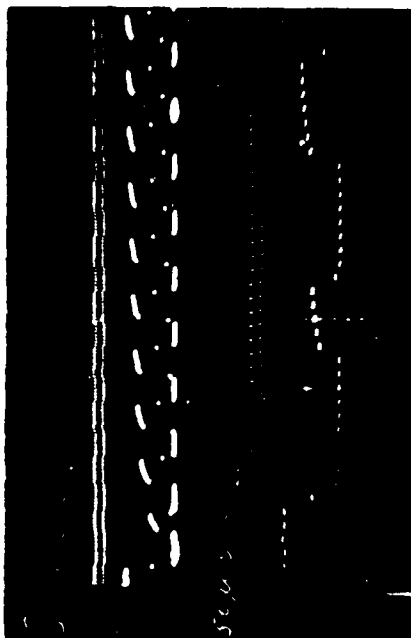
Figure 5-10. CCD shift register, prompt ionizing radiation upset.



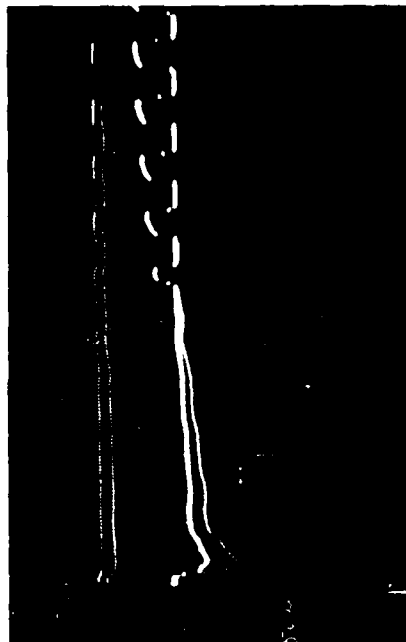
Ser. No. 15 1.2 x 10<sup>5</sup> R/sec  
 Comments Ones and zeros input  
Upper Trace: 2V/DIV; 200  $\mu$ sec  
Lower Trace: 2V/DIV; 50  $\mu$ sec



Ser. No. 15 2 x 10<sup>6</sup> R/sec  
 Comments Ones and zeros input  
Upper Trace: 2V/DIV; 200  $\mu$ sec  
Lower Trace: 2V/DIV; 50  $\mu$ sec

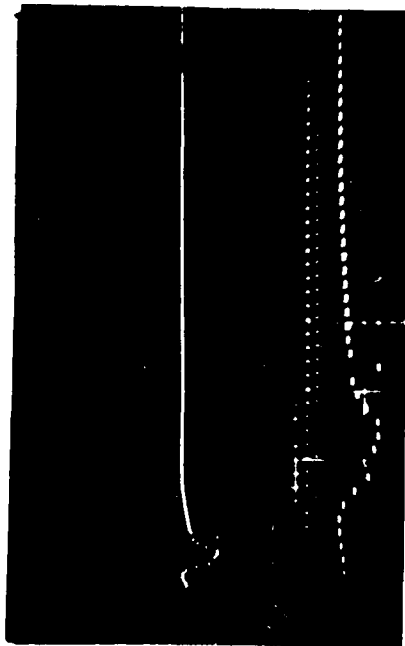


Ser. No. 15 4.8 x 10<sup>5</sup> R/sec  
 Comments Ones and zeros input  
Upper Trace: 2V/DIV; 200  $\mu$ sec  
Lower Trace: 2V/DIV; 50  $\mu$ sec

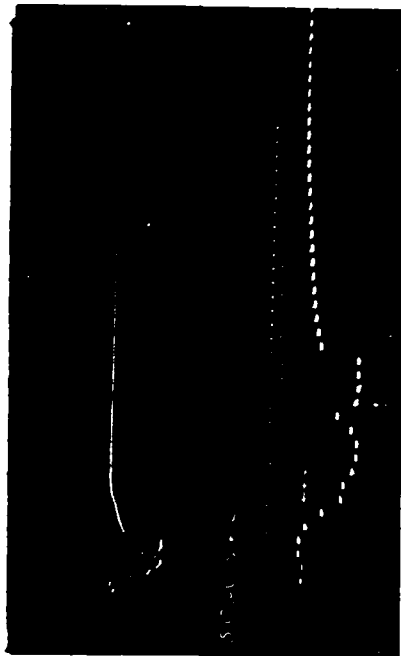


Ser. No. 15 4.1 x 10<sup>6</sup> R/sec  
 Comments Ones and zeros input  
Upper Trace: 2V/DIV; 200  $\mu$ sec  
Lower Trace: 2V/DIV; 50  $\mu$ sec

Figure 5-11. CCD shift register, prompt ionizing radiation upset.



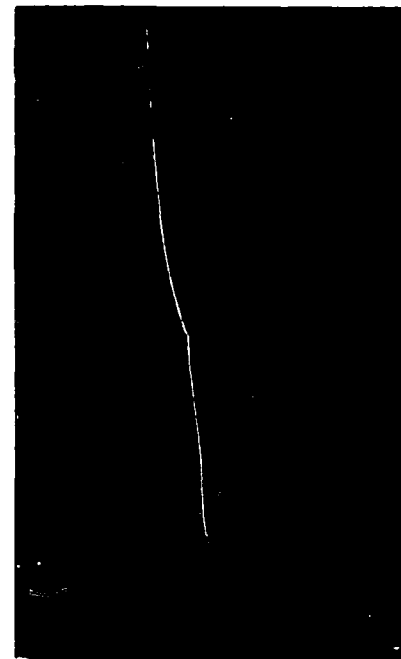
Ser. No. 15  $8 \times 10^4$  R/sec  
 Comments Upper Trace: 2V/DIV; 200  $\mu$ sec  
 Lower Trace: 2V/DIV; 50  $\mu$ sec



Ser. No. 15  $1.2 \times 10^5$  R/sec  
 Comments Upper Trace: 2V/DIV; 200  $\mu$ sec  
 Lower Trace: 2V/DIV; 50  $\mu$ sec



Ser. No. 15  $4.2 \times 10^6$  R/sec  
 Comments Upper Trace: 2V/DIV; 200  $\mu$ sec  
 Lower Trace: 2V/DIV; 50  $\mu$ sec



Ser. No. 15  $8.6 \times 10^6$  R/sec  
 Comments Upper Trace: 2V/DIV; 200  $\mu$ sec  
 Lower Trace: 2V/DIV; 50  $\mu$ sec

Figure 5-12. CCD shift register, prompt ionizing radiation upset.

board with a flat-pack test socket, was inserted into the experiment cylinder of the Gammacell with all cabling routed out through the top orifice. This allowed for in-source biasing of the device and immediate measurements when the cylinder was raised. External cable changes were required when testing the half-adder.

A plot of exposure time versus total absorbed dose is maintained on a monthly basis for the Gammacell. Thus, the required exposure time for given dose on the test samples was easily obtained. As added verification of the received dose, thermal luminescent dosimeters (TLD's) were occasionally attached to the test fixture.

The shift registers were tested first. Pre and Post-irradiation data consisted of oscilloscope photographs of the data output from the device and X-Y recorder plots of surface potential versus gate voltage for two of the on-chip test FET's. These photographs (as well as real-time observation) indicated the effect of radiation on the functional operation of the shift register and allowed the measurement of charge transfer inefficiency (CTI). By measurement of the gate voltage shift on the X-Y plots, the threshold voltage change was read directly. Sample total dose test data is contained in Section 5.3.2.

Data input to the shift registers consisted of an alternate pattern of eight zeros and eight ones. No "fat-zero" was used; therefore the initial CTI values are not optimum. The initial bias voltages and clocking ranges for the shift registers are given as follows:

<u>Terminal</u>	<u>Voltage</u>
$\phi_1$	0 to +10
$\phi_2$	0 to +10
$\phi_3$	0 to +10
$\phi_R$	8.5 to 18
$\phi_D$	0.8 to 8.2
$V_{GG}$	+ 8.0
$\phi_{OUT}$	+ 3.0
$C_2$	+ 4.0
$V_{DD}$	+15.0
$C_1$	+2 to 7.6
$V_{SS}$	- 8.0

With these values, the following initial CTI's were measured for the four shift register samples:

<u>Sample No.</u>	<u>CTI</u>
1	.002
3	.002
4	.004
18	.0009

After irradiation to approximately 500 Rads(Si) total dose, each shift register began to experience severe degradation of functional operation. This was manifested as a rapid rise of the zero bits in the data pattern up to the logic one level. This pattern persisted even after the devices were removed from the Co<sup>60</sup> source. By the time each device had received 1000 Rads(Si), the device data output was no longer usable with respect to logic levels.

At this point, a readjustment of bias voltages was suggested. It was found by shifting the inject diode ( $\phi_D$ ) voltage swing negatively by from 1 to 3 volts for all samples, that functional operation could be restored with a distinct pattern of ones and zeros. For sample numbers 1 and 3, operation could be maintained in this manner (by continual adjustment of  $\phi_D$ ) up to levels of approximately 20,000 Rads(Si). Sample numbers 4 and 18 could not be operated past 10,000 Rads(Si).

Irradiation was continued up to 58,000 Rads(Si) for sample number 1 and to 96,000 Rads(Si) for sample number 3. Measurements of post-radiation CTI are as follows:

<u>Sample No.</u>	<u>Dose</u>	<u>CTI</u>
1	12,000	.003
1	58,000	.0104
3	25,000	.0125
3	96,000	.0140

Threshold voltage shifts were measured on sample numbers 1 and 4. The FET's on number 1 showed a maximum shift of -0.75 volts at 58,000 Rads(Si).

Next, the two half-adder samples were tested. A four-trace oscilloscope was used to monitor the two inputs and the sum and carry outputs of the device. Thus, the ability of device to perform its arithmetic function was under observation.

The functioning of both half-adder samples began to fail at approximately 1600 Rads(Si) total dose. The effect was that of the logic one sum bits going to zero and the logic zero carry bits going to one. As with the shift registers, an adjustment of bias was tried. This time clock phase four ( $\phi_4$ ) was shifted 1 to 2 volts positively to restore operation. With this adjustment, the half-adders gave good functioning up to 9600 Rads(Si). Past this level, both samples would only operate up to approximately 12,000 Rads(Si) with another adjustment of  $\phi_4$ .

The ability to restore the functional operation of both the shift register and the half-adder after total dose irradiation by adjustment of biases indicates that the effects observed may be related to threshold voltage shift. However, functional operation of the devices began to degrade at only about 1000 Rads(Si) while the threshold shifts measured on the test FET's did not exceed 1 volt at levels as high as 58,000 Rads(S8). It is not likely that the devices' functional operation would be sensitive to the even smaller (not measured) shifts which would occur at low total doses. It is suspected that the functional aberrations observed at low total doses are related to charging effects on the several coaxial cables which lead to the test fixture and which were immersed in the  $\text{Co}^{60}$  source with the test sample.

After the final dose, two shift register samples were "baked" in a laboratory oven at  $200^{\circ}\text{C}$  for approximately 18 hours in an attempt to restore functional operation. Both samples recovered to their pre-rad operational states using the original values of bias. Also, the threshold shifts of the FET's were reversed with the post-bake plots retracing the pre-rad plots.

Towards the end of the NE1-1 total dose tests, it was discovered that the oxide layer of the -1 lot had been improperly processed. Since this would be a limiting factor in the total dose hardness of the CCD, it was agreed to package a new set of test devices from a new lot (NE1-3) and re-test to, hopefully, higher total dose levels. The new samples would also be tested at revised biases as determined from the -1 tests.

Total dose tests were performed on new NE1-3 shift registers and half-adders in June of 1978 using the same methods as in the -1 tests. Surprisingly, the -3 samples proved to be even more susceptible to total dose with functional operation failing at as low as 500 Rads(Si) in spite of the revised biases. In addition, a radiation-induced interaction of the test FET's with device operation was observed. It was found that by biasing the gates of the test FET's with a large voltage, the device could be restored to a semi-operational state.

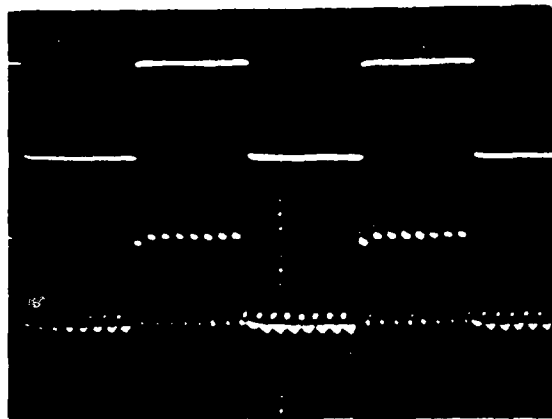
At present, the cause of the FET interaction at very low total dose has not been determined, but deterioration of the Teflon insulation in the test fixture's coaxial cables due to high total doses is suspected. Construction of a new test fixture to verify this suspicion was not attempted due to the limited test time available. Instead, it was elected to passively (no bias applied) irradiate a -3 wafer exclusive of any test fixture, and post-test on a wafer probe station. This would allow several shift-registers (for which the probes and driving electronics were already set up) to be tested functionally while the test FET's on each die remained unbonded.

A wafer was irradiated to a total dose of 30,000 Rads(Si) and then returned to the probe station. Of the several shift registers on the wafer that were probed, each was functional and had good output data waveforms; the only noticeable change was an increase in CTI (similar to -1 measurements). The same bias voltages were used for pre and post irradiation measurements.

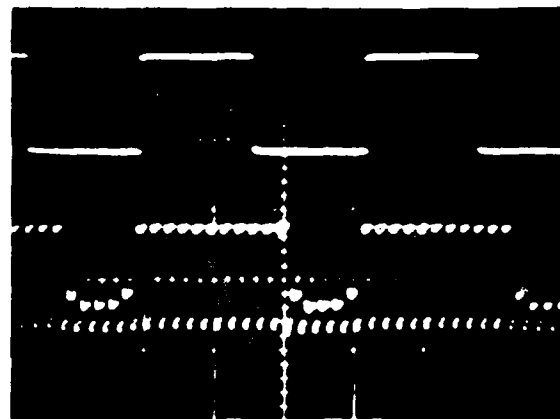
Although the wafer tests show promising results for the NE1 CCD's (total dose hardness comparable to other tests in the literature), additional testing should be performed with bias voltages applied to the devices while under irradiation. This is a worst-case situation for N-channel devices since the positive gate voltages tend to drive trapped ionization-produced charge toward the oxide-silicon interface. Preferably, separate test fixtures should be used for irradiation and post-irradiation measurements. In addition, dark current measurements in the shift register which were neglected due to time constraints should be performed. Once adequate total dose characterization is obtained, neutron tests can be performed.

### 5.3.2 Total Ionizing Dose Test Data

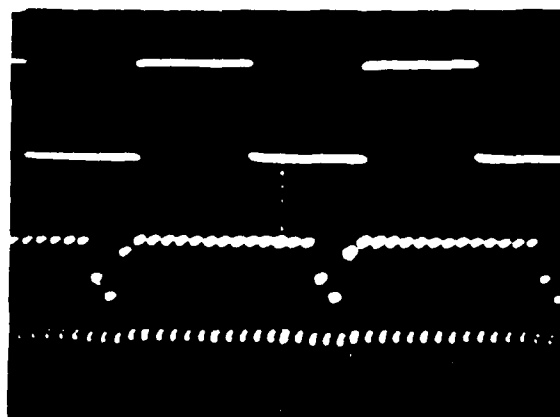
Figures 5-13 through 5-16 represent typical oscilloscope photographs of the CCD shift register and half-adder operation over the range of total ionizing doses received. During the irradiation, as waveform degradation became excessive, device biases ( $\phi_D$ ,  $\phi_4$ ) were adjusted to achieve the most acceptable output waveforms possible. For each sample the final photo gives the maximum total dose for which a bias adjustment could produce reasonable operation.



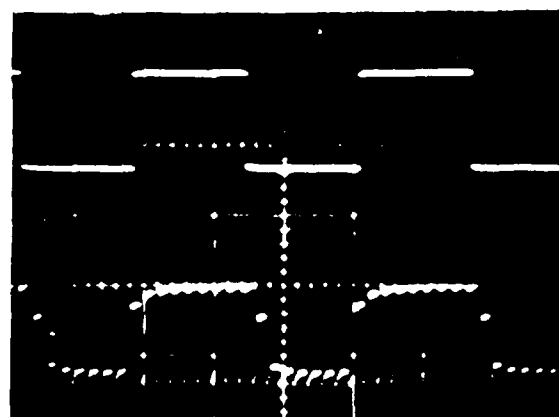
Pre-rad



500 Rads(Si)



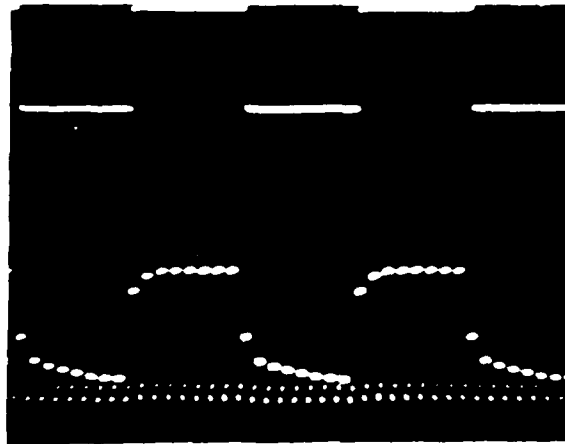
2000 Rads(Si)



22,000 Rads(Si)  
(after inject diode  
adjustment)

Top trace: Input (5v/div.)  
Bottom trace: Output (2v/div.)  
Time scale: 50 microseconds/div.

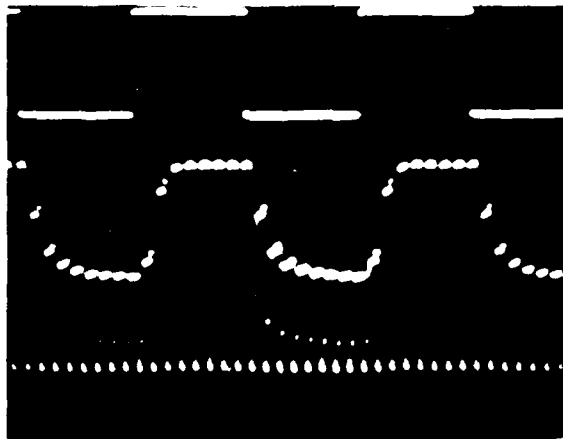
Figure 5-13. Shift Register Output vs. Total Dose (Sample #1)



Pre-rad



4100 Rads(Si)



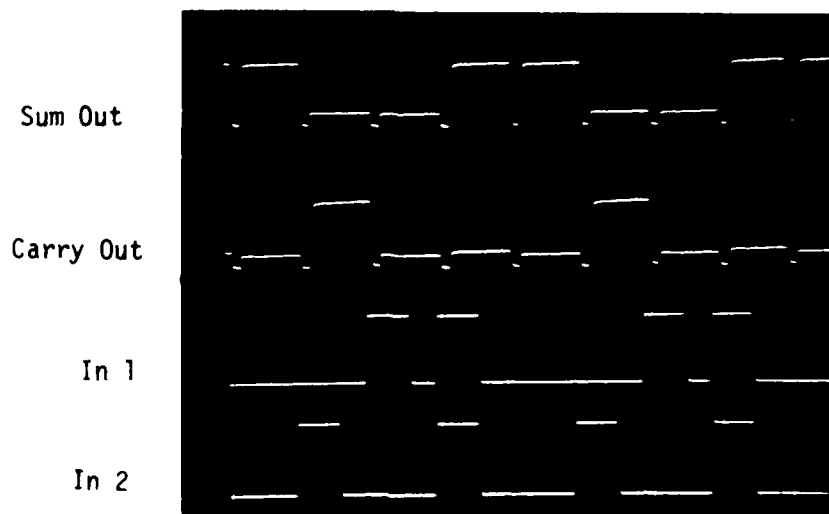
11,000 Rads(Si)  
(after inject diode  
adjustment)



25,000 Rads(Si)  
(after inject diode  
adjustment)

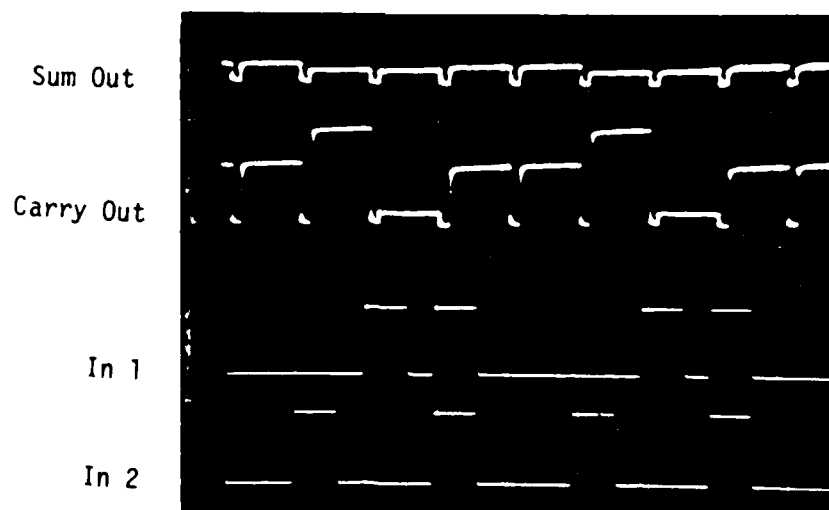
Top trace: Input (5v/div.)  
Bottom trace: Output (2v/div.)  
Time scale: 50 microseconds/div.

Figure 5-14. Shift Register Output vs. Total Dose (Sample #3)



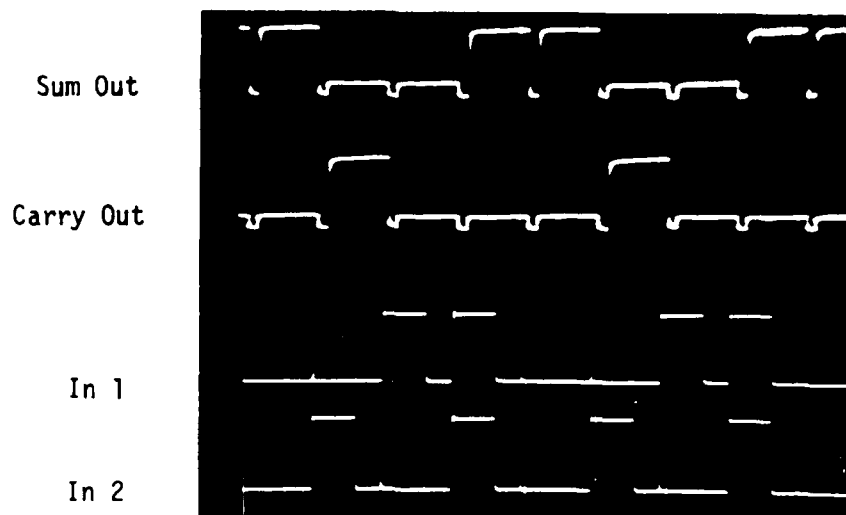
Pre-rad

V: 2v/div. H: 10 microseconds/div.



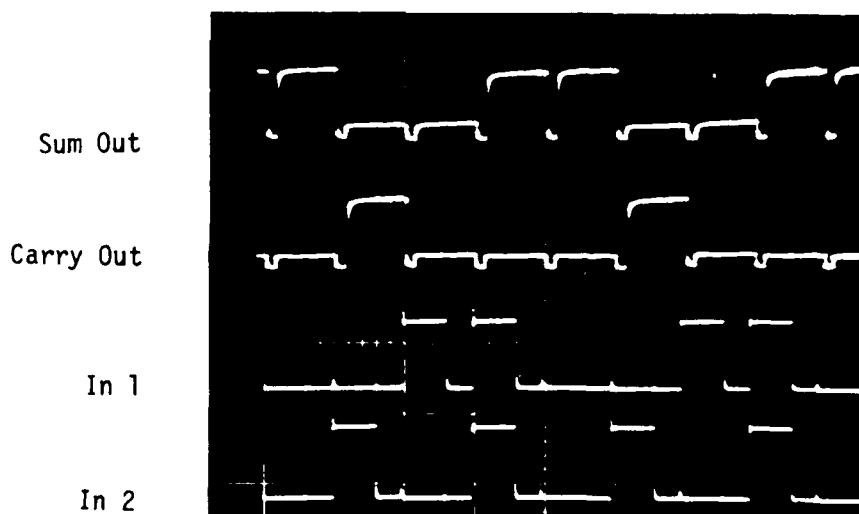
1600 Rads(Si)

Figure 5-15. Half-Adder Output vs. Total Dose (Sample #58)



1600 Rads(Si) (with  $\phi_4$  adjust)

V: 2v/div. H: 10 microseconds/div.



9600 Rads(Si) (with  $\phi_4$  adjust)

Figure 5-16. Half-Adder Output vs. Total Dose (Sample #58)

## 6. SIGNAL AND DATA PROCESSING APPLICATIONS

### 6.1 INTRODUCTION

The arithmetic capabilities of DCCL chips can be utilized in filtering applications: correlation, convolution, and fast transforms such as Fourier, Hadamard, and Hilbert. The inherent structure of these functions allows them to be cast into flow-form which is ideal for DCCL pipeline computations. The flow form of the structure allows timing and data routing to replace much of the program memory and control logic found in general purpose processors.

A large number of different flowform signal processing functions can be formed using only two types of DCCL Large Scale Integrated (LSI) chips. One chip provides the arithmetic function (AU) while the other provides memory and control (MC).

### 6.2 APPLYING THE DCCL CONCEPTS

The basic arithmetic functions to be realized are addition/subtraction, multiplication and scaling (multiplication by a power of two). The arithmetic accuracy required for the different applications, as we have seen, can vary widely; however, the more stringent applications such as Itakura voice processing, can be satisfied with 16-bit multiplication accuracy and addition/subtraction accuracy required for the different applications such as Itakura voice processing, can generally be satisfied with 16-bit computational accuracy. In some cases a double precision add/subtract capability of 32-bits is required. A DCCL chip configuration with this capability is shown in Figure 6-1. To allow the sequence of arithmetic operations to be performed in different orders, corresponding to different applications, multiplexers are placed at the input to the adder and multiplier. A multiplexer is also provided at the output so that results of the different operations can be selected.

Control inputs are accepted by the arithmetic chip to route the data through the desired elements so that a prescribed sequence of operation is performed.

For example, the radix two form of the FFT kernel or "butterfly" can be accomplished with six add/subtract operations and four multiplications. Initially, the sum of the real parts of the complex inputs is computed and

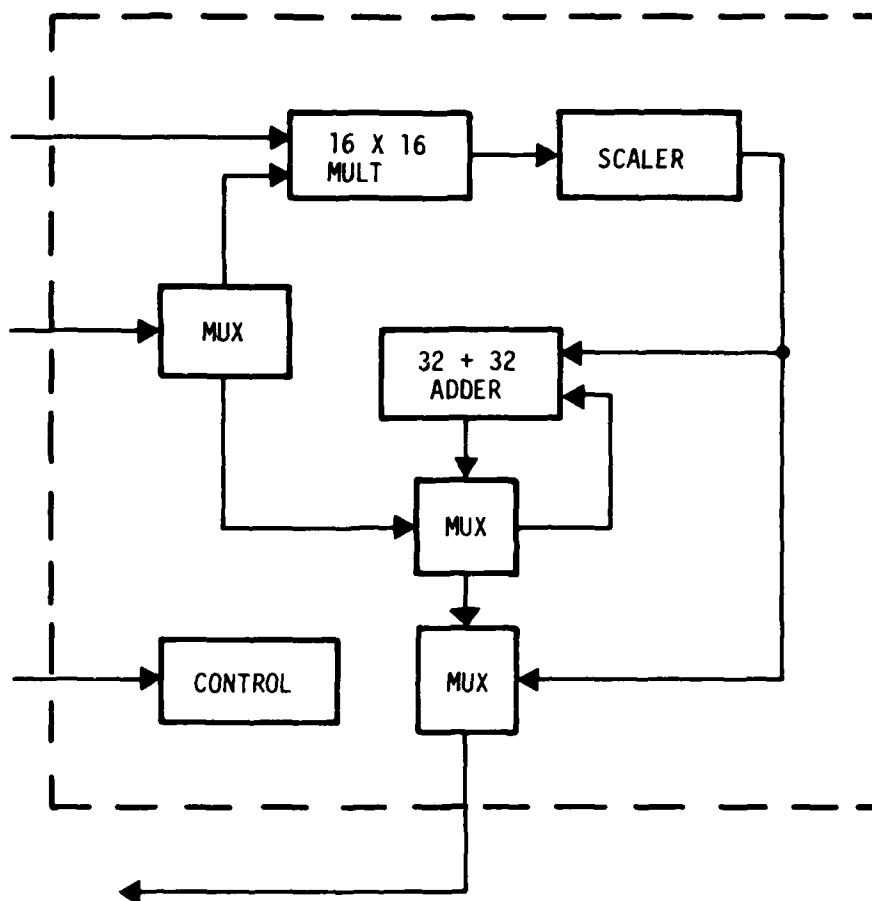


Figure 6-1. DCCL arithmetic unit chip.

the result applied to the output for storage. Next, the sum of the imaginary parts is computed and applied to the output. The third and fourth steps consist of computing the difference between the real parts and the difference between the imaginary parts, respectively. These differences are then routed through the multiplier where they are multiplied by the sine and cosine "twiddle factors". Four passes through the multiplier are required to compute the four products. The final steps in the "butterfly" computation which complete the complex multiply, are to sum one pair of products and to compute the difference of the other pair. These two results are then returned to storage.

To perform a correlation computation, the control inputs to the arithmetic chip cause the output of the adder to be fed back to the input thereby operating as an accumulator. The sequences of the two input variables to be correlated are then applied to the multiplier and the product accumulated. Registers for latching the data words are not shown in Figure 6-1 because storage is implicit in the operation of DCCL.

The fundamental consideration in applying DCCL is the throughput delay. Best computational efficiency is obtained using pipeline techniques. Although in many of the important applications, the computations can be cast into a flow-form suitable for pipelining, there is also a need for general purpose computer operations such as executing branching and jump instructions. Conditional instructions of this type require a comparison to be made before the next step in the program is determined. Due to the delay through the DCCL arithmetic logic, it is difficult to perform general purpose computing efficiently. With these characteristics of DCCL arithmetic in mind, it is important to tailor the control chip to match the characteristics of the AU.

The basic timing can be broken up into blocks of  $N$  clock intervals where  $N$  exactly matches the delay through the AU: typically this may be between 16 to 32 clock intervals. Control of the DCCL arithmetic unit can be divided into block and intra-block instructions. The intra-block instruction controls allow pipelined operations to be performed, like the FFT, where data words are added and then subtracted on successive clock pulses. By changing the block instructions, the intra-block instructions can be changed after each block of  $N$  clock pulses. For example, the AU can perform successive sums and differences on one block of  $N$  samples followed by a multiply and accumulate on the next block of  $N$  samples. Since the results of an arithmetic operation becomes available at the arithmetic unit output after  $N$  samples, branching, skip, and jump instructions can be performed at the block rate. Thus, the AU can either perform flow-form types of computations at a high rate or general purpose computations at a lower (by a factor of 16 to 32) block rate.

The separation of the control of the AU into block and intra-block functions is inherent in the shift register type of architecture for the DCCL control chip as shown in Figure 6-2. The blocks of shift register memory

may be either conventional data memory or shift register read only memory (ROM) where a metallization mask determines how many of the blocks are to be ROM as well as the contents of the ROM. Multiplexers at the input and output control the flow of data and program instructions to and from the AUs.

Each memory block in Figure 6-2 consists of shift registers and recirculation logic. Nominally, the block would be 16 or 32 samples long with 16 shift registers in parallel corresponding to a 16-bit/word parallel data format. The shift register block has a tap after  $N-1$  samples so that data can be recirculated back to the input after either  $N$  or  $N-1$  sample delays. This allows the memory blocks to be operated either as recirculating memory or as a delay line time compressor (DELTAIC) so that as the data processes through the register, the oldest sample is replaced by the new input sample.

When the DCCL control chip is operated with the DCCL arithmetic unit, the two data outputs are selected by the multiplex gates and applied to the AU inputs, while the arithmetic unit output is fed back to the input MUX. The lower multiplex gate on the right in Figure 6-2 selects the control values from either the ROM shift registers or a data shift register; thus, the controller operation can proceed either according to a program stored in the ROM or be changed by input values. The input values can be from either an external source (e.g., an interrupt) or from values computed by the DCCL arithmetic unit.

When operated at the slower block rate, both the data and the next program control value can be time-interleaved so that both are computed in a single  $N$  clock interval block time. With a 4 MHz clock rate and  $N = 32$ , both operations can be accomplished in 8  $\mu$ sec.

### 6.3 SPECIFIC NRL/DCCL APPLICATIONS

TWO APPLICATIONS OF DCCL to specific systems were considered (at different points in time) in response to mutual TRW/NRL desires. The first system application, which comprised the great majority of the project duration, was for a DCCL Itakura transform chip(s). As the program progressed, two conditions emerged which changed its direction and goals. First, the original need for the Itakura transform function dissipated as a result of changes in a parallel voice processing program (which was intended to use this transform chip). Second, as the chip development progressed, estimates of the design

and layout effort required to realize the Itakura function began to indicate that these efforts were beyond the scope of the original contract. As a result of these two conditions, a sorting application emerged as a more useful project goal. By mutual agreement, a new goal of designing a number sorting chip was under taken.

The following paragraphs describe these two applications from the stand-point of DCCD implementation.

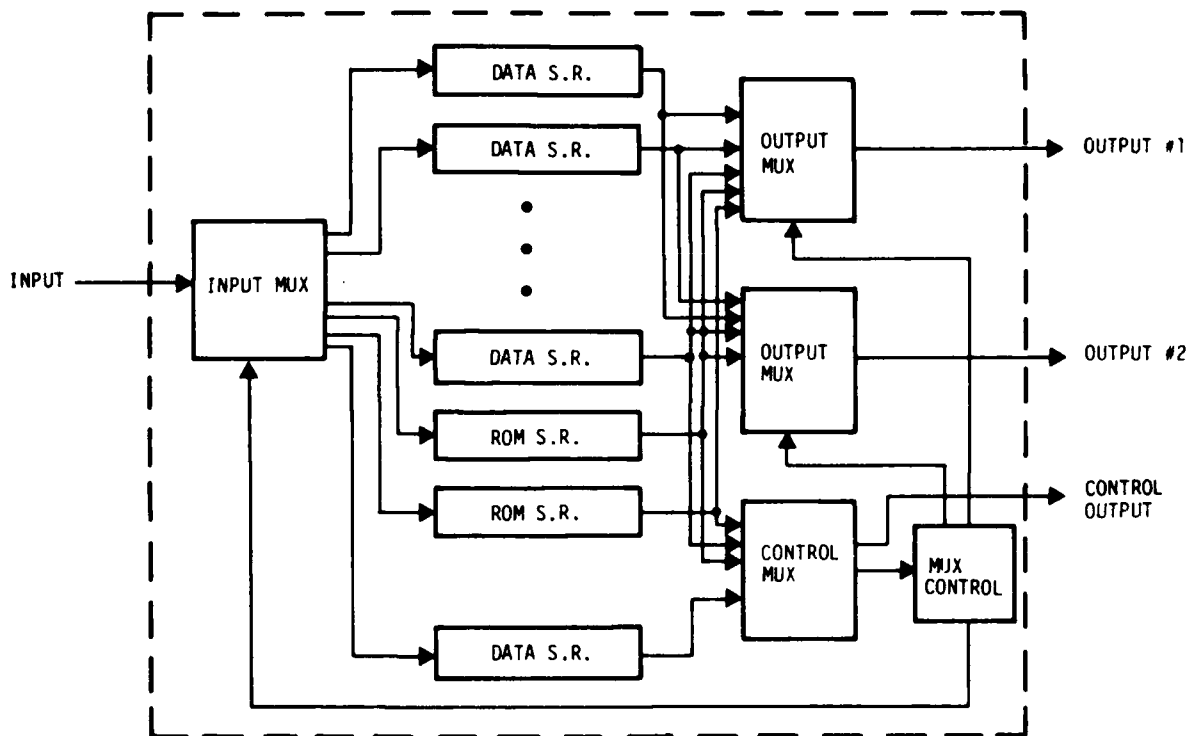


Figure 6-2. DCCL controller chip.

### 6.3.1 Itakura Transform Application

Secure voice processing is a potential application for the pair of DCCL chips. The problem, stated simply, is to digitize the speech signal so that the security feature can be implemented by performing numerical operations on the data. Unfortunately, digitizing the speech directly (e.g., using PCM) results in a greatly increased bit rate. In order to reduce the bit rate so that it can be transmitted over existing audio channels, it is necessary to perform the secure voice processing which, in essence, compresses the bandwidth by source coding.

One of several voice processing techniques is to employ a linear predictive coding (LPC) algorithm (ITAKURA, F. et al, 1972). The procedure for the analyzer part of the voice processor consists of passing a signal through ten identical stages (as shown in Figure 6-3). In each stage a Parcor (ITAKURA, F. et al., 1972) coefficient,  $K_i$   $i = 1, 2, \dots 10$ , is determined and these ten coefficients in addition to pitch and voicing information are sent to the receiver where the speech is reconstructed.

As indicated in Figure 6-3, the Parcor coefficients can be written

$$K_i = \frac{\rho_i - 1}{P_i - 1}$$

where the  $\rho_i$  are correlation values and the  $P_i$  are the mean square forward prediction errors (or backward prediction errors). The  $\rho_i$  and  $P_i$  can be written

$$\rho_i = \sum_{j=1}^N A_{i-1} B_{i-1}$$

and

$$P_{i-1} = E [A_{i-1}^2]$$

where  $E$  denotes expectation. The  $i^{\text{th}}$  stage forward (and backward) prediction errors,  $A_i$  and  $B_i$  are related to the previous stage values, and the Parcor coefficient,  $K_i$  by

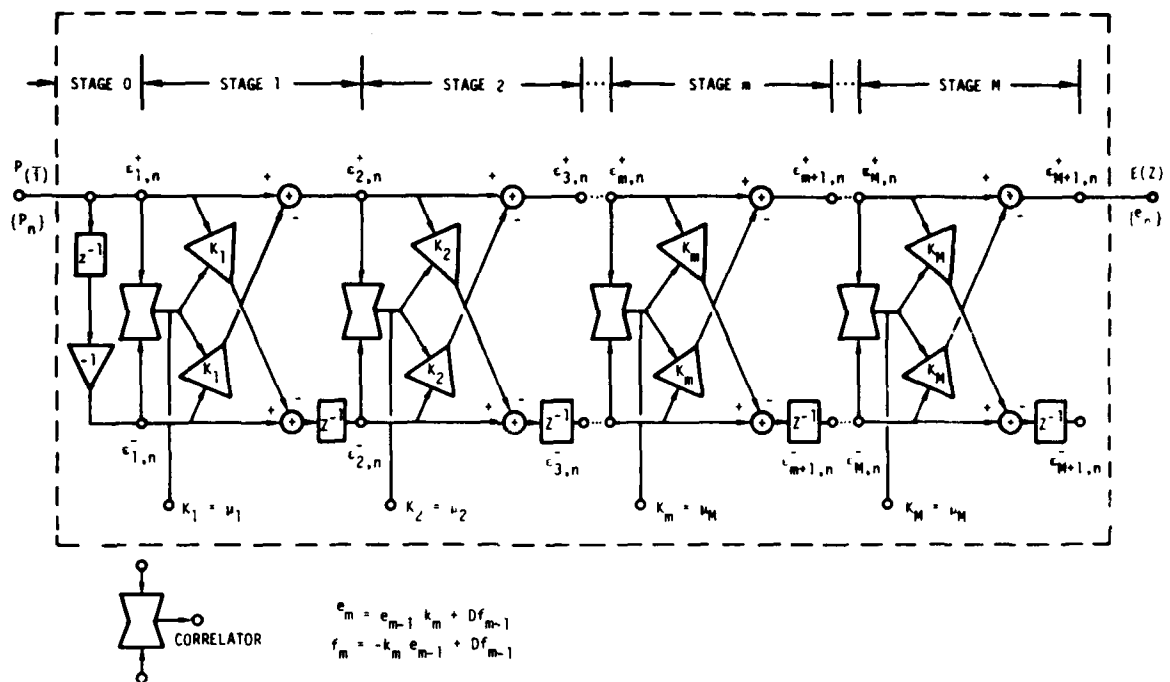


Figure 6-3. Itakura analyzer.

$$A_i = A_{i-1} - K_i B_{i-1}$$

and

$$B_i = B_{i-1} + K_i A_{i-1}$$

In practice, the summation over  $N$  samples which forms the correlation is replaced by lowpass filtering. The expected value of the prediction error is approximated by subtracting the product of the Parcor coefficient times the correlation from the value in the previous state. A block diagram indicating the operations necessary to realize an Itakura analyzer stage is shown in Figure 6-3.

Due to the relatively long propagation delay through the DCCL arithmetic unit, and the desire to employ pipeline computation for best speed and efficiency, it is necessary to separate the computation into a number of steps. Each Itakura analyzer section can be computed with a sequence of seven passes through the arithmetic chip to perform the following operations:

(1) Multiply  $A_{i-1} \cdot B_{i-1}$

(2) Perform lowpass filter computation

$$P_{i-1} = 2^{-k} (A_{i-1} B_{i-1}) + (1-2^{-k})P_{i-2}$$

(3) Compute  $\frac{1}{P_{i-1}}$

(4) Compute  $K_k = \frac{\rho_{i-1}}{P_{i-1}} = \rho_{i-1} \left( \frac{1}{P_{i-1}} \right)$

(5) Update  $P_i = P_{i-1} - K_i \rho_{i-1}$

(6) Update  $A_i = A_{i-1} - K_i B_{i-1}$

(7) Update  $B_i = B_{i-1} - K_i A_{i-1}$

In the above list of operations, each can be accomplished in a straightforward manner by applying the appropriate controls to the arithmetic chip. The divide operation can be implemented by a recursive algorithm, which requires a ROM table lookup to estimate the inverse value followed by two multiplications and an addition (HUTCHINS, S. E. et al., 1975). Typically, a conventional ROM would be used; however, a DCCL ROM could be used if the longer access time could be tolerated.

A primary difficulty in implementing the Itakura analyzer in an efficient pipeline fashion with DCCL is that the result of one pass through the AU must be available before the next can commence. This, of course, holds true for each of the ten stages in the Itakura analyzer. The solution to this

problem is to employ interleaving.<sup>(10)</sup> By accepting, for example, a 10 sample delay; the first operation on the list for each stage can be computed during the N clock pulse interval corresponding to the propagation time through the AU. On the next pass through the AU the second operation on the list is performed for each of the ten interleaved stages. After the last operation of the first analyzer stage has been completed, the time position of the result is shifted one clock interval utilizing the variable length shift register (or DELTIC) in the control chip so that the time position corresponds to the interleaving for the second analyzer stage. This procedure is repeated to complete the ten-stage analyzer computation. Although this distribution in time of the computation of different analyzer sections and the interleaving of the operations would require a complicated indexing scheme with a general purpose computer; with the shift register structure of the DCCL control chip the required control becomes simple and straight-forward.

### 6.3.2 Sort and Merge Applications

The majority of most general computer time is spent sorting and reassembling numbers, yet there is no LSI device available that has been designed to do this function efficiently. In August 1978, work on the voice processor application was stopped to permit a study of the feasibility of designing a digital CCD Sort and Merge chip.

This section discusses the different Sort and Merge designs that resulted from this design/study effort.

#### 6.3.2.1 DCCL Sort and Merge Technique No. 1

In every system application considered, the unsorted numbers are received in a continuous stream of 2's Complement Numbers of 16 or 32 parallel bits. The words may be converted from parallel to serial format before entering the CCD chip in order to reduce the number of input pads. On the chip the input is converted back from a serial to parallel format with a CCD shift register.

The largest of two 2's Complement Numbers is determined by subtracting one of the numbers from the other and examining the binary value of the most significant or sign bit. Subtraction of 2's Complement Numbers is performed by complementing one of the numbers and then adding together the complemented number, the other number, and a binary one.

EXAMPLE 1. To subtract  $B = 4$  from  $A = 15$

Complement  $B = 0\ 0\ 1\ 0\ 0$ ;  $\bar{B} = 1\ 1\ 0\ 1\ 1$

$A = 0\ 1\ 1\ 1\ 1$

ADD  $\underline{0\ 0\ 0\ 0\ 1}$

$0\ 1\ 0\ 1\ 2 = +\ 10$

Sign Bit  $\uparrow$

The binary "0" value of the Sign-Bit indicates that  $A > B$  (i.e.  $+10$ )

EXAMPLE 2. Compare  $A = 4$  and  $B = 15$

Complement  $B = 0\ 1\ 1\ 1\ 1$ ;  $\bar{B} = 1\ 0\ 0\ 0\ 0$

$A = 0\ 0\ 1\ 0\ 0$

ADD  $\underline{0\ 0\ 0\ 0\ 1}$

$1\ 0\ 1\ 0\ 2 = -\ 10$

Sign Bit  $\uparrow$

The binary "1" value of the Sign-Bit indicates that  $A < B$  (i.e.  $-10$ )

The same method of comparing 2's Complement Numbers by subtraction holds true for negative 2's Complement Numbers.

It can be seen from the examples given above that only the sign-bit is required to determine which of the two numbers is the larger; the actual magnitude of the difference is not required.

In order to generate the sign-bit, we must add together the most significant bit of the complemented number,  $\bar{B}_m$ , the most significant bit of the other number,  $A_m$  and a carry bit. The carry-bit,  $C_m$ , is generated by adding the rest of the complemented number,  $\bar{B}_{m-1} - \bar{B}_0$ , the rest of the other number,  $A_{m-1} - A_0$  and the binary "1" bit,  $C_0$ .

The truth table for the carry-bit,  $C_1$ , generated by adding together the least significant bits of the complemented word,  $\bar{B}_0$ , the other word  $A_0$  and the binary "1" input,  $C_0$  is shown in Table 6-1.

Table 6-1. Truth Table for the Generation of a Carry from a Full-Adder

Inputs			Output
$A_0$	$B_0$	$C_0$	$C_1$
0	0	0	0
0	0	1	0
0	1	0	0
0	1	1	1
1	0	0	0
1	0	1	1
1	1	0	1
1	1	1	1

The Boolean expression for the truth table is:

$$C_1 = A_0 B_0 + (A_0 + B_0) C_0 \quad (1)$$

The Boolean expression for the second least significant carry can be written in a similar manner:

$$C_2 = A_1 B_1 + (A_1 + B_1) C_1. \quad (2)$$

If the carry input factor,  $C_1$ , in Equation (2) is replaced with its Equation (1) value, the expression for  $C_2$  becomes:

$$C_2 = A_1 B_1 + (A_1 + B_1) (A_0 B_0) + (A_1 + B_1) (A_0 + B_0) C_0. \quad (3)$$

The carry outputs for the remainder of the 32-bits can be expressed by an extension of Equation (3). The carry-bit charge packets can be generated in a simple manner in DCCL by cascaded AND gates as shown in Figure 6-4.

It was shown in the previous examples that only the most significant sum bit is required to determine which of two numbers is the larger. The expression for the most significant sum bit is:

$$S = A \bar{B} \bar{C} + \bar{A} B \bar{C} + \bar{A} \bar{B} C + A B C. \quad (4)$$



Since Equation (4) involves complemented terms it is necessary to use a floating-gate cell; and with three inputs we must use a full-adder.

Each AND function is performed during one phase of a three phase clock period and therefore with the exception of the most significant bit will require  $(N-1)/3$  clock periods to perform the comparison and generate the next to most significant carry bit (where  $N$  = number of bits per word).

If cascaded dual half-adders are used to generate the most significant sum bit, two clock periods are required. The comparator will then require a minimum clock frequency of

$$f_c = [(N-1)/3 + 2] f_0 \quad (5)$$

where  $f_0$  is the clock frequency of the numbers entering the comparator.

The unsorted 2's complement numbers enter the Sort and Merge chip serially so that the first numbers have to be retained in a memory for comparison with later numbers. The method that we have devised for the temporary store to perform a serial to parallel conversion and transfer the parallel numbers, through a 1 to 4 multiplexer, into four parallel registers which are filled sequentially. The first number enters Register  $A_1$ , shown in Figure 6-5. The clocks to Register  $A_1$  are then inhibited holding the first number in Register  $A_1$ . The second number then enters Register  $B_1$ . The clocks to Register  $B_1$  are then inhibited thereby holding the second number in Register  $B_1$ . Similarly, the third number enters Register  $C_1$  and is held.

Simultaneously with the third number entering Register  $C_1$ , the Register Select Gates AND 1 and AND 2 are enabled so that the first and second numbers enter their respective Restore and Convert circuits ( $RC_1$  and  $RC_2$ ). The Restore and Convert circuits sense the binary value of the input charge, by comparing it with another charge of fixed size. Based on the result of this comparison, a MOS flip-flop is toggled to the appropriate binary state. The flip-flop provides a digital voltage output that corresponds to the binary value of the input charge. The Restore and Convert circuit also provides an output voltage that is the complement of the binary value of the input charge. The true digital voltage output from  $RC_1$  and the complemented digital voltage output from  $RC_2$  are converted to charge packets that are then applied to the AND gates and full-adder of the comparator.

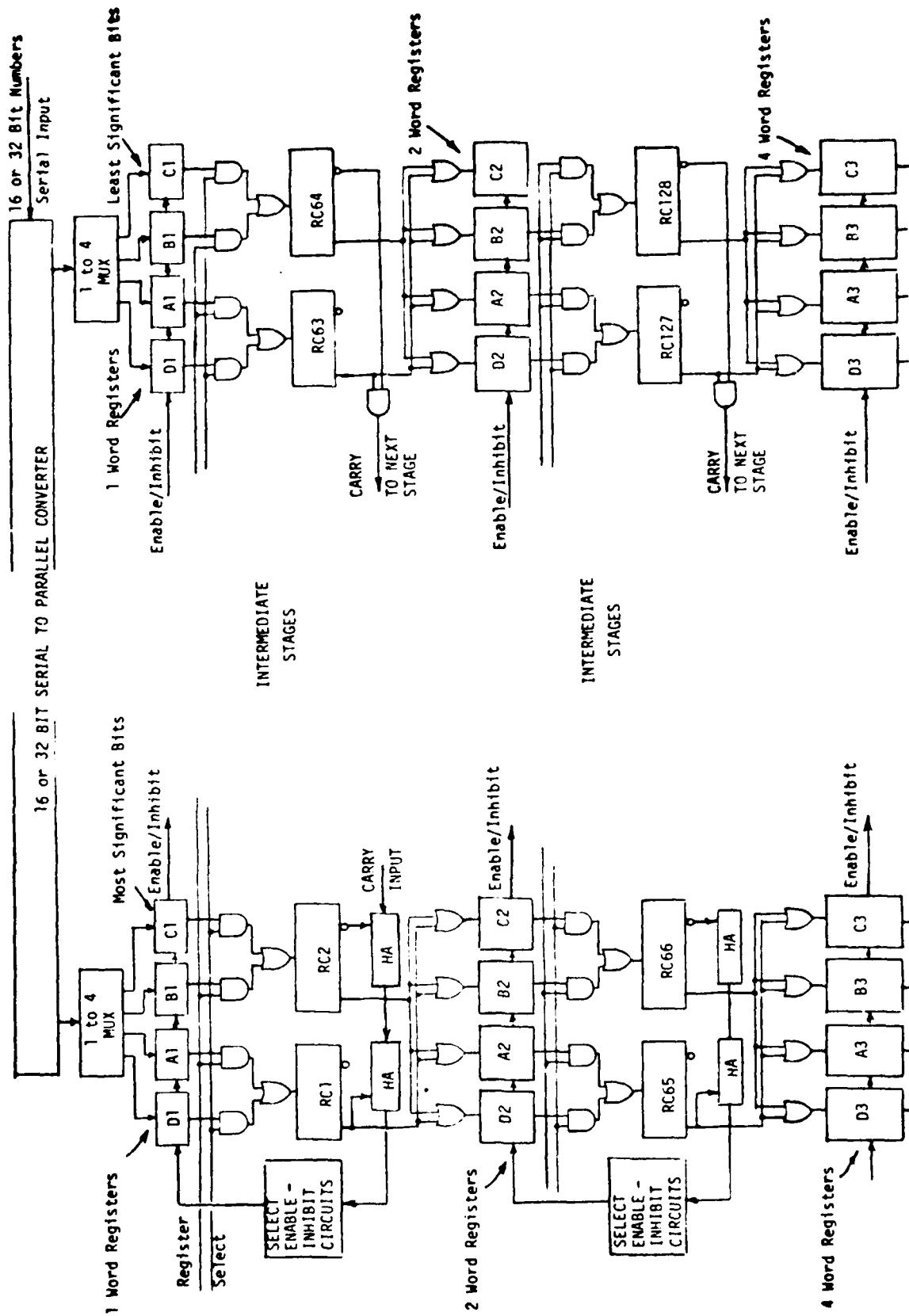


Figure 6-5. Block diagram showing how four registers are interleaved. Note that each Restore and Convert (RC) Cell is shared by two Storage Registers and that each Comparator is shared by four Storage Registers.

The comparison of the first and second numbers takes place during one cycle of the input clock rate for the unsorted numbers.

Depending upon the binary value of the most significant sum bit from the number comparison, either the A1 or B1 registers and the output from its corresponding RC circuit are enabled. The clock signal to the register that is holding the larger (or smaller, if that is the order of the sort) of the first and second numbers is enabled and that number is transferred into register A2. Register A2 can store two numbers.

The fourth number then enters Register D1 and the clocks to register D1 are inhibited thereby retaining this value in the D1 register. Simultaneously with the fourth word entering register D1, the clocks to the register containing the number remaining in either registers A1 or B1 are enabled and that number is transferred into register A2.

The fifth number enters and is held in Register A1; this starts a new cycle of the first comparison level. Simultaneously with the fourth word entering register A1, the Register Select Gates AND 3 and AND 4 are enabled so that the first and second numbers enter their respective Restore and Convert circuits (RC1 and RC2) and the comparator. Numbers 3 and 4 are then sorted in a similar manner to 1 and 2 and placed into Register B2. Numbers 5 and 6 are sorted and placed in Register C2 and numbers 7 and 8 sorted and placed in Register D2.

While the four numbers are being sorted and placed into Registers C2 and D2 the four numbers in Registers A2 and B2 are sorted and placed in Register A3. Register A3 can hold four numbers. Sorting is carried out by comparing the first number entered into Register A2 with the first number that was entered into Register B2. The clocking to the register containing the larger of the two numbers (or smaller, if that is the order of the sort) is enabled so that the number is transferred into Register A3 and is replaced by the second number transferred into Register A2 or B2. A comparison then takes place between the number retained by the inhibited clock register and the number replacing the one just transferred out.

This sequence of comparison and shift continues until all four numbers in Registers A2 and B2 are transferred into Register A3 leaving Registers A2 and B2 empty for the ninth, tenth, eleventh and twelfth numbers.

Sorting and storing the numbers continues through the remaining stages with the length of the storage registers doubling at each stage until the required quantity of numbers are held in two registers. The numbers in these two registers are then compared once more and then transferred into a parallel to serial converter before transferring off the chip on a single serial line.

A three phase clock system may be used for the registers and by making  $\phi_3$  more positive than the other two phase, and by making a  $\phi_3$  clock line unique for each of the registers; each register can be either enabled or inhibited by switching the  $\phi_3$  clock lines and allowing the common  $\phi_1$  and  $\phi_2$  clock lines to continuously run.

Using Equation (5), which was derived previously for a 3-phase clocking system, and assuming an unsorted 16-Bit word rate of  $f_0 = 1$  MHz; the required DCCL clock rate is

$$f_c = [(16-1/3 + 2)]f_0$$

$$= 7.0 \text{ MHz}$$

In September 1978, a half-adder design that would operate comfortably at a clock speed of 7.0 MHz was not available. This subsequently resulted in the abandonment of this approach from a design risk standpoint. One year later a 4-phase ACD2 half-adder was operated at 5.0 MHz with a predicted upper operating limit of 10 MHz. If Equation (5) is modified for 4-phase operation, it becomes;

$$f_c = [(16-1/4 + 2)]f_0 \quad (6)$$

Now, for a unsorted 16-Bit word rate of  $f_0 = 1$  MHz, the required DCCD clock frequency is only 5.75 MHz. At this point in time, this sorting technique appears to be a feasible DCCL option.

#### 6.3.2.2 DCCL Sort and Merge Technique No. 2

Investigation of a second technique was initiated in November 1978. This approach integrated the magnitude comparison and the sort store into single, bit size, logic blocks as shown in Figure 6-6.

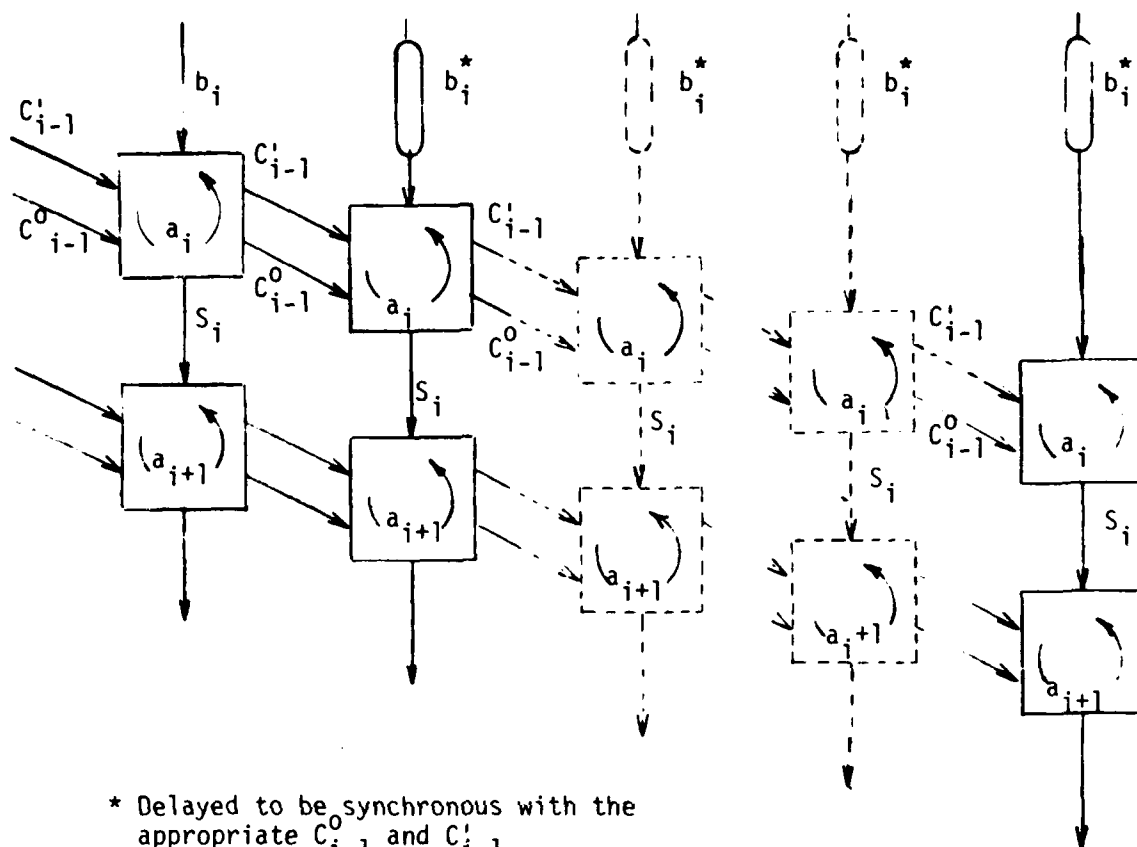


Figure 6-6. Block diagram of a sort and merge algorithm with the features of allowing the bit length of the numbers being compared to be expandable in the row direction and the quantities of sorted numbers to be expandable in the column directions.

The description of this sort and merge algorithm begins by assuming that the first word,  $a_1$ , has been entered and stored in the first row of logic blocks, with the most-significant-bit (MSB) in the left block. The next number,  $b_1$ , enters the first row of logic blocks and the MSB of  $b_1$  is compared with  $a_1$  to determine which has the higher binary value. If  $a_1$  is equal to  $b_1$ , then a control signal,  $C_{i-1}^o$ , equal to a binary 0, is generated and transmitted to the second-most-significant logic block, this binary 0 level indicates that no determination on the number size has been made at the

MSB's and a comparison now has to be made at the second or lower binary level. In addition to the  $C_{i-1}^0$  signal, the MSB logic block will generate an output bit,  $S_i$ , that is of the same binary value as  $a_i$  or  $b_i$  (remember that  $a_i = b_i$  in the present case). This  $S_i$  signal is transmitted as the  $b_i$  input to the next row of logic blocks.

For the case when  $a_i$  and  $b_i$  do not have equal MSB values, the control signal,  $C_{i-1}^0$ , equal to a binary 1, is generated. This  $C_{i-1}^0$  signal, a second control to the rest of the logic blocks in that row, indicating that no further comparisons are necessary. In addition to the  $C_{i-1}^0$  signal, a second control signal  $C_{i-1}^1$  is generated and also transmitted to the remaining logic block in the row. The  $C_{i-1}^1 = \text{binary } 1$  when  $b_i = \text{binary } 1$  and  $C_{i-1}^1 = \text{binary } 0$  when  $a_i = \text{binary } 1$ . If  $a_i$  is a binary 1, the stored number  $a_i$  in that row is output as  $S_i$  to the next row of logic blocks and  $b_i$  is stored for the next comparison. However, if  $b_i$  is binary 1, the  $b_i$  number is output from the logic block row to the next lower row and  $a_i$  is restored for a subsequent comparison.

A truth table of the four input and output terms of a logic block are shown in Table 6-2. The max-terms and min-terms derived from Table 6-2 can be reduced to the four logic equations (7 through 10) shown below.

$$S_i = \overline{C_{i-1}^0} (a_i + b_i) + C_{i-1}^1 a_i + \overline{C_{i-1}^1} b_i \quad (7)$$

$$C_i^0 = C_{i-1}^0 + a_i \overline{b_i} + \overline{a_i} b_i \quad (8)$$

$$C_i^1 = C_{i-1}^0 C_i^1 + \overline{C_{i-1}^0} \overline{b_i} \quad (9)$$

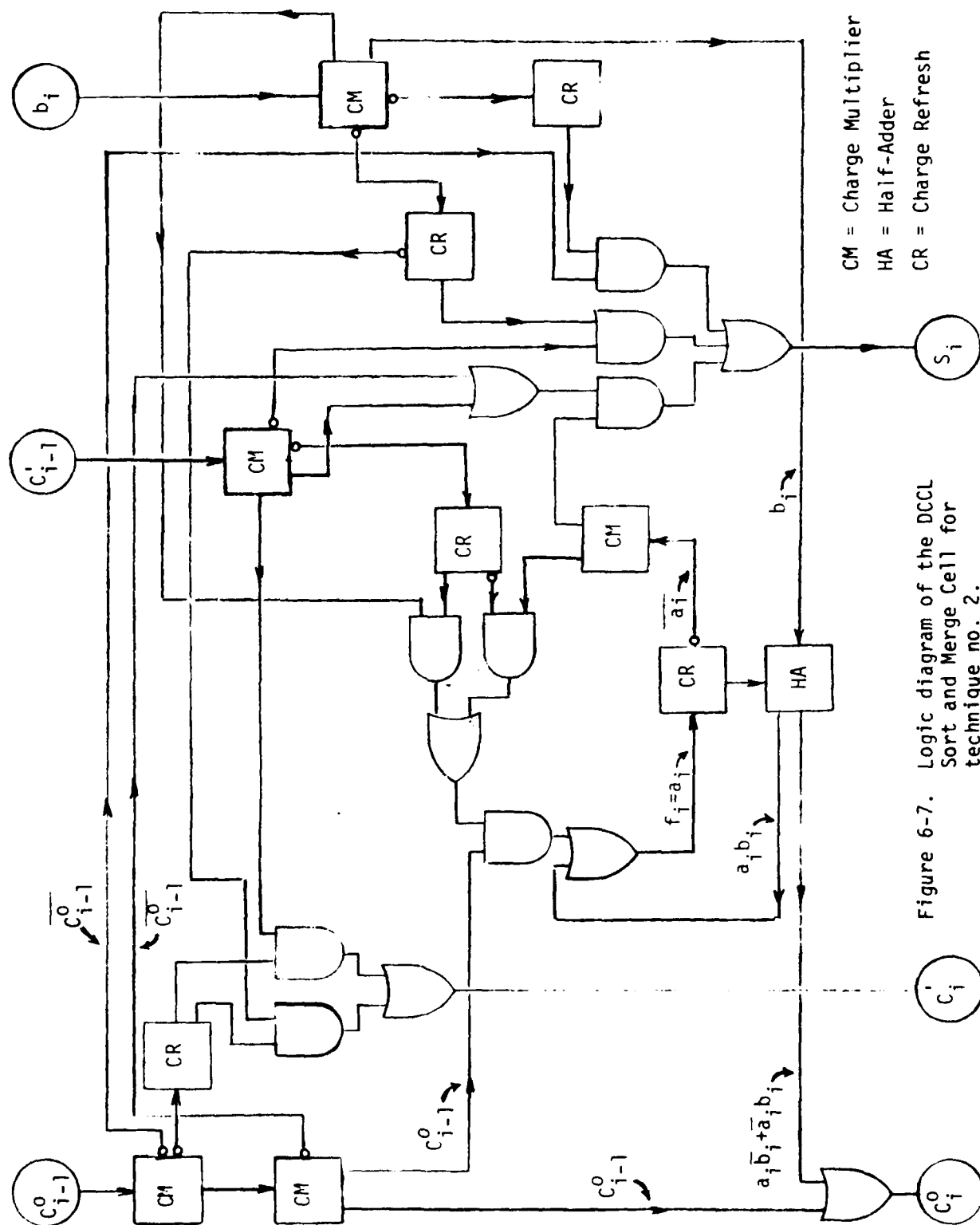
$$f_i = C_{i-1}^0 (C_{i-1}^1 b_i + \overline{C_{i-1}^1} a_i) + a_i b_i \quad (10)$$

Table 6-2. Signal and control lines for a single sort and merge logic block.

INPUTS				OUTPUTS			
$C_{i-1}^0$	$C_{i-1}^1$	$a_i$	$b_i$	$S_i$	$C_i^0$	$C_i^1$	$f_i$
0	0	0	0	0	0	X	0
0	0	0	1	1	1	0	0
0	0	1	0	1	0	X	1
0	0	1	0	1	1	1	0
0	1	0	0	0	0	x	0
0	1	0	1	1	1	0	0
0	1	1	1	1	0	X	1
0	1	1	0	1	1	1	0
1	1	0	0	0	1	1	0
1	1	0	1	0	1	1	1
1	1	1	1	1	1	1	1
1	1	1	0	1	1	1	0
1	0	0	0	0	1	0	0
1	0	0	1	1	1	0	0
1	0	1	1	1	1	0	1
1	0	1	0	0	1	0	1

To implement these four equations, each input or control term must have a fan-out of up to five. Fortunately we can use some of the inherent DCCL features to reduce this requirement. As an example, if  $a_i$  and  $b_i$  are the two inputs to a DCCL half-adder, the sum output will be  $a_i \bar{b}_i + \bar{a}_i b_i$  which is a major part of the  $C_i^0$  expression, while the carry output from the same half-adder will be the  $a_i b_i$ , part of the  $f_i$  expression.

Figure 6-7 shows the logic design for the new algorithm that integrates the magnitude comparison and the sort store technique described above. The Figure 6-7 DCCL cell requires five charge refresh cells, five charge



fan-out cells, one half-adder, eight AND gates and six OR gates. A computer analysis shows that at a CCD gate density of 3.4 mils/gate, this 71 gate SAM design will require an area of 15.5 x 15.5 mils and, a 2 MHz clock rate, will dissipate 143 microwatts of  $CV^2f$  power.

One problem with this sorting approach is how to empty the sorted numbers from the SAM chip and how to load the first unsorted words into the chip. These two difficulties can be overcome by simply keeping the two control line inputs to the most significant bit at  $C^0_{i-1} = 1$ ,  $C'_{i-1} = 0$  when reading out the chip. The  $C^0_{i-1} = 1$  indicates that no further comparisons are necessary and the  $C'_{i-1} = 0$  indicates that the stored data must be outputted to the next lower level. The output stored data is replaced by a vector that is equal to the largest positive number. The  $C^0_{i-1} = 1$ ,  $C'_{i-1} = 0$  controls are shifted down, clocking the sorted numbers out of the chip.

The first unsorted number of the next block immediately follows the vector which is now the  $a_i$  in store. Since the unsorted number will be smaller or equal to  $a_i$ , the vector will be outputted to the next lower level.

From the logic diagram shown in Figure 6-7, it can be seen that there are sixteen places where the signal paths (CCD channels) cross. This large number of crossovers and fan-outs required result in a large area per word requirement. For a reasonable die size, the number of chips required to implement this sorting technique is large in comparison with other sort and merge approaches. Consequently, this approach was abandoned in January 1979.

#### 6.3.2.3 DCCL Sort and Merge Technique No. 3

Investigation of a radix exchange algorithm for the DCCL Sort and Merge application was initiated in January 1979. In the radix exchange algorithm, a M long list of unsorted N-bit wide words are sorted by decision logic into two registers, depending on the binary value of the most significant bit as shown in Figure 6-8. In order to keep the two sorted stacks in their sorted positions during future sort separations, a delimiter binary-one bit is added to the left of the most-significant-bit on the first and last words of each stack. At the end of the input word list, two lists, resulting from the first (MSB) sort, are separated into their respective registers.

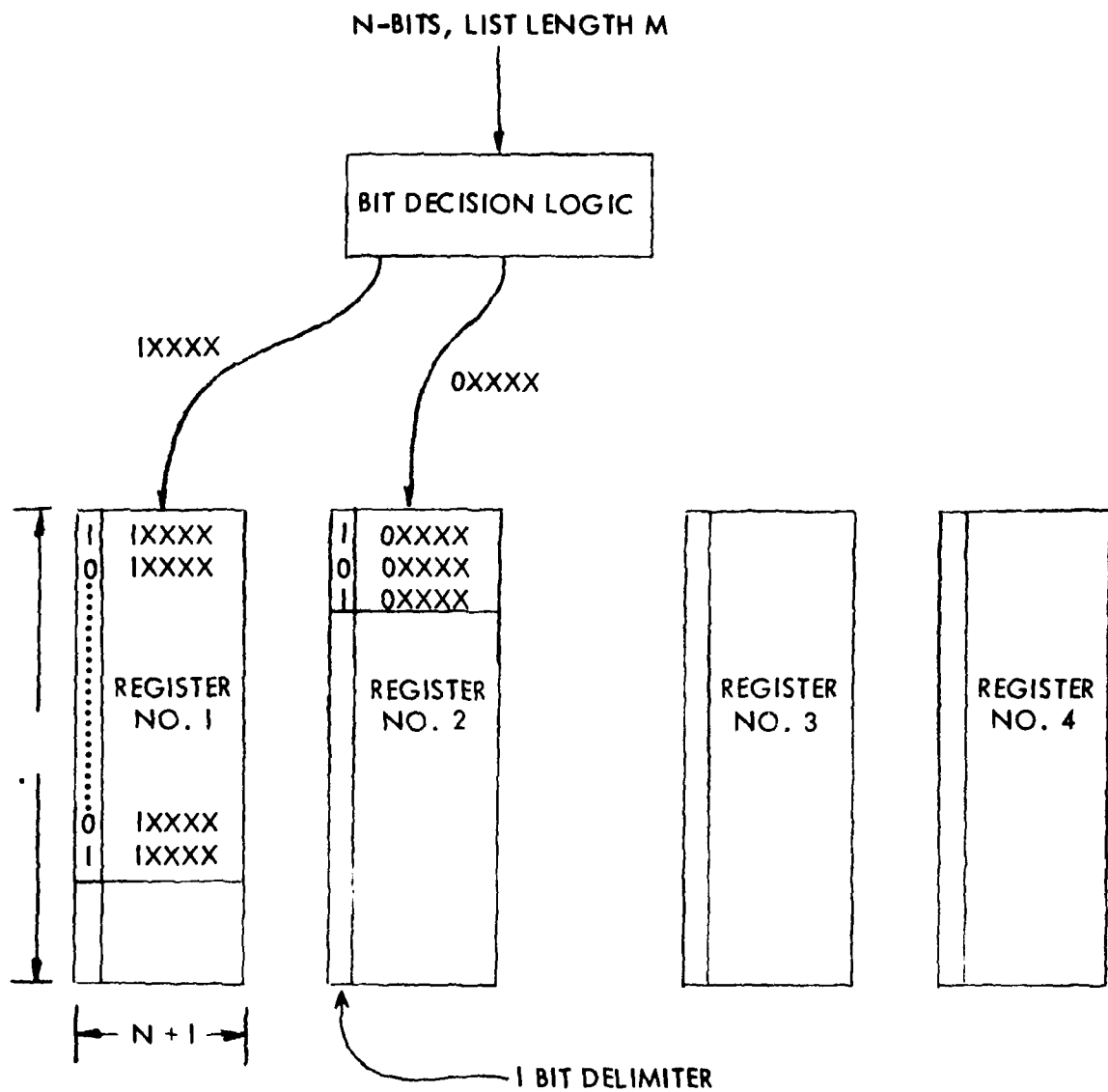


Figure 6-8. First step of the radix exchange sort and merge algorithm.

The clocks to register 2 (MSB = 0) are inhibited while those rerouted through the decision logic (Figure 6-9). On this second pass, the words are sorted into registers 3 and 4, depending on the binary value of the second-most-significant-bit. Again, delimiter bits are added to the first and last words in each stack. The clocks to register 1 are then inhibited and reverse order clocks to register 2 are enabled, emptying register 2 through the decision logic, into registers 3 and 4. Again, at the end of the sort, delimiters are added to the first and last words in each stack.

The clocks to register 4 are then inhibited and reverse clocks to register 3 are enabled, emptying through the decision logic into the now empty registers 1 and 2 (Figure 6-10). On this third pass, the words are sorted depending upon the binary value of the third-most-significant-bit. When a delimiter-bit is reached, the clocks to register 3 are inhibited, new delimiter bits are added to the stacks in registers 1 and 2 and the reverse clocks to register 4 are then enabled. The words in register 4 then empty through the decision logic until a delimiter-bit is reached. At that stage, the clocks to register 4 are inhibited and the reverse clocks to register 3 enabled. This process continues until all words have been sorted according to the binary value of each bit.

The long registers required for this sorting technique are configurable as SPS-CCD arrays since it is required that the data flow through these registers be bi-directional, the necessity for a bi-directional (LIFO as well as FIFO) SPS memory design emerged. A LIFO capability satisfies the Sort and Merge application needs and a normal SPS (LIFO) capability provides for recirculation in one stack while data is being inserted or removed from other stacks (a feature which allows for increasing the length of the sorted numbers). To provide for data recirculation, it was necessary to include a recirculating/input switch. Also, to permit data read-out from either end of the SPS it was necessary to have two charge comparator circuits as shown in Figure 6-11.

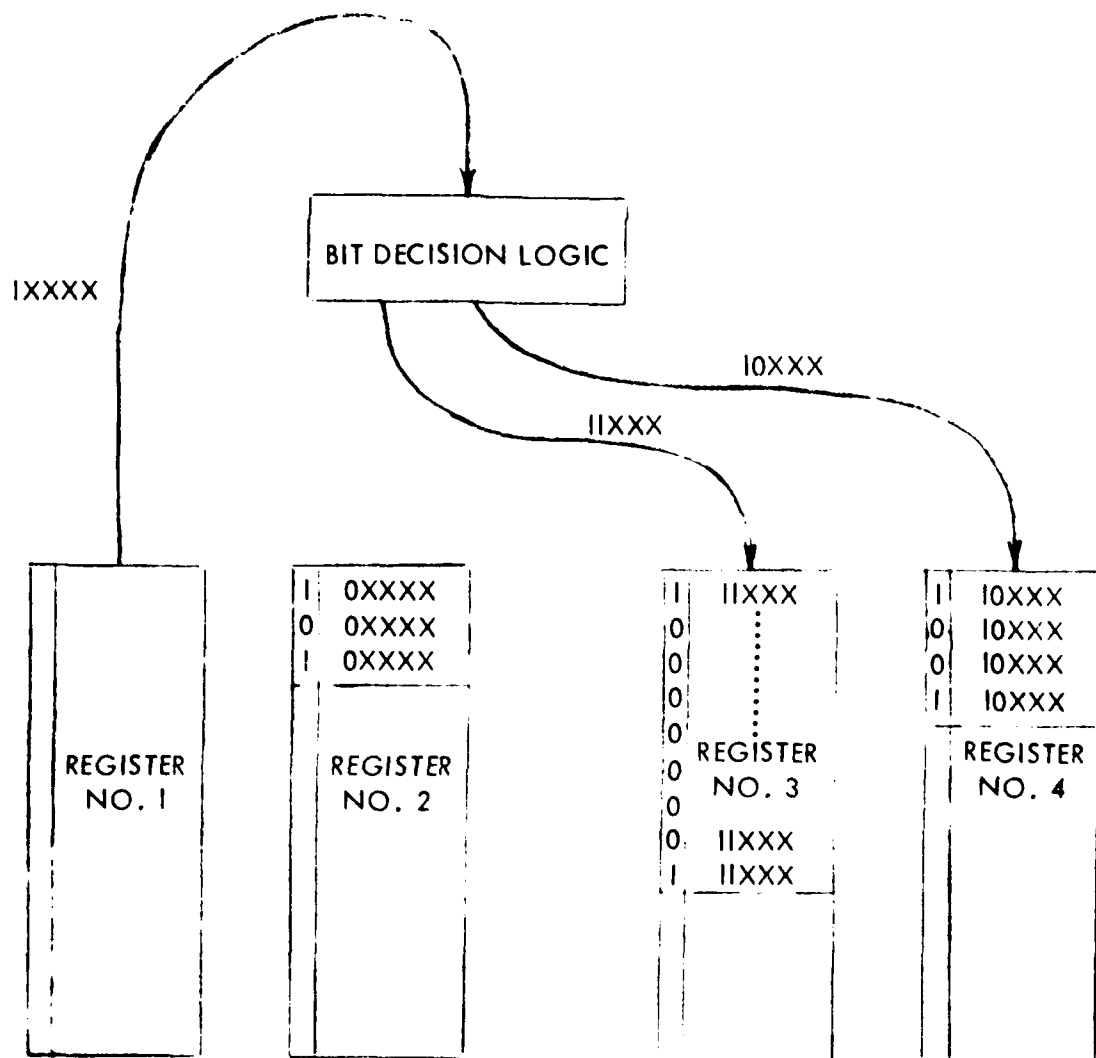


Figure 6-9. Second step of radix exchange sort and merge algorithm.

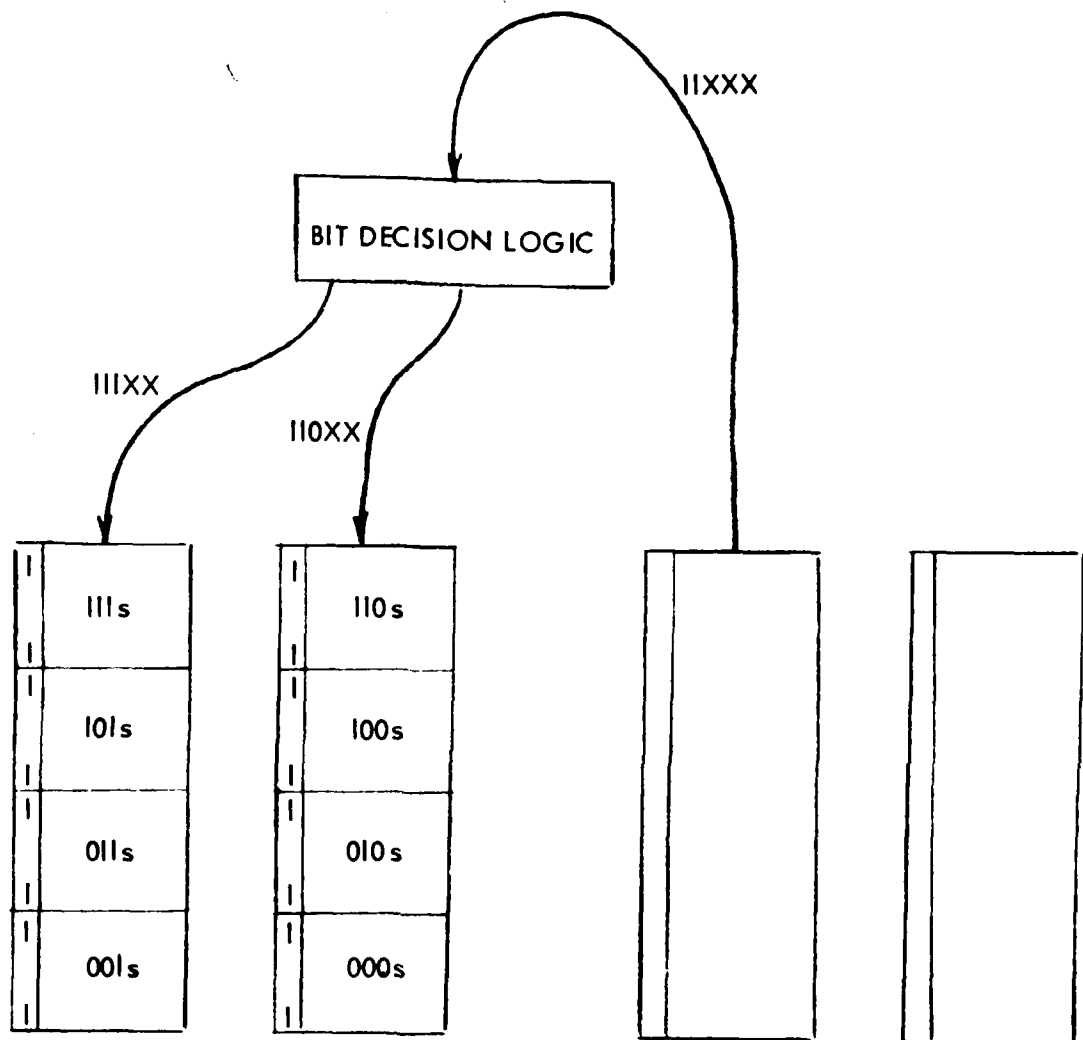


Figure 6-10. Step 3, Repeat Step 2 for register no. 2.  
Step 4, Reverse procedure no. 1.

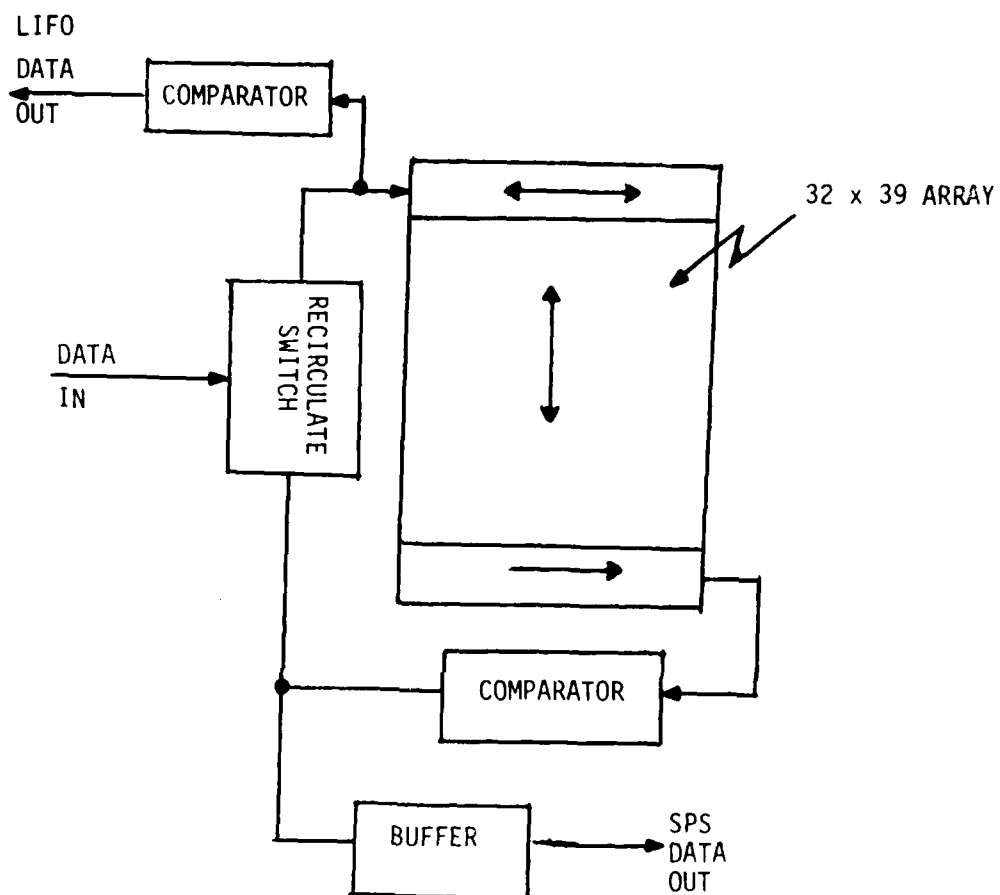


Figure 6-11. Block diagram of test cell FIFO/LIFO CCD memory.

#### 6.3.2.4 The Sort and Merge (SAM) FIFO/LIFO Design

The following paragraphs describe the operation of a FIFO/LIFO SPS memory designed for the radix exchange sort and merge algorithm described in Section 6.3.2.3.

##### 6.3.2.4.1 Interlaced FIFO SPS Design

One of the inherent problems encountered in the designing of a high density SPS memory is the serial to parallel and parallel to serial transfer interface. The use of a four-phase clocking scheme permits the use of the same polysilicon level for all serial/parallel transfer gates, as shown in Figure 6-12.

The intermediate solution to increasing the density of a SPS and still keeping within the same design and processing rules is to reduce the storage areas. Significant reduction of the gate length,  $L$ , is limited by the design and processing rules for shrinkage and alignment. The ability to reduce the storage area is, therefore, limited to a reduction in the gate width,  $W$ .

As  $W$  is decreased, the unused space,  $S$ , between the parallel registers increases. To make use of this space, the novel interlace technique, shown in Figure 6-13, can be used. As can be seen from Figure 6-13, another set of parallel registers have been inserted between the original ones.

Interlacing of the parallel data is achieved by first transferring data from the input serial register into parallel registers when charge packets are under  $\phi_1$  gates. Following this, the input register is loaded again and the serial to parallel transfer performed when the data charge packets are under the  $\phi_3$  gates thereby completing the serial to parallel interleaving operation.

The serial to parallel transfer clock pulses are spaced 16.5 high speed clock cycles apart as can be seen from the timing and potential flow diagrams shown in Figure 6-14 and 6-15.

Referring to Figure 6-15 the charge transferred under the parallel phase 1 gate spreads back under the transfer gate during the time that the charge under the phase 3 serial gate transfers under the phase 1 parallel gate. This has no adverse effect. The parallel to serial transfer is more difficult

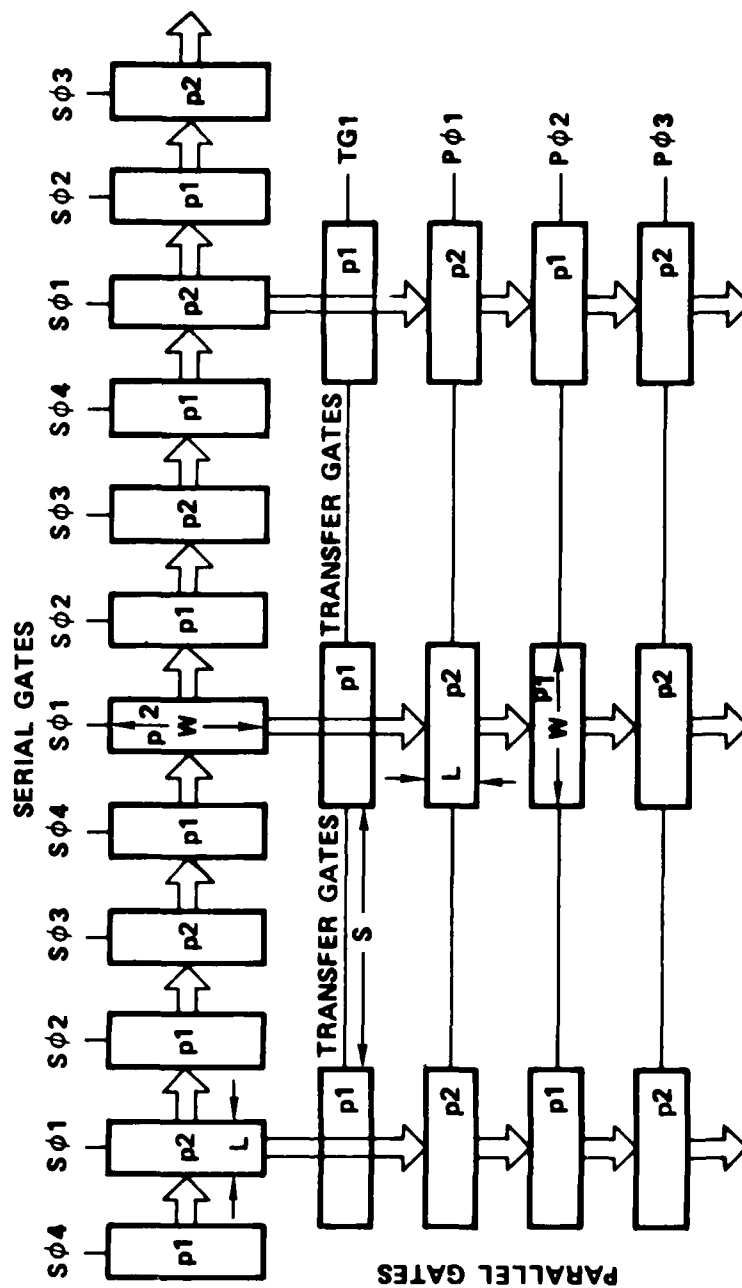


Figure 6-12. Block diagram of a standard SPS structure.

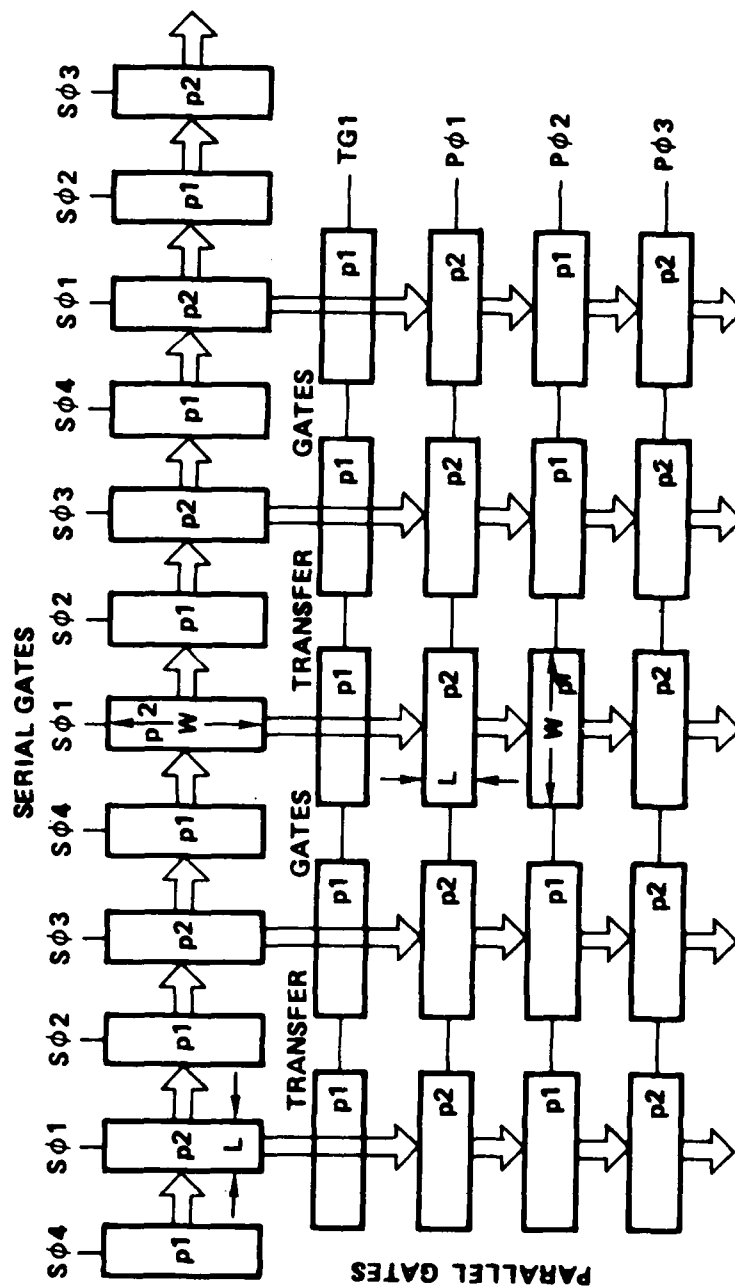


Figure 6-13. Serial to parallel interface of an interlaced SPS structure.

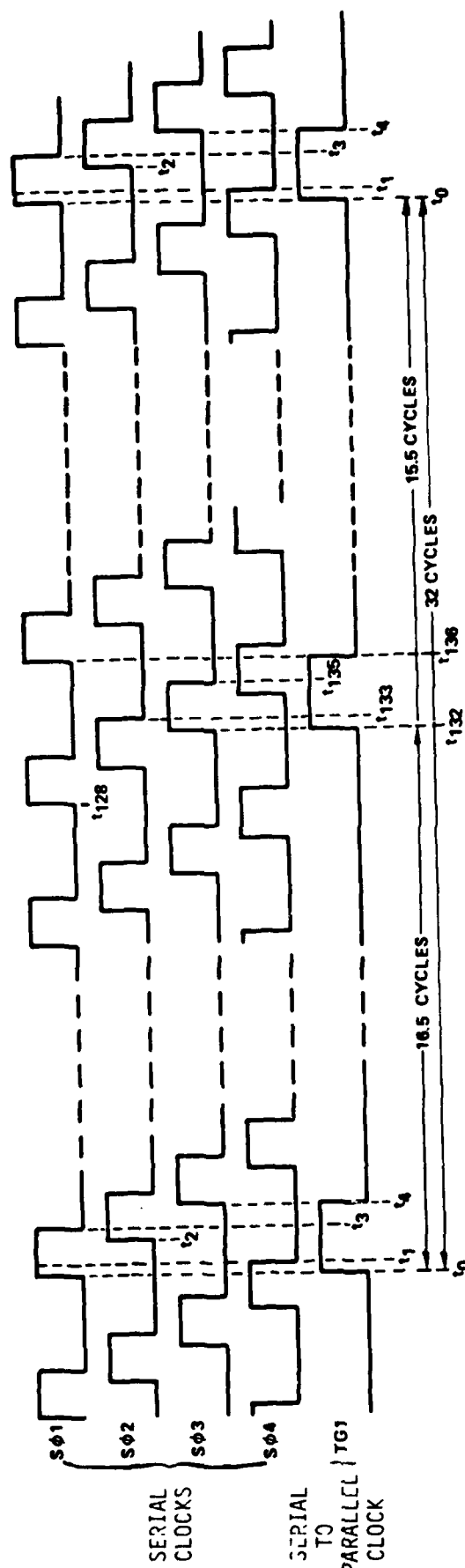


Figure 6-14. Timing diagram for the serial register and a serial-to-parallel transfer.

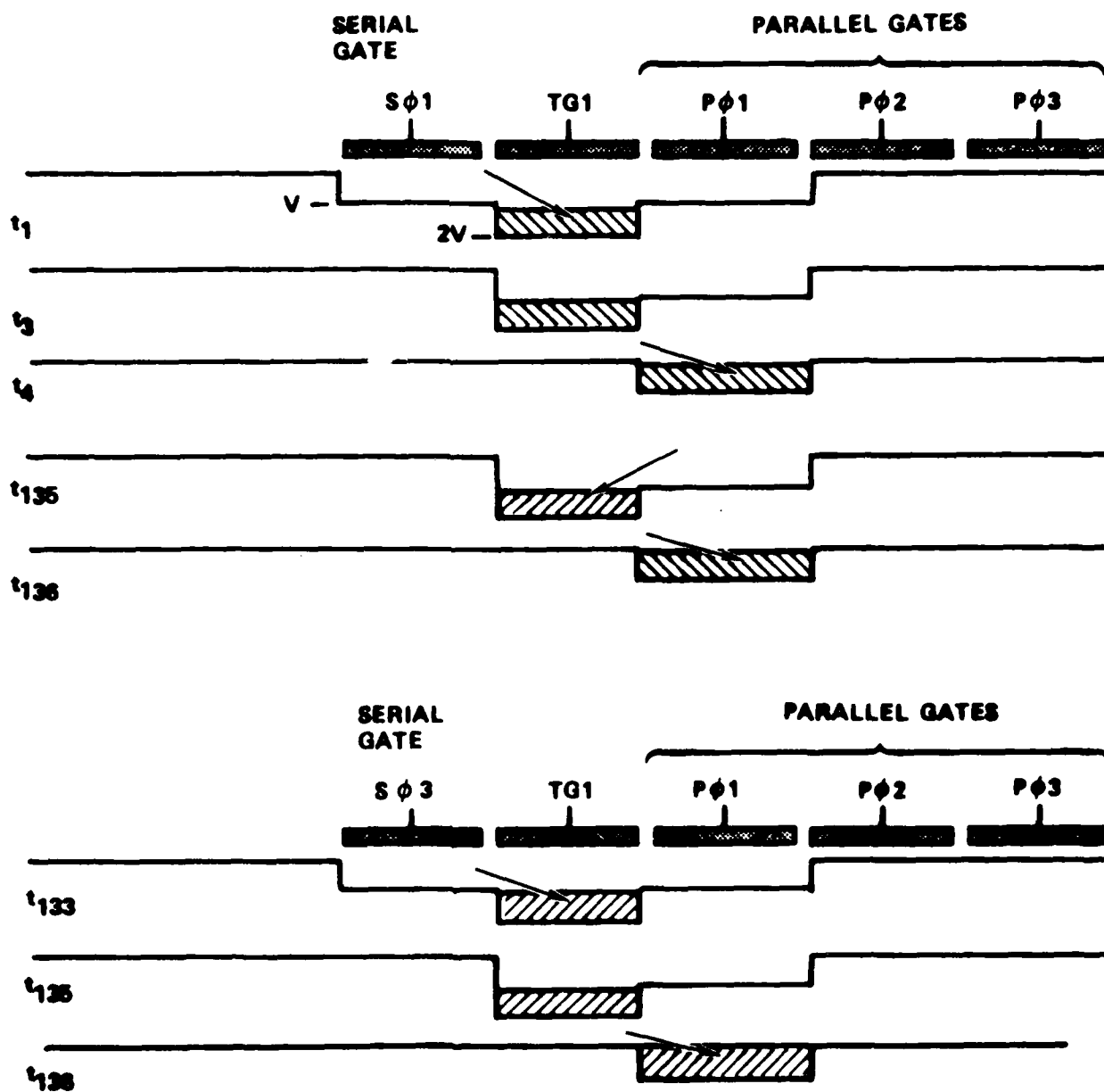


Figure 6-15. Potential diagram showing transfer of charges from the serial to parallel register in the interleaved SPS memory.

since we have to consider the mode when there are charge packets in adjacent last 4 parallel gates. Referring to Figure 6-16, parallel charge packets are first transferred to the serial register when the serial 01 clocks are at their positive level. Next, the parallel charge packets transferred to the serial register when the serial 03 clocks are at their positive level thereby completing the parallel to serial de-interleaving operation.

In order to accomplish this transfer successfully, we employ a large temporary storage gate area (TG2) that is connected to a dc voltage. In addition to a second storage area (TG3) connected to a clock line as shown in Figures 6-16 and 6-17. The transfer from the parallel register to the serial register is accomplished through the TG4 gate. The purpose of the additional TG3 temporary storage gate is to reduce the distance and time of charge transfer from TG2 to the 01 or 03 serial register gate.

The charge packet may transfer out of and back into the TG4 storage gate in a similar manner to the serial-to-parallel transfer. Again, this will have no adverse effect. The timing relationship between the four serial clocks and the transfer clocks is shown in Figure 6-18.

#### 6.3.2.4.2 Interlaced FIFO/LIFO SPS Memory Design

The design of an SPS memory capable of operating as either a FIFO or LIFO required a scheme for changing the direction of charge transfer both within the registers and also between parallel and serial registers.

The clock waveforms of the serial register 4-phase overlapping clocks are shown in Figure 6-19 along with the clocks phases necessary to transfer in the opposite direction. By examining these waveforms it can be seen that to change the direction of the charge transfer, it is only necessary to interchange two of the clock phases; as an example, gates attached to 01 and 03 in the forward direction are changed to 03 and 01 respectively. Gates that are attached to clock lines 02 and 04 are unchanged.

The serial to parallel transfer described above for the SPS memory cannot be used for the LIFO since it will not enable the reverse transfer from parallel to serial. Therefore it is necessary to use the same serial-to-parallel transfer structure described for the interlaced SPS for both serial-to-parallel and parallel-to-serial transfers for the LIFO memory.

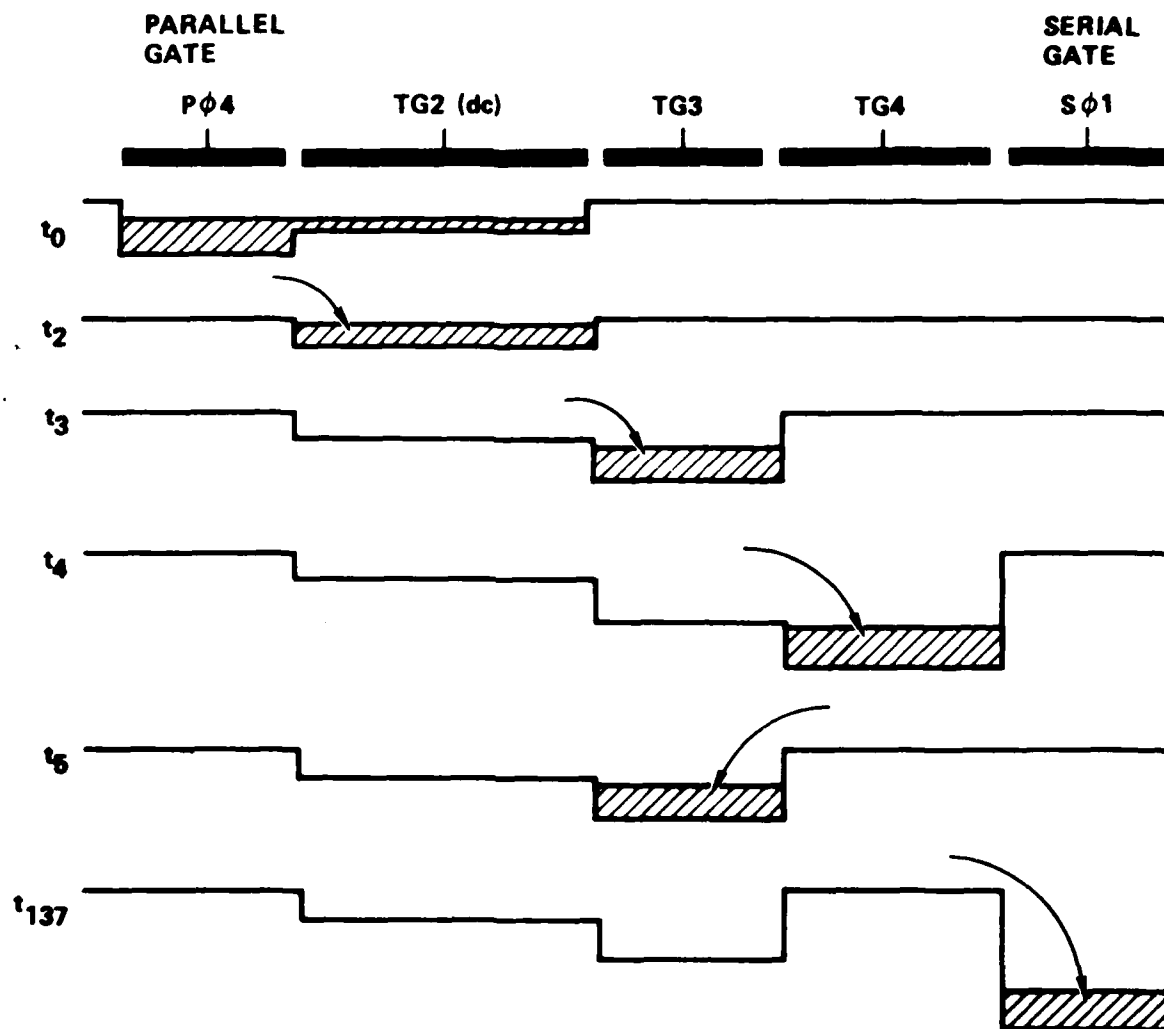


Figure 6-16. Potential diagram showing transfer of charges from parallel to serial register in the interleaved SPS memory.

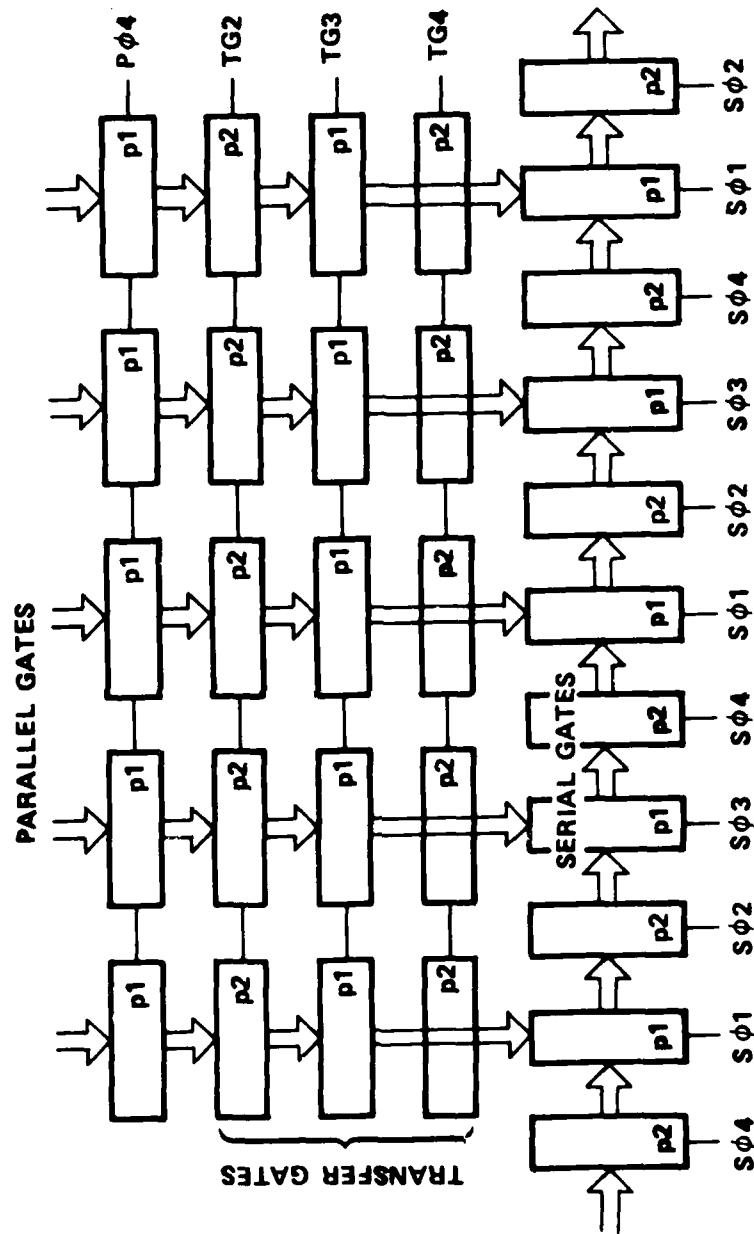


Figure 6-17. Parallel to serial interface for the interleaved SPS structure.

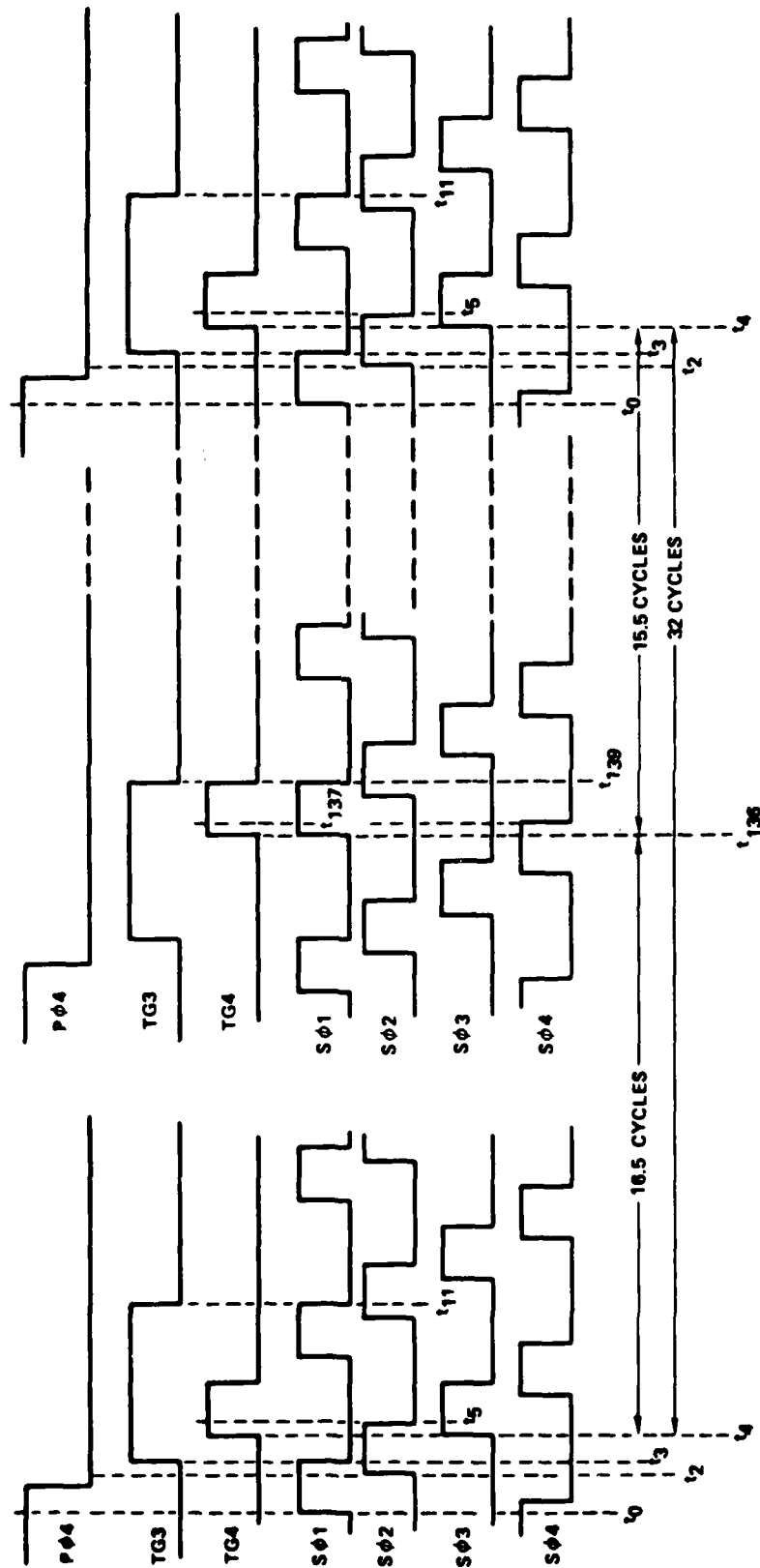


Figure 6-18. Timing diagram for the serial register and the parallel-to-serial transfer.

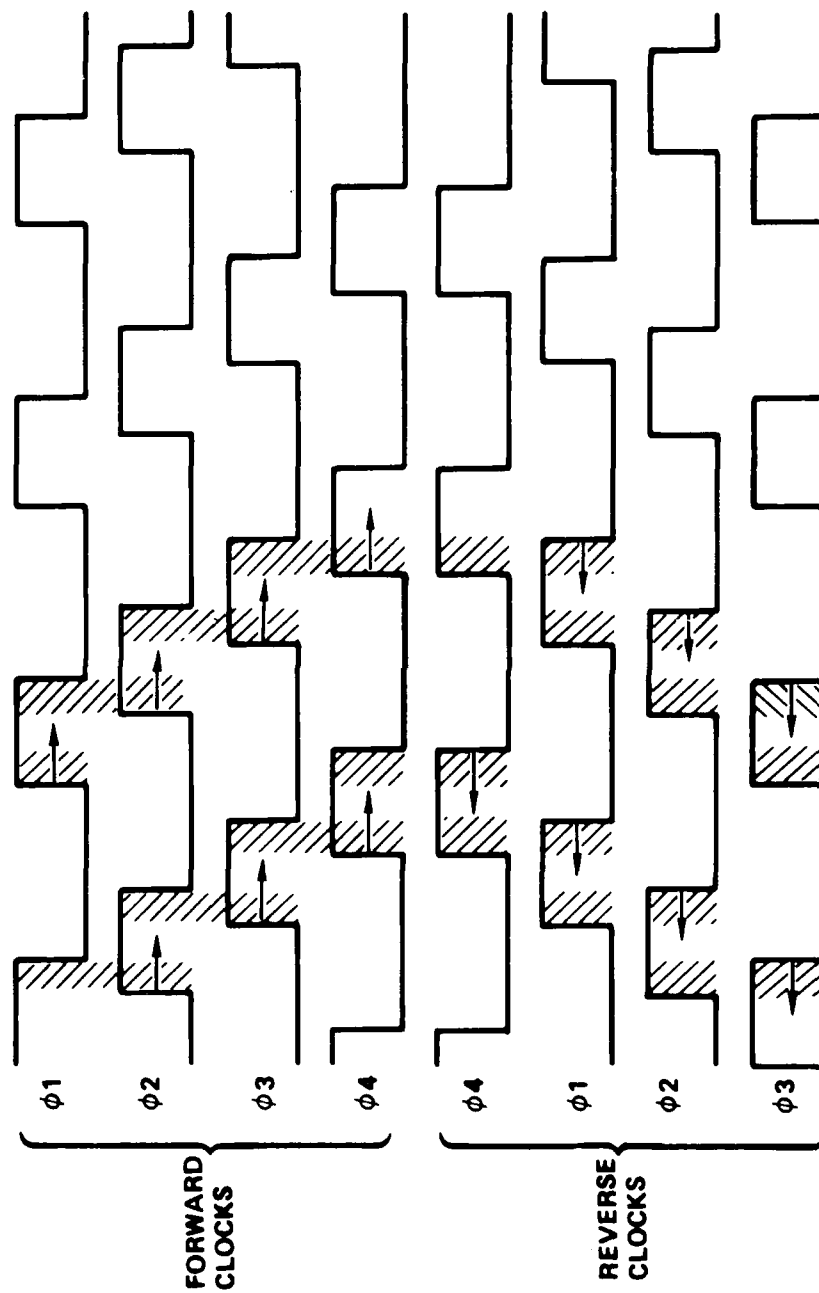


Figure 6-19. Forward and reverse four-phase clocks.

When the data transfers from the serial to parallel registers, either at the top in the normal SPS read-in, or at the bottom in the LIFO read-out mode, the transfer clocking arrangement has to be changed as shown in Figure 6-20. The three-gate transfer is changed to a single gate transfer and two parallel clocks. The  $\phi_1$ ,  $\phi_2$ ,  $\phi_3$  and  $\phi_4$  parallel clocks are switched to  $\phi_2$ ,  $\phi_1$ ,  $\phi_4$  and  $\phi_3$  respectively.

In switching the direction of transfer, we do not have to increase the number of storage gates, so no gaps occur in the data. However direction of charge transfer can only occur during the period when both the  $\phi_1$  and  $\phi_2$  parallel clocks and  $\phi_2$  or  $\phi_4$  serial clocks are at their positive levels.

In order to read data out of the input serial register, we add an extra output port to the first  $\phi_1$  serial input gate as shown in Figure 6-21.

Two additional  $\phi_4$  clock lines are required, these both have the same phase and voltage as the standard  $\phi_4$  serial clocks but in addition must have the capability of being switched to ground independently. The gates attached to these additional  $\phi_4$  clock lines ( $\phi_{4A}$  and  $\phi_{4B}$ ) act as charge barriers when the lines are switched to ground.

The typical input clocking and gating for the SPS memory is shown in Figure 6-20 and the same physical structure with the clocking switched to LIFO read-out mode is shown in Figure 6-21. Note that when the clocks were switched from write to read the  $\phi_1$  and  $\phi_3$  clock lines were reversed to change the direction of charge flow as described previously.

The design of this FIFO/LIFO memory was performed and incorporated into a test mask cell. Program funding and schedule constraints did not however, permit the functional evaluation of this design.

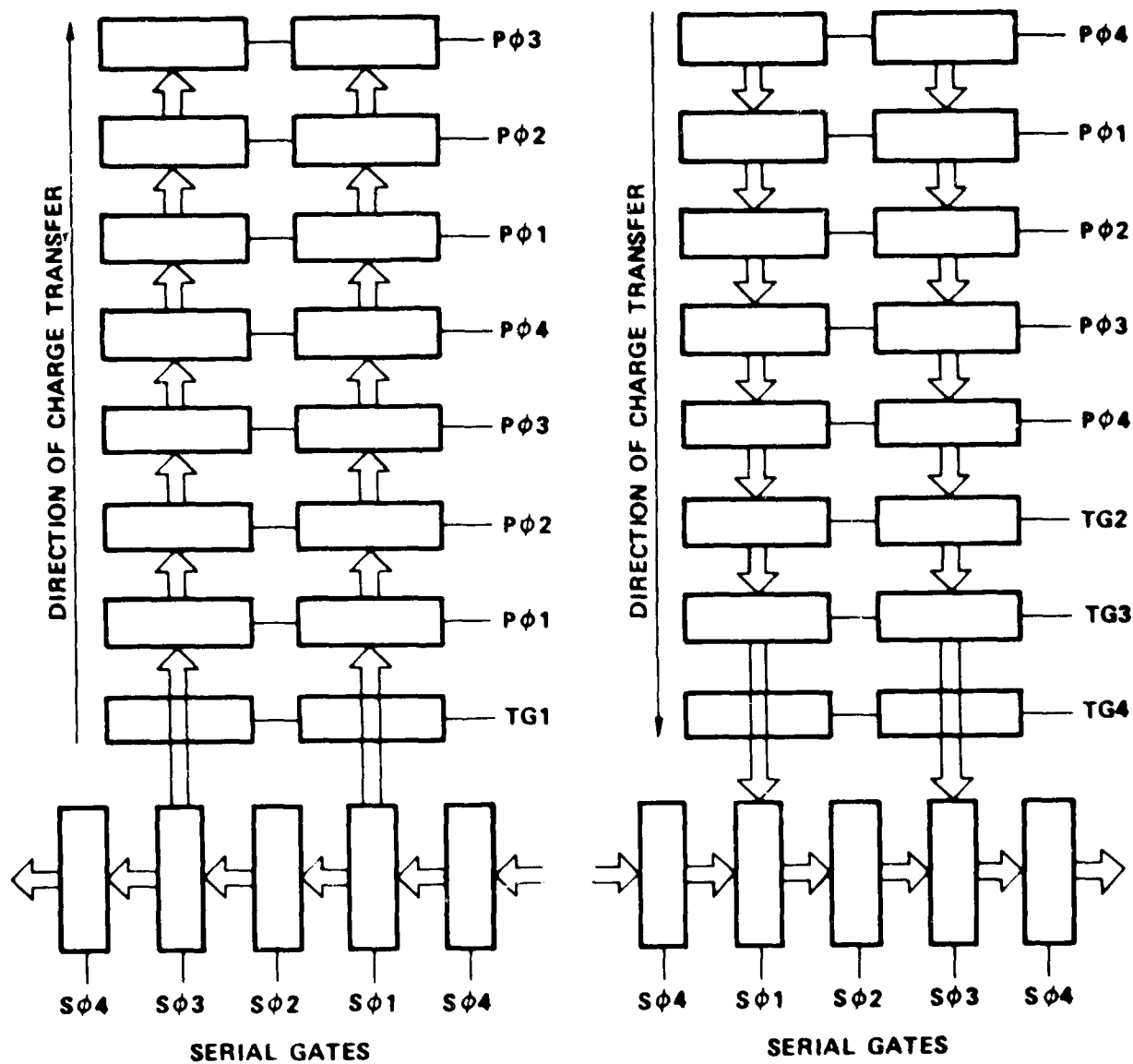


Figure 6-20. Clocking system required to change from LIFO read-out to read-in.

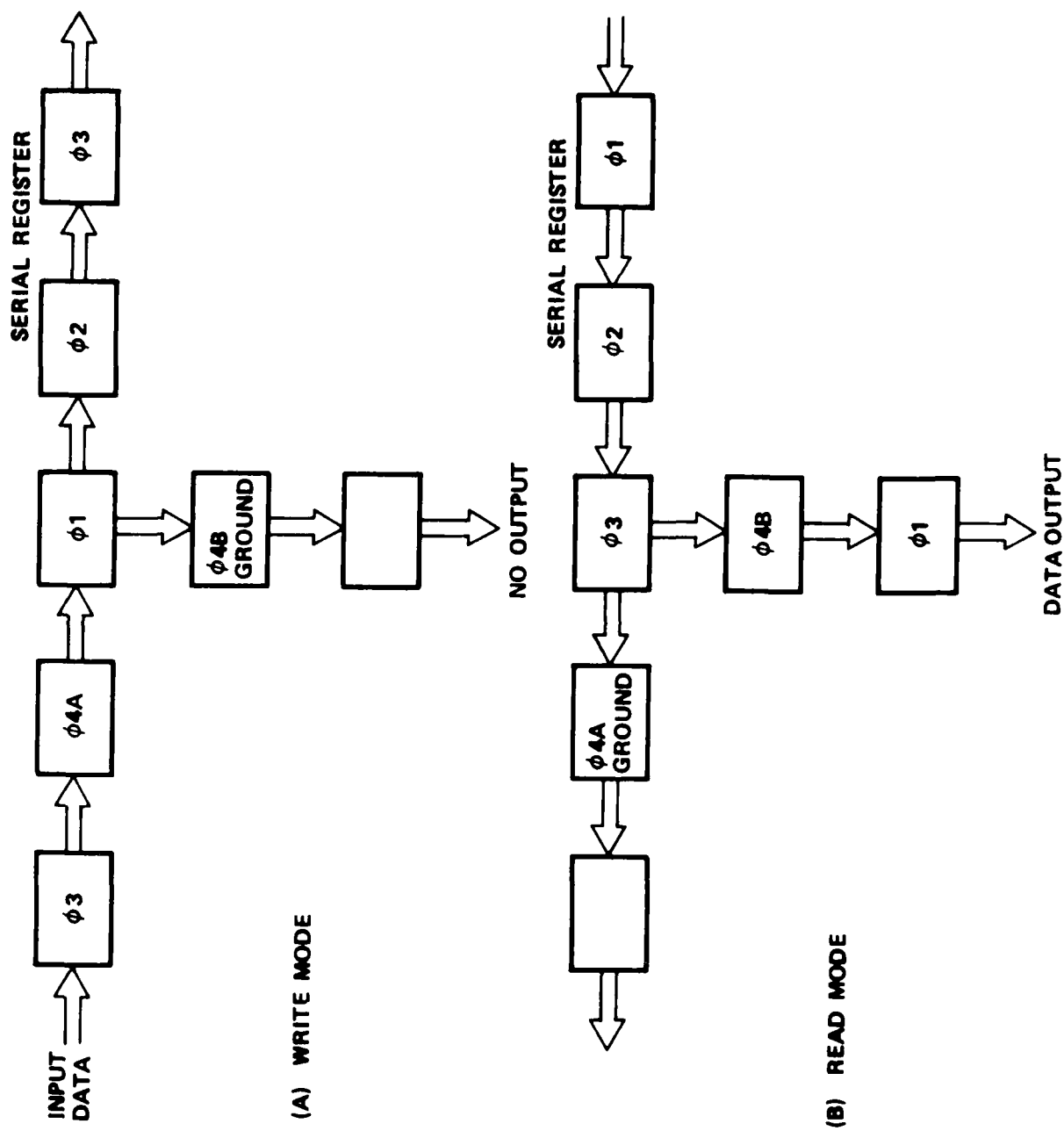


Figure 6-21. Input and output data flow block diagram for the LIFO memory.

## 7.0 DCCD WAFER PROCESSING

### 7.1 INTRODUCTION

Processing of digital charge-coupled devices (DCCD's) has undergone an extensive evolution over the past 5 years affecting every step of the processing technology. Key objectives of CCD process development were increased circuit density, not only to reduce the number of chips needed to build a complex signal processing system, but to enable higher clock rates as well. Every aspect of MOS processing technology was involved; this resulted in major changes in processing methods and device/circuit design and layout methods.

A summary of CCD Processing Laboratory accomplishments during the 1975 - 1979 period include:

1. Development of a process technology that resulted in successful fabrication of key DCCD building blocks (e.g.: full adder; half adder; refresh cell).
2. Produced several generations of DCCD chips that performed in a uniform, repeatable manner.
3. Developed standardized processing procedures and controls, also, in-process monitoring, that resulted in tighter device tolerances with resulting increases in circuit density and performance.
4. Simplified and calibrated major processing steps; this included field and gate oxide growth; polysilicon, nitride and metallization depositions; dopant implantation and drive procedures; photoresist coating, development and removal methods; and plasma etching of polysilicon and nitride films.
5. Increased the level of automation of key processing steps; this included gate oxide growth, photoresist coating, and plasma etching of poly and nitride films.

### 7.2 PROCESSING EVOLUTION

Current processing technology used to produce DCCD's include a long list of processing changes that were the result of thousands of man hours of wafer processing, pains-taking test and evaluation, subsequent design

rule changes, and equipment modification. Some of the more important processing changes that permitted fabrication of DCCD circuit building blocks included:

1. Conversion from P-channel to N-channel devices, as a means of increasing device uniformity and higher clock frequencies.
2. Improving circuit yields by process step simplification.
3. Rejecting the polysilicon gate/metal gate technology in favor of a dual poly-gate technology.
4. Employing a uniform 1,000Å gate oxide under poly I and II gate levels.
5. Reducing field oxide thickness to 10,000Å, to insure satisfactory step coverage by metal conductor patterns.
6. Developing a plasma etch technology, to insure high density polysilicon gate structures.
7. Doping of Poly I and II level films with Phosphorus, rather than employing both N and P type dopants, with possible contamination of thin gate oxides by Boron.
8. Standardizing metal sintering temperature at 400°C, for significantly reduced  $Q_{SS}$ .
9. Employing TEOS in lieu of SILOX or thermally grown  $SiO_2$  for smooth step coverage by metal conductor lines.
10. Improved contact hole etching techniques, enabling a significant reduction in both poly and metal line widths.
11. Identifying the depletion barrier or BUMP phenomenon, occurring at the edge of Poly I structures; this structural anomaly reduces gate control over charge packets, resulting in a series of barriers between gates that may reduce the transfer efficiency of CCD devices.
12. A P-type buried channel lot was fabricated in 1977 that demonstrated buried channel operation of a 10-bit shift register. This verified the changes made to the DP-3 process to provide buried channel operation.

PROCESS EVOLUTION	1975	1979
1. <u>Metallization</u>		
Line Width	7.5u	5.0u
Thickness	20,000Å	10,000Å
Metallization System	Pure Aluminum	4% Cu-doped Al
Substrate Heating	Deposited at Ambient (25° C)	Deposited at 300°C
2. <u>Contact Holes</u>	7.5u x 7.5u	2.5u x 5.0u
3. <u>Line Separation</u>	7.5u	1.27u
4. <u>Oxide Cut (windows)</u>	2.5u	1.27u
5. <u>Poly Gate Overlap</u>	2.5u	1.9u
6. <u>Gate Levels</u>	Polysilicon and Metal	Both gate levels are Polysilicon
7. <u>Gate Oxides</u>	Poly Level - 1,000Å Metal Level- 2,000Å	Gate oxides for both levels are 1,000Å or less.
8. <u>Etching Methods</u>	Wet Etching Processes Only	Plasma Etching used for Poly; Nitride - Wet Etch used for Oxides; Metal
9. <u>Field Oxide</u>	15,000Å	7,000 - 8,000Å THK.
10. <u>Channel Definition</u>	15,000Å Field Oxide Cut	Channel Stops used to define channel
11. CCD Technology Selected	P-Channel	N-Channel

A comparison can be made of the basic processing that was used to produce DCCD devices in 1975 with current processing methods. A comparison of resulting device parameters can also be used as a gage of the progress made during this 5 year period.

### 7.3 PROCESSING HISTORY

The very first wafer lots produced in 1975 were designated N1 through N4. The circuit under development at that time was the full adder, which used a floating gate to control one of two paths between the adder input and the SUM output. Lots N1 and N2 were fabricated with 1,000A gate oxides under the polysilicon electrodes. Initial objectives were to determine whether the full adder structure could be processed as designed and detect any possible failure mode. There was some concern over the thickness of the field oxide (15,000A), as a high "step" was formed upon etching the channel cut. Thin photoresist covering the edge of this cut could permit the formation of pinholes in the oxide during contact hole etching.

Lots N3 and N4 employed the "standard" DCCD process. These lots basically evaluated a combination of thermal oxide protective film in combination with a thin phosphosilicate glass, to prevent the formation of pinholes. These two lots had other problems associated with the operational characteristics of the full adders; both poly-gate FETs and metal gate FETs had severe threshold voltage problems; this included high  $V_t$  values for the poly-gate FETs and shorted metal-gate FETs. It was suspected at that time that both boron and phosphorus had completely penetrated the gate oxides, producing the high thresholds and shorts. The substrate material used for the N1 through N4 lots was N-type <100> 1 - 3 ohm-cm.

NAV-5 and NAV-6 were then produced; both lots had 500A of thermal oxide under the floating gate and 2,000A thermal oxide between the floating poly-gate and the "carry" (metal) gate. Surface potential plots of the metal and poly gate test FETs of NAV-5 indicated that the phosphorus used to dope the poly gate had penetrated the 500A gate oxide. NAV-6 received a lower temperature dopant drive-in schedule;  $V_t$  values looked normal.

NAV-7 and NAV-8 were produced during May 1975. Lot 7 employed 1,000A gate oxides and did not indicate phosphorus penetration through the gate oxide. Lot 8 was a departure from standard processing procedure as a complex oxide/nitride gate dielectric was employed. Unfortunately, this lot did not produce testable devices as the etching of the FET source-drains also attacked the polysilicon covering the CCD devices.

NAV-9 was produced with a 600A gate oxide. Results were indeterminate due to circuit functional problems. NAV-10 and NAV-11 were then fabricated, using the identical process sequence of NAV-9. These lots employed both all wet and all dry oxides as a means of isolating the floating gate element; none of the combinations selected cured the charge accumulation problem, thereby indicating the necessity for a design change.

#### 7.3.1 Introduction of the "DP" Mask Series

In order to overcome difficulties with the full adder's floating gate configuration, several device structures were conceived that allowed discharge or presetting of the floating gate itself. Before these new device designs were included in the DP-1 mask set, a small test device mask set, designated DP-0 was designed, which permitted verification of the floating gate FET discharge concept.

The floating gate amplifier was subsequently modified to incorporate a FET discharge device for its floating gate structure. The DP-0 mask set was generated using the slip mask technique. This technique was pursued in order to reduce mask costs by allowing several mask levels to be combined on one reticle. The circuits included on DP-0 required 6 mask levels; this necessitated two reticles consisting of 3 levels each. It must be realized that this technique decreased the number of usable circuits, since during the processing steps, some potential circuit positions are not available as a result of slip mask operation. As DP-0 was created to evaluate basic circuit concepts, it was agreed that 20 die positions were sufficient to verify design concepts. Approximately 30 circuits were obtained on the available 2-inch wafers.

Two DP-0 lots were initiated during this period (September 1975). DP-0-1 had both oxides (on either side of the poly floating gate) grown in a wet atmosphere, while DP-0-2 wafers had both oxides surrounding the floating gate grown in a dry atmosphere. Oxide thickness under the polysilicon electrode was 1,000A, while the oxide under the metal electrode was 2,000A. The field oxide thickness was 15,000A. The polysilicon film was phosphorus doped and was covered by a "poly protect" nitride film. Both poly and nitride films were plasma etched. PMOS source-drains were doped by diffused boron. Pure aluminum was used as metallization; sintering was accomplished at 450°C in a nitrogen ambient followed by sintering at the same temperature in hydrogen.

Four DP series lots were fabricated during the months of September - October 1975. Basic variations were made in gate oxide thickness for both poly and metal gate structures as follows:

LOT DESIG.	GATE OXIDE LEVEL	THICKNESS	WET/DRY THERMAL OXIDE	TEMPERATURE
DP-0-1	Poly Level	1,000A	Wet	920°C
	Metal Level	2,000A	Wet	920°C
DP-0-2	Poly Level	1,000A	Dry	1075°C
	Metal Level	2,000A	Dry	1075°C
DP-0-3	Poly Level	1,000A	Dry	1075°C
	Metal Level	2,000A	Wet	920°C
DP-0-4	Poly Level	1,000A	Wet	920°C
	Metal Level	2,000A	Wet	920°C

The use of a slip mask on DP-0 lots proved to be successful. Information gathered on the DP-0 lots were reflected in DP-1 mask designs. Tests of DP-0 circuits indicated that the addition of the discharge FET to the floating gate structure insured that floating gate performance would no longer be susceptible to charge accumulation on the gate structure.

DP-0-5 was produced on <111> material; this material was selected as a means of raising the field oxide threshold voltages. Substrate bias was used on previous lots fabricated on <100> material; in order to avoid this circuit complication, <111> material was used in the hopes that it would produce devices with higher threshold voltages. An additional oxidation step was included following polysilicon gate definition. This oxidation step was designed to prevent source-to-drain shorts resulting from poly-gate definition, standard PMOS source-drain and diffusion and drive procedures.

Lot DP-0-6, completed in December 1975, did not provide useful devices due to metal discontinuities at many polysilicon-to-metal contact regions.

During the initial months of 1976, several DP-1 lots were completed and tested. In general, the process used for these lots followed the same step sequence employed on the DP-0 lots. A "poly protect" mask was added to the processing sequence, to prevent etching the field oxide under the polysilicon structures. The resulting undercut of the poly lines produced steps that were difficult to cover by the Aluminum interconnects. In addition, TEOS was again used as a protective film to cover poly structures on lot DP-1-2; lots DP-1-1 and 3 were fabricated without a TEOS film. Electrical tests performed on these lots indicated a large number of breaks in the metal conductors where they traversed combined field oxide and polysilicon edges.

DP-1-5 and DP-1-6 were therefore fabricated with a TEOS film over poly gate structures. A second processing change increased the gate oxide thickness under the metal gates to 3,000A. Subsequent electrical testing of these lots indicated metal gate oxide contamination; the decision was then made to process the following lots without a TEOS film: DP-1-7; lot DP-1-9 was produced as a divided lot, having no TEOS film; however, the lot was divided so that 2 of the 4 wafers were fabricated with a poly protect mask. The DP-1-9 lot produced devices that provided needed test results. Information acquired was used in the redesign of the DP-1 mask set; also, for the DP-2 mask set, which contained an 8 + 8 bit adder, a 3 x 3 bit multiplier and a 4 + 4 bit adder employing the half adder design. DP-1-10 was fabricated during June 1976, again employing a TEOS film over the polysilicon gates and supporting structures. As the DP-1-10 mask set included the circuit corrections discovered during tests on earlier lots, functioning multiplier and adder arrays were obtained.

#### 7.3.1.1 The Double Polysilicon Process

During the month of August 1976, two DP-2 lots (DP-2-1 and DP-2-2) were started using the new double poly process. This required some modification of the DCCD process sequence. Although the poly-metal gate process was considered a simpler process, problems with metal step coverage were sufficiently severe to necessitate conversion to the new processing approach. As the new DP-2 series was fabricated with slip masks, alignment problems became an over-riding consideration in producing useful lots. Although the mask supplier provided TRW with a new, more closely aligned set of slip masks, the problem of using the slip mask set continued. The initial DP-2 lots produced with these masks necessitated special alignment procedures; the circuits were aligned by ignoring the alignment targets and aligning the contact hole mask to the polysilicon structures already on the wafers, as well as the observable diffused areas.

Tests performed on the DP-2 8 + 8 adder array indicated a large number of Schottky diode occurrences on clock lines; these unwanted diodes were injecting charges into the channels. An investigation of this occurrence showed that the diodes occurred where an aluminum contact was made to polysilicon over a 1,000A channel oxide. The large number of potential aluminum-to-poly contact failures on the 8 + 8 array made it impossible to find a failure-free device for functional tests. The full adder test cell also suffered from the same aluminum-to-poly contact problem.

Additional process modifications were made during this period (October 1976) to determine the gate oxide thickness relationship between Poly I and II gate levels; DP-2-3 was a split lot, with half the wafers having 1,000/2,000A gate oxides, while the other half were made with 1,000/3,000A. Results as to which oxide combination produced the most usable devices were inconclusive, due to alignment problems with the slip mask set, which produced unusable devices. Reoccurring problems forced the decision to have the DP-2 mask set remade as a conventional set, with a separate reticle for each mask layer. A variety of experiments were performed to eliminate contact problems, with heavy concentration on selecting the most appropriate sintering temperatures.

The new conventional mask set for DP-2 circuits was obtained during December 1976 and was designated as DP-2A. This new mask set was used to produce lot DP-2A-1. The nitride step normally used to define Poly II was deleted. The Poly II gate film was therefore doped during the PMOS source-drain diffusion sequence. Low voltage thresholds obtained when this lot was tested were attributed to boron penetration through the gate oxide during the TEOS densification cycle that occurs at higher temperatures. The poor results with this lot necessitated a return to the nitride protective film to prevent boron penetration of the gate oxides during PMOS source-drain diffusions. During this period, lot DP-2A-2 was completed. This lot was produced with a conventional Arsenic-doped Poly II layer. DP-2A-2 had difficulties with the source-drain diffusion process. The sheet resistance of the diffused region was extremely high resulting in poor device operating characteristics.

#### 7.3.1.2 The Switch to N-Channel DCCD Technology

Early in 1977, the decision was made to fabricate an N-channel DP-2A lot. The motivating force for this decision was improvement of the data rate through the arithmetic arrays. As predicted, tested transistors operated in the depletion mode; however gate voltage versus surface potential ( $V_g V_s$ ) curves were recorded by applying a large back-bias to the substrate. Clock voltages were computed for the DP-2A-1N N-channel devices, to permit testing of the various arithmetic arrays.

Lot DP-2A-1N was made with P-type  $\langle 100 \rangle$  17 - 30 ohm-cm wafers; the process was similar to the P-channel process, except that phosphorus was used for the source-drain (NMOS) diffusions.  $X_{jS-D}$  depth was approximately 1 $\mu$ . Initial results indicated surface "channels" that were created at the PN junctions; this produced high leakage diodes. These "channels" were probably caused by the oxide fixed charge or  $Q_{ss}$ . New wafer lots were initiated using 0.8 ohm-cm material; the objective here was to prevent unwanted channel formation. Lot DP2-2N employed 0.8 ohm-cm material, while lot DP2-3N used 3-5 ohm-cm material. Testing of these new lots was minimal; it was realized early in the testing cycle that these lots would produce devices with excessive surface leakage currents, which is not unexpected for N-channel devices without channel stops. The decision was made to concentrate on DP3 designs, which were specifically designed for N-channel operation.

#### 7.3.1.3 The DP3 Series

The DP3 series of lots contained an 8 x 8 multiplier array, a 16 + 16 adder array and various test cells and experimental circuits. In April 1977, the first DP3 masks were received and device lots were initiated. A process definition effort was also started for a buried channel version of DP3.

Lots DP3-1 and DP3-2 were completed during May 1977. Problems were experienced with polysilicon definition, due to photoresist lifting (poor adhesion). The process was improved by subjecting the sample wafers to a 30-minute oxidation at 900°C previous to photoresist coating; also, the AZ111 photoresist developer was further diluted. Some difficulties were experienced with contact hole and metal line definition due to overetching. Exposure time and development were adjusted to solve this problem. Gate voltage vs surface potential plots were generated for several positions on each DP3-1 wafer. These curves were satisfactory for the oxide thickness used. Gate shorts were found to be quite prevalent on this lot, so a complete gate short characterization was undertaken; 60 serviceable die locations were found on 5 wafers. The decision was made to define all MOSFET channels with both thick oxide (10,000Å) and channel stops. This device design approach prevented breakdown between the inversion charge layer and the channel stop in MOSFET structures.

Lot DP3-3BC was initiated during this period. This lot was fabricated using a buried channel process (N-Buried Channel) that was similar to the surface channel process. It had an additional photoresist step (implant mask) and a B<sub>11</sub> ion implant to produce the buried channel. Three different implants were used for this lot:

1.  $1 \times 10^{12}$  @ 100 KEV Boron B<sub>11</sub>
2.  $2 \times 10^{12}$  @ 100 KEV Boron B<sub>11</sub>
3.  $1 \times 10^{12}$  @ 150 KEV Boron B<sub>11</sub>

Upon completion of DP3-3, it was found that better poly and metal resolution was obtained with a 10,000A field oxide than with 15,000A. It was concluded that added field oxide film thickness would be necessary to optimize channel, polysilicon and metal line definition. DP3-3 provided poor yields determined by extremely close proximity of the channel to adjacent diffusions, which resulted in punch-through at low voltages. Lot DP3-4 was then initiated and an attempt was made to maximize channel-to-diffusion separation by changing the photoresist process.

Lot DP3-3BC was completed during this period and buried channel operation was demonstrated.

Lot DP3-4 was completed during the month of July 1977. Initial field oxide thickness was held to 8,000A. The final field oxide under Poly II was 7,000A. As a result of previous channel-to-diffusion punch-through, the spacing between these two areas was increased from 5.0u to 7.5u, requiring a major mask set revision. Lots made with the revised mask set were designated DP-3A.

The first lot of 10 DP3A-1 were completed during August 1977; this lot was processed with an 8,000A field oxide and 1,000A/2,000A gate oxides for poly I and II. The yield obtained from this lot was satisfactory permitting characterization of the arithmetic cells.

Two additional lots, DP3A-2 and 3 were completed during September 1977 and also provided satisfactory device yields. A new lot (DP3A-4) was started with a more lightly doped 8 - 12 ohm-cm substrate material. This lot produced devices with very low source diode breakdown (punch-through). Lot DP3A-6BC was then started with the channel region implanted with phosphorus (Dose:  $1.5 \times 10^{12} \text{ cm}^{-2}$  @ 100 KEV; drive-in was 36 HRS @  $1075^{\circ}\text{C}$ ).

Lot DP3A-6BC was completed in November 1977. This lot employed a field oxide of 15,000A which resulted in a number of shorts between Poly I and II levels. The transition of polysilicon films from field oxide to channel level caused fracturing of the oxide layers between the two poly levels. The resultant topography created yield problems due to broken metal lines as well.

Lot DP3A-7 was completed during this period and was processed using 10 ohm-cm substrate material. Differences between this lot and its predecessors included the following:

1. FETs were fabricated in implanted tubs that provided a 4 ohm-cm background for the NMOS devices.
2. The field oxide height was reduced from 15,000A to 10,000A resulting in some improvement in shorting problems seen with the previous lots.

An in-depth evaluation of key device characteristics indicated the presence of a depletion barrier between poly I and II levels, this so-called "bump" occurred at the edges of poly I gate structures and is caused by the lifting of the polysilicon film during growth of the poly II gate oxide. SEM photographs, represented by Figure 7-1, illustrate the distortion of the poly I gate structure at its edges. The non-planarity created at the edge of the gate reduces the control provided by the gate, resulting in a series of barrier structures that reduce the transfer efficiency of these devices. In essence, a succession of bumps act like a continuous series of charge traps that can affect half-adder or full adder operation.

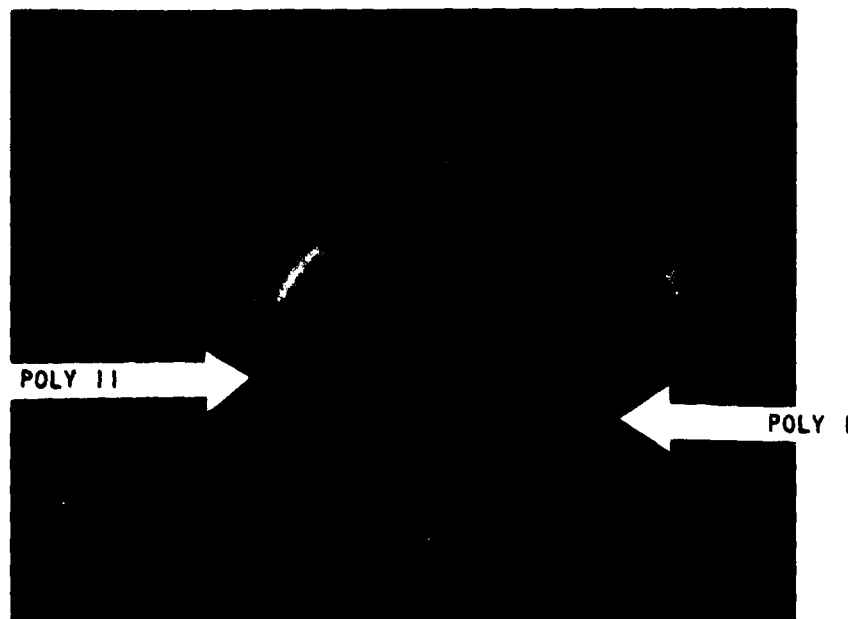


Figure 7-1. An SEM photograph showing the vertical tilt at the end of the poly I gate.

Lot DP3A-8 was completed in December 1977; this lot employed gate oxides of 800A and 2400A. This large difference in gate oxide thickness was chosen in order to provide a large difference in poly I and II surface potentials in an attempt to overcome the race conditions described in the November 1977 Interim Report.

Tests performed on DP3A-8 produced working devices, however, test results obtained from the cascaded dual half adder indicated very poor transfer efficiency; the results from these tests indicated that the change from the conventional 1000A/2000A gate oxide configuration was a poor one, as the transfer efficiency of these test devices deteriorated with the 800A/2400A gate oxide thicknesses. Based on these initial test results, it was decided to suspend further testing of devices and DCCD cells on this lot.

Two additional lots, DP3A-9, -10 were initiated during this period; the specific goal of these lots was to eliminate or substantially reduce the "bump" problem. Upon completion, lot DP3A-10 provided very uniform VgVs plots, indicating a 4 volt potential difference between poly I and II curves. The wafers of this lot were specifically processed to reduce the size of the interface barriers between poly I and II gates. Testing of the so-called charge barrier or "bump" indicated a spread of values which were not significantly better than was obtained from lot DP3A-8. The special "bump removal" processing involved removal of poly I material along the edge of each gate structure. This material is normally undercut and therefore unsupported during chemical etching of the oxide areas to be occupied by poly II gate and gate oxide films. In the event that the poly I unsupported edge is NOT etched away, the subsequent poly II gate oxide growth fills in the undercut region and causes this fringe to lift up. This lifting effect provides increased gate oxide thickness along poly I gate edges, thereby creating the intergate potential barrier or "bump."

#### 7.3.1.4 The Nitride Sandwich Experiment

A second approach to insure reduction or possible elimination of the intergate barrier was devised and included as a process sequence modification on lot DP3A-9. This lot employed an  $\text{Si}_3\text{N}_4$  -  $\text{SiO}_2$  dielectric sandwich.

that provides an absolutely planar dielectric surface under poly I and II gate structures. Some significant processing problems were presented by the  $\text{Si}_3\text{N}_4$  -  $\text{SiO}_2$  dielectric layers. A tough, etch-resistant silicon-oxy-nitride film was formed on the wafer's surface during oxidation of poly I gate structures, preceding deposition of the poly II film. This silicon-oxy-nitride film did not etch uniformly in the barrel-type plasma etcher which normally is used to etch and define source-drain regions for input and output FET circuits. This tough film was removed, however, by a phosphoric acid etch bath, which also affected adhesion of the photoresist film protecting the surface of the wafer. An extended bake of the photoresist was tried, before the phosphoric acid bath, in an attempt to solve this problem.

Extensive test and evaluation of DP3A-9 provided the following information:

1. Examination of the oxide-nitride-dielectric sandwich indicated an oxide thickness of 800A; the nitride layer was approximately 600A thick, providing a dielectric with a total equivalent value equal to 1,100A oxide ( $\text{SiO}_2$ ).
2. CV curves showed significant distortion from those normally expected, which could not be attributed to lot contamination. (BT stress tests verified the absence of alkali ion contamination.)
3. Further testing of poly capacitors employing the  $\text{Si}_3\text{N}_4$  -  $\text{SiO}_2$  sandwich, indicated extremely low leakage characteristics. (This particular lot did not receive extensive device or cell testing as it was fabricated specifically to evaluate the basic characteristics of the dielectric film sandwich as a means of solving the intergate "bump" phenomenon.)

#### 7.3.2 NE-1 and NE-2 Test Patterns

The design of a DP5 chip containing a 32-bit adder/subtractor/exclusive-OR array had become so complex, that it was decided to generate a series of N-channel test patterns which would prove out segments of the DP5 design. The NE-1 mask set therefore contained twelve separate N-channel test structures. The second test chip, designated NE2, contained a multiplier cell capable of multiplication of two 5-bit 2's complement numbers and deliver the product as a 9-bit 2's complement number. It also contained twelve cascaded full adders with their carry outputs taken to bonding pads.

Three NE1 lots were fabricated during February 1978, using the baseline N-surface channel process sequence. In addition, an NE2 lot was also processed using boron-implanted 25 ohm-cm P-type material, to reduce its resistivity to less than 10 ohm-cm. The resultant devices were to be compared with those on NE1-1 which was fabricated of 25 ohm-cm as well. The difference in impurity concentration between the three NE1 lots was sufficiently different to determine the impact of starting material resistivity on DCCD device performance. Test results from lot NE1-1 were satisfactory and operating device characteristics were obtained. Initial tests of lot NE2-1 were suspended due to excessive dark current.

Fabrication of an N-buried channel lot (NE1-IBC) was also started during this period. It was produced with 20 ohm-cm P-type material. The phosphorus (channel) implant was  $1 \times 10^{12} \text{ cm}^{-2}$  @ 150 KEV. The boron channel stop implant was  $1 \times 10^{14} \text{ cm}^{-2}$  @ 100 KEV. High temperature annealment ( $1075^{\circ}\text{C}$ ) of implant damage was reduced to a minimum to provide devices that would withstand high ionizing radiation doses.

A new surface channel lot designated NE1-3 was started in April 1978; its purpose was to produce half adders and shift registers for radiation hardness evaluation. Several nominal process modifications were suggested as a means of achieving desired goals, which included resistance-heated evaporation of the aluminum metallization film. Mechanical abrasion of the backs of all NE1-3 wafers was used to create stacking faults; these faults are used to trap heavy metal ions that migrate through the substrate during high temperature processing steps. In addition, heavy phosphorus gettering of wafer backs ( $\text{N}^+$  gettering) was also employed during NMOS source-drain doping to reduce the number of "S" pits and dislocation sites, thereby lowering the dark current in the completed devices.

As the NE1-3 wafer lot was to be subjected to extensive ionizing radiation tests, CCD Processing personnel endeavored to locate a source of resistance-heated metallization, without success. This lot was therefore metallized with Cu-doped Aluminum, using our standard E-beam deposition system. It was felt at the time that these devices would have their inherent radiation resistance reduced by employing E-beam deposited metal. Subsequent tests verified that these devices could withstand an ionizing dose of  $10^4$  to  $10^5$  rads (Si).

Lot NE1-4 was started in May 1978, as a means of further evaluating the compound dielectric sandwich of  $\text{SiO}_2$  -  $\text{Si}_3\text{N}_4$ . An error in the processing sequence cause the lot to be scrapped; it was replaced immediately by NE1-5.

NE1-5 was produced as a twelve wafer lot. Its purpose was to determine the effectiveness of the compound dielectric sandwich and to determine whether this type of dielectric would create any unique device operating characteristics. This lot was divided as follows:

1. Gate dielectrics consisted of 600A of  $\text{SiO}_2$ , followed by CVD-deposited  $\text{Si}_3\text{N}_4$  with a thickness of 200A.
2. Gate dielectrics consisting of 600A of  $\text{SiO}_2$ , followed by CVD-deposited  $\text{Si}_3\text{N}_4$  with a thickness of 400A.
3. Two standard control wafers with conventional 1,000A of  $\text{SiO}_2$  were also included.

Results from this lot were inconclusive due to an equipment malfunction during the  $\text{Si}_3\text{N}_4$  deposition operation.

#### 7.3.2.1 SILMAT-Processed Wafers

Lot NE1-6S was a ten wafer lot produced in May 1978. Its purpose was to evaluate SILMAT-processed material to determine whether it produced devices with significantly lower dark current values. These wafers were obtained from Silicon Materials Inc., Sunnyvale; these specially processed wafers are supposed to reduce heavy metal contamination as well as reduce "S" pits and other crystalline defects which are considered dark current generation sites. Three control wafers were included with this lot which were back abraded and heavy phosphorus gettered by CCD Processing Lab people. This was done to determine whether the SILMAT process provided any significant improvement in device characteristics, or whether the same results could be obtained by in-house processing. This NE1-6S lot was also processed with the compound dielectric of  $\text{SiO}_2/\text{Si}_3\text{N}_4$ .

Initial test results of the NE1-6S lot indicated that the bump height of those wafers processed with a conventional 1,000A  $\text{SiO}_2$  gate oxide was essentially the same as those wafers processed with the 200A  $\text{Si}_3\text{N}_4$ /600A  $\text{SiO}_2$  gate dielectric. The SILMAT-processed material produced devices that

were similar in operating characteristics to devices produced with conventional in-house gettering. As a result it was decided to continue to use in-house gettered material, rather than go through the expense and additional handling required to obtain SILMAT-processed material. All subsequent lots were mechanically abraided and heavy phosphorus doped to reduce sources of dark current.

#### 7.3.2.2 Buried Channel Operation

Lot NE1-1BC was produced in March 1978, however, meaningful test results from this lot was not obtained until June. (Refer to Section 7.3.5 for processing information.) A buried channel CCD shift register demonstrated satisfactory performance by operating in a frequency range of 60 kHz to 3 MHz. Transfer efficiency for these devices was between 0.995 and 0.998 and compared favorably to devices operating in a surface channel mode. The speed of the buried channel device was limited on the low side by dark current and on the high side by CCD gate lengths (1.5 mil) and mutual induction transients in the clock phases.

The source of the excessive dark current that previously plagued these devices was identified as coming from the guard ring buried channel implants, as regulated by the phased gates. Operating these gates at sufficiently large voltage levels permitted excess charge injection into the channel. This charge came from the generation centers in the depletion regions.

In August 1978, the decision was made to discontinue making NE1 lots. The desire to complete the DP5 mask set (32-bit adder/subtractor/exclusive-OR array) also necessitated suspension of any work on the NE2 design (3 x 5 array).

The first DP5-1 lot was completed in October 1978. During the deposition of poly I, an interruption of the process occurred due to a power outage causing a discontinuity in the CVD deposition cycle. Though the correct amount of poly film was deposited after the system was put back into operation, the discontinuity somehow extended the etch rate so that fine filaments of polysilicon remained on the field oxide. These filaments were too fine to notice during periodic inspection following plasma etching of the poly layer. They were discovered, however, when high resistance shorts were found between adjacent poly lines. The DP5-1 lot was therefore rejected as untestable.

Due to the large size of the DP5 chip (approximately 0.4 inch on a side) the alignment targets across the wafer were spaced too far apart for normal alignment. This problem was corrected by changing the location of the alignment target near the edge of the chip, to a location near the chip's center. The redesigned mask set, incorporating this modification, was designated DP5A.

It was also determined that the scribe line areas on two layers were omitted, adding to the alignment problem. This error was also corrected on the DP5A mask revision.

While awaiting the DP5A revised mask set, some tests were performed on the half adder of DP5-1 and some useful results were obtained; however, the large number of poly I layer shorts made it impossible to accurately control test conditions.

In January 1979, lot DP5A-1 was completed and delivered to test. Several mask errors, such as omitted contacts to polysilicon gates, were found by careful inspection of the mask set during processing. All mask errors appeared to be in the 32-bit arithmetic array; no errors were found in the test devices. The decision was made at that point not to start any new lots until another complete inspection of all test devices and the arithmetic array could be performed and appropriate corrections made.

In essence, this completed the work accomplished on the Navy's DCCD development program. No new DP5A lots were fabricated as the ultimate complexity of this large 32-bit array would seem to defeat the ability of the design group to uncover all potential errors without a commitment of manpower and time beyond the remaining resources of the program.

Despite the difficulties encountered on this program, a viable, repeatable process was generated that has since been employed to fabricate a number of complex DCCD LSIs. Two significant programs, such as the AZIMUTH CORRELATOR DEVICE (ACD) and the FAST HADAMARD TRANSFORM (FHT) chips have employed the identical processing sequence generated during the final phase of the Navy Program. A detailed listing of this DCCD processing sequence is provided in Table 7.1.

TABLE 7.1. THE DCCD DOUBLE POLYSILICON PROCESS FLOW CHART

STEP	OPERATION	REMARKS
1.	Select Wafer Material; Record Thickness and Resistivity	10 ohm-cm P-type Mtl. <100>
2.	Clean Wafers	Standard 5 min. Buf Dip
3.	Field Oxidation	F.O. Thickness = 8,000A @ 1,075°C
4.	Apply Photoresist for Channel Stop Cut	Positive Resist AZ111
5.	Etch Channel Stop Cut	
6.	Strip & Clean Photoresist	
7.	Oxidation and N <sub>2</sub> Anneal of Channel Stop Cut	Oxide Thickness = 200A @ 920°C
8.	Implant Channel Stop	Boron (B <sub>11</sub> ) $2 \times 10^{14}$ @ 100 KeV
9.	Clean Surface of Oxide followed by Anneal of Implant Damage	15 min. @ 1,075°C in N <sub>2</sub>
10.	Apply Photoresist for Channel Cut	Resist AZ111
11.	Etch Channel Oxide	
12.	Strip & Clean Photoresist	
13.	Buffered Dip and Clean	Insures Clean Silicon Surface Before Gate Oxide Growth Cycle
14.	Oxidation and N <sub>2</sub> Anneal of Channel Cut	Oxide thickness = 1,000A @ 920°C
15.	Polysilicon I Film Deposition	CVD Deposition; Poly film thickness = 4,000A
16.	N <sup>+</sup> Diffusion	N <sup>+</sup> Furnace @ 950°C
17.	Photoresist Preparation	Clean Poly Surface, Followed by Oxidation of Poly Surf @ 900°C (Permits better adhesion of Photoresist)
18.	Apply Photoresist to Poly I Film	HMDS and Photoresist 1350J
19.	Buffered Dip and Plasma Etch	Provides Poly I Pattern
20.	Plasma Etch Wafer Backs	
21.	Strip & Clean Photoresist	
22.	Etch Channel Oxide and Clean	This Etch Prepares Silicon Surface for Poly II Gate Oxide Growth Cycle

STEP	OPERATION	REMARKS
23.	Oxidation and N <sub>2</sub> Anneal for Poly II Gate Oxide	Oxide Thickness = 1,000A @ 920°C
24.	Polysilicon II Film Deposition	CVD Deposition; Poly Film Thickness = 3500A
25.	N <sup>+</sup> Diffusion	N <sup>+</sup> Furnace @ 950°C
26.	Buffered Dip	To Remove Phosphorus From Surface
27.	Photoresist Preparation	Oxidation of Poly Surface at 900°C (Permits better adhesion of Photoresist)
28.	Apply Photoresist to Poly II Film	HMDS and Photoresist 1350J
29.	Buffered Dip and Plasma Etch	Defines Poly II Pattern
30.	Plasma Etch Wafer Backs	
31.	Strip & Clean Photoresist	
32.	Photoresist Preparation	10 min. @ 900°C in N <sub>2</sub>
33.	Apply Photoresist For NMOS Source-Drains	Photoresist AZ111
34.	Etch Oxide in Source-Drain Regions	
35.	Strip & Clean Photoresist	
36.	N <sup>+</sup> Diffusion For Source-Drains	N <sup>+</sup> Furnace @ 950°C
37.	Buffered Dip followed by Resistivity Check	Insures sufficient doping of S-D's
38.	TEOS Deposition and Densify	TEOS Thickness = 5000A; TEOS deposited at 730°C, with densification at 920°C
39.	N <sup>+</sup> Getter and Photoresist Prep.	N <sup>+</sup> Furnaced Used
40.	Apply Photoresist For Contact Holes	Photoresist AZ111
41.	Etch Contact Holes (Vias)	Buffered HF Used to Clear Holes
42.	Strip & Clean Photoresist	
43.	Deposit Metal (Aluminum + 4% Cu)	Metal Film Thickness = 10,000A Front; 5,000A wafer backs
44.	Apply Photoresist to Metal Film	HMDS and Photoresist 1350J
45.	Etch Metal Interconnection Pattern	
46.	Strip & Clean Photoresist	
47.	Sinter Metal	Approx. 1 hr. @ 400°C

STEP	OPERATION	REMARKS
48.	SILOX Deposition	SILOX Thickness = 4000A with 3% Phos.
49.	Apply Photoresist to SILOX Film	HMDS and Photoresist 1350J
50.	Etch SILOX Passivation Pattern	
51.	Strip & Clean Photoresist	

#### 7.4 THE IMPACT OF THE DCCD PROGRAM ON TRW'S PROCESSING TECHNOLOGY

The difficulties encountered in both the design and fabrication of DCCD LSI's emphasized the necessity of tight process standardization which could only be brought about by extensive process automation. As the chief advantages of DCCD's include very high cell density coupled with MHz clock rates, the necessity of very tight device geometries and very accurate processing is apparent. As a result of the many problems requiring solution in order to standardize DCCD fabrication, TRW had decided to embark on a relatively extensive automation program, in an attempt to provide DCCD device yields comparative to those obtained by other state-of-the-art MOS technologies. The automation program will include all major processing technologies:

##### 7.4.1 Mask-to-Wafer Alignment

This effort involves the purchase of proximity alignment equipment capable of one micron line resolution. It will provide cassette-to-cassette wafer transfer, deep UV light sources (235 nm) and split field imaging. Projection alignment equipment significantly increases mask life and will be considered during the next major upgrade of the MOS Processing Facility.

TRW has also purchased an E-beam direct writing system that can be used for patterning micron-sized gate, conductor and interconnection patterns, channel stop, and P<sup>+</sup> guard ring patterns directly onto the photoresist-coated wafers.

Direct-Step-On-Wafer equipment is also being considered for the MOS Fabrication Facility as a means of improving line tolerances, reducing geometries, and significantly increasing LSI density.

##### 7.4.2 Photoresist Coating, Developing and Removal

Current line widths are now at the 3 - 4 micron level. The densities demanded of custom LSI circuits during the early 1980's will necessitate a photolithographic technology capable of delivering 1 - 2 micron lines in a day-to-day production environment. TRW has already purchased the most advanced wafer handling equipment available (GCA Wafertrac Equipment), which will soon be installed in the MOS Processing Facility. This equipment is capable of automatic scrub/bake, coat/bake, develop/bake operations; all

wafers are transported to the various processing stations by means of air bearing tracks. Wafers are inserted and removed from the processing sequences by means of cassette-to-cassette wafer handling equipment. The entire system is microprocessor programmed and any subsystem malfunction is brought to the attention of operators by automatic alarms. Removal of operator manipulation from this key processing sequence insures uniform processing of wafers and therefore higher yields.

Within the next few years, Wafertrac equipment will provide automatically scrubbed, baked, photoresist-coated and baked wafers directly to the projection alignment station, where cassettes will feed uniformly processed wafers directly to a microprocessor-controlled aligner, that provides 0.2 micron alignment accuracy, based upon automatic pattern recognition system capabilities.

#### 7.4.3 Microprocessor-Controlled Diffusion Furnaces

As MOS device geometries are reduced to dimensions that provide short-channel operation, Xj distances related to source-drain implants will be reduced to 0.2 - 0.3 microns. The control of implant drive-in temperatures and time must necessarily be quite precise to permit the fabrication of devices that operate with the desired threshold, punch-through and breakdown voltages. Ultimately, tight control over furnace zone temperatures and drive-in periods can be obtained by means of microprocessor controllers; these devices continuously monitor all three heat zones of each furnace and provide an alarm should one of these zones change temperature by more than  $\frac{1}{4}$ -degree Centigrade.

Other important aspects of microprocessor controlled furnaces include low temperature growth ( $900^{\circ}\text{C}$ ) of gate and intermediate field oxides, with subsequent ramping of these tubes to a higher temperature ( $1,000^{\circ}\text{C}$ ) for proper annealment. The ability to ramp diffusion furnaces up and down without removing wafers from the tube reduces the number of tubes required by a processing facility. Also, it reduces handling of the wafer boats, as a wafer lot can go through a doping and diffusion cycle at different temperatures, without being removed from the tube in which the initial doping is accomplished.

#### 7.4.4 Dry Etching of Polysilicon, Nitride, Oxide and Metal Patterns

The MOS Processing Laboratory currently uses both wet and dry etching of LSI films, although the direction of the etching technology shows a clear preference for dry (plasma) etching over wet chemistry processes. Processing of MOS and DCCD devices indicate the need for greater precision in etching critical self-aligned gate structures. This implies little or no undercut of gate patterns and metallization patterns where line widths are less than 2 microns.

Current laboratory capabilities include a barrel-type plasma etcher, that provides less than a 1 : 1 undercut. As gate and interconnection line widths decrease to less than 2 microns, there will be a general demand for planar plasma etching equipment capable of providing true anisotropic etching capabilities. TRW has recently purchased planar etching equipment and will soon employ it as a means of defining poly-gate levels of MOS and DCCD LSI's.

#### 7.5 DCCD TECHNOLOGY SUMMARY

DCCD fabrication processes for both the DP and NE series of devices evolved through many mask layout iterations. These changes were needed to improve circuit operating parameters, such as dynamic range and transfer efficiency. Each new generation of circuits which employed higher density geometries, also necessitated significant changes in the DCCD processing sequence, or a different arrangement of processing steps. Most of these technology variations involved poly I and II gate layout patterns. Table 7.2 lists the various DP and NE generations, including significant differences between generations.

Table 7.2 DP and NE Design Generations.

Circuit Designation	Mask Type	Gate Technology	Remarks
N1 through N4	Conventional	Poly & Metal	*Field Oxide = 15,000Å *P-Channel Technology *Gate Oxides: 1000/2000 Å
NAV5 through NAV11	Conventional	Poly & Metal	*Technology concentrated on Floating Gate Devel.
DP-0	Slip Masks	Poly & Metal	*Test circuits designed to verify Floating Gate FET discharge concept; *6 mask levels required *Poly Protect film used
DP-1	Slip Masks	Poly with Poly Protect Mask/Metal	*TEOS used as a protective film over poly, to help metal step coverage * Gate Oxides: 1000/3000 Å
DP-2, (-2A)	Slip Masks(-2) Poly/Poly also Conventional Masks(-2A)		*Contained 8 + 8 Adder *Contained 3 x 3 Multiplier *First use of Double Poly Gates *Arsenic doping of Poly Films *Switch to N-Channel on lot DP-2A-1N
DP-3, (-3A)	Conventional (-3A, mask revision)	Poly/Poly	*Contained 8 x 8 Multiplier *Contained 16 + 16 Adder *First lot of Buried Channel *Thick Field Oxide & Channel Stops used together to define CCD Channel * Field Oxide = 10,000Å for improved poly & metal line definition *10 ohm-cm P-type material *Intergate Barrier or "Bump" identified and SEM photos *First attempt to deposit SiO <sub>2</sub> /Si <sub>3</sub> N <sub>4</sub> Dielectric

Circuit Designation	Mask Type	Gate Technology	Remarks
NE-1	Conventional	Poly/Poly	*Contained 12 N-Channel Test Structures *25 ohm-cm material used *NE1-1BC first N-Buried Channel Lot *Mechanical Abrasion of Wafer Backs used for 1st time in combination with heavy N <sup>+</sup> Gettering to lower dark current. *NE-1-6S used to evaluate SILMAT-processed material
NE-2	Conventional	Poly/Poly	*Contained 12 cascaded full adders; also multiplier cell *one lot only fabricated
DP-5	Conventional	Poly/Poly	*Contained 32-bit Adder/Subtractor/Exclusive-OR *Chip Size = 0.4" x 0.4" *Circuit used full Adder design.

#### 7.5.1 Mask Generations

Although conventional mask sets were selected for the first mask generations of this program (N1 - N4; NAV5 - NAV11), a commitment to slip mask use was made during fabrication of DP-0, -1 and -2 series. Slip masks were selected for the DP series primarily to save program funds. The very complexity of the DCCD technology required many mask level changes to correct layout errors, occasional errors created by the computer graphics system (Applicon System), and circuit modifications based upon test circuit performance.

Slip masks provided three or four mask levels per plate; during the alignment of successive mask levels, the slip mask was displaced in either the X or Y direction. Combining four mask levels onto one plate reduced mask fabrication costs and facilitated quick lot turn-around. The major problem with slip masks involved alignment difficulties created by extensive mask "run-out" and "rotation" between successive mask levels. Normal lens aberrations did not permit the mask manufacturer (Electromask, inc.) to compensate for dimensional tolerance variations between mask levels.

While slip masks were used for DP-0, DP-1 and DP-2 mask generations, alignment difficulties, combined with low yields, necessitated the abandonment of this approach in favor of conventional mask sets, which provided superior results. Conventional mask sets were therefore used for the later versions of DP-2A and DP-3 and -3A series. Further improvements in circuit yields could have been obtained if proximity or projection alignment equipment had been available to produce these high density circuits.

#### 7.5.2 Gate Technology

Two significantly different approaches were evaluated during the early phases of this program to determine the most reliable and reproducible method of fabricating CCD gate structures. Aluminum metal gate structures were initially selected for Poly II levels, as it basically requires a simpler process than polysilicon gate structures. Aluminum gates were used on DCCD series N1 through N4; NAV5 through NAV11; DP-0; also, DP-1. None of the processes used to fabricate these various DCCD generations employed an isoplanar technology; the resulting topography of these various designs were quite complex and metal step coverage became a significant factor in obtaining workable devices. The DCCD processing technology was extensively reworked for DP-2, to permit the use of a dual polysilicon technology. The use of poly for both gate levels resulted in a significant improvement in step coverage as well as device yields.

Initially, the polysilicon films were deposited in an RF-heated reactor, which permitted in-situ doping and annealment of these films with limited success. The problems encountered with RF reactor deposition centered around

film thickness uniformity, it became a significant problem to control polyfilm thicknesses to better than 20%. In addition, the deposition reaction required the use of hydrogen as a reducing agent; this created the potential for explosions, forcing the decision to build a hot wall CVD reactor.

In 1976, MEC personnel completed the design and fabrication of a CVD reactor for polysilicon deposition. This tube has been used successfully during the latter half of this DCCD program. In general, the CVD polysilicon deposition system produced very uniform films of required thickness ( $\sim 4,000\text{\AA}$ ), superior in uniformity to that obtained from the RF-heated system. Following a one hour pump-down, the polysilicon film is deposited at approximately  $630^{\circ}\text{C}$ ; deposition of the  $4,000\text{\AA}$  film required 20 minutes. The only significant drawback of this system is the necessity to dope the polysilicon film in an  $\text{N}^+$  or  $\text{P}^+$  furnace, to insure polysilicon gate and interconnection patterns of sufficiently low resistivity. Separate doping lengthens and complicates the processing sequence. In-situ doping of polysilicon films will be the subject of an intensive development effort in the near future, to reduce operator handling and increase processing yields. Its only limitation appears to be the necessity to deposit, then dope the poly film in a conventional manner, which extends processing length and complexity. Some companies now producing LSI devices employ in-situ doping of these films, however, the details of this technology innovation is considered "company proprietary" information. Doping and diffusion systems manufacturers have not yet solved this problem, as systems incorporating this important feature are not yet available.

#### 7.5.2.1 Gate and Field Oxide Undercut Problems

Significant gate oxide undercut was encountered during fabrication of initial DP series lots; this became a significant yield loss problem following adoption of the double polysilicon gate process (DP-2 Series).

Several process changes were made to avoid this problem. A special photoresist masking step was used to cover polysilicon gates and interconnects before oxide cuts were made. This special "poly protect" masking step

successfully prevented oxide undercut, as shown in Figure 7-2. Note that severe oxide undercut as shown in Figure 7-2 would result in broken metallization lines caused by poor step coverage. The "poly protect" processing sequence did much to eliminate yield losses caused by this phenomenon.

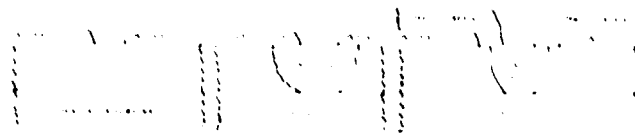


Figure 7-2. Polysilicon Protect Configuration.

- a. - Polysilicon pattern defined.
- b. - Oxide etched without "poly protect" masking step, showing undercut of polysilicon gate-interconnection pattern.
- c. - Oxide etched with "poly-protect" showing no undercut of polysilicon region, permitting smooth transition for subsequent metallization coverage.

It is unfortunate that wet etching processes must still be used to define field and gate oxide cuts; oxide undercut can be significantly reduced by plasma etching techniques, particularly planar plasma etchers that provide an anisotropic etch capability. Reactive ion etching is still a relatively new technology innovation and etching oxides by this method is a very slow process. Although ion milling was available as a means of defining field and gate oxide cuts, it was not used during the course of this program; this etching technique is not selective in its removal of film material and would have necessitated an extensive experimental program to insure good device yields.

#### 7.5.2.2 Gate Control by Means of Gate Oxide Thickness Adjustment

An extensive number of processing variations were made and evaluated to improve gate control of charge packets. Poly I and II gate oxide thicknesses were varied from 1000/2000Å to 1000/3000Å; later variations included 800/2400Å. Both boron and phosphorus-doped poly II layers were made, in an attempt to simultaneously dope source-drain and self-aligned polygate structures. Doping polygate structures with boron provided poor results, as source-drain drive-in time and temperature requirements usually resulted in boron penetration of the relatively thin gate oxides with resultant doping of the channel. In most instances, this changed the threshold voltage characteristics of the devices sufficiently to make the circuit untestable.

A review of Section 7.3, Processing History, indicates that a DP-1 wafer lot was produced by doping source-drain regions and poly II gate structures simultaneously. This was an attempt to simplify the DCCD process by eliminating the nitride layer which was used at that point in process development. As a poly II protect mask against boron doping of the already Arsenic-doped poly film, the nitride film also prevented boron diffusion and doping of the gate oxide, with resultant changes in channel threshold characteristics. Elimination of the nitride protect film on this DP-1 lot produced very low threshold voltages, as well as some depletion-type devices. As previously stated, boron penetration through the gate oxide was suspected. In the worst case, boron penetration will form a heavily doped P-type region immediately beneath the gate oxide, resulting in depletion type devices. Subsequent tests of DP-1 devices verified this occurrence. A common technique used in the study of impurity penetration through gate oxide involves measurement of the depth of the junction formed by the impurity's penetration. A determination of the time necessary for penetration of the  $\text{SiO}_2$  gate oxide layer, to a particular depth in the silicon can be made.

It is obvious that significant electrical effects due to boron penetration will occur in CCD devices long before a PN junction is detected. At the onset of boron penetration, ionized boron atoms will cause the formation of a positive charge layer at the  $\text{Si/SiO}_2$  interface, shifting the flatband voltage of the MOS device. Movement of the flatband voltage can be detected as an equivalent

change in the MOS device's threshold voltage. C-V measurements carried out on test capacitors, clearly showed boron penetration. In addition, boron penetration was not uniform and varied across the wafer, as determined by variations in test transistor threshold voltage measurements.

As a result of depletion-type device formation, boron doping of polygate structures associated with PMOS devices was abandoned in favor of in-situ doping with arsenic during RF deposition of the polysilicon film.

DCCD technology advancements will require thin polygate structures and interconnections ( $\sim 2,000\text{\AA}$ ). As these polygate film thicknesses decrease, it will complicate doping these films to achieve films of high conductivity. One approach toward solving this problem involves modifying CVD deposition to enable in-situ doping of the polysilicon; a second, less conventional, approach is refractory metal deposition and drive-in, providing a metal-doped polysilicon film of exceedingly low resistivity. Both of these technology approaches will be attempted within the near future.

#### 7.5.2.3 Thermally Grown Field and Gate Oxides

The DCCD fabrication process employs relatively low temperatures ( $920^{\circ}\text{C}$ ) gate oxides; field oxides are grown at  $1075^{\circ}\text{C}$ . In general, wet oxidation cycles are used, as dry oxidation cycles take approximately X5 the growth period needed for a wet cycle. Wet oxides are grown by steam oxidation of the silicon substrate; the steam is produced by an in-situ reaction of  $\text{H}_2$  and  $\text{O}_2$  gasses supplied to an oxy-hydrogen torch that provides the super-heated steam. Measured  $Q_{ss}$  values were approximately  $2 \times 10^{11} \text{ cm}^{-2}$ ; in this instance,  $Q_{ss}$  represents fixed surface states or interface charges that occur during the thermal oxidation cycle.  $N_{ss}$ , or fast surface state density, values were usually in the  $10^9/\text{cm}^2\text{eV}$  range. As great care is taken to prevent furnace contamination by mobile (alkali) ions, HCl steaming of furnaces is done on a periodic basis, B-T stress testing of furnaces in the MOS/CCD Processing Lab usually indicates mobile ion concentrations that are less than the sensitivity of the C-V measurement equipment.

Gate or field oxides prepared by wet thermal oxidation of the silicon substrate, generally have positive charges associated with the oxide layer; as a result, the underlying silicon will be depleted or inverted, if it is P-type, or will evidence accumulation if it is N-type. These charge states may be classified in at least four general categories.

The nature of these oxide charge states in relation to the  $\text{SiO}_2/\text{Si}$  interface is indicated in Figure 7-3. These include:

1.  $Q_{ss}$  - fixed surface states or interface charges
2.  $Q_o$  - mobile charges within the oxide (caused by alkali ion contamination)
3.  $N_{st}$  - surface recombination centers, which act as generation sites of unwanted dark current leakage
4.  $N_t$  - trapping sites within the oxide, that are susceptible to ionizing radiation; this affects both threshold voltage and transfer efficiency of exposed devices.

$Q_{ss}$  or fixed charge is apparently quite close to the  $\text{SiO}_2/\text{Si}$  interface; its density can vary from almost zero to approximately  $2 \times 10^{11}$  electronic charges/ $\text{cm}^{-2}$ . Mobile ion charges are usually the result of processing contamination that can be introduced by operator oversights, contaminated solvents, photoresist developer solutions, or diffusion furnace tube devitrification.  $N_{ss}$  is a measure of fast surface states; the density of such active surface states can range from less than  $10^{10}/\text{cm}^2\text{-ev}$  to significantly higher values. It is believed that the presence of these fast surface states depends upon processing conditions, while the silicon potential determines whether or not they are charged.

Positively charged traps in the oxide, referred to as  $N_t$ , have been observed after exposure of a MOS device to X-rays, electron streams, or other ionizing radiation. The concentration of these traps is of the order of  $10^{18} \text{ cm}^{-3}$ .

Surface charge has also been identified as a factor in grossly modifying MOS device performance; it occurs on the outer surface of an oxide, and can usually be attributed to surface contamination. Usually this charge is a result of ion migration in the vicinity of a biased junction. As stated, surface charge migration requires a conduction surface, which is usually brought about through surface contamination.

Gate and Field oxidations are about to undergo a relatively dramatic change in processing methods, brought about by pressurized oxidation systems that operate at temperatures well below  $900^\circ\text{C}$ . These furnaces will be micro-processor controlled with real-time monitoring of each temperature zone, to

insure uniform, repeatable results. It is not inconceivable that both gate and field oxides will be grown in the same furnace tubes, with micro-processor controlled adjustments made on the basis of preprogrammed oxidation and annealment cycles.

#### 7.5.2.4 Clean Gate Oxide Technology

The MOS/CCD Processing Laboratory has investigated and developed a clean gate oxide technology for CCD fabrication. Early experiments using conventional oxidation systems showed that reproducible fixed charge values could be obtained only with new quartz tubes; however, these values deteriorated rapidly with time. Reproducible fixed charge values ( $Q_{ss}$ ) were found when double wall quartz tubes were used, however even these relatively stable values drifted over an extended period of time. Changes in  $Q_{ss}$  were also attributed to substrate crystal orientation, with greater changes in  $Q_{ss}$  occurring in  $\langle 111 \rangle$  than with  $\langle 100 \rangle$  substrates. A more rapid increase in  $Q_{ss}$  was also observed in oxides grown in Spectrosil furnace tubes than in GE #204 quartz tubes; it was claimed that Spectrosil quartz is practically free from metallic impurities, with total impurity concentrations equal to one part per million. A spectroscopic analysis of the quartz used in these tube indicated a sodium content of approximately 20 ppm, which appeared as its major impurity. An analysis of GE #204 tube quartz indicated an aluminum content of 40 to 50 ppm; also, sodium (20 to 30 ppm) content as well.

Experiments directed toward elimination of high  $Q_{ss}$  produced some interesting results; it appears that very fast quenching during removal of wafers from the furnace hot zone can reduce fixed charge ( $Q_{ss}$ ) to a minimum. When oxides with very small fixed charge values ( $1 \times 10^{11} \text{ cm}^{-2}$ ) were quenched in  $\text{LN}_2$  to  $-200^\circ\text{C}$ , or annealed in gaseous  $\text{N}_2$  at a relatively low furnace temperature ( $550^\circ\text{C}$ ), fixed charge could be virtually eliminated and experimental curves close to the theoretical values can be obtained. It is suspected that aluminum and sodium atoms that are found in thermally grown oxide, originate in the quartz furnace tubes and are the source of the observed increase in  $Q_{ss}$  values. The changes in fixed charge caused by rapid cooling or quenching may be the result of a shift in the state of the aluminum atoms, from an interstitial to a substitutional position in the oxide lattice structure.

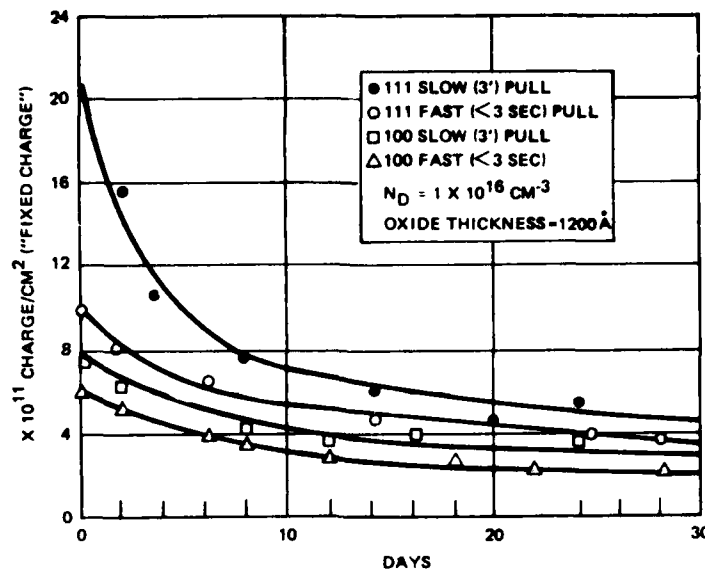


Figure 7-3. Fixed Charge as a Function of Quartz Tube Age.

#### 7.5.2.5 Polysilicon Gate Technology

From its inception, polysilicon electrodes were used as an integral part of the DCCD processing technology. The use of polysilicon gates also facilitates the use of self-aligned gate structures, which cannot be implemented effectively with a metal gate technology. Polysilicon films therefore became a very important feature of the DCCD structure. The chemical and physical characteristics of these films had to be carefully controlled and deposition, doping, and etching had to be worked out in detail.

Polysilicon films have been deposited by thermal decomposition of Silane in an RF-heated, horizontal epitaxial reactor, using Hydrogen as the carrier gas. The resultant crystalline structure is very sensitive to deposition conditions. The film's crystalline structure determines its electrical characteristics, particularly its resistivity. A temperature of  $650^{\circ}\text{C}$  is the optimum deposition temperature for polysilicon films formed in an RF-type epi reactor. Films formed at higher temperatures usually had a poorer, less uniform, coarse-appearing structure. The deposition rate at  $650^{\circ}\text{C}$  was approximately 1000Å/minute. Since these films were used as conductors and in some instances, as diffusion masks, no dopants were added

to lower the resistivity of the film. Neither DCCD device or circuit performance was adversely affected by the higher resistivity gate and interconnecting structures.

Increased circuit complexity forced reconsideration of polysilicon film doping; despite the difficulties encountered in doping RF-deposited polysilicon films, techniques were developed to provide in-situ doping to insure improved conductivity of relatively long polysilicon traces.  $\text{BBR}_3$  was employed to diffuse boron into the polysilicon films;  $\text{POCl}_3$  was used to diffuse phosphorus into polysilicon films; both dopants lowered film resistivity. When it was discovered that these dopants often penetrated the thin gate oxides beneath the doped polygate structures, arsenic was selected as the best alternative, to prevent this unwanted occurrence. Diffusion temperatures of  $950^\circ\text{C}$  provided the most reliable, uniform results.

#### 7.5.2.5.1 The Single Level Polysilicon Process

This process was employed during the initial phases of the DCCD program. It required N-type silicon wafers, with a resistivity of 3 to 5 ohm-cm and  $\langle 100 \rangle$  orientation, to minimize surface charge. At first, a 15,000A thick field oxide was grown by means of the dry oxidation-wet  $\text{N}_2$ -dry  $\text{N}_2$  oxidation cycle. The CCD channels were defined by means of positive photoresist, followed by a wet oxide etch; the gate oxide grown in the channel area was 1,000A thick and was produced in a gate oxidation furnace, operating at  $920^\circ\text{C}$ ; wet oxidation was achieved by means of an oxy-hydrogen torch. These steps were followed by deposition of a 3500A polysilicon film that occurred in an RF-heated epi reactor. Initially, the poly film was phosphorus-doped in a separate diffusion furnace before in-situ doping was achieved. The poly film was then covered by a nitride film ( $\text{Si}_3\text{N}_4$ ), approximately 200A to 400A thick. The nitride film was slightly oxidized, to improve photoresist adhesion. The CCD gate patterns were then defined, followed by plasma etching of both nitride and polysilicon films in a barrel-type plasma etcher. Poly definition was followed by an additional oxidation step; this was performed to increase the thickness of the oxide covering the channel region. The additional oxidation acted as a channel mask to insure that boron penetration did not occur during source-drain diffusions. This boron diffusion followed

definition and etching of field oxide over the source-drain regions. The  $\text{Si}_3\text{N}_4$  covering the polygate structure was then removed by chemical etching, to insure that the polysilicon pattern was not disturbed. Channel oxide between polysilicon gates was then removed, so that a new, clean gate oxide could be thermally grown for eventually deposited and defined metal gate patterns.

Etching of the channel oxide between polysilicon gates was followed by the growth of a 2000Å thermally-grown oxide, that covered both the exposed channel areas as well as the defined polysilicon gate and interconnection pattern. Contact holes through this oxide layer were then defined and etched; this was followed by an aluminum film deposition. The aluminum film was then defined into a combined metal gate pattern as well as a circuit interconnection and termination pad pattern. Sintering of these wafers occurred at  $450^\circ\text{C}$ . The sintering sequence employed both gaseous  $\text{N}_2$ , followed by sintering in  $\text{H}_2$ . Circuits fabricated during the early phases of this program did not receive a SILOX passivation step.

#### 7.5.2.5.2 The Double Polysilicon Process

A two-level polysilicon process was adopted and used for DP-2, DP-3 and DP-5 series. The processing sequence is quite similar to that provided in Table 7.1. Device cross-sections are provided in Figure 7-4.

A switch was made to N-channel DCCD technology, which occurred with lot DP-2A-1N ("N" for N-channel). The N-channel process is therefore significantly different than the preceding P-channel single level polysilicon process. The N-channel double polysilicon process required 10 ohm-cm <100> P-type starting material. Initially, an 8,000Å field oxide was grown by means of wet oxidation at  $1075^\circ\text{C}$ . This step was followed by a channel stop cut and subsequent implant, that defined CCD channel perimeters. Annealment of channel stop implant damage was followed by CCD channel definition; this included removal of field oxide over all CCD channel areas. A second oxidation and anneal of the channel regions produced a clean gate oxide in all channel areas, that was approximately 1,000Å thick. This was followed by CVD deposition of the first polysilicon film (approx. 4,000Å thick), which was patterned into Poly I gates and interconnecting structures. (As previously noted, the poly I film was

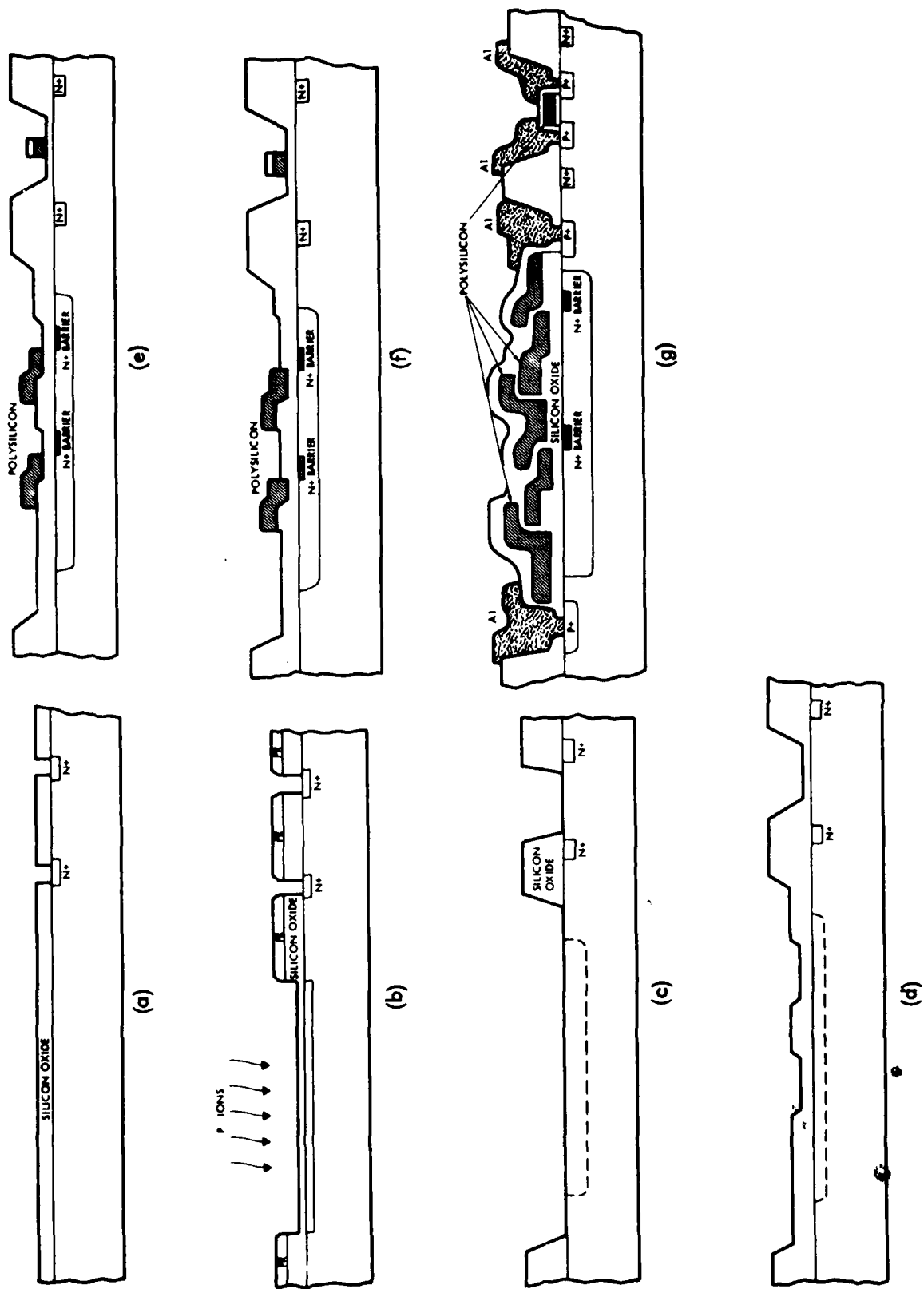


Figure 7-4. LSM-2 process for CCD device fabrication.

doped by an  $N^+$  diffusion at  $950^{\circ}C$ , to insure good polygate conductivity.) Definition of poly I gate structures was accomplished by means of plasma etching in a barrel-type etcher.

A second channel etch at this point in the process prepared the channel's surface for the growth of a new, clean, poly II gate oxide film of 1,000A in thickness; this step was followed by CVD deposition of the poly II film. Thermal oxidation of the channel to provide the poly II gate oxide also grew an insulating oxide layer over all poly I structures; this is of particular importance to prevent poly I and II shorts from occurring in those areas where poly II gates overlapped poly I gates.

The poly II film was deposited 3500A thick; it was also  $N^+$ -doped as well. Following the  $N^+$  doping of the poly II film, the wafers were processed through a buffered "dip" that removed excess phosphorus from the wafer's surface. NMOS source-drains were then defined and subsequently doped in the  $N^+$  furnace. Source-drain doping was followed by a buffered dip and resistivity check to insure that appropriate doping level of source-drains was achieved.

A TEOS film, 5,000A thick, was deposited over the surface of the wafers and densified at  $920^{\circ}C$ . These wafers were then inserted into the  $N^+$  furnace, to provide a thin phosphorus coating over the wafer's surface for  $N^+$  gettering of heavy metal ion impurities. Contact holes were then etched through the TEOS and thermally-grown oxides to provide vias to poly gates and source-drain areas. 10,000A of copper-doped aluminum was then deposited by means of electron beam gun evaporation in an ultra-high vacuum deposition system. The metal interconnection and termination pad pattern was then defined, followed by a sintering step of one hour at  $450^{\circ}C$ .

The surface of the wafer was protected by means of a deposited passivation film of SILOX, approximately 4,000A thick. The SILOX was then patterned to expose circuit termination pads, completing the fabrication process. The process herein presented, has been used for the fabrication of all DCCD circuits, designed within the last 18 months.

### 7.5.3 Progress Towards an Isoplanar Technology

The complexity of DCCD technology has brought about a reduction in device yields that is not in keeping with its overall potential. The density of DCCD LSI's will soon be at a point where it will be impractical to decrease poly and metal line widths and spaces without a significant decrease in film thicknesses as well. Further increases in DCCD circuit density will be brought about through adoption of a multilevel metal interconnection technique, that will permit three levels to be used for intracell and intercell connections. The key to this technology milestone will be a further reassessment of device and circuit geometry, directed towards an isoplanar topography.

Additional emphasis will be placed on thinner field oxides as well as thinner polysilicon gate and supporting interconnections. Intermediate metal level thicknesses will be limited to a few thousand Angstroms, in lieu of the 10,000A now used for top level metallization. The ability to design cell structures that simplify circuit topography will become a critical consideration, in order to achieve higher density and good yields. The most significant factor that will detract from DCCD device yields will be step coverage or level-to-level transition of micron-wide poly or metal lines. Both CCD design and processing people now believe that poly and metal line step coverage or line breakage is one of the major problems challenging high yields and good performance of DCCD devices. A unique combination of thermally-grown field oxides used in combination with deposited and densified  $\text{SiO}_2$  films, may help solve this problem and permit the realization of this technology's true potential.

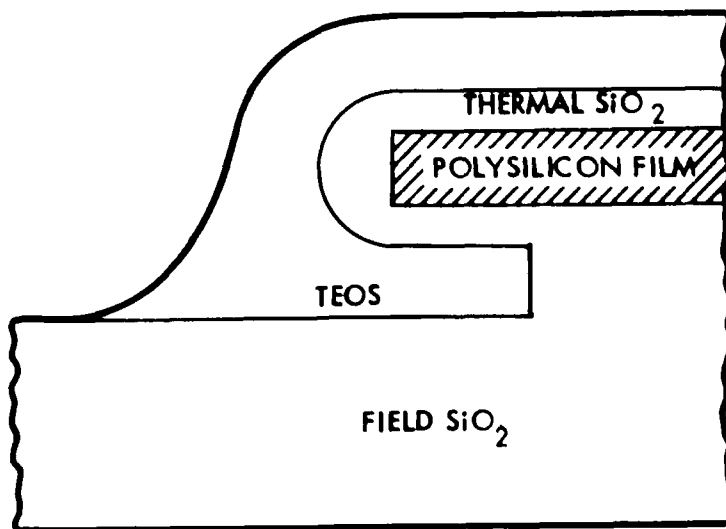


Figure 7-5. Undercut Polysilicon Step Covered by a TEOS Film.

#### 7.5.4 Metallization Problems and Solutions

A metal step coverage problem was identified during the early phases of the DCCD program as seen in the photograph of a DP-0 circuit.

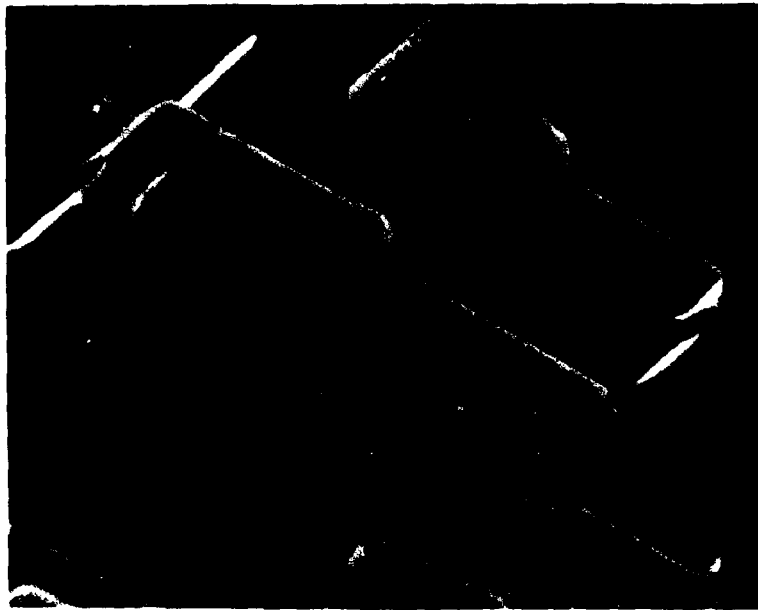


Figure 7-6. Breaks in the Al Metallization - DP-0 Circuit.

The cavity caused by the undercut field oxide is shown in the SEM photograph. A simplified drawing which illustrates the cavity created by the undercut oxide is shown in Figure 7-5; this cavity was created during etching of the 1500A oxide covering the areas to be occupied by metal gates in addition to the steep walls of the polysilicon film edge. Traversing this step, with its built-in cavity, is difficult for narrow line widths of aluminum metallization; LSI circuits have many thousands of these oxide steps which must be traversed by metal lines. Unless an absolutely reliable method is provided to insure conductor continuity for the many thousands of conductors and interconnections that comprise a complex LSI circuit, yields will be

virtually nil. These problems were encountered during the early phases of this program on N1 through N4, NAV5 through NAV11, and on DP-0 and DP-1 circuits.

A concerted effort was made, at this stage of processing technology development, to solve the metal step coverage problem. Filling these so-called cavities by means of a deposited film of oxide, appeared to offer a potential solution. Both SILOX and TEOS were evaluated. Films formed by thermal decomposition of Tetraethyl-ortho-silicate (TEOS), produced very smooth transitions over polygates with undercut gate oxides; this is illustrated by the drawing in Figure 7-5. Whereas TEOS was capable of filling in the undercut region beneath the polygate edge, SILOX was deficient, coating the surface and edges of the polygates only. The decision to incorporate densified TEOS as a practical solution to this problem resulted in an immediate improvement in device yields.

Incorporating the new TEOS layer required an extra mask level. The resultant process involved depositing TEOS over the polysilicon film before the "poly protect" mask operation. After the "poly protect" masking step, the oxide in the channel was etched away and fresh gate oxide was regrown. Figure 7-7 shows a metallized poly step covered with TEOS, indicating good coverage, whereas Figure 7-6 is an SEM of a metallized poly step without TEOS. Metal discontinuities can be observed in this area; also, note the steepness of the poly step, which is responsible for the metal step coverage problem.

The problem of depositing and defining reliable metal gate structures used on early DCCD circuits, was eliminated by adopting a double poly process for the DP-2, DP-3 and DP-5 series lots. Excellent step coverage was obtained. In addition, the "poly protect" step was also eliminated, simplifying the DCCD process sequence.

Some additional step coverage problems occurred with DP-2 circuits as shown in Figure 7-5.

AD-A084 829

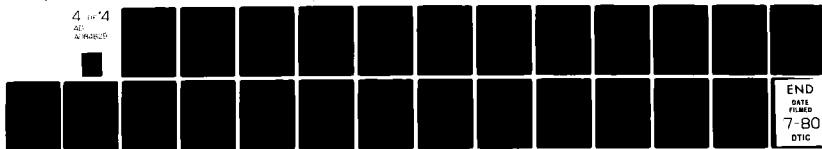
TRW DEFENSE AND SPACE SYSTEMS GROUP REDONDO BEACH CA F/G 9/1  
CHARGE COUPLED DEVICES IN SIGNAL PROCESSING SYSTEMS. VOLUME V. --ETC(U)  
DEC 79 R A ALLEN, J M ANDERSON, F G HAMILTON N00014-74-C-0068

NL

UNCLASSIFIED

4 11-14

AL  
A-14-14-14



END  
DATE  
FILMED  
7-80  
DTIC

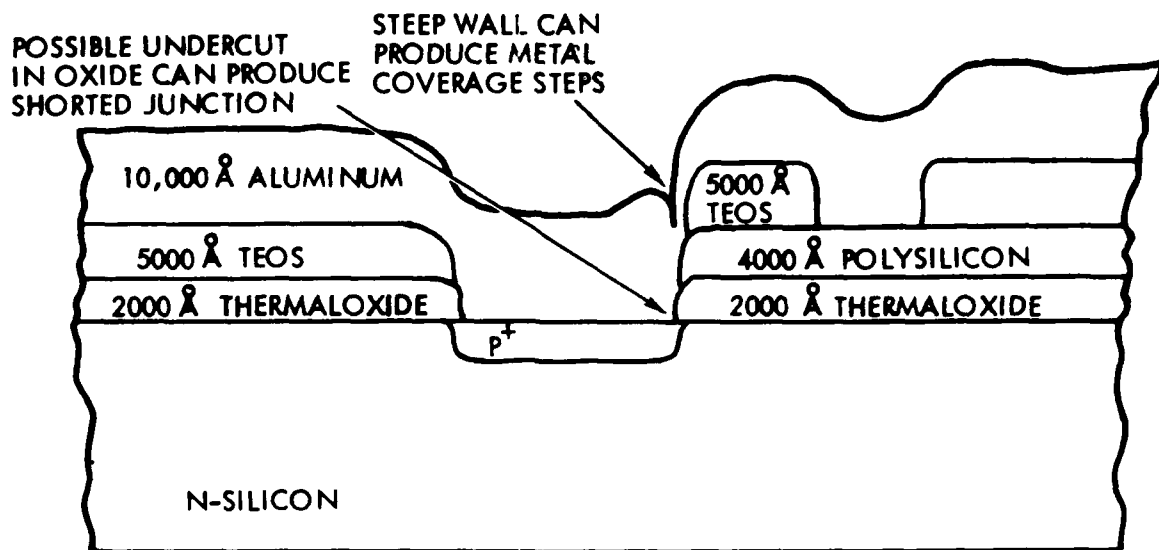


Figure 7-7. Source/Drain Contact to Poly Contact Structure.

Coincident edges of polysilicon traces over oxide cuts provided very steep steps that significantly reduced chances of reliable, unbroken step coverage. Note that the polysilicon trace does not overhang nor protect the edges of the  $P^+$  diffusion; any undercut of the gate oxide beneath the edge of the polysilicon film permits the deposited aluminum to short the  $P^+$  region to the N-substrate. This design oversight was corrected on DP-3 designs.

Additional metallization problems encountered during the early phases of this program included the selection of a satisfactory metal sintering temperature. The metal sintering temperature was lowered to  $400^{\circ}\text{C}$  during the processing of DP-2 lots. Test results indicated that this time vs temperature sequence was not sufficient to cancel X-ray damage produced during electron beam gun deposition of the aluminum metallization film. Additional problems encountered included poor ohmic contacts to both diffusion areas and polygate interconnections. Schottky diodes also affected CCD performance. In subsequent lots, a temperature of  $450^{\circ}\text{C}$  was again used to prevent the appearance of unwanted Schottky diodes and good ohmic contacts to diffusion and poly contact regions were again established.

Another metallization problem was uncovered when a high percentage of shorts-to-substrate occurred when metal contacts were made to poly structures that lay over thin thermally-grown oxides (1,000 - 2,000A thick). This design approach was carefully deleted from all future cell layouts, starting with the DP-3 series.

## 8.0 COMPUTER AIDED DESIGN

### 8.1 INTRODUCTION

At the time DCCL was in its developmental stages, existing computer aided design (CAD) systems serviced only transistor oriented technologies. Thus, at the outset, these existing systems were not useful for DCCD designs. The approach taken in developing a CAD system for DCCD designs was to evolve both the CAD system and the DCCD development simultaneously. The goal was to find the best trade-offs between the restrictions of CAD systems and the flexibility of layout. The result of this effort is a complete MOS/CCD design and layout system which provides front to back LSI photo mask production in periods of two to three months.

### 8.2 DEVELOPING A CCD DESIGN/LAYOUT CAD SYSTEM

CAD systems have been completely structured around transistor devices. For such CAD systems the devices and interconnects are represented symbolically. The symbols are designed in very specific ways for each device such that when the mere symbols are put together by the system rules (often referred to as spacing guides) the CAD software automatically assembles the actual chip layout. Such is the case for the oxide aligned transistor (OAT) technology developed by TRW.

The fundamental feature of CCD designs, which sets it apart from the other members of the MOS family, is that there are not necessarily any source or drain diffusions by which basic devices can be coupled together into a functional node structure. CCD's are primarily made up of overlapping gate electrodes which involves such considerations as getting the desired number of gates into a space allocation and defining the CCD channel properly (by making certain that the gate oxide and channel stop definition patterns are continuous and properly positioned under the gate electrode). Thus, existing CAD LSI layout systems had few provisions that were directly applicable to CCD devices initially.

In the experimental stages of CCD development the devices are simple and are evaluated individually at the wafer level. At this stage the demands placed on a CAD system are few. It merely provides a quick and convenient way of getting the simple configurations off the drawing board and onto mask plates. The test configurations are digitized into the computer one or two rectangles at a time with the finest positioning grid available. The grid units here are Applicon Graphic System (AGS) units of which there are 32,000 by 32,000. The scaling that was chosen for CCD was 40 AGS = 1.0 mil. Although this approach offers almost total flexibility in layout, there are some drawbacks.

Relative to the more automated layout systems, the piece-wise assembly of the various devices and configurations is immensely time consuming in addition to incurring a high potential for error. If there were no other approach to CCD design/layout, it would most certainly be very impracticable as an LSI technology. Clearly, for CCD to become a useful element of the MOS design family, some trade-offs, had to be made between CAD system restrictions and design and layout flexibility.

### 8.3 EVOLUTION OF DCCD AS AN LSI TECHNOLOGY

There are four main aspects to the approach

(1) Develop a technique of quickly and safely manipulating very large sections of a design data base: The most powerful feature available on the AGS system is the ability to nest cells. Nesting cells is a technique whereby a cell, consisting of a collection of components and basic devices, can be nested in another cell (this is nesting two levels deep). This means that the first cell's position in the data base is controlled by the positioning of the latter. AGS provides for up to 16 levels of nesting. This, in itself, presents the problem of keeping track of the device and component allocations between the levels.

(2) Develop a schematic representation of the design: This includes a schematic representation of CCD that is compatible with existing schematic forms for MOS. The schematic would allow a number of people, other than the design engineer, to effectively check designs before they go into fabrication. Schematics are also known to be helpful in testing for trouble shooting purposes in any technology.

(3) Develop a symbology for all the basic DCCD devices and interconnect: Developing a system of symbology to be used on the AGS for layout would form the heart of a workable CAD system. Rough layout diagrams could be generated with symbols in a very short time, and thus, chip dimensions and operating specifications could be sized early in a program.

(4) Obtain an effective automatic design rule check: Automatic design rule checking is becoming an essential part of the overall CAD system for LSI designs. The goal in this part is to not be limited to checking only spacing rules of the symbols but rather to check the spacing rules of the actual output patterns.

#### 8.4 PRESENT MOS/CCD DESIGN AND LAYOUT SYSTEM

The present CAD system for MOS/DCCD takes full advantage of the LSI graphics capability afforded by AGS. A fully developed system of schematics for the MOS/DCCD is now in use. A partial automatic design rule check is being used as part of the die design check procedure and a complete design/layout manual has been created which provides a framework and source documentation for the entire CAD system that has been developed.

MOS/DCCD layouts now use the nested cell capability of the AGS. At this point in time, the maximum number of nesting levels currently employed in MOS/DCCD layouts is set at four. The allocations between the nesting levels are as follows: Level 0 contains fixed components such as standard transistors, capacitors, standard subsections of shift register, and fundamental components of the DCCD half adder and charge fan-out. Level 1 controls everything on level 0 plus the additional components that complete the basic devices (i.e. half adders, charge fan-out, MOS signal interface, MOS timing and control and logic signal generators). Level 2 controls level 1 (and therefore level 0) plus all components of interconnect which tie basic devices into larger functional blocks. These functional blocks can be repeated, moved with the data base, and moved to other data bases with great ease. All internal relationships are maintained automatically by the AGS software. Level 3 controls the functional blocks, their interconnect, and all peripheral interconnect of pads, reticle alignment targets and chip identification number.

A system of schematics has been developed for the MOS/DCCD technology. Figure 8-1 shows a listing of all schematic symbols and descriptions. This system has been implemented on the AGS and thus enjoys all the advantages of editing, cell replication and nested cell data base management. A full set of formal schematics is created for each design before it enters the check cycle. The schematics provide an effective means of controlling the design and layout throughout the entire process. The schematics have also proven to be invaluable in the trouble shooting and testing of new designs.




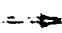
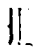
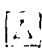
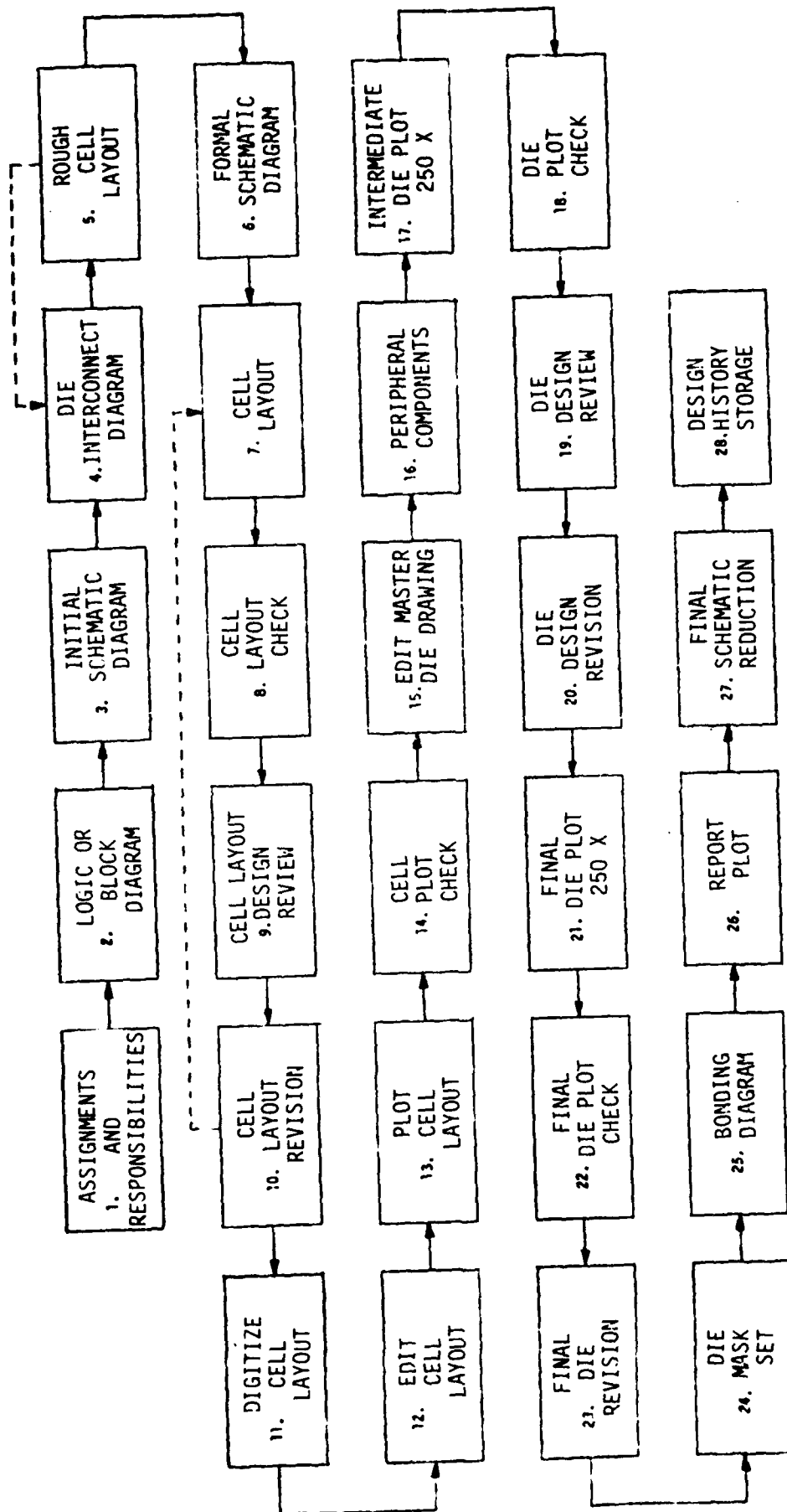
	POLY 1 ELECTRODE
	POLY 2 ELECTRODE
	SIGNAL OR CLOCK LINE USUALLY IN METAL
	CHARGE TRANSFER
	NAND2
	CELL CENTER
	TERMINATION ON TO A PAD AND/OR A GATE LINE
	FROM DATA BUFFER FILES ARE
	FROM DATA BUFFER FILES ARE

Figure 8-1. Index of schematic symbols and descriptions.

The DCCD design process now includes a form of automatic design rule check. It is run on the CDC time sharing system (TSS) at TRW. This design check code was configured specifically for the TRW triple diffused (3-D) technology. Thus, there is a limited amount of design check that it can do for the MOS/CCD technology. The design checks that are currently being done by this code are for minimum contact hole coverage by metal, minimum rectangle dimensions on all levels and minimum spacing between rectangles within a given level. In all these checks, the minimum dimension is specified by the user for each level submitted. The program flags all rectangles that are directly involved in any dimension that is less than the specified minimum. The remaining design checks for minimum spacing and overlap are done visually between the following levels:

CHANNEL OXIDE	- CHANNEL STOP
POLYSILICON I	- POLYSILICON II
CHANNEL STOP	- POLYSILICON I & II
SOURCE/DRAIN	- { CHANNEL OXIDE POLYSILICON I & II
CONTACT	- { CHANNEL STOP CHANNEL OXIDE POLYSILICON I & II METAL
PASSIVATION	- METAL

A complete MOS/DCCD design and layout manual has been created. It covers every major aspect of the CAD system that has been developed for MOS/DCCD. Figure 8-2 shows a top level flow diagram, taken from the manual, showing all the major steps in the present design and layout procedure.



DCCD DIE DESIGN FLOW DIAGRAM

Figure 8-2. Flow diagram of the complete die design and layout procedure taken from the DCCD design/layout manual.

## 9.0 RELATED DCCD PROJECTS

The following sections provide a general description of several DCCD projects which were created by the DCCD technology resulting from this program.

### 9.1 FAST HADAMARD TRANSFORM PROJECT

Data communications have become an important compliment to military avionics in many command and control applications. Data transmission is now accomplished by digital communication systems that take advantage of their greater efficiency and superior error control. Television, however, has continued to use analog signal processing techniques. This is a result of the high data rates (typically 60 Mbps) and concomitant wide bandwidths required by conventional Pulse Code Modulation (PCM) of video. Typical parameters required for good fidelity include sampling rates of 10 MHz (minimum), with 6 to 8 bits per sample. Never-the-less, the switching, storage and processing advantages of digital data have led many commercial and military applications to favor digital television transmission. Fortunately, digital television coding techniques have shown that significant compression of high data rates can be achieved through exploitation of spatial, temporal and spectral (color) redundancy present in normal color video data.

Transform coding algorithms perform a one or two dimensional unitary transformation on the input data followed by some form of quantization of the resulting coefficients. At the receiver, the inverse transform is performed to restrict the original data within particular degradation limits. The Hadamard, Fourier, Maar, Slant, and Cosine transforms all possess qualities desirable for data compression.

The chief disadvantage of transform encoding are implementation complexity related to large data block sizes (needed for effective de-correlation) and high sampling rates. With two (spatial) dimensional data blocks, that can take advantage of spatial picture correlation, computation rates become intense. For example, using the straightforward FFT, an 8 x 8 sample data block requires 3 "butterfly" operations per sample. Besides the complex multiply and add functions, special logic must be included to limit numerical

noise effects. Such systems are practical only through the use of LSI technology to reduce subsystem chip and component complexity. For general applicability, a sufficient data range is provided by a Hadamard transform chip that performs a single stage of a pipeline version transform algorithm. The design of a Fast Hadamard Transform (FHT) chip allows the same device to be used at any stage of either the forward or reverse transform for data block sizes as large as  $8 \times 8$  (Figure 9-1). In addition, all of the multiplex clocking and control is included on chip.

The interconnection of four typical FHT cells is shown in Figure 9-2. Each cell consists of two full-adders, four multiplexing AND gates, and a feedback delay. The I/O multiplex signals in a FHT A5 (first Hadamard stage, 5th significant bit) or FHT A6 (first Hadamard stage, 6th significant bit) require a single clock phase delay, while in the B5 and B6 stages (second Hadamard stage, fifth and sixth bits), they require two clock phase delays. These delays are part of the Hadamard encoding technique and double at each stage as the data progresses across the chip.

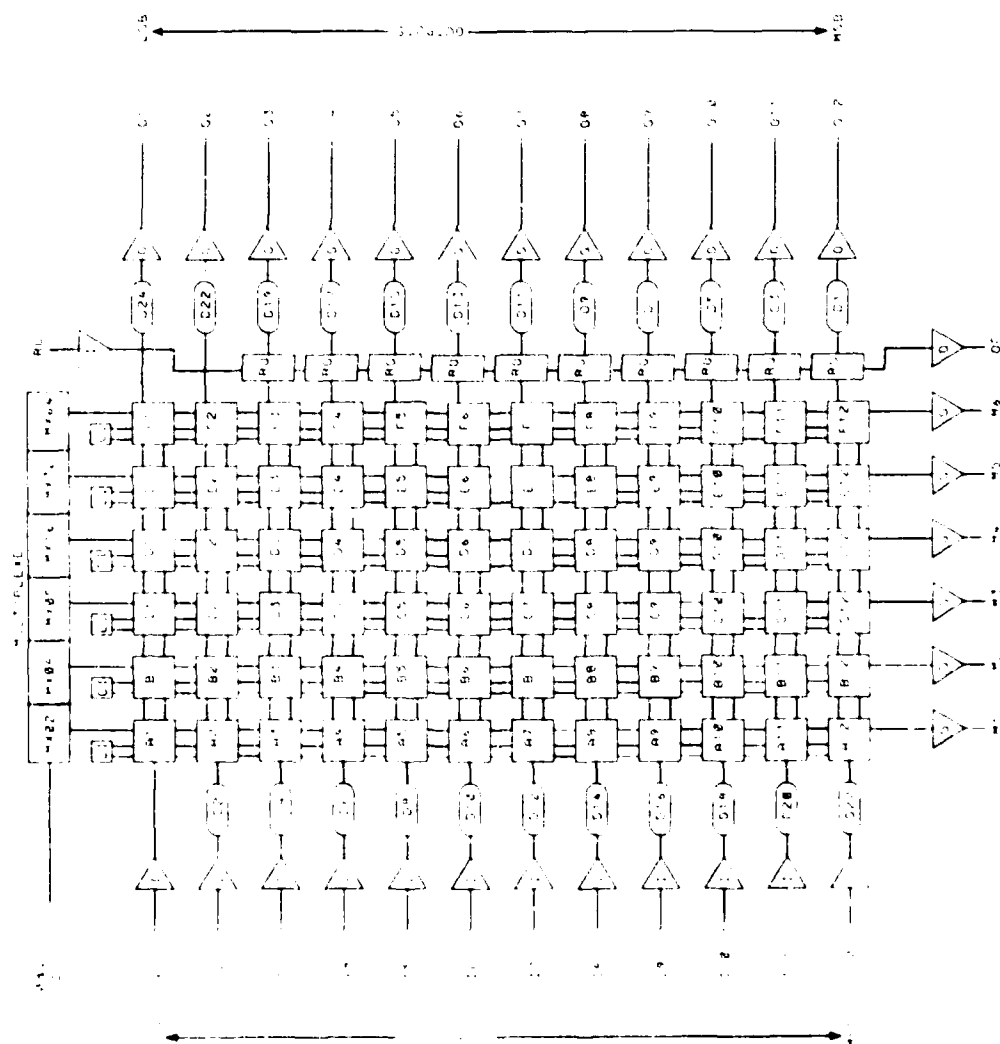
The carry-bit from Stage A5 transfers vertically to Stage A6 after a one-bit delay through the full-adder and the input data to Stage A6 must also be delayed by one-bit to ensure that they arrive synchronously with the carry-bit. This skewing of the data is inherent in any DCCL pipeline array to accommodate the finite charge transfer times.

All of the arithmetic, multiplexing, and digital CCD Logic functions required for the FHT chip were designed for inclusion on a test chip designated FHT-0 (see Section 4.4 for functional results).

The  $8 \times 8$  version of the FHT chip has a completed initial layout at this time. This chip is required to operate at 2.4 MHz, dissipate less than 750 mw, and measures just under 400 mils on a side.

## 9.2 AZIMUTH CORRELATOR DEVICE

Arrays of ACD circuits are intended for use in Synthetic Aperture Radar (SAR) on-board data processors for space missions. In the first planned application, an array of 1024 ACDs will be used to perform azimuth correlations in a Developmental Model SAR Processor (DMSP). The DMSP functional block diagram, Figure 9-3, shows the relationship of the azimuth correlator to the other



NOTES

- - HADAMARD CELL
- - SELECT 7/12 (ROUND OFF)
- (D17) NUMBER - AMOUNT OF DELAY
- △ - 16/128 BUFFER (OUTPUT)
- ▽ - 16/128 BUFFER (INPUT)
- - OVERFLOW ERROR BIT
- - CARRY AND CARRY INTO ARRAY
- △ - DELAYED MULTIPLEXER CONTROL SIGNAL N=1-6

Figure 9-1. Block diagram of the 64 point Fast Hadamard Transform Chip.

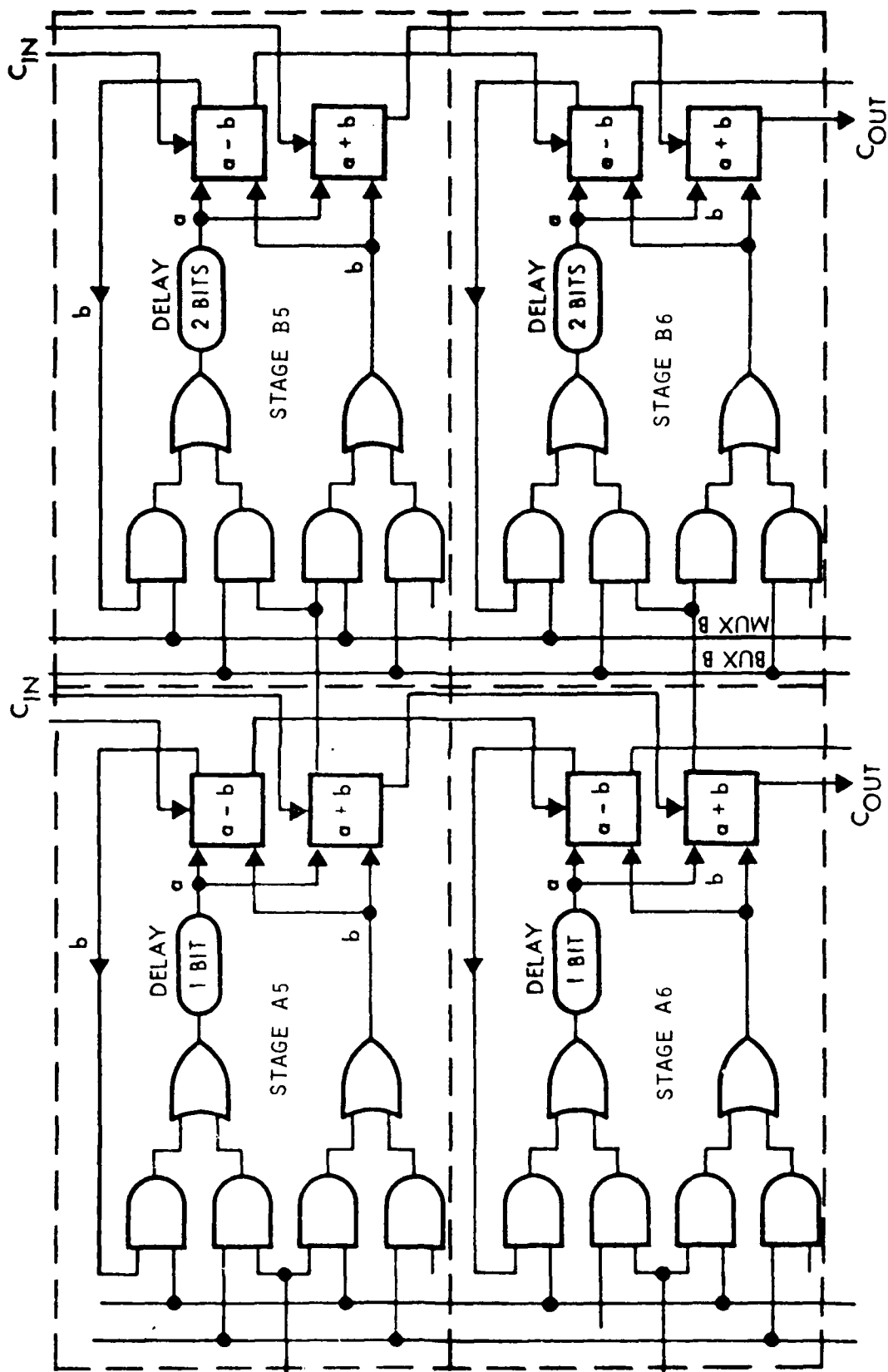


Figure 9-2. Four Typical FHT Cells.

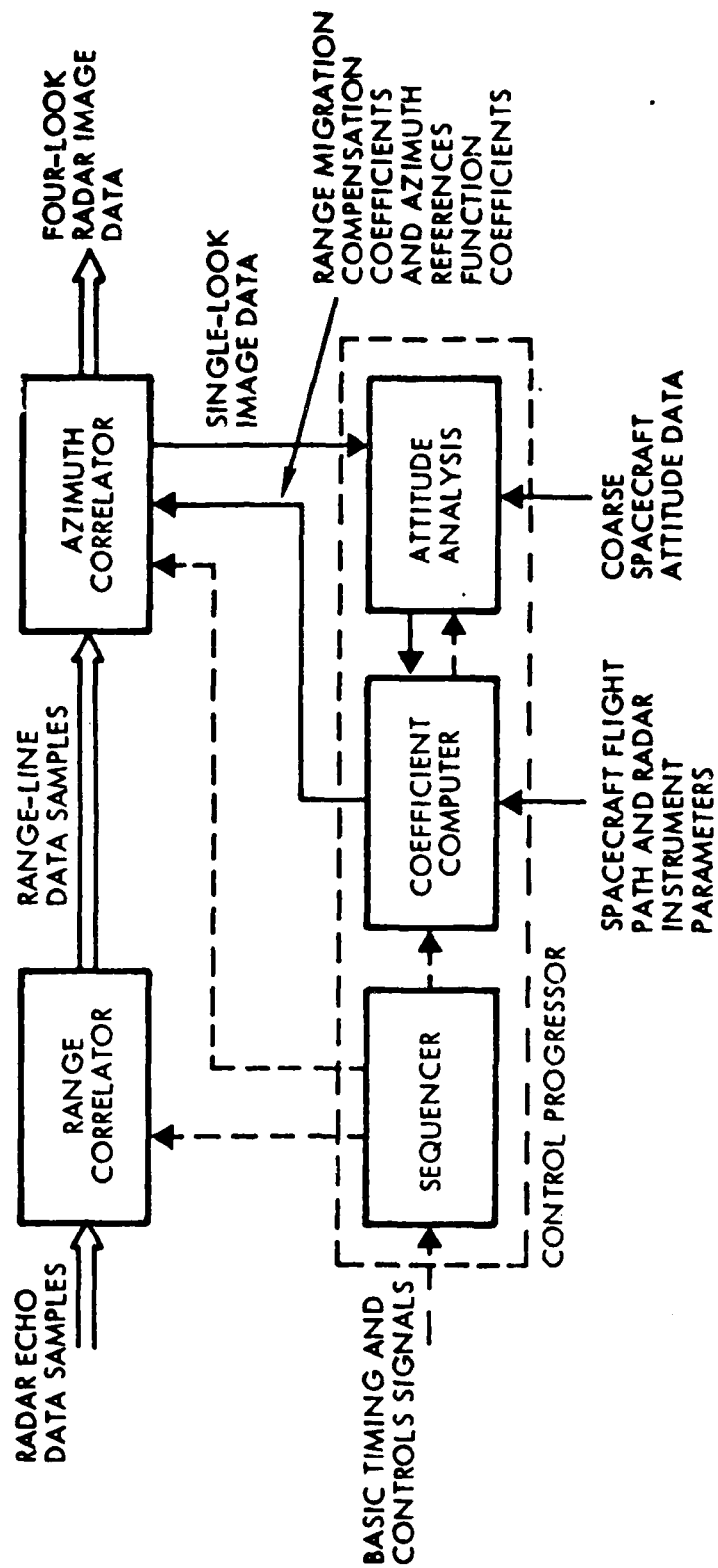


Figure 9-3. Developmental Model SAR Processor Block Diagram.

elements of the DMSP. The ACD receives data from the range correlator via the ACD input sample bus; this is provided as a contiguous sequence of "range-lines." Each range-line comprises 2560 complex data samples accompanied by several sync signals. The basic operation performed by the ACD during a range-line processing cycle is to select the appropriate set of 1024 complex data samples from each range-line, multiply each data sample by the appropriate complex azimuth reference function (ARF) coefficients and add this product to the appropriate cell in the accumulator register. (New sets of reference function coefficients are required for each new set of range-line data samples input to the ACD during an image-line processing cycle.) In the DMSP, an image-line processing cycle will involve 1020 range-lines. At the end of an image-line processing cycle, each ACD circuit outputs its accumulated 1024 complex image-line samples. The image-line memory is filled with zero levels during the image-line readout process and a new image line is initiated.

A functional block diagram of the Azimuth Correlator Device is shown in Figure 9-4. This DCCD chip contains both a complex parallel multiplier and a large array of CCD memories.

The primary functional blocks for the ACD were designed, fabricated, and tested on two evaluation masks designated ACD-0 and ACD-2. The performance results to date on these circuits are described in Sections 4.2 (Adder), 4.3 (Multiplier), and 4.5 (Memory).

### 9.3 SORT AND MERGE (SAM)

A key requirement of an EW pulse processor is its ability to use the information that characterizes each pulse (i.e., Time of Arrival (TOA), Angle of Arrival (AOA), Pulse Width, and Pulse Amplitude) and classify or sort, each pulse into groups having similar parameters. Thus, all pulses having an AOA within specific boundary constraints. Pulses having a similar Pulse Repetition Interval (PRI) that are within an AOA boundary are capable of being grouped. Further processing can then be performed on selected groups having particular parameters, while other groups can be ignored. This can significantly reduce the required processing as most signal environments contain far more pulses that are not of interest than those that are of interest. Figure 9-5 shows a functional block diagram of a pulse processing algorithm which can be

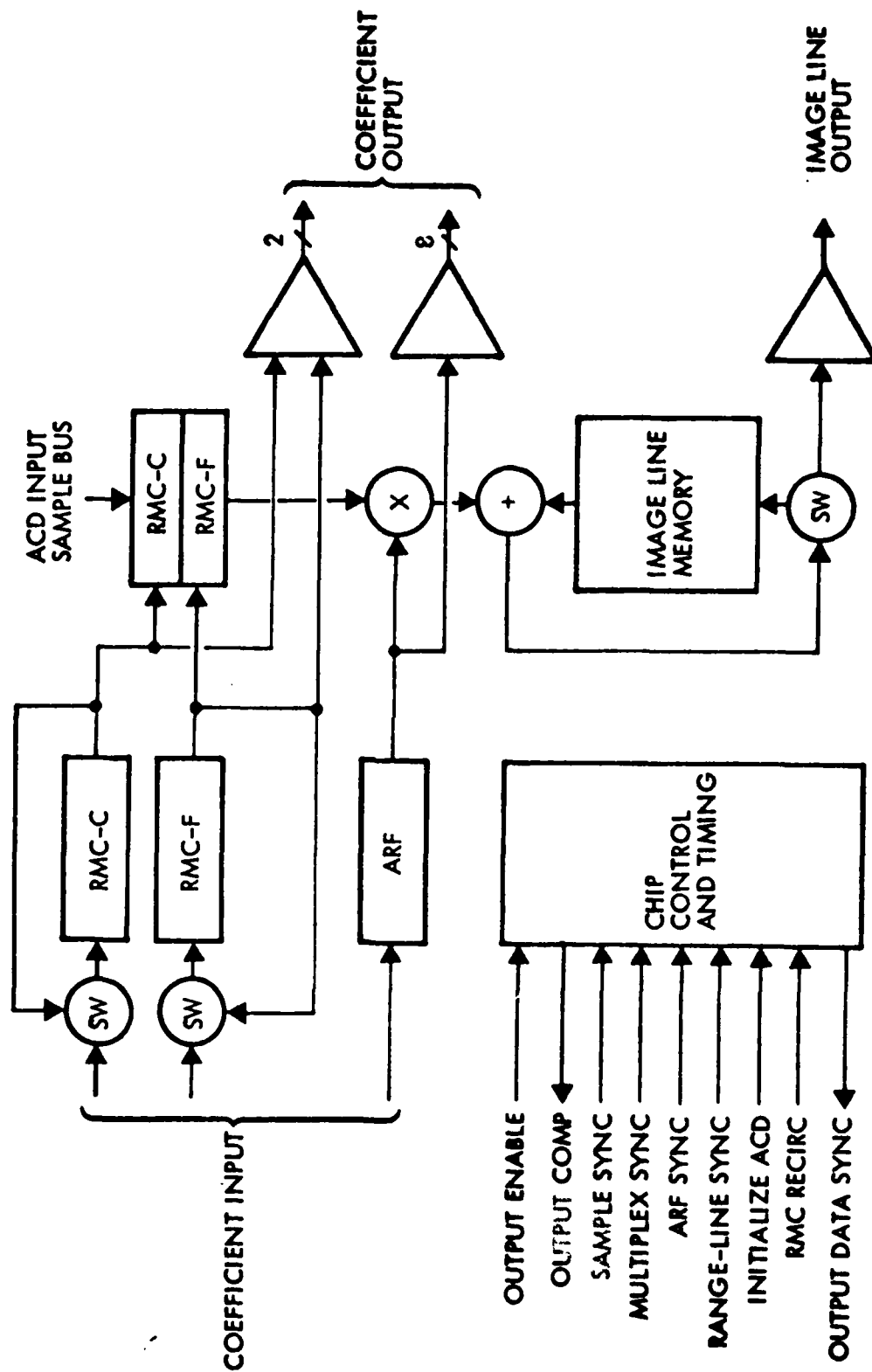


Figure 9-4. Functional block diagram of the ACD.

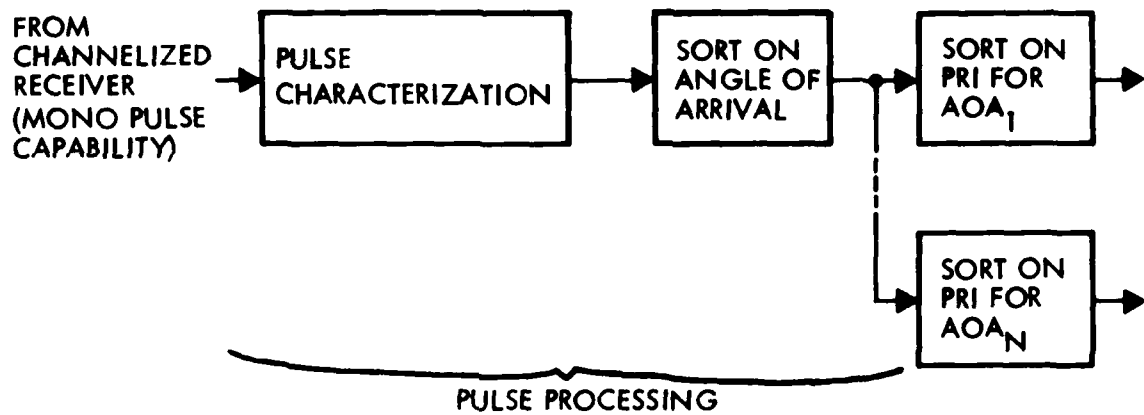


Figure 9-5. EW pulse processing algorithm.

applied to a batch of characterized pulses to eliminate those pulses that are received from angular locations (related to the receiver) that are not of interest. Pulses that have been processed and geo-located (with a rather coarse resolution of  $1/128^{\text{th}}$  of a circle) are then sorted for PRI. This final sorting groups pulses by potential emitters and thereby reduces the load of any post processing equipment.

The possibility of using DCCD to perform the sort and merge functions required for EW processors emerged in late 1978. A number of techniques were studied for compatibility with DCCD implementation. These are discussed in some detail in Section 6.3.

These studies concluded that the most favorable candidate for a DCCD sort and merge system is a radix exchange algorithm (see Section 6.3.2). In the radix exchange algorithm, an M long list of unsorted N-bit wide words are sorted by decision logic into two registers, depending on the binary value of the most significant bit. Since a last-in-first-out (LIFO) memory is required to store the sorted N-bit wide words, the application of a high bit density CCD memory to the sort and merge function was apparent. A 1.2K-bit experimental LIFO was designed and placed on the ACD-2 test mask for evaluation. Unfortunately, program cost and schedule constraints did not permit the functional evaluation of this design.

#### 9.4 THE TWENTE REPORT

An internal report on digital charge coupled devices has been written by J.W.M. Jansen and published,<sup>(11)</sup> by Twente University of Technology, Enchede, The Netherlands. This study was initiated as a result of technical papers that described DCCD logic cells as well as the results obtained from work performed on this contract.

The Twente report contains a comprehensive analysis of a DCCL "AND" gate and a half-adder. It also describes the design and test results of a n-channel, double-polysilicon, DCCL evaluation chip. This chip contained a half-adder, an AND/OR-gate, a signal regeneration (fan-out) circuit and two multiple value logic circuits. The regeneration (fan-out) circuit differs from TRW designs as it converts charge into a voltage; fan-out then creates new charge packets.

The half-adder uses a floating-capacitor as the charge sensing node of the charge transfer electrode in an identical manner to the DP1 design. Since the carry output is taken from the master side of the charge sense electrode instead of the T-gate, charge regeneration is not achieved (again similar to the DP1 design). A simple pseudo-one phase clocking scheme was used for these designs. This scheme requires a single clock line plus a d-c clock line. In order to provide directionality a dc biasing voltage is required to produce a surface potential step. Correctly functioning AND/OR gates and half-adders were demonstrated for clock speeds from 10 kHz to 500 kHz.

## 10.0 RECOMMENDATIONS FOR FUTURE WORK

### 10.1 DESIGN

The demonstrated frequency and noise immunity performance of the latest DCCD multiplier (6 x 4 bit 2's complement) and adder (10 + 10 bit) designs provide the basic circuit functions needed for constructing larger arithmetic and computational blocks.

The next step towards the realization of these blocks should include a task for the evaluation and characterization of the interfaces between DCCD logic and arithmetic circuits. Candidate designs for this interface development include the serial correlator and code generator applications described in the first (Volume I: Digital Signal Processing) study phase of this program. The serial correlator application is particularly attractive in that it provides an opportunity to interface multipliers, adders, and memory. Preliminary sizing for an 8 bit version of this correlator yields a comfortable chip size of approximately  $13 \text{ mm}^2$ .

Another task recommended for inclusion into future program efforts is a DCCD design scaling investigation. The ability to perform dimensional scaling on DCCD devices is essential if they are to remain competitive with the current speed/power projections for future NMOS and CMOS devices. One primary activity anticipated for this task is the need to develop a ultra sensitive circuit for reliably detecting the reduced charge levels resulting from this dimensional scaling.

Finally, it is recommended that the task of developing on-chip support circuits be performed. This task will included the design and development of high speed, low power circuits for on-chip clock generation, bias voltage generation, addressing, decoding, and general input output functions such as tri-state buffers and level shifters. Emerging candidate technologies for this application are short channel CMOS and/or dynamic NMOS.

## 10.2 PROCESSING

Although the present DCCD processing sequences and techniques provide reliable, repeatable circuit performance characteristics, continued process development is required if functional density and operating speed improvements are to continue. The following paragraphs describe the key items identified as achievable goals for the next phase of DCCD process development.

Additional effort is required to maximize circuit density by reducing contact hole size and poly gate lengths, along with supporting interconnection patterns and metallization patterns. Reduction of critical line widths may be achieved through anisotropic etching (dry/plasma/reactive ion etching) of these fine patterns that control circuit density.

Elimination of the undesirable intergate charge barrier or "bump" may be feasible, by developing a reliable  $\text{SiO}_2/\text{Si}_3\text{N}_4$  dielectric sandwich, that can be used in lieu of a conventional gate oxide. A sufficient amount of work has already been done to improve chances of success in this important area. Such a compound dielectric may permit polygate doping concurrently with associated self-aligned source-drains. Concern over Boron penetration of thin gate oxides (500Å) could be set aside, as the density of the nitride film would prevent dopant penetration of the CCD channel during polygate and source-drain doping steps.

Major improvements in polysilicon film deposition can be made, in order to achieve significantly thinner films (2000Å) with similar or perhaps lower film resistivity. New techniques in CVD-deposited polysilicon may enable in-situ doping, thus simplifying polysilicon deposition procedures. This would include reduced operator handling of wafers with corresponding increases in yields. Further gains in LSI yields are also potentially available if significantly thinner films can be deposited that are subsequently doped by a refractory metal that provides low resistivity values (0.5 - 5 ohms/sq). Thin poly films having high conductivity, also supports the quest for a basically isoplanar technology and higher circuit yields.

Higher circuit densities for DCCD chips may also be obtained by employing multilayered interconnections; this implies an additional level of metal interconnections in addition to the existing levels of polysilicon and metal. For example, state-of-the-art interconnection system might be comprised of a polysilicon level for CCD and MOS gates and interconnecting leads. Densified TEOS or SILOX would be used to separate this first level from a second metal interconnection level comprised of refractory metal(s) such as Tungsten or Ti:W. A patterned layer of refractory metal can withstand sintering temperatures of 450°C forming good ohmic contacts to the polysilicon structures. In addition, an insulating layer of SILOX can be deposited over the high density refractory metal lines without causing pattern dissolution. The top level of metallization can be patterned of aluminum or copper-doped aluminum, which in turn would be protected by a passivation layer of SILOX. There are a number of critical parameters that must still be worked out for such a complex multilevel interconnection system to be successful.

## 11.0 PATENTS AND PUBLICATIONS

### 11.1 PATENTS

The following section lists the patents awarded (and pending) that result from the digital charge coupled devices technological development program.

Patent No. 4,170,041. Inventor T. A. Zimmerman and R. Handy  
Logic Gate Utilizing Charge Transfer Devices

This is the basic half-adder and full-adder digital CCD with the addition of a control gate between the input "OR-gate" (D-gate) and the slave side of the charge transfer electrode.

Patent No. 4,135,104. Inventor R. A. Allen  
Regenerator Circuit

This is a digital half-adder in which the CARRY output is changed from the master side of the charge transfer electrode to the "OR-gate", (T-gate). This modification results in an automatic fully regenerated CARRY charge packet. A second modification causes a binary one charge packet to be inserted into one of the inputs each clock cycle, and the complement of the input binary value to be available at the output plus a fully regenerated charge packet of the same binary value as the input charge packet.

Patent Pending, Docket No. 12-002. Inventor R. A. Allen  
CCD Channel Crossover

This invention enables charge packets being transferred in a typical CCD manner in two separate shift-registers to intersect without interference.

Patent Pending, Docket No. 12-035. Inventor R. A. Allen  
DCCD Latch Circuit

A modification to a DCCD half-adder in which the exclusive-OR (SUM) output is connected back to the input to form a latch circuit. Set and re-set inputs are available.

Patent Pending, Docket No. 12-036. Inventor R. A. Allen  
DCCD Frequency Divider

A modification to a DCCD half-adder in which the AND (CARRY) output is connected back through a shift-register to one of the inputs. A binary one charge packet is inserted into the other input at each clock phase. The frequency is  $f_o = f_c(n+1)/2$  where  $f_c$  is the clock frequency and  $n$  is the number of shift-register stages in the feedback path.

Patent Pending, Docket No. 12-037. Inventor R. A. Allen  
DCCD Fan-Out Generator

A digital CCD that uses the input charge packet to control the state of a charge transfer electrode. This electrode then controls through which output ports two or more full-charge packets are transferred. It is possible to obtain either two or three charge packets of the same or the binary complement of the input charge packet.

## 11.2 PUBLICATIONS

All of the following technical publications discuss digital charge coupled devices, either as tutorial papers that described the technology or as descriptions of system applications.

1. T. A. Zimmerman, "Charge Coupled Devices in Signal Processing Systems: The Analog and The Digital Approach", 1974 National Telecommunications Conference, San Diego, December 1974
2. T. A. Zimmerman, "The Digital Approach to Charge Coupled Device Signal Processing", IEEE Advanced Solid State Components for Signal Processing, 1975 Circuits and Systems Conference, pp 69-82, April 1975
3. C. S. Miller, T. A. Zimmerman, "The Application of Charge Coupled Devices to Digital Signal Processing", International Communications Conference, San Francisco, pp 2-20/2-24 June 1975
4. C. S. Miller, T. A. Zimmerman, "Applying the Concept of a Digital Charge Coupled Device Arithmetic Unit", Second International Conference on the Application of Charge Coupled Devices, pp 199-207, San Diego, Oct. 1975
5. T. A. Zimmerman, R. A. Allen, "Charge Coupled Device Digital Arithmetic Functions: Experimental Results", Third International Conference on the Application of Charge Coupled Devices, pp 190-196, September 1976
6. R. A. Allen, R. J. Handy, J. E. Sandor, "Charge Coupled Devices in Digital LSI", International Electron Devices Meeting, pp 21-26, December 1976

7. R. A. Allen, "Digital CCD Arithmetic Technology," Digest of Papers, Compcon 77, pp. 342-344, March 1977.
8. T. A. Zimmerman, D. F. Barbe, "A New Role for Charge-Coupled Devices: Digital Signal Processing", Electronics, pp. 97-103, March 1977.
9. C. S. Miller, C. F. Motley, R. A. Allen, "Digital Charge Coupled Device Technology and Digital Filters Applications," EASTCON-77, Proceedings, pp. 30-1A/30-1H, September 1977.
10. T. A. Zimmerman, R. A. Allen, R. W. Jacobs, "Digital Charge Coupled Logic (DCCL)", IEEE Journal of Solid-State Circuits, pp. 473-485, October 1977.
11. R. A. Allen, D. J. Spencer, C. S. Miller, "LSI Video Compression and Computational Module Utilizing Digital Charge Coupled Devices," AGARD Conference, Proceedings, pp. 3.8-1/3.8-5 Quebec, October 1977.
12. E. Hyman, R. A. Allen, "The Development and Application of a Digital Charge Coupled Logic (DCCL) Arithmetic Unit," 1978 International Conference on the Application of Charge Coupled Devices, Proceedings pp 3A-53/3A-57, San Diego, October 1978.
13. T. A. Zimmerman, "Charge Coupled Devices," Quest, New Technology of TRW Defense and Space Systems Group, Autumn 1978, Vol. 2, No. 2, pp. 70-92.
14. D. J. Spencer and J. M. Anderson, "A Real Time Video Bandwidth Reduction System based on a CCD Hadamard Transform Device," Proceedings of the IEEE 1974 NAECON, Vol. 3, pp. 1218-1231, May 15-17, 1979.

## 12.0 REFERENCES

1. T. A. Zimmerman, R. A. Allen, R. W. Jacobs, "Digital Charge Coupled Logic," JSSC, Vol. SC-12, No. 5, October 1977.
2. M. F. Tompsett, "A Simple Charge Regenerator for use with Charge-Transfer Devices and the Design of Functional Logic Arrays," IEEE J. Solid-State Circuits, Vol. SC-7, pp. 237-242, June 1972.
3. T. A. Zimmerman and C. S. Miller, "Charge Coupled Devices in Signal Processing Systems, Vol. I, Digital Signal Processing," July 1974.
4. T. A. Zimmerman, R. J. Handy, R. A. Allen, E. E. Swartlander, D. J. Heath, J. E. Sandor, "Charge Coupled Devices in Signal Processing Systems," Vol. III, Digital Function Feasibility Demonstration, March 1976.
5. R. A. Allen, M. Penberg, T. A. Zimmerman, "Charge Coupled Devices in Signal Processing," Vol. IV, Digital Array Feasibility, June 1978.
6. T. A. Zimmerman and R. A. Allen, "Charge Coupled Device Arithmetic Functions: Experimental Results," Third International Conference on the Application of Charge Coupled Devices, Edinburgh, Proceedings, pp. 190-196, September 1976.
7. C. S. Wallace, "A Suggestion for a Fast Multiplier," IEEE Trans. Electronic Computers, Vol. EC-13, pp. 14-17, February 1964.
8. J. R. Logan, "A Square-Summing, High-Speed Multiplier," Computer Design, pp. 67-70, June 1971.
9. L. G. Heller and H. S. Lee, "Digital Signal Transfer in Charge Transfer Devices," J. of Solid State Circuits, SC-9, pp. 116-125, 1973.
10. C. S. Miller and T. A. Zimmerman, "Applying the Concept of a Digital Charge Coupled Device Arithmetic Unit," Second International Conference on the Application of Charge Coupled Devices, 1975.
11. J.W.M. Jansen, "Basic Logic Functions Using Charge Coupled Devices," Internal Report 1217.2850, Twente University of Technology, Afdeling Electrotechniek, Laboratorium Vastest of Electronica, P.O. Box 217, Enschede, The Netherlands.